AD

AD661088

USAAVLABS TECHNICAL REPORT 67-17

AIRCRAFT PASSENGER-SEAT-SYSTEM RESPONSE TO IMPULSIVE LOADS

By

James W. Turnbow
Jack A. Collins
J. Robert Cromack
Nils P. Myklestad

August 1967

U. S. ARMY AVIATION MATERIEL LABORATORIES
FORT EUSTIS, VIRGINIA

CONTRACT DA 44-177-AMC-360(T)
ARIZONA STATE UNIVERSITY
TEMPE, ARIZONA
AND
AVIATION SAFETY ENGINEERING AND RESEARCH
A DIVISION OF
FLIGHT SAFETY FOUNDATION, INC.

Distribution of this document is unlimited

314

Disclaimer

When Government drawings, specifications, or other data are used for any purpose other than in connection with a definitely related Government procurement operation, the United States Government thereby incurs no responsibility nor any obligation whatsoever; and the fact that the Government may have formulated, furnished, or in any way supplied the said drawings, specifications, or other data is not to be regarded by implication or otherwise as in any manner licensing the holder or any other person or corporation, or conveying any rights or permission, to manufacture, use, or sell any patented invention that may in any way be related thereto.

Disposition Instructions

Destroy this report when no longer needed. Do not return it to originator.

DEPARTMENT OF THE ARMY
U. S. ARMY AVIATION MATERIEL LABORATORIES
FORT EUSTIS, VIRGINIA 23604

This report has been prepared by the Aviation Safety and Engineering Research Division of the Flight Safety Foundation and Arizona State University under the provisions of Contracts DA 44-177-AMC-254(T) and DA 44-177-AMC-360(T). It consists of an investigation of the dynamic response of seat passenger systems to crash-induced floor accelerations through a computer analysis of the problem; an investigation of seat strength and load deformation characteristics; and an investigation of conceptual seat-system designs.

The results of this study disclosed data on the use of load limiters in reducing seat loads and the effect of using shoulder harnesses. The study also presents several seat restraint designs.

Task 1A024701A12101
Contract DA 44-177-AMC-360(T)
USAAVLABS Technical Report 67-17
August 1967

AIRCRAFT PASSENGER-SEAT-SYSTEM RESPONSE TO IMPULSIVE LOADS

AvSER 66-20

by

James W. Turnbow
Jack A. Collins
J. Robert Cromack
Nils P. Myklestad

Prepared by

Arizona State University
Tempe, Arizona
and
Aviation Safety Engineering and Research
Phoenix, Arizona
a Division of
Flight Safety Foundation, Inc.

for

U. S. ARMY AVIATION MATERIEL LABORATORIES
FORT EUSTIS, VIRGINIA

Distribution of this
document is unlimited

BLANK PAGE

SUMMARY

These report presents the results of an investigation of the dynamic response of typical aircraft passenger-seat systems to impulsive loading. It is divided into four chapters as follows:

Chapter 1 describes the mathematical model consisting of a visco-elastic occupant (control of joint stiffness through muscle tension) and an elastic-plastic seat structure. A comparison is made of the computer output and a full-scale dynamic test of a modern transport seat using instrumented dummies.

Chapter 2 presents a spectrum of design data based on results obtained from the computer program. The design variables studied include:

1. Seat displacement with respect to the aircraft floor in the fore-aft direction.
2. Seat belt load.
3. Vertical force reaction on the front seat legs.
4. Vertical force reaction on the rear seat legs.
5. Horizontal force on the seat legs in the fore-aft direction.
6. Pelvic displacement with respect to seat.
7. Pelvic deceleration of the occupant in the fore-aft direction.
8. Maximum velocity of the occupant's head.

The concept of load limiting is presented, and the effect of load limiting on the above design variables is studied. In addition, the effect of pulse shape and amplitude is presented through the use of an array of triangular, trapezoidal, and other pulses. The effects of passenger weight, seat belt slack, and shoulder harness are studied.

Chapter 3 presents a discussion of load limiting and other structural and detail design concepts appropriate to maintaining good restraint of the occupant. Stress concentrations under dynamic load are explored, and the results of experimental tests are presented to show that components which have stress raisers may absorb only very small amounts of energy prior to failure. Static and dynamic tests have been conducted on typical seat components, and load-carrying capacity is compared under these conditions.

Chapter 4 discusses the problem of head impact for the jackknifing passenger when restrained by seat belt alone. A computer study has been made which allows a correlation of head impact velocity and "cushioning material" thickness with the presently known human tolerance limits to deceleration. It is shown that the permissible head impact velocities will probably be in the order of one-third to one-half those which result in the 64-foot-per-second impacts described in Chapter 2.

The data presented in this report were necessarily computed and plotted over a period of several months. During this same time, the computer program was undergoing constant modification and improvement. For these reasons, the data presented are not in every case directly comparable. While the trends are qualitatively correct throughout the data presented, the use of the results for quantitative purposes must be undertaken with caution since the results of such quantitative comparisons could be misleading in some cases. Appendix III is included to illustrate quantitative changes which have occurred in improving the computer program.

FOREWORD

The work discussed in this report was conducted jointly by the Aviation Safety Engineering and Research (AvSER) Division of the Flight Safety Foundation (FSF) and the School of Engineering of Arizona State University (ASU) under the provisions of Contracts DA 44-177-AMC-254(T) and DA 44-177-AMC-360(T) with the U. S. Army Aviation Materiel Laboratories.* Funds for this study were provided in equal amounts by the National Aeronautics and Space Administration, the United States Army, the United States Navy, and the United States Air Force. The study was guided and monitored by Mr. I. Irving Pinkel and Mr. John H. Enders, both of NASA. Mr. Joseph L. Haley, Jr., served as project engineer for AvSER; Dr. James W. Turnbow, Professor of Engineering, served as principal investigator for Arizona State University.

Major contributions to this effort were made by the following staff personnel at Arizona State University:

James P. Avery, Ph. D., Professor of Engineering
Jack A. Collins, Ph. D., Professor of Engineering
Nils O. Myklestad, Ph.D., Professor of Engineering
Wilbur C. Schoeller, Ph. D., Professor of Engineering
James W. Turnbow, Ph. D., Professor of Engineering
J. Robert Cromack, M. S. E., Research Engineer

The authors wish to extend acknowledgement to the following graduate and undergraduate students who supplied valuable assistance in the study:

Mr. F. Richard Campbell, Graduate Student
Mr. Victory Lee, Undergraduate Student
Mr. Paul R. Mohr, Graduate Student
Mr. Salmon A. Soule, Graduate Student
Mr. S. C. Martin Spoor, Graduate Student
Mr. Peter L. Versteegen, Undergraduate Student

Appreciation is extended to Mr. K. C. Hagerman, Chief Metallurgist for the Reynolds Metals Company, Phoenix, Arizona, for providing the spectrographic analysis of the aluminum used in the stress concentration tests at no cost to the project.

*Formerly U. S. Army Transportation Research Command.

Grateful appreciation is also extended to the Sandia Corporation, Albuquerque, New Mexico, for providing the use of their facilities and the Hy-Ge testing machine at no cost to the project. Particular thanks are due Mr. Olden Burchet of Sandia Corporation and his staff for arranging their schedule to allow the dynamic stress concentration tests to be performed.

CONTENTS

CONTENTS (Contd.)

CONTENTS (Contd.)

CONTENTS (Contd.)

ILLUSTRATIONS

ILLUSTRATIONS (Contd.)

ILLUSTRATIONS (Contd.)

ILLUSTRATIONS (Contd.)

ILLUSTRATIONS (Contd.)

ILLUSTRATIONS (Contd.)

ILLUSTRATIONS (Contd.)

ILLUSTRATIONS (Contd.)

ILLUSTRATIONS (Contd.)

ILLUSTRATIONS (Contd.)

TABLES

INTRODUCTION

With the rapid growth of air transportation subsequent to World War II, increasing attention has been focused on the causes of passenger injuries in severe, although potentially survivable, crashes. In many accidents the probable cause of injuries has been traced to the failure of the occupant's seat restraint system. These failures have permitted seated occupants to be thrown against objects either inside or, in some cases, outside the aircraft. In some severe accidents, in which the occupant's restraint system did not fail, injuries have been caused by the flailing of body extremities into the adjacent seat.

In an effort to determine the magnitude of the forces acting on aircraft passengers during aircraft crashes, the National Aeronautics and Space Administration (formerly the National Advisory Committee for Aeronautics, NACA) conducted a series of full-scale aircraft crash tests with instrumented dummies in the early 1950's. These tests yielded excellent results on the magnitude of forces acting on the floor of aircraft under varying crash conditions. Later NACA studies by Pinkel and Rosenberg[7] on the dynamic response of seat structures to impact loads gave a better insight into the problem, but insufficient data were obtained to permit the FAA (formerly Civil Aeronautics Administration, CAA) to write new seat specifications which would take advantage of the NACA results obtained to that date. The results obtained by the NACA research, however, did not go entirely unused, because the CAA did increase the static strength of seats by a factor of 50 percent, from a longitudinal load factor of 6G to a factor of 9G. These new strength requirements were issued in 1954 before the advent of turboprop and turbojet aircraft in this country.

The use of 9G seats has, no doubt, reduced the number of fatalities which would have occurred. For example, accident investigators have revealed that some 9G seats were torn from the floor in accidents while adjacent seats remained in place; these observations would indicate that the decelerative loads imposed were just about equal to the ultimate strength of the seat, and that 6G seats would certainly have failed under the same conditions.

No new requirements on the longitudinal strength of seats have been written since 1954; however, a request to incorporate a seat back "breakover" feature to alleviate head impact injuries is now in effect. Seat manufacturers have also applied energy-absorption techniques to seat back structures to some extent in an attempt to alleviate the problem of extremity impacts. Energy-absorbing devices in the seat frame have also been

offered by some seat manufacturers in an effort to insure seat retention against deceleration values which exceed the 9G static strength requirement; however, the true potential of such systems has not been fully explored.

There seems to be little doubt that aircraft accidents will continue to occur, regardless of the efforts expended to prevent them. If this premise is accepted, then the only remaining method of reducing the fatality and injury rate will be an improved rate of survival in severe crashes.

With this premise in mind, the Aviation Crash Injury Steering Committee* of the Cornell-Guggenheim Aviation Safety Center first met in late 1961 to discuss the best approach for improved crash survival in aircraft accidents. In this meeting, and in several subsequent meetings in 1962, an overall approach to the crash injury problem was outlined. The Committee recommended that a literature search and retrieval system be set up on the subject of Impact Acceleration Technology. This work was accomplished by the Aviation Safety Engineering and Research Division of the Flight Safety Foundation in the latter part of 1962 and 1963.

Upon completion of the literature survey, the Steering Committee met again in 1964 to specify in more detail the tasks which should be conducted in the crash injury field. The Committee divided the tasks into four broad areas as listed:

1. An investigation of crash-induced floor accelerations.

2. An investigation of the dynamic response of seat-passenger systems to crash-induced floor accelerations through a computer analysis of the problem.

3. An investigation of seat strength and load-deformation characteristics.

4. An investigation of conceptual seat-system designs.

The above outline was used as a basis for work which was to be accomplished over a 2-year period beginning in October 1964.

---

*This Committee is composed of representatives from the following agencies: United States Air Force, United States Navy, United States Army, Civil Aeronautics Board, Federal Aviation Agency, Air Force Institute of Pathology, National Aeronautics and Space Administration, and Aircraft Industries Association/Air Transport Association.

On the basis of the above outline, a study was jointly funded by the National Aeronautics and Space Administration, the United States Air Force, the United States Navy, and the United States Army. Mr. I. Irving Pinkel, Chief of the Fluid Systems Components Division of NASA, was selected for the technical monitorship of the project. Mr. John H. Enders of the Office of Aeronautics, NASA, also contributed advice and counseling on the project. The U. S. Army Aviation Materiel Laboratories (USAAVLABS) was selected to negotiate and administer a contract to accomplish the study. The contract was given by USAAVLABS to the Flight Safety Foundation and Arizona State University. This report summarizes the 2-year effort on the last three tasks outlined. Another report is being prepared by AvSER describing the probable crash-induced floor accelerations for transport aircraft.*

A Phase I report[1] was prepared in September 1965 covering the first year's effort. This report has not been published, but is available on a loan basis from Arizona State University. Further details of the computer program and of the preliminary studies of the load-deformation characteristics of seats are presented in the Phase I report. These studies led to the load-limiter design concept discussed in Chapters 2 and 3 of this report.

*USAAVLABS Technical Report 67-16, "Floor Accelerations and Passenger Injuries in Aircraft Accidents".

CHAPTER 1

THE COMPUTER SIMULATOR

INTRODUCTION

During the first year's effort (1964-65), the objectives of this study included the following:

1. Develop an accurate mathematical model of the seat-passenger system.
2. Derive the differential equations of motion.
3. Develop a computer program for solving these equations numerically for various crash pulses.
4. Perform calculations to ascertain the effect of varying those parameters which affect the response of the seat-passenger system.

It is, of course, clear that the accuracy of the results depends in part upon the completeness of the mathematical model established in item 1. An overly simplified mathematical model will yield results of questionable value, while an overly complex model becomes cumbersome, leading to difficulty in the avoidance of human errors in controlling the input variables. For these reasons, a mathematical model was chosen which appeared to represent the practical limit of complexity. This mathematical model is shown in Figure 1. It is a two-dimensional one in which all

motion is assumed to take place in a vertical plane of symmetry.

The computer program was checked out only a short time before the completion of the first year's effort; therefore, very few calculations could be performed under item 4.

The extension of the project into the period 1965-66 permitted the addition of the following objectives:

5. Check the method of analysis against a dynamic test using dummy occupants in a typical aircraft seat.
6. Perform calculations to establish the effectiveness of using a "load limiter" on the seat in the longitudinal direction.
7. Develop a subroutine which will represent a real seat as accurately as possible and from which reliable values can be obtained for the reaction components.
8. Simplify and reorganize the overall computer program so as to make it as efficient and readable as possible.
9. Develop a program that would reduce computer time by using a smaller time increment for the seat than for the passenger.
10. Perform additional design calculations as needed for the design of improved seats.

All but one of these objectives were reached; item 9 had to be given up because the program became too complex.

Item 7 turned out to be by far the most important, and also the most time-consuming, part of the project and was not completed until near the end of the contract period. The first useful seat routine which was developed incorporated a longitudinal "load limiter" and permitted buckling of the front legs and plastic stretching of the rear legs of the seat. This computer routine did not, however, satisfy exactly the differential equations connecting the deformations, reactions, and accelerations of the seat. To compensate for this, the computer was programmed to automatically cut down the time increment to improve the accuracy. The result was that each calculation took about 20 minutes to perform when the originial accuracy requirement, as written into the program, was used. In order to speed things up, the accuracy requirement was relaxed so that a calculation could be performed in about 5 minutes, and for most cases this proved to be sufficiently accurate. Those calculations that were of insufficient accuracy could easily be spotted and redone with greater accuracy, since calculations were being made with various load-limiter settings at that time and since the plotting of curves readily indicated any variations. However, when calculations were performed to ascertain the effect of varying the input to the program, the original accuracy requirement was reinstated.

This made it doubly important to complete the new seat routine (item 7), and it turned out to be worth the effort because the time to complete one calculation was reduced from 20 minutes to about 4 minutes without loss of accuracy. Only a limited number of calculations presented in this report were ultimately computed using the new routine. However, it will now be used for all future work. Test runs were made with both routines to insure that the data obtained earlier were valid. Excellent agreement in the test runs was obtained.

MATHEMATICAL MODEL

In this two-dimensional analysis, the passenger and seat are considered to have a plane of symmetry, and all masses and forces are located in this plane. Schematically, then, the system is as shown in Figure 1, where the passenger has been represented by eight concentrated masses at the most important joints of the body. The seat is considered to be a rigid body except for the legs and attachment fittings. The motion of the passenger and seat is given with respect to the x, y coordinate system shown in Figure 2. This is a non-Newtonian coordinate system fixed with respect to the cabin floor, with the x axis pointing forward along the floor and the y axis perpendicular to the floor. The seat belt is assumed to be attached at point A of the seat, which lies on the y axis when the seat is undeformed. The other end of the seat belt is assumed to be attached to the large mass at the pelvis so as to form a nonlinear spring between the

two points. Similarly, the shoulder harness is assumed to act as a horizontal spring between the back of the seat and the mass at the neck and shoulders, at a distance d above the seat cushion.

Referring to Figure 2, the reaction from the floor on the seat is assumed to act at the seat belt attachment point, because this makes it unnecessary to speculate on how these forces are really transmitted to the seat until this information is obtained from the seat analysis study and test program. This results in the simplest possible subroutine for the seat.

The tension in the seat belt is given by the pair P_B; its mathematical length L_B is the distance from A to m_1, which is less than half its real length. During the crash, its mathematical length increases by an amount δ, which is a function of time; the angle θ_B between the mathematical seat belt and the horizontal is also a function of time.

The compression in the seat cushion is indicated by the pair P_C, and the friction between the passenger and the seat cushion is indicated by the force $\mu_S P_C$ on the seat and the equal and opposite force acting at m_1 and the moment $\mu_S P_C L_B \sin\theta_B$ acting on the thigh of the passenger. The moment pair M_C between the seat cushion and the thigh of the passenger is due to the fact that the pair P_C does not really go through m_1 but is located farther forward and depends on the angle θ_2.

The forces R_{x3} and R_{y3} are the reactions from the floor on the feet of the passenger, and at first these reactions cause great difficulty in the analysis. This difficulty was removed, however, by considering the flexibility of the passenger's feet.

The moment pairs $M_{2,3}$, $M_{2,4}$, $M_{4,5}$, $M_{5,6}$, $M_{5,7}$, and $M_{7,8}$ are all due to muscular action of the passenger during the crash and are considered to be of such value at the beginning of impact as to insure static equilibrium.

The point C in Figure 2 is the mass center of the seat, and it has coordinates c_1 and c_2 in a coordinate system which coincides with the seat back and seat cushion. The mass of the seat is m_s, and its moment of intertia about C is I_s.

The coordinates of point A of the seat are x_s and y_s, and the coordinates of the n^{th} mass are x_n and y_n. By expressing these latter coordinates in terms of x_s, y_s, $L_B + \delta$, and θ_2 to θ_8, a system with twelve degrees of freedom is obtained. The twelve generalized coordinates are then:

$q_1 = \theta_s$, $q_2 = x_s$, $q_3 = y_s$, $q_4 = \delta$, $q_5 = \theta_B$, $q_6 = \theta_2$, $q_7 = \theta_3$, $q_8 = \theta_4$, $q_9 = \theta_5$, $q_{10} = \theta_6$, $q_{11} = \theta_7$, $q_{12} = \theta_8$.

NUMERICAL ANALYSIS

The numerical analysis consists in first obtaining twelve differential equations of motion involving the twelve generalized coordinates and their first and second derivatives with respect to time. They will also involve

all the forces on the system, so it is assumed that separate subroutines can be written which connect these forces and the generalized coordinates.

It is also assumed that all the generalized coordinates and their first derivatives, and also all the forces, are known at a particular time, t_n. The twelve differential equations can then be solved for the second derivatives of the generalized coordinates at $t = t_n$.

Letting Δt be a sufficiently small time increment, it follows that the second derivatives are constant during this time increment as a first approximation. Letting q stand for any one of the generalized coordinates, the first approximations to q_{n+1} and $\dot{q}_{n+1}$ at $t = t_{n+1} = t + \Delta t$ are calculated from the simple formulas

$$q'_{n+1} = q_n + \dot{q}_n \Delta t + \tfrac{1}{2}\ddot{q}_n \Delta t^2 \tag{1}$$

$$\dot{q}'_{n+1} = \dot{q}_n + \ddot{q}_n \Delta t \tag{2}$$

With these values, the subroutines for obtaining the forces at t_{n+1} are then executed.

This now gives approximate values for all the generalized coordinates and their first derivatives, as well as for the forces, at t_{n+1}. With these values, the second derivatives at t_{n+1} are found and approximate values for $\ddot{q}_{n+1}$ (called $\ddot{q}'_{n+1}$) are obtained.

In order to obtain more accurate values at t_{n+1}, it is now assumed that $\ddot{q}_n$ is constant for the n^{th} time interval to obtain a second approximation for q_{n+1} and $\dot{q}_{n+1}$. Assuming that this is sufficiently accurate so that no further iterations are necessary, the equations

$$q_{n+1} = q_n + \dot{q}_n \Delta t + \frac{1}{6} (2\ddot{q}_n + \ddot{q}'_{n+1}) \Delta t^2 \tag{3}$$

$$\dot{q}_{n+1} = \dot{q}_n + \frac{1}{2}(\ddot{q}_n + \ddot{q}'_{n+1}) \Delta t \tag{4}$$

give the generalized coordinates and their first derivatives at $t = t_{n+1}$. With these values, the subroutines for finding the forces are again executed and the second derivatives at the beginning of the $n + 1^{st}$ time interval are then obtainable. This process is repeated for every small time increment, Δt, until the motion has been obtained for the entire crash period.

DIFFERENTIAL EQUATIONS OF MOTION

The x, y coordinate system is fixed in the airplane, and it is assumed that the x axis is close enough to being horizontal so that no gravity effect need be considered in this direction, but will be given its full value in the negative y direction. The acceleration components of the coordinate system and the cabin floor during a crash are given as a_x and a_y.

The method now consists of using d'Alembert's principle in a translating coordinate system, and by adding the inertia forces on each mass particle, the passenger-seat combination may be considered to be in static

equilibrium at any instant. This permits the taking of moments about the joints, thus leading to the exact number of equations to match the number of generalized coordinates.

Since the three differential equations of motion of the seat involve only three of the generalized coordinates, these equations are written first:

$$I_S\ddot{\theta}_S = (\text{dee} - c_2)P_H + c_1\left[P_B\sin(\theta_B + \theta_S) + R_y^S\cos\theta_S + R_x^S\sin\theta_S\right] -$$
$$c_2\left[\mu_S P_C + P_B\cos(\theta_B + \theta_S) + R_x^S\cos\theta_S - R_y^S\sin\theta_S\right] +$$
$$P_C\left[(L_B + \delta)\cos(\theta_B + \theta_S) - c_1\right] + M_C - R_S^M \qquad (5)$$

Considering motion of point C in the x and y directions gives

$$m_S\left[a_x + \ddot{x}_S + (c_2\cos\theta_S - c_1\sin\theta_S)\ddot{\theta}_S\right]$$
$$= (\mu_S\cos\theta_S - \sin\theta_S)P_C + P_B\cos\theta_B + P_H + R_x^S \qquad (6)$$

$$m_S\left[a_y + \ddot{y}_S - (c_1\cos\theta_S + c_2\sin\theta_S)\ddot{\theta}_S + g\right]$$
$$= P_B\sin\theta_B - P_C(\cos\theta_S + \mu_S\sin\theta_S) + R_y^S \qquad (7)$$

Applying d'Alembert's principle to the concentrated masses at the knees and feet and summing the moments about the knee joint and hip joint leads to the two equations

$$m_3L_3\left[(a_x + \ddot{x}_3)\sin\theta_3 + (a_y + g + \ddot{y}_3)\cos\theta_3\right.$$

$$= M_{2,3} + L_3(R_{y3}\cos\theta_3 + R_{x3}\sin\theta_3) \tag{8}$$

$$m_2L_2\left[(a_x + \ddot{x}_2)\sin\theta_2 + (a_y + g + \ddot{y}_2)\cos\theta_2\right] +$$

$$m_3L_2\left[(a_x + \ddot{x}_3)\sin\theta_2 + (a_y + g + \ddot{y}_3)\cos\theta_2\right] +$$

$$m_3L_3\left[(a_x + \ddot{x}_3)\sin\theta_3 + (a_y + g + \ddot{y}_3)\cos\theta_3\right]$$

$$= M_c - M_{2,4} + (R_{y3}\cos\theta_2 + R_{x3}\sin\theta_2)L_2 +$$

$$(R_{y3}\cos\theta_3 + R_{x3}\sin\theta_3)L_3 - \mu_S P_C(L_B + \delta)\sin(\theta_B + \theta_S) \tag{8a}$$

It is immediately seen that this last equation can be simplified by means of Equation 8 to yield

$$(m_2 + m_3)L_2\left[(a_x + \ddot{x}_2)\sin\theta_2 + (a_y + g + \ddot{y}_2)\cos\theta_2\right] +$$

$$m_3L_2\left[(\ddot{x}_3 - \ddot{x}_2)\sin\theta_2 + (\ddot{y}_3 - \ddot{y}_2)\cos\theta_2\right]$$

$$= M_C - M_{2,3} - M_{2,4} + L_2(R_{x3}\sin\theta_2 + R_{y3}\cos\theta_2 -$$

$$\mu_S P_C(L_B + \delta)\sin(\theta_B + \theta_S) \tag{9}$$

The neck is now treated as if it had a single hinge at its base and a concentrated mass, representing the head, at its top. Thus,

$$m_6L_6\left[(a_x + \ddot{x}_6)\cos\theta_6 - (a_y + g + \ddot{y}_6)\sin\theta_6\right] = -M_{5,6} \tag{10}$$

Treating the arms similarly to the legs yields the two equations

$$m_8L_8\left[(a_x + \ddot{x}_8)\cos\theta_8 + (a_y + g + \ddot{y}_8)\sin\theta_8\right] = -M_{7,8} \tag{11}$$

$$\begin{aligned} &m_7L_7\left[(a_x + \ddot{x}_7)\cos\theta_7 + (a_y + g + \ddot{y}_7)\sin\theta_7\right] + \\ &m_8L_7\left[(a_x + \ddot{x}_8)\cos\theta_7 + (a_y + g + \ddot{y}_8)\sin\theta_7\right] + \\ &m_8L_8\left[(a_x + \ddot{x}_8)\cos\theta_8 + (a_y + g + \ddot{y}_8)\sin\theta_8\right] = -M_{5,7} \end{aligned} \tag{11a}$$

By means of Equation 11, the last equation can be simplified to

$$\begin{aligned} &(m_7 + m_8)L_7\left[(a_x + \ddot{x}_7)\cos\theta_7 + (a_y + g + \ddot{y}_7)\sin\theta_7\right] + \\ &m_8L_7\left[(\ddot{x}_8 - \ddot{x}_7)\cos\theta_7 + (\ddot{y}_8 - \ddot{y}_7)\sin\theta_7\right] = M_{7,8} - M_{5,7} \end{aligned} \tag{12}$$

Mass m_4 is supposed to be concentrated at the base of the chest, and for simplicity it is assumed that there also is a hinge at this point. Taking moments about this hinge then gives the equation

$$\begin{aligned} &m_6L_6\left[(a_x + \ddot{x}_6)\cos\theta_6 - (a_y + g + \ddot{y}_6)\sin\theta_6\right] - \\ &m_8L_8\left[(a_x + \ddot{x}_8)\cos\theta_8 + (a_y + g + \ddot{y}_8)\sin\theta_8\right] - \\ &(m_7 + m_8)L_7\left[(a_x + \ddot{x}_7)\cos\theta_7 + (a_y + g + y_7)\sin\theta_7\right] - \\ &m_8L_7\left[(x_8 - x_7)\cos\theta_7 + (y_8 - y_7)\sin\theta_7\right] + \\ &(m_5 + m_6 + m_7 + m_8)L_5\left[(a_x + \ddot{x}_5)\cos\theta_5 - (a_y + g + \ddot{y}_5)\sin\theta_5\right] + \end{aligned}$$

$$m_6L_5\Big[(\ddot{x}_6 - \ddot{x}_5)\cos\theta_5 - (\ddot{y}_6 - \ddot{y}_5)\sin\theta_5\Big] +$$

$$(m_7 + m_8)L_5\Big[(\ddot{x}_7 - \ddot{x}_5)\cos\theta_5 - (\ddot{y}_7 - \ddot{y}_5)\sin\theta_5\Big] +$$

$$m_8L_5\Big[(\ddot{x}_8 - \ddot{x}_7)\cos\theta_5 - (\ddot{y}_8 - \ddot{y}_7)\sin\theta_5\Big] = -P_HL_5\cos\theta_5 - M_{4,5}$$

By means of Equations 10, 11, and 12, this can be simplified to

$$(m_5 + m_6 + m_7 + m_8)L_5\Big[(a_x + \ddot{x}_5)\cos\theta_5 - (a_y + g + \ddot{y}_5)\sin\theta_5\Big] +$$

$$m_6L_5\Big[(\ddot{x}_6 - \ddot{x}_5)\cos\theta_5 - (\ddot{y}_6 - \ddot{y}_5)\sin\theta_5\Big] +$$

$$(m_7 + m_8)L_5\Big[(\ddot{x}_7 - \ddot{x}_5)\cos\theta_5 - (\ddot{y}_7 - \ddot{y}_5)\sin\theta_5\Big] +$$

$$m_8L_5\Big[(\ddot{x}_8 - \ddot{x}_y)\cos\theta_5 - (\ddot{y}_8 - \ddot{y}_7)\sin\theta_5\Big]$$

$$= M_{5,6} - M_{5,7} - M_{4,5} - P_HL_5\cos\theta_5 \qquad (13)$$

The final moment equation is taken about the hip joint, where mass m_1 is concentrated. This gives

$$m_6L_6\Big[(a_x + \ddot{x}_6)\cos\theta_6 - (a_y + g + \ddot{y}_6)\sin\theta_6\Big] -$$

$$m_8L_8\Big[(a_x + \ddot{x}_8)\cos\theta_8 + (a_y + g + \ddot{y}_8)\sin\theta_8\Big] -$$

$$(m_7 + m_8)L_7\Big[(a_x + \ddot{x}_7)\cos\theta_7 + (a_y + g + \ddot{y}_7)\sin\theta_7\Big] -$$

$$m_8L_7\Big[(\ddot{x}_8 - \ddot{x}_7)\cos\theta_7 + (\ddot{y}_8 - \ddot{y}_7)\sin\theta_7\Big] +$$

$$(m_5 + m_6 + m_7 + m_8)L_5\Big[(a_x + \ddot{x}_5)\cos\theta_5 - (a_y + g + \ddot{y}_5)\sin\theta_5\Big] +$$

$$m_6L_5\Big[(\ddot{x}_6 - \ddot{x}_5)\cos\theta_5 - (\ddot{y}_6 - \ddot{y}_5)\sin\theta_5\Big] +$$

$$(m_7 + m_8)L_5\left[(\ddot{x}_7 - \ddot{x}_5)\cos\theta_5 - (\ddot{y}_7 - \ddot{y}_5)\sin\theta_5\right] +$$

$$m_8L_5\left[(\ddot{x}_8 - \ddot{x}_7)\cos\theta_5 - (\ddot{y}_8 - \ddot{y}_7)\sin\theta_5\right] +$$

$$(m_4 + m_5 + m_6 + m_7 + m_8)L_4\left[(a_x + \ddot{x}_4)\cos\theta_4 - (a_y + g + \ddot{y}_4)\sin\theta_4\right] +$$

$$(m_5 + m_6 + m_7 + m_8)L_4\left[(\ddot{x}_5 - \ddot{x}_4)\cos\theta_4 - (\ddot{y}_5 - \ddot{y}_4)\sin\theta_4\right] +$$

$$m_6L_4\left[(\ddot{x}_6 - \ddot{x}_5)\cos\theta_4 - (\ddot{y}_6 - \ddot{y}_5)\sin\theta_4\right] +$$

$$(m_7 + m_8)L_4\left[(\ddot{x}_7 - \ddot{x}_5)\cos\theta_4 - (\ddot{y}_7 - \ddot{y}_5)\sin\theta_4\right] +$$

$$m_8L_4\left[(\ddot{x}_8 - \ddot{x}_7)\cos\theta_4 - (\ddot{y}_8 - \ddot{y}_7)\sin\theta_4\right]$$

$$= -P_H(L_4\cos\theta_4 + L_5\cos\theta_5) - M_{2,4}$$

By means of Equations 10, 11, 12, and 13, this can be simplified to

$$(m_4 + m_5 + m_6 + m_7 + m_8)L_4\left[(a_x + \ddot{x}_4)\cos\theta_4 - (a_y + g + \ddot{y}_4)\sin\theta_4\right] +$$

$$(m_5 + m_6 + m_7 + m_8)L_4\left[(\ddot{x}_5 - \ddot{x}_4)\cos\theta_4 - (\ddot{y}_5 - \ddot{y}_4)\sin\theta_4\right] +$$

$$m_6L_4\left[(\ddot{x}_6 - \ddot{x}_5)\cos\theta_4 - (\ddot{y}_6 - \ddot{y}_5)\sin\theta_4\right] +$$

$$(m_7 + m_8)L_4\left[(\ddot{x}_7 - \ddot{x}_5)\cos\theta_4 - (\ddot{y}_7 - \ddot{y}_5)\sin\theta_4\right] +$$

$$m_8L_4\left[(\ddot{x}_8 - \ddot{x}_7)\cos\theta_4 - (\ddot{y}_8 - \ddot{y}_7)\sin\theta_4\right]$$

$$= M_{4,5} - M_{2,4} - P_HL_4\cos\theta_4 \qquad (14)$$

The last two equations are obtained by summing all the forces on the passenger (including inertia forces) in the x and y directions. This leads to

$$(m_1 + m_2 + m_3 + m_4 + m_5 + m_6 + m_7 + m_8)(a_x + \ddot{x}_1) +$$
$$(m_2 + m_3)(\ddot{x}_2 - \ddot{x}_1) + m_3(\ddot{x}_3 - \ddot{x}_2) + (m_4 + m_5 + m_6 +$$
$$m_7 + m_8)(\ddot{x}_4 - \ddot{x}_1) + (m_5 + m_6 + m_7 + m_8)(\ddot{x}_5 - \ddot{x}_4) +$$
$$m_6(\ddot{x}_6 - \ddot{x}_5) + (m_7 + m_8)(\ddot{x}_7 - \ddot{x}_5) + m_8(\ddot{x}_8 - \ddot{x}_7)$$
$$= R_{x3} + P_C(\sin\theta_S - \mu_S\cos\theta_S) - P_B\cos\theta_B - P_H \tag{15}$$

$$(m_1 + m_2 + m_3 + m_4 + m_5 + m_6 + m_7 + m_8)(a_y + g + \ddot{y}_1) +$$
$$(m_2 + m_3)(\ddot{y}_2 - \ddot{y}_1) + m_3(\ddot{y}_3 - \ddot{y}_2) + (m_4 + m_5 + m_6 +$$
$$m_7 + m_8)(\ddot{y}_4 - \ddot{y}_1) + (m_5 + m_6 + m_7 + m_8)(\ddot{y}_5 - \ddot{y}_4) +$$
$$m_6(\ddot{y}_6 - \ddot{y}_5) + (m_7 + m_8)(\ddot{y}_7 - \ddot{y}_5) + m_8(\ddot{y}_8 - \ddot{y}_7)$$
$$= R_{y3} + P_C(\cos\theta_S + \mu_S\sin\theta_S) - P_B\sin\theta_B \tag{16}$$

Since θ_S, x_S, and y_S already are generalized coordinates of the system, Equations 5, 6, and 7 can be solved directly for $\ddot{\theta}_S$, $\ddot{x}_S$, and $\ddot{y}_S$. In the rest of the equations, the x's and y's and their derivatives must first be replaced by generalized coordinates and the resulting equations solved simultaneously for their second derivatives. This very lengthy process has been previously described in detail[1]. Here it is sufficient to note that all of the above equations contain the x and y components of acceleration of the aircraft itself, as well as the reactions and internal

forces of the system. Each of these reactions and internal forces is found by a subroutine of the computer program. A simplified flow chart for the main program is shown in Appendix I. The acceleration of the aircraft is found by a series of subroutines which cover a wide range of pulse shapes.

SUBROUTINES FOR CALCULATING ACCELERATIONS

There are seven aircraft acceleration subroutines which are incorporated in the FORTRAN program and can be called into action by specifying the proper value of the code number LL in the input data. Only the acceleration in the x direction is calculated directly in each case, and the acceleration in the y direction is then given as

$$a_y = -Qa_x \tag{17}$$

where Q is a constant which is specified in the input data as QUO. The severity of the crash is indicated by the reduction in velocity of the aircraft during the time considered, which is indicated by Δv. Following the primary pulse, the acceleration is always considered to be zero. Figure 3 shows the pulse shapes and the data that must be specified for each pulse.

SUBROUTINE FOR CALCULATING FORCES

Seat Belt and Shoulder Harness

The actual stretching of the seat belt is given by the quantity DSB = $\delta - S_B$, where S_B is the initial slack in the belt. The force in the seat belt is then represented by the formula

$$P_B = k_{B1}(DSB) + k_{B2}(DSB)^2 + k_{B3}(DSB)^3 + k_{B4}(DSB)^4 + k_{B5}\dot{\delta} \qquad (18)$$

when $\delta > S_B$; when $\delta \leq S_B$, we have $P_B = 0$. This formula must consider the difference between the mathematical belt and the real belt and also take into account the compressibility of the passenger's abdomen. For a 3-inch Navy Dacron seat belt for which information is available, the coefficients are $k_{B1} = 200$, $k_{B2} = -206$, $k_{B3} = 84$, and $k_{B4} = 12$. The static load versus elongation characteristics of this belt are shown in Figure 4. The coefficient k_{B5} expresses the nonelastic part of the force, and it was arbitrarily set equal to 50.

The actual stretching of the shoulder harness is given by the quantity $XXSH = X_5 - X_{05} - S_H$, where X_{05} is the initial X coordinate of the passenger's shoulder and S_H is the initial slack in the harness. The force P_H is zero when $X_5 - X_{05} \leq S_H$, and when $X_5 - X_{05} > S_H$ it is given as

$$P_H = k_{H1}(XXSH) + k_{H2}(XXSH)^2 + k_{H3}\dot{X}_5 \qquad (19)$$

For the few calculations for which the shoulder harness was considered, values of the constants were arbitrarily selected to be $k_{H1} = 200$, $k_{H2} = 100$, and $k_{H3} = 5$.

Seat Cushion

If P_{OC} is the initial value of P_C, then further values of P_C are given by

$$P_C = P_{OC} + k_{C1}\left[L_B \sin\theta_{OB} - (L_B + \delta)\sin(\theta_B + \theta_S)\right] +$$
$$k_{C2}\left[L_B \sin\theta_{OB} - (L_B + \delta)\sin(\theta_B + \theta_S)\right]^3 +$$

$$k_{C3}\left[\dot{\delta}\sin(\theta_B + \theta_S) + (L_B + \delta)(\dot{\theta}_B + \dot{\theta}_S)\cos(\theta_B + \theta_S)\right] \quad (20)$$

where θ_{OB} is the initial value of θ_B. The value of M_C may then be written as

$$M_C = KP_C(\theta_2 + \alpha) \quad (21)$$

where K is estimated or obtained from actual tests and α is calculated from the initial conditions. The values used for the coefficients were $k_{C1} = 300$, $k_{C2} = 100$, $k_{C3} = -50$, and $K = 25$.

The friction force between the passenger and the seat is given by $\mu_S P_C$, where μ_S is the coefficient of friction. In order to have the friction force in the correct direction at all times, and also to effect a smooth transition when the velocity changes sign, μ_S is expressed as

$$\mu_S = \dot{x}_1 - \dot{x}_S \quad (22)$$

as long as $\dot{x}_1 - \dot{x}_S \leq \mu$, and

$$\mu_S = \mu \frac{\dot{x}_1 - \dot{x}_S}{|\dot{x}_1 - \dot{x}_S|} \quad (23)$$

when $|\dot{x}_1 - \dot{x}_S| > \mu$, where μ is the maximum value of the coefficient of friction.

Reaction From Floor on Passenger's Feet

As long as the feet are in contact with the floor, the vertical component of reaction is given by

$$R_{y3} = R_{y3}^{(0)} - 10{,}000y_3 - 1{,}000\dot{y}_3 \quad (24)$$

and whenever $R_{y3} \leq 0$, then $R_{y3} = 0$ and $R_{x3} = 0$.

Similarly,

$$R_{x3} = R_{x3}^{(0)} - 10{,}000(x_3 - x_{03}) - 1{,}000\dot{x}_3 \qquad (25)$$

when $R_{y3} > 0$ and $|R_{x3}| \leq \mu_F R_{y3}$; but as soon as $|R_{x3}| > \mu_F R_{y3}$, then R_{x3} is given by

$$R_{x3} = -\mu_F R_{y3} \qquad (26)$$

where μ_F is the coefficient of friction between the floor and the feet.

The consideration of a rigid floor and static friction on the passenger's feet greatly complicated the problem at first; but with the introduction of Equations 24 and 25, these complications were completely overcome. Equations 24 and 25 merely state that the combination of the floor and the passenger's feet is equally flexible in the horizontal and vertical directions and that the motion is damped. Damping is introduced wherever possible because it has the quality of smoothing out the motion and thereby increasing the accuracy of the calculations. The constants 10, 000 and 1, 000 in Equations 24 and 25 are wholly arbitrary and are chosen large enough so that only a negligibly small negative vertical deflection of the feet is permitted.

In order to effect a smooth transition from the static to the dynamic condition, let

$$\mu_F = \dot{x}_3 \qquad (27)$$

until $|\dot{x}_3|$ becomes greater than the estimated coefficient of friction, μ_1.

After that,

$$\mu_F = \mu_1 \frac{\dot{x}_3}{|\dot{x}_3|} \tag{28}$$

Moment Pairs due to Muscular Tension

Since the distortion of a human body is limited by tension in muscles and ligaments, such restrictions must be introduced into the analysis in order for it to be realistic. The following equations have proved to be effective in accomplishing this:

(29a)

If $tem_1 = 0.2 + \theta_2 - \theta_3$,

and $(tem_1 \leq 0)$, then $\quad M'_{2,3} = a_{2,3} \dfrac{\dot{\theta}_3 - \dot{\theta}_2}{|\dot{\theta}_3 - \dot{\theta}_2| + 0.1}$

If $(tem_1 > 0)$, then $\quad M''_{2,3} = M'_{2,3} + b_{2,3} tem_1 (\dot{\theta}_3 - \dot{\theta}_2 - 10)$

(29b)

If $tem_2 = \theta_4 - \theta_2 - 1.1$,

and $(tem_2 \leq 0)$, then $\quad M'_{2,4} = a_{2,4} \dfrac{\dot{\theta}_4 - \dot{\theta}_2}{|\dot{\theta}_4 - \dot{\theta}_2| + 0.1}$

If $(tem_2 > 0)$, then $\quad M''_{2,4} = M'_{2,4} + b_{2,4} tem_2 (\dot{\theta}_4 - \dot{\theta}_2 + 10)$

(29c)

When $(\theta_4 + 0.3 \geq \theta_5 > \theta_4)$, then $\quad M'_{4,5} = a_{4,5} \dfrac{\dot{\theta}_5 - \dot{\theta}_4}{|\dot{\theta}_5 - \dot{\theta}_4| + 0.1} + M^{(0)}_{4,5}$

Let $tem_3 = \theta_5 - \theta_4 - 0.3$.

If $(\theta_5 > \theta_4 + 0.3)$, then $\quad M''_{4,5} = M'_{4,5} + b_{4,5} tem_3 \left(\dot{\theta}_5 - \dot{\theta}_4 + 10 \dfrac{\theta_5 \quad \theta_4}{|\theta_5 \quad \theta_4|} \right)$

If $(\theta_5 \leq \theta_4)$, then $\quad M_{4,5} = b_{4,5} \left[\dot{\theta}_5 - \dot{\theta}_4 + 10(\theta_5 - \theta_4) \right] + M^{(0)}_{4,5}$

When $(\theta_5 + 1.2 \geq \theta_6 > \theta_5)$, then $M'_{5,6} = a_{5,6} \dfrac{\dot{\theta}_6 - \dot{\theta}_5}{\left|\dot{\theta}_6 - \dot{\theta}_5\right| + 0.1} + M^{(0)}_{5,6}$

Let $tem_4 = \theta_6 - \theta_5 - 1.2$.

If $(\theta_6 > \theta_5 + 1.2)$, then $M''_{5,6} = M'_{5,6} + b_{5,6} tem_4 (\dot{\theta}_6 - \dot{\theta}_5 + 10)$ (29d)

If $(\theta_6 \leq \theta_5)$, then $M_{5,6} = b_{5,6}\left[\theta_6 - \theta_5 + 10(\theta_6 - \theta_5)\right] + M^{(0)}_{5,6}$

If $tem_5 = \theta_5 + \theta_7 - 3.2$,

and $(tem_5 \leq 0)$, then $M'_{5,7} = a_{5,7} \dfrac{\dot{\theta}_5 + \dot{\theta}_7}{\left|\dot{\theta}_5 - \dot{\theta}_7\right| + 0.1} + M^{(0)}_{5,7}$ (29e)

If $(tem_5 > 0)$, then $M''_{5,7} = M'_{5,7} + b_{5,7} tem_5 (1 + \dot{\theta}_5 + \dot{\theta}_7)$

If $tem_6 = 0.2 + \theta_7 - \theta_8$,

and $(tem_6 \leq 0)$, then $M'_{7,8} = a_{7,8} \dfrac{\dot{\theta}_8 - \dot{\theta}_7}{\left|\dot{\theta}_8 - \dot{\theta}_7\right| + 0.1} + M^{(0)}_{7,8}$ (29f)

If $(tem_6 > 0)$, then $M''_{7,8} = M'_{7,8} + b_{7,8} tem_6 (\dot{\theta}_8 - \dot{\theta}_7 - 1)$

In these equations the terms with super zero are the initial values required for static equilibrium, and the primed and double primed expressions are applicable under the conditions indicated at the left.

Subroutine for the Seat

The subroutine for the seat was by far the most difficult one, and hence the last to be perfected.

Figure 5 shows the three reactions R_x^S, R_y^S, and R_S^M, all acting at the seat belt attachment point, as they are incorporated in the original program. Figure 6 shows the real reactions R_x^S, R_y^F, and R_y^R, all acting at the cabin floor on the legs of the seat. The relation between the two sets of reactions is evidently

$$R_y^S = R_y^F + R_y^R \tag{30}$$

$$R_S^M = R_x^S\, y_S + R_y^F d - R_y^R e \tag{31}$$

If R_y^F is known, then

$$R_y^R = R_y^S - R_y^F \tag{32}$$

$$R_S^M = R_x^S\, y_S + R_y^F (d + e) - R_y^S e \tag{33}$$

and if R_y^R is known, then

$$R_y^F = R_y^S - R_y^R \tag{34}$$

$$R_S^M = R_x^S\, y_S + R_y^S d - R_y^R (d + e) \tag{35}$$

From Equations 33 and 35, it follows that

$$R_y^F = \frac{R_S^M + R_y^S e - R_x^S\, y_S}{d + e} \tag{36}$$

$$R_y^R = \frac{R_x^S\, y_S + R_y^S d - R_S^M}{d + e} \tag{37}$$

The seat routine now revolves around Equations 5, 6, and 7, which are the differential equations of motion for the seat. In order to simplify the equations, the quantities z_1 through z_8 are introduced, where

$$z_1 = (\text{dee} - c_2)P_H + M_C + P_C(L_B + \delta)\cos(\theta_B + \theta_S) + c_1\left[P_B\sin(\theta_B + \theta_S) - P_C\right] - c_2\left[\mu_S P_C + P_B\cos(\theta_B + \theta_S)\right]$$

$$z_2 = c_1\sin\theta_S - c_2\cos\theta_S$$

$$z_3 = \frac{1}{m_S}\left[P_B\cos\theta_B + P_H + P_C(\mu_S\cos\theta_S - \sin\theta_S)\right] - a_x$$

$$z_4 = c_1\cos\theta_S + c_2\sin\theta_S$$

$$z_5 = \frac{1}{m_S}\left[P_B\sin\theta_B - P_C(\cos\theta_S + \mu_S\sin\theta_S)\right] - g - a_y$$

$$z_6 = I_S - m_S z_8 z_2 \qquad z_7 = \frac{I_S}{m_S} + z_4(z_4 + e)$$

$$z_8 = y_S - z_2 \qquad z_9 = d + e$$

$$z_{10} = z_4 - d \qquad z_{11} = z_4 + e$$

Equations 5, 6, and 7 can now be solved for the second derivatives to yield

$$\ddot{\theta}_S = \frac{1}{I_S}(z_1 - R_S^M + R_y^S z_4 + R_x^S z_2) \tag{38}$$

$$\ddot{x}_S = z_2\ddot{\theta}_S + z_3 + \frac{R_x^S}{m_S} \tag{39}$$

$$\ddot{y}_S = z_4\ddot{\theta}_S + z_5 + \frac{R_y^S}{m_S} \tag{40}$$

They can also be solved for the reaction components to yield

$$R_S^M = z_1 + R_y^S z_4 + R_x^S z_2 - I_S\ddot{\theta}_S \tag{41}$$

$$R_x^S = m_S(\ddot{x}_S - z_2\ddot{\theta}_S - z_3) \tag{42}$$

$$R_y^S = m_S(\ddot{y}_S - z_4\ddot{\theta}_S - z_5) \tag{43}$$

It is seen that the six variable quantities involved are $\ddot{\theta}_S$, $\ddot{x}_S$, $\ddot{y}_S$, R_S^M, R_x^S, and R_y^S. In addition, Equations 30 to 37 also introduce the quantities R_y^F and R_y^R. During the development of the program, any three of these quantities are obtained from either the relationships between force and deformation or the requirement that $\dot{x}_S$, $\dot{y}_S$, and $\dot{y}_S'$ must never become negative. This last requirement is tantamount to requiring that the seat not be permitted to vibrate during the crash, and it is the key to the success of the subroutine; without it, computer time was increased by an order of magnitude. In many cases the calculations could not be performed at all because the small time increments required created excessive scatter in the calculated values.

The following special equations were developed for the seat routine:

Given R_x^S, R_y^R, and $\ddot{\theta}_S$

First $\ddot{x}_S$ is obtained from Equation 39. Next R_S^M is obtained in terms of R_y^S from Equation 35. Substituting this into Equation 38 gives R_y^S:

$$R_y^S = \frac{I_S\ddot{\theta}_S - z_1 + R_x^S z_8 - R_y^R z_9}{z_{10}} \tag{44}$$

Then, $\ddot{y}_S$ may be obtained from Equation 40 and R_y^F from Equation 34.

Given R_x^S, $\ddot{y}_S$, and R_y^F

In this case R_S^M is found from Equation 33 and substituted into Equation 38. This equation may then be solved for $\ddot{\theta}_S$ in terms of R_y^S, and the resulting expression may be substituted into Equation 40, which then may be solved for R_y^S in terms of known quantities only. The resulting equation is

$$R_y^S = \frac{I_S(\ddot{y}_S - z_5) - z_4\left[z_1 - R_x^S z_8 - R_y^F z_9\right]}{z_7} \tag{45}$$

The value of R_y^R is then obtained from Equation 32, R_S^M from Equation 31, $\ddot{\theta}_S$ from Equation 38, and $\ddot{x}_S$ from Equation 39.

Given $\ddot{x}_S$, $\ddot{y}_S$, and R_y^F

In this case R_x^S is found in terms of $\ddot{\theta}_S$ from Equation 42, and R_S^M in terms of R_y^S from Equation 33. These expressions may then be substituted in Equation 38 to give

$$\ddot{\theta}_S = \frac{\left[z_1 - R_y^F z_9 + m_S z_8(z_3 - \ddot{x}_S) + R_y^S z_{11}\right]}{z_6} \tag{46}$$

This value of $\ddot{\theta}_S$ may now be substituted into Equation 40, which then may be solved for R_y^S to give

$$R_y^S = \frac{\ddot{y}_S - z_5 - \frac{z_4}{z_6}\left[z_1 - R_y^F z_9 + m_S z_8 (z_3 - \ddot{x}_S)\right]}{\frac{z_4}{z_6} z_{11} + \frac{1}{m_S}} \tag{47}$$

$\ddot{\theta}_S$ can now be found from Equation 46, R_x^S from Equation 42, and R_y^R from Equation 32, which completes the determination of all desired quantities.

<u>Given $\ddot{x}_S$, R_y^F, and R_y^R</u>

In this case R_x^S is found in terms of $\ddot{\theta}_S$ from Equation 42, R_y^S from Equation 30, and R_S^M from Equation 31. These expressions may then be substituted into Equation 38 to yield

$$\ddot{\theta}_S = \frac{\left[z_1 + R_y^F z_{10} + R_y^R z_{11} - z_8 m_S (\ddot{x}_S - z_3)\right]}{z_6} \tag{48}$$

The value of $\ddot{y}_S$ is now found from Equation 40, and R_x^S from Equation 42, which completes the determination of all desired quantities.

The procedure now is as follows: As long as $\dot{x}_S$, $\dot{y}_S$, and $\dot{y}_S''$ are all positive, the reactions are calculated from the displacements as indicated by Figures 7 and 8.

For the horizontal reaction,

$$R_x^S = - k_{x1} x_S - k_{x2} \dot{x}_S \tag{49}$$

until the absolute value of the reaction reaches the load-limiter value R_A; after that, $R_x^S = -R_A$. This is illustrated in Figure 7. The coefficient $k_{x1} = R_A/x_{SE}$, where x_{SE} is the elastic deflection of the seat in the x direction and k_{x2} is a damping coefficient.

For the front legs, the force-displacement pattern of Figure 6 also holds, and here R_B is the buckling load, y''_{SE} the elastic shortening of the leg, and y''_{SC} the amount of shortening corresponding to complete collapse of the leg. This latter value is arbitrarily set equal to 5 inches; and when y''_S reaches y''_{SC}, the computer prints "Seat Failed" and the calculations stop. Thus,

$$R_y^F = k_y^F + k_{y1}^F y''_S + k_{y2}^F \dot{y}''_S \tag{50}$$

until the buckling load is reached; after that, $R_y^F = R_B$. The coefficient k_y^F is obtained from statics, $k_{y1}^F = R_B/y''_{SE}$, and k_{y2}^F is a damping coefficient.

For the rear legs, the force-displacement pattern is assumed to be as shown in Figure 8, where y'_{SE} is the limit of elastic deflection and R_E is the corresponding value of the reaction. For simplicity, both the front and rear legs are considered to be vertical in the calculations. Thus, for the elastic part of the curve,

$$R_y^R = k_y^R - k_{y1}^R y'_S - k_{y2}^R \dot{y}'_S \tag{51}$$

as long as $y'_S \leq y'_{SE}$; after that,

$$R_y^R = -R_E - k_{y2}^R \dot{y}_S - k_{y3}^R (y'_S - y'_{SE}) \tag{52}$$

for the plastic part of the curve.

Whenever any one of the quantities $\dot{x}_S$, $\dot{y}_S$, or $\dot{y}''_S$ becomes so small that it would become negative during the next time interval, its derivative is given such a value that if it were constant the quantity in question would become zero at the end of the time interval. In this way only small negative values are permitted for the quantities $\dot{x}_S$, $\dot{y}_S$, and $\dot{y}''_S$. When any one of the quantities $\ddot{x}_S$, $\ddot{y}_S$, or $\ddot{y}''_S$ is given in this way, a different set of equations is used to obtain the reactions, but in all cases the differential equations of equilibrium are satisfied, and the required equations are always available among Equations 30 through 50. Appendix II gives a detailed flow chart for this seat routine.

INITIAL VALUES

The initial values of the muscle forces are obtained by putting all accelerations equal to zero in the moment equations so as to obtain static equilibrium, except that in Equation 8 the value for $M_{2,3}^{(0)}$ is arbitrarily given by

$$M_{2,3}^{(0)} = 0 \tag{53}$$

From Equations 10, 11, and 12, then

$$M_{5,6}^{(0)} = m_6 L_6 \; g \; \sin\theta_{06} \tag{54}$$

$$M_{7,8}^{(0)} = m_8 L_8 \; g \; \sin\theta_{08} \tag{55}$$

$$M_{5,7}^{(0)} = M_{7,8}^{(0)} - m_{7,8} L_7 \; g \; \sin\theta_{07} \tag{56}$$

Similarly, from Equation 13,

$$M_{4,5}^{(0)} = M_{5,6}^{(0)} - M_{5,7}^{(0)} + m_{5,8} L_5 \; g \; \sin\theta_{05} \tag{57}$$

If the passenger's feet are on the floor before the crash, then

$$X = \sin\theta_{03} = \frac{y_{OS} + L_B \sin\theta_{OB} - L_2 \sin\theta_{02}}{L_3} \tag{58}$$

A value of $X \geq 1$ means that the feet do not reach the floor, and the following values are appropriate:

$$\theta_{03} = \frac{\pi}{2} \qquad\qquad R_{x3}^{(0)} = R_{y3}^{(0)} = 0 \tag{59}$$

If $X \leq 0$, then

$$\theta_{03} = \sin^{-1} X \tag{60}$$

and $R_{x3}^{(0)}$ and $R_{y3}^{(0)}$ are arbitrarily given the values

$$R_{x3}^{(0)} = 0 \tag{61}$$

$$R_{y3}^{(0)} = 0 \tag{62}$$

Also, the initial values of the friction coefficients are set equal to zero, or

$$\mu_{OS} = 0 \tag{63}$$

$$\mu_{OF} = 0 \tag{64}$$

For the seat cushion, it follows that

$$P_{OC} = mg - W_3 \tag{65}$$

$$M_{OC} = W_2 L_2 \cos\theta_2 \tag{66}$$

The value of α is then given as

$$\alpha = \frac{M_{OC}}{KP_{OC}} - \theta_{02}$$

This calculation is built into the program.

The initial value of $M_{2,4}$ is assumed to be zero because it will be balanced by the back of the seat as the passenger leans against it. All other initial values are calculated automatically.

COMPARISON OF CALCULATION AND EXPERIMENT

A dynamic seat test has been made using two dummies in a typical aircraft seat. The acceleration-time curve obtained in the test is indicated by the dotted curve in Figure 9. A computer calculation was then made by using the triangular acceleration-time curve shown by the solid line of Figure 9. The dashed curves in Figures 10 through 13 are taken from the test data. The corresponding calculated quantities are shown by the solid curves in the same figures. The agreement is considered to be satisfactory. In particular, the peak values are very close, which is the most im-

portant information for design purposes. Further comparisons are needed between experiment and the computer solution, however, with particular emphasis on the behavior of live subjects. The effect of muscle tension on the response of the subject may be of considerable consequence, especially at the lower levels of floor deceleration.

OTHER OUTPUT

The design section of this report (Chapter 2) presents the primary computer output developed in this study. As a matter of interest, however, Figure 14 shows the actual calculated displacements of a dummy for a particular acceleration-time curve, and Figure 15 shows the same for a dummy with shoulder harness. In each case the displacement of the dummy is extreme. This fact strongly suggests that future correlation of data on the human tolerance to decelerative loading with the computed passenger response will be needed to bring about a complete understanding of the significance of the computer input. The figures, nevertheless, indicate the capability of the method in studying the response of the system.

CHAPTER 2

A SPECTRUM OF DESIGN DATA BASED ON RESULTS FROM THE COMPUTER PROGRAM FOR DYNAMIC RESPONSE OF SEAT-PASSENGER SYSTEMS

INTRODUCTION

It requires only a brief consideration of the model of the seat-passenger system shown in Figure 2 and the nearly two hundred input and output variables listed in Table II to conclude that a complete investigation of the effects and interactions of all the variables is impractical, if not impossible. The picture becomes even more complex when one recognizes that the output variables may be strongly affected by the characteristics of the crash pulse, and that a wide variety of crash-pulse conditions can readily occur. When one further considers that other factors such as the angle of incidence of the crashing aircraft, seat belt charactertistics, passenger weight, and force-deflection characteristics of the seat all may exhibit an important influence on the resulting forces, displacements, velocities, and accelerations of the seat and the occupant, it becomes very clear that much judgement is required in making meaningful calculations.

Therefore, it is not claimed that the results and data presented in this report are comprehensive. Indeed, they are not. However, an attempt has been made to select those combinations of variables which would seem to be of the most significance from the standpoint of design interest.

By proceeding in this way, two objectives have been met: (1) a demonstration of the potential design utility of the computer program described in Chapter 1, and (2) the accumulation of a limited amount of design data for practical or typical ranges of the more important input variables and several crash pulse conditions.

While every effort has been made to select reasonable and typical values and ranges for all input variables, some of the values require further confirmation before firm design configurations can reasonably be based on the results from the computer program. Caution is therefore advised in the use of these results for final design purposes, and the designer must carefully evaluate the applicability of all input data tabulated in Table II, as well as the data on the curve of interest.

The data presented in this chapter are intended to presage the potential of the computer program in solving seat design problems under crash conditions. These data represent only a meager beginning, but certain very interesting trends can nevertheless be observed. Much significant work remains for the future.

INPUT CHARACTERISTICS AND CONCEPTS USED IN THE STUDY

DESIGN VARIABLES STUDIED

The vastness of the variable space involved in a computation of the complexity of the one described in Chapter 1 makes essential the judicious choice of output variables of primary interest. For this reason, the

following eight output variables were selected as being of utmost interest to the seat designer:

1. Seat displacement with respect to the aircraft floor in the fore-aft direction.
2. Seat belt load.
3. Pelvic displacement with respect to the seat.
4. Vertical force reaction on the front seat legs.
5. Vertical force reaction on the rear seat legs.
6. Horizontal force on the seat legs in the fore-aft direction.
7. Pelvic deceleration of the occupant in the fore-aft direction.
8. Maximum velocity of the occupant's head.

In the presentation of the data in the figures, the order of presentation is consistent in all cases with the order set in the above list.

THE LOAD-LIMITER CONCEPT

In the course of this investigation, it has been determined that the use of a load limiter is in many cases very beneficial. A load limiter is a device which has a force-deflection characteristic such that the deflection is essentially zero until the load reaches a preset magnitude and then deflects indefinitely while maintaining the preset load. Such a characteristic is shown graphically in Figure 16. When a load limiter is placed in series with a seat, for example, the force on the seat can never exceed the preset force level of the load limiter. More details regarding load-

limiter devices are presented in Chapter 3, but it should be noted that the data presented in this chapter are all based on the use of a seat in series with an ideal load limiter, i.e., one with a force-deflection characteristic as shown in Figure 16. The load-limiter setting is in every case noted either on the curve or on the common data sheet preceding the curve group.

CRASH-PULSE CHARACTERISTICS

The acceleration-time characteristic of the crash pulse is an important input to the calculation of the magnitudes of the design variables. The computer program has been written so that essentially any crash pulse can be used simply by putting a new subroutine into the calculation. Even the most complex actual crash pulse can be approximated well through use of harmonic analysis. For purposes of the current study, however, it was decided to utilize several acceleration-time patterns of relatively simple geometry but, nevertheless, with acceleration peaks and crash durations approximating "typical" aircraft crashes. Consequently, the data presented are all for pulse shapes which are triangular, sinusoidal, trapezoidal, triangular with secondary spikes, or repeated triangular acceleration-time patterns.

An array of various crash pulses conceived to facilitate the study of the selected design variables is presented in Figure 17. Not all of these pulses have thus far been utilized in the current study due to time limitations. Table III presents a series of comparisons that would be possible

if data were available for all of the pulse shapes shown in Figure 17. Several of these comparisons are presented in the data discussed later in this chapter, but some remain for future investigation.

Pulse 3 of Figure 17 is a symmetrical triangle with a 20G peak and 0.20-second duration, representing a velocity change of about 64 feet per second. This pulse has been used as a "standard" pulse, and the results from this pulse are repeatedly plotted as a basis of comparison throughout the data presented.

One further observation is appropriate here. All of the crash pulses used in generating the data presented in this report correspond to a velocity change of 64 feet per second. This includes triangles, sinusoids, trapezoids, triangles with spikes, and repeated triangles. While it is true that some of the pulses sketched in Figure 17 correspond to other velocity changes, none of these has been used to generate data for this report.

The crash-pulse acceleration-time geometry is noted on the common data sheet preceding the curve group, where an appropriate reference is given to Figure 17 for detailed pulse specifications.

ANGLE OF INCIDENCE OF CRASH

The angle of incidence of the crash is an important variable in determining the magnitude of the design variables for a given crash pulse. In the inital study reported here, the program is written so that the vertical acceleration component is at all times a fixed proportion of the horizontal

acceleration component. The vertical acceleration-time pulse is always in phase and geometrically similar to the horizontal acceleration-time pulse, and the vertical component is equal to the horizontal component mutliplied by the tangent of the angle between the resultant acceleration vector and the floor line as shown in the small sketch of the seat in the following figures. The basic pulse (referenced on the common data sheets preceding each curve group and sketched in Figure 17) is the horizontal pulse, that is, the pulse applied parallel to the floor.

PRESENTATION OF DATA

DATA GROUPING

A spectrum of data useful for preliminary design and overall comparison purposes is plotted and discussed in the following paragraphs. To make the presentation as clear as possible, the curves have been grouped into 13 sets; each set is self-contained in a separate group at the end of this report.

DESCRIPTION OF VARIABLES STUDIED

Design Variables as Functions of Time for Triangular Crash Pulses

Figure 18 through 26 display the data pertinent to this discussion. These nine curves show seat displacement, seat belt load, and pelvic deceleration as functions of time for three different load-limiter settings and five different triangular crash pulses. All pulses represent a 64-foot-per-second velocity change. The following observations may be made:

1. As load-limiter setting is decreased, the required seat displacement is increased. Approximately 10 inches of displacement is required, at worst, for the conditions investigated.
2. Generally, as the peak of the triangular pulse occurs later in the pulse (longer rise time), the required seat displacement is increased.
3. The largest seat displacements are required by the combination of a late peak in the crash pulse together with a low load-limiter setting.
4. The maximum seat belt load is virtually independent of the rise time, although the time at which it occurs is a function of rise time.
5. Generally, the maximum seat belt load increases as the load limiter is set at higher force levels.
6. Pelvic acceleration levels range from about 40 to 80 percent higher than the input crash-pulse peak acceleration. The condition is worse for the higher load-limiter settings.

Design Variables as Functions of Time for Trapezoidal Crash Pulses

Figures 27 through 34 display the data pertinent to this discussion. The eight curves show in sequence the eight design variables of interest as functions of time for two trapezoidal crash pulses. These are Pulses 16 and 18 shown in Figure 17. The standard pulse, Pulse 3, is plotted for

reference. All pulses represent a 64-foot-per-second velocity change. Only a single value of load-limiter setting is presented. The following observations may be made:

1. No outstanding or unusual trends are apparent.
2. The 40G peak short-duration trapezoid results in early peak values in all design variables.
3. The 20G peak trapezoid behaves somewhat like a 20G triangle with an early peak.
4. The maximum pelvic acceleration associated with the 40G pulse is only about 42G, while the pelvic acceleration associated with the 20G pulse is about 31G. The maximum pelvic acceleration value for the 40G trapezoid occurs on a primary peak, while for the 20G trapezoid the maximum value occurs on a secondary peak.

Design Variables as Functions of Time for Sinusoidal Crash Pulses

Figures 35 through 42 display the data pertinent to this discussion. The eight curves show in sequence the eight design variables of interest as functions of time for two sinusoidal pulses. These are Pulses 13 and 15 shown in Figure 17. The standard pulse, Pulse 3, is plotted for reference. All pulses represent a 64-foot-per-second velocity change. Only a single value of load-limiter setting is presented. The following observations may be made:

1. Seat displacement required is about the same for both sinusoidal

pulses as for the standard triangular pulse.

2. The seat belt load is about the same for the 20G sinusoidal pulse as for the 20G standard triangular pulse, and even for the 40G sinusoidal pulse the seat belt load is only about 20 percent greater.

3. The 40G peak short-duration sinusoid results in early peak values in all design variables.

4. The maximum pelvic acceleration with the 40G pulse is only about 42G, while the pelvic acceleration associated with the 20G pulse is about 31G. The maximum pelvic acceleration value for the 40G sinusoid occurs on a primary peak, while the maximum value for the 20G sinusoid occurs on a secondary peak.

5. Maximum values of occupant head velocity are about the same for both sinusoidal pulses.

Effects of Changing the Load-Limiter Setting

Figures 43 through 50 display the data pertinent to this discussion. The eight curves show in sequence maximum values of the eight design variables of interest as functions of load-limiter setting. A family of curves representing five different triangular pulses is shown. These are Pulses 1, 2, 3, 4, and 5 shown in Figure 17. All pulses represent a 64-foot-per-second velocity change. The following observations may be made:

1. As the load limiter is set to lower values, the required seat

displacement increases. Approximately 10 inches of seat displacement is required for the worst case investigated.

2. The time in the triangular crash pulse at which the peak value of acceleration occurs has a marked effect on the required seat displacement. A late peak represents the most severe condition.
3. Maximum seat belt load is a strong function of load-limiter setting. The seat belt load, and hence the force on both seat and passenger, can be significantly lowered by lowering the load-limiter setting.
4. All vertical and horizontal reactions are strong functions of load-limiter setting. Hence, all forces, and therefore stresses, and therefore structural weights, are significantly reduced by lowering the load-limiter setting.
5. Maximum pelvic displacement with respect to the seat is not much affected by load-limiter setting.
6. The maximum pelvic acceleration can be significantly reduced by lower load-limiter setting for most crash pulses studied.
7. The maximum head velocity is little affected by the load-limiter setting.

Effects of Rise Time in Triangular Crash Pulses

Figures 51 through 58 display the data pertinent to this discussion. The eight curves show in sequence the eight design variables of interest as

functions of rise time of the triangular pulse. A family of curves representing five different load-limiter settings is shown. All pulses represent a 64-foot-per-second velocity change. The following observations may be made:

1. For any given load-limiter setting, the required seat displacement is not a very strong function of crash pulse rise time.
2. Seat belt load, pelvic displacement with respect to the seat, all vertical and horizontal force reactions on the seat, pelvic acceleration, and head velocity are all essentially independent of the rise time of the crash pulse.

Effects of Changing the Peak Values of Triangular Crash Pulses

Figures 59 through 66 display the data pertinent to this discussion. The eight curves show in sequence the eight design variables of interest as functions of time for the different triangular pulses. These are Pulses 3 and 11 shown in Figure 17. Both pulses represent a 64-foot-per-second velocity change. Only a single value of load-limiter setting is presented. The following observations may be made:

1. Seat displacement required is about the same for both the 40G peak and the 20G peak triangular crash pulses.
2. The seat belt load for the 40G triangular pulse is less than 20 percent greater than for the 20G peak triangular pulse.
3. The 40G peak short-duration triangle results in early peak

values in all design variables.

4. The maximum pelvic acceleration with the 40G pulse is only about 40G, while the pelvic acceleration associated with the 20G pulse is about 30G. The maximum pelvic acceleration value for the 40G triangle occurs on a primary peak, while for the 20G triangle the maximum value occurs on a secondary peak.

5. Maximum values of occupant head velocity are about the same for both triangular pulses.

Effects of Secondary Spikes in the Crash Pulse

Figures 67 through 74 display the data pertinent to this discussion. The eight curves show in sequence the eight design variables of interest as functions of time for two different triangular pulses with secondary short-duration spikes. These are Pulses 23 and 26 shown in Figure 17. The standard pulse, Pulse 3, is plotted for reference. All pulses represent a 64-foot-per-second velocity change. Only a single value of load-limiter setting is presented. The following observation may be made:

The required seat displacement, maximum values of seat belt load, pelvic displacement with respect to the seat, all vertical and horizontal seat reactions, pelvic acceleration, and head velocity are essentially unaffected by the presence of secondary spikes in the crash pulse.

Effects of Repeated Peaks in the Crash Pulse

Figures 75 through 82 display the data pertinent to this discussion. The eight curves show in sequence the eight design variables of interest as functions of time for two different repeated-triangular-pulse configurations. These are Pulses 29 and 30 shown in Figure 17. The standard pulse, Pulse 3, is plotted for reference. All pulses represent a 64-foot-per-second velocity change. Only a single value of load-limiter setting is presented. The following observations may be made:

1. The required seat displacement is somewhat increased by the occurrence of multiple or repeated peaks in the crash pulse.
2. The maximum values of seat belt load, pelvic displacement with respect to the seat, all vertical and horizontal seat reactions, pelvic acceleration, and head velocity are essentially unaffected by multiple peaks in the crash pulse. The time of occurrence is, however, somewhat later for the pulses studied.

Effects of Ratio of Vertical to Horizontal Acceleration Components on Seat

Figures 83 through 90 display the data pertinent to this discussion. The eight curves show in sequence the eight design variables of interest as functions of time for three different ratios of vertical to horizontal acceleration components on the seat. These curves are shown only for the standard Pulse 3 and one value of load-limiter setting. From these data,

the following observations may be made:

1. As the ratio of the "vertical" acceleration pulse to the "horizontal" acceleration pulse is increased, i.e., as tangent θ is increased, the required seat displacement increases.
2. The seat belt loads, pelvic displacement with respect to the seat, and occupant head velocity are virtually independent of the ratio of vertical to horizontal acceleration components for the range investigated.
3. Pelvic acceleration, especially the secondary peaks, seems to be rather sensitive to the angle θ. The angle whose tangent is 0.2 yields a pelvic acceleration of 31G, while the bracketing values of tangent θ equal to 0 and 0.4 yield maximum acceleration peaks of only about 17G. This conclusion is based on very meager data, however, and needs further study before definite conclusions can be drawn.

Effects of Passenger Weight

Figures 91 through 98 display the data pertinent to this discussion. The eight curves show in sequence the eight design variables of interest as functions of time for two different passenger weights. These curves are shown only for the standard Pulse 3 and one value of load-limiter setting. The following observations may be made:

1. The required seat displacement is significantly larger for the heavy passenger.

2. The seat belt load, pelvic displacement with respect to the seat, and all vertical and horizontal reaction forces on the seat are significantly greater for the heavy passenger.
3. The pelvic acceleration is greater for the lightweight passenger.
4. The head velocity is slightly greater for the heavy passenger.

Effects of Slack in the Seat Belt

Figures 99 through 106 and 107 through 114 display the data pertinent to this discussion. The eight curves in each group show in sequence the eight design variables of interest. In the first group the maximum values of the variables are plotted versus load-limiter settings for three values of seat belt slack. In the second group the variables are plotted as functions of time for a load-limiter setting of 25G. The crash pulse used is Pulse 1 shown in Figure 17. The following observations may be made:

1. At load-limiter settings greater than about 4528 pounds, the equivalent of a 20G acceleration force on a 187-pound man, the amount of slack in the seat belt has little effect on the required seat displacement. At load-limiter settings below about 4528 pounds, increasing the amount of slack means that an increase is required in the available seat displacement.
2. The maximum seat belt load is essentially independent of the amount of seat belt slack in the range of load-limiter settings

investigated. At high load-limiter settings, above about 30G equivalent force on the 187-pound occupant, the seat belt load is actually decreased with an increased amount of seat belt slack.

3. The amount of slack in the seat belt does not greatly affect any of the maximum vertical or horizontal reaction forces on the seat.
4. The maximum pelvic deceleration is greatly affected by the existence of seat belt slack. For 5 inches of seat belt slack, the maximum pelvic acceleration is on the order of three times as great as for the condition of no slack; for 2 inches of seat belt slack, the maximum pelvic acceleration is nearly double that for no slack.

Effects of Shoulder Harness

Figures 115 through 123 display the data pertinent to this discussion. The nine curves show in sequence the nine design variables of interest as functions of time for the condition of seat belt only and the condition of seat belt with shoulder harness. The curves are shown only for the standard Pulse 3 and for one value of load-limiter setting. The following observations may be made:

1. The seat displacement required with shoulder harness is significantly less than with seat belt only.
2. The maximum seat belt load with shoulder harness is only about 20 percent as much as for seat belt only. Of course, the

shoulder harness takes some of the load, but the total seat belt plus shoulder harness load is, at a maximum, only about 60 percent as much as the seat belt load for seat belt only.

3. The maximum pelvic displacement with respect to the seat is only about half as much with shoulder harness as without shoulder harness.

4. The vertical force reactions on the seat are virtually the same with and without shoulder harness.

5. The total horizontal force reaction on the seat with shoulder harness is reduced to about 80 percent of the horizontal force reaction on the seat without shoulder harness.

6. The maximum pelvic acceleration is reduced from about 31G to about 21G by the use of shoulder harness.

7. The maximum head velocity is reduced by a factor of 3 through the use of shoulder harness.

8. The shoulder harness loads are relatively low. Due to the similarity of the force field on a seat with shoulder harness and an aft-facing seat, one might infer that investigations of aft-facing seats should be reopened.

CONCLUSIONS AND RECOMMENDATIONS

It is evident that the spectrum of data presented here is miniscule when viewed as a part of all important and interesting combinations of the variables that might be studied; yet at the same time, the 106 pages of graphical data border on being so voluminous as to be meaningless. Lest those observations obscure the real value and potential of the computer program described in Chapter 1, it should be emphasized again that, once a specific set of input conditions is specified, it is a matter of only minutes with this program before design information regarding forces, reactions, displacements, velocities, and accelerations is printed out and available. If human tolerances were well defined, the domain of acceptable design data would be established and methodical seat design would be possible. Unfortunately, much remains to be done in the area of defining human tolerance to jerk and acceleration, particularly in the forward-facing situation with seat belt restraint only.

On the other hand, limited though they are, the data presented and discussed above do provide some insight into the problem of seat design for crash survival. Based on the observations made in the preceding paragraphs, the following general conclusions may be drawn based on the ranges of the variables studied:

1. The use of a load limiter is generally effective in reducing loads

on the seat in all directions and in reducing accelerations on the occupant. Hence, seat weight might be significantly reduced by use of a load limiter.

2. For a practical range of crash conditions, the maximum required seat displacement, i. e., load-limiter stroke, is on the order of about 10 inches. This is in the range of practical feasibility.

3. The seat belt load is not much affected by rise time and is not very sensitive to pulse shape so long as the pulses all correspond to the same velocity change. Furthermore, the seat belt loads are not much affected by changing the ratio of vertical to horizontal acceleration components.

4. Significantly smaller dynamic overshoot factors are associated with higher crash-pulse acceleration peaks than with lower crash-pulse acceleration peaks. For example, 20G crash pulses generate 31-36G pelvic accelerations, while 40G crash pulses generate only 40-42G pelvic accelerations. These observations are true rather independently of the crash-pulse shape so long as the velocity change associated with all the pulses is the same.

5. Head velocity of the occupant is virtually the same, from 800 to 1,000 inches per second, for all conditions investigated, with the notable single exception where shoulder harness was used. The shoulder harness reduces the occupant head velocity by a factor of about 3.

6. Short-duration spikes in the crash-pulse acceleration-time characteristic, either early or late, seem to have virtually no effect on any of the design variables and for all practical purposes may be ignored.

7. The presence of repeated peaks in the crash pulse acceleration-time characteristic seems to have virtually no effect on any of the design variables so long as the velocity changes associated with the pulses are all the same.

8. Pelvic acceleration seems to be rather sensitive to the ratio of vertical to horizontal acceleration components.

9. Seats must be designed for heavy passengers from a seat strength standpoint; but if load limiters are properly set for heavy passengers, the accelerations on lightweight passengers are significantly higher. Some study of load limiters which can be adjusted according to passenger weight is indicated.

10. Maximum seat belt load is essentially independent of the amount of slack in the belt for the range investigated.

11. Reaction forces on the seat are not greatly affected by the amount of slack in the seat belt when the seat belt only is used.

12. The maximum pelvic acceleration is greatly affected by seat belt slack, being progressively worse for greater amounts of slack.

13. The introduction of shoulder harness significantly reduces the <u>total</u> horizontal force reaction on the seat. The same statement

may be appropriate for an aft-facing seat.

14. The maximum passenger pelvic acceleration and head velocity are significantly reduced by the introduction of shoulder harness. The same statement could be made for an aft-facing seat.

15. The possibility of an occupant's "submarining" under the seat belt does not emerge as a serious problem in any of these studies.

16. Due to the reduced seat loads and passenger accelerations and head velocities obtained for the case with shoulder harness, and by inference, for the aft-facing seat, these cases should be given further study.

While the foregoing conclusions are based on limited data, they do seem to provide useful insight for the seat designer interested in crashworthiness. The observations regarding shoulder harness effects are especially interesting in military crew and troop seat application. It is recommended that before any of the data or conclusions are used for design purposes, the specific input conditions be carefully studied for specific applicability. Meanwhile, it is recommended that these and other important design variables be further studied, extended, and verified.

CHAPTER 3

DESIGN CONCEPTS AND FEASIBILITY STUDIES FOR SEAT SYSTEMS UNDER CRASH-PULSE LOADING

INTRODUCTION

Numerous design concepts have emerged in the course of this study through evaluation of the computational data presented in Chapter 2, through studing the results of acceleration tests on anthropomorphic dummies, through studying actual accident reports, by conducting special experiments to demonstrate fundamental concepts, by making feasibility studies, by discussing the subject with experts, and through the more subjective processes of conceptual ideation. Many of the concepts are not new, and some of them may not be practical. Data supporting the feasibility of some of the concepts are sketchy; however, the concepts discussed here are based on engineering data and analysis and are supported by preliminary feasibility studies in most cases. More comprehensive data and more accurate analyses may generate new concepts or modify those presented here.

THE CONCEPT OF LOAD LIMITING

Perhaps one of the most important concepts studied is that of load limiting. While this is not a new idea, the real feasibility and practicability of using a load limiter have not been well demonstrated heretofore. While the data presented in Chapter 2 are not exhaustive in this regard, they do

cover a wide range of conditions, and it may be stated conclusively that for all conditions studied, the use of a load limiter with appropriate characteristics will result in lower forces on the seat, lower forces on the passenger, and lower passenger accelerations for any given crash configuration. A further and very important observation is that, under the most serious crash conditions studied, a maximum of only about 10 inches of load-limiter stroke, that is, forward displacement of the seat, is required; and for most crash conditions, a stroke of 4 to 6 inches is enough. These displacements are well within the practical range for aircraft seating, whether commercial or military.

The utility and feasibility of the load-limiter concept are not only supported by the data of Chapter 2 but by the results of a special series of experiments as well[1]. While it is not the function of this report to recommend specific configurations for load limiting, a few general observations regarding feasibility are in order. Generally, load limiters for aircraft seating may be divided into three broad categories: (1) structurally integral load limiters; (2) external load limiters, that is, devices between the seat structure and the connection to the airframe; and (3) combinations of structurally integral and external devices.

STRUCTURALLY INTEGRAL LOAD LIMITERS

Structurally integral load limiters may take the form of either a special device or devices incorporated in the seat structure, or the structural

members themselves might be designed to provide the load-limiting function. Figure 124 shows schematically a load-limiting diagonal in the seat structure. Several observations are apparent when one considers the typical dimensions shown and the data of Chapter 3, which indicate that a 10-inch forward seat motion may be desired. These observations are:

1. To obtain the desired load-limiter stroke, the seat must undergo a vertical displacement which brings it within about 6 inches of the floor.
2. The vertical seat displacement provides a measure of load limiting in the vertical direction, which may be considered an advantage.
3. The vertical seat displacement may generate leg injuries due to the close approach to floor level. This is a disadvantage.
4. Large angular deflections of each joint and at the floor attachment sites must be provided.
5. Large changes in length must be sustained by structural members; for example, the diagonal in Figure 124 must undergo a change in length of over 30 percent without failure.
6. "Bottoming" of the load limiter must be avoided. For example, in Figure 124, when the parallelogram reaches a dead center position, the load limiter becomes ineffective and the forces and accelerations on the seat and passenger may jump to intolerable

levels if the situation requires further stroking of the load-limiting device.

7. Forces on the seat structure are not well defined and are always a function of the crash pulse magnitude. Hence, seat design cannot be based on a well-known force system, and the result may be either a weight penalty associated with overdesign or seat failure associated with underdesign.
8. Stress concentration problems must be considered carefully and evaluated under the conditions of crash-pulse impact loading.
9. In general, high ductility is to be desired, with an attendant sacrifice in strength or weight.

Some of the above observations may be viewed as advantages and others as disadvantages, depending on other design constraints. They are merely presented here for consideration.

EXTERNAL LOAD LIMITERS

External load limiters take the form of a device in series with the seat structure but independent of the structure. For example, in Figure 125, an external load limiter is attached between the seat structure and the airframe to provide load limiting in the horizontal direction. In Figure 126, external load limiting is used in both the vertical direction and the horizontal direction. A combination of external and structurally integral load limiting is shown in Figure 127. In studying external load limiters and

comparing them with structurally integral load limiters, the following observations may be made:

1. The stroking action of the external horizontal load limiter has no effect on the height of the seat.
2. If the load limiter were incorporated in the seat tiedown track, it is possible for any reasonable stroke, certainly 10 inches or more, to be accommodated without bottoming.
3. It is necessary to provide separate load limiting in the vertical direction in the form of buckling legs, collapsible foam under the seat, or other means.
4. Essentially no angular deflections in the structural joints are required, no matter what the magnitude of the load-limiter stroke.
5. Essentially no change in length is required for any structural member in the seat, no matter what the magnitude of the load-limiter stroke.
6. "Bottoming" of the load limiter must be avoided. Otherwise, the load limiter becomes ineffective and the forces and accelerations on the seat and passenger may jump to intolerable levels.
7. Maximum forces on the seat structure are very well defined, no matter what the crash pulse configuration, because the load limiter will permit only a predetermined force level. Hence, seat design can be based on a well defined force system, and neither weight penalty due to uncertain loading and overdesign nor

failures due to uncertain loading and underdesign need be tolerated.

8. Stress concentration problems must be considered carefully, but need only be evaluated up to the force levels of the selected load-limiter setting.

9. In general, there is no strong need for high ductility in the structural members; consequently, high strength materials may be utilized in the seat structure to effect a weight saving.

To illustrate the feasibility of incorporating an external load limiter in the tiedown track,the configuration of Figure 128 is suggested. The floor track, which might also serve as an airframe structural member to conserve weight, has an upper "wavy" flange, as shown. The seat tiedown connection clamps to the wavy flange so as to secure the seat in place. A horizontal force on the seat causes the flange to be drawn through the tiedown attachment. Due to plastic deformation and friction, the load is limited at a rather constant level, depending on the materials and geometrical configuration of the track flange and the tiedown fixture.

The following analytical approximation for the force level at which the load is limited has been developed:

$$F_{LL} = \frac{F_b}{1 - \frac{n\mu d}{\sqrt{c^2 + d^2}}} \qquad (67)$$

where

$$F_b = \frac{2n}{c}\left[\frac{P_{max} + P_{yp}}{2}\right]\left[\frac{d - d_{yp}}{2}\right]$$

$$P_{yp} = \frac{8IS_{yp}}{ct}$$

$$d_{yp} = \frac{P_{yp}c^3}{24EI}$$

$$P_{max} = \left[0.9\left(\frac{d}{d_{lim}}\right)(P_{lim} - P_{yp})\right] + P_{yp}$$

$$P_{lim} = \frac{4E_rI}{c(r + \frac{t}{2})}$$

$$d_{lim} = \frac{P_{lim}c^3}{24E_rI}$$

$$E_r = \frac{3S_{yp}(2r + t)}{2t}$$

n = effective number of clamped track undulations.

μ = coefficient of friction between track and tiedown fixture.

d = distance from top to bottom of track undulations (Figure 128).

c = distance from crest of one undulation to valley of next one (Figure 128).

I = area moment of inertia of cross section of track flange.

S_{yp} = yield strength of track flange material.

t = thickness of track flange.

E = modulus of elasticity of track flange material.

r = radius of curvature of fixture die (Figure 128).

b = flange width.

Although Equation 67 is only an approximation, it has been experimentally verified for a few points, and agreement with experiment is close enough to permit use of the equation for feasibility studies. Table IV shows the calculated and the measured results for two cases. The measured results were relatively uniform over large deflections of the load limiter. However, the device was rate sensitive, and for cross-head speeds of approximately 2 inches per minute, the measured force increased from 20 to 70 percent above the values cited in Table IV.

In any event, it may be observed that within the range of reasonable and practical dimensions shown in Table IV, the load-limiting force levels are in the required useful range. It is therefore suggested that the concept of external load limiters between the seat leg tiedown and the floor track is not only useful but feasible as well. Further development would be required, however.

WEIGHT ESTIMATES FOR LOAD-LIMITED SEATS

An approximate analysis has been developed and computer programmed for the purpose of estimating the percent change in weight of the seat structure as the load-limiter setting is changed. While the analysis is approximate, it does give an insight into the trend to be expected in weight savings by utilizing the concept of load limiting. Figure 129 shows a typical result based on the analysis for one selected set of conditions as specified on the figure. It may be noted that the seat weight is decreased as the load

limiter is set to lower values. For example, at a load-limiter setting of approximately 4528 pounds, which is about the equivalent of a 20G acceleration level on a 187-pound man and the seat, it may be observed from Figure 129 that the seat structural weight, using a slenderness ratio of L/R = 20, is only about 62.5 percent of the required weight of a rigidly mounted seat under the same set of crash conditions.

While the weight estimates shown in Figure 129 are approximate, to be sure, they indicate a significant trend to weight savings for load-limited seats. These estimates are on the conservative side, and actual weight savings would be greater than indicated. This is true largely because the maximum forces on the structure are known with high accuracy when a load limiter is used. This means that the designer can work to a specific design load and avoid overdesign to account for contingency loads.

The overall conclusion, then, is that the evidence indicates a weight advantage for load-limited seats. Further investigation of this concept is therefore indicated.

FLOOR DISTORTION AND ITS EFFECT ON SEAT DESIGN

Two primary types of floor distortion might be generated by an aircraft crash which could cause failure of the seat structure or tiedown connections. First, a floor distortion might take the form of a "bulge" or "dish" in the floor surface between the seat leg tiedown connections as shown in

Figure 130. This would produce a rotation of the seat legs relative to the floor surface, resulting in a connection failure if deflection limits for the attachments were exceeded. Second, a twisting or warping of the floor surface, as shown in Figure 131, could take place which might produce a distortion of the seat structure great enough to result in a seat or connection failure due to the additional loads imposed on the seat structure.

Each of these two modes of floor distortion is considered separately in the following paragraphs.

FLOOR BULGING

The angular displacement or rotation of the seat leg with respect to the floor surface may be expressed in terms of the magnitude of the bulge. Assuming the bulge to be a circular arc passing through adjacent tiedown points, as shown in Figure 132, the relative rotation of the legs may be computed as follows: Referring to Figure 132 for the definition of symbols,. we may write from geometric considerations:

$$\Delta_B = \rho(1 - \cos\psi)$$

$$\frac{d}{2} = \rho \sin\psi$$

$$\frac{2\Delta_B}{d} = \frac{1 - \cos\psi}{\sin\psi} \qquad (68)$$

Expanding the right side of Equation 68 in a Maclaurin series, we have

$$\frac{2\Delta_B}{d} = \frac{\psi}{2} + \frac{\psi^2}{24} + \ . \ . \ . \qquad (69)$$

For a sufficiently small angle, ψ, the first term alone will suffice to provide an approximate value of ψ. Hence,

$$\psi \doteq 4\left(\frac{\Delta_B}{d}\right) \qquad (70)$$

If the floor distortion in a survivable crash does not produce a ratio of $\frac{\Delta_B}{d}$ greater than 0.10, as is likely, then the maximum ψ to be accommodated would be

$$\psi_{max} \doteq 4(0.1) = 0.4 \text{ radian} \qquad (71)$$

or

$$\psi_{max} \doteq 23^{\circ} \qquad (72)$$

Such a relative rotation would cause failure of many types of button-in-track tiedown connections. In designing tiedown connections, therefore, attention should be given to increasing the limits of acceptable relative rotation without failure. This concept is discussed further in a later section of this chapter.

FLOOR WARPING

Under a twisting action, the original plane surface ABCD of Figure 131 is warped into an anticlastic (saddle-shaped) surface A'B'C'D'. Under these conditions, either (1) one or more seat legs must buckle or stretch, (2) the seat pan must twist, or (3) a combination of these modes must take place.

The mode of seat structural distortion and the magnitudes of the associated forces introduced by the distortion would depend on the relative stiffnesses of the structural components. For example, the compressive buckling load for a seat leg is always less than the plastic extension load for this same leg; hence, if legs were to deform, compressive buckling loads would govern. These loads have been found experimentally to range from 5,000 to 10,000 pounds for typical seat structures examined.* However, torsional stiffness for that section of the seat pan which lies between seat leg assemblies is generally small enough to preclude leg buckling; instead, the seat pan merely twists. To quantify this discussion, a numerical example will be considered. Referring to Figure 131, we may define the following terms:

T = torque applied.

d = distance between fore and aft legs.

$\beta = \beta_1 + \beta_2$ = angular rotation of one side of the seat pan with respect to the other side.

F = force in seat legs required to supply torque T to seat pan.

Then,
$$T = K\beta \tag{73}$$
where

K = a torsional rigidity constant obtained by standard analytical procedures.

*Tests conducted as reported in Reference 1.

For a typical seat, K was computed to be about 50, 000 inch-pounds per radian. A plausible maximum floor warpage angle, β, would be 0.15 radian, corresponding to the displacement of point A (out of the plane B'C'D') equal to 0.15 times the length d. That is,

$$\beta \doteq \frac{\Delta_B}{d} \doteq 0.15 \text{ radian} \tag{74}$$

$$T = K\beta = 50{,}000\ (0.15) = 7{,}500 \text{ inch pounds} \tag{75}$$

The associated leg force, F, is then related to the torque, T, by

$$F \cdot d = T \tag{76}$$

Hence, for a distance, d, of 15 inches,

$$F = \frac{T}{d} = \frac{7500}{15} = 500 \text{ pounds} \tag{77}$$

As this load is an order of magnitude less than leg buckling loads, it would govern; consequently, it would be the additional force introduced in the seat legs as a consequence of floor warping. The points of critical importance would again be the tiedown connections, since the leg distortion loads would be directly superposed upon the acceleration-induced force at these connections.

DESIGN CONCEPTS

The seat designer may anticipate possible floor bulging or warping and take appropriate measures in seat structural design to minimize the adverse effects.

To accommodate the leg rotations with respect to the floor surface arising

from floor bulging, several design configurations may be conceived. Two of these are presented below.

1. A deliberate "yield hinge" of sufficiently ductile material may be incorporated in the tiedown connection design as shown in Figure 133. This yield hinge would need to be designed so that plastic bending without failure would occur adjacent to the connection. It would be necessary for the design to accept leg rotation up to a value greater than would ever be anticipated as a result of floor bulging.
2. A frictional connection could be used so that slippage between contacting surfaces would take place under leg rotation. This concept is illustrated in Figure 134, where leg "yoke" plates are tightened against a floor track plate. The plates would bend to accommodate side-to-side leg rotation and slip to accommodate fore-aft leg rotation.

For the problem of floor warping and consequent seat structure distortion, the critical design parameter appears to be the torsional rigidity of the seat pan. If the torsional rigidity is low, only small warpage forces are introduced into the seat structure. However, for seat pans very stiff in torsion, the warpage forces may either cause a leg to buckle or, worse, overload a tiedown connection, causing failure. A high torsional rigidity in the seat pan might arise from integrating the stiff lateral cross tubes

with the seat pan so that the tubes must also twist with the seat pan. Consequently, it may be desirable to connect the cross tubes with the seat pan in such a way that the seat pan is free to twist independently of the cross tubes.

The general conclusion that one may reach based on the foregoing feasibility analyses is that tiedown connections should be so configured as to provide angular displacements in all directions. In fact, all structural joints should be capable of large angular displacements in all directions without failure. These concepts are closely related to the requirements already stated with regard to structurally integral load limiting. Hence, a seat designed properly for structurally integral load limiting would probably also satisfactorily accommodate floor buckling and warping under crash conditions.

STRESS CONCENTRATION UNDER CRASH-PULSE LOADING

An extensive study of crash-induced failures of aircraft seating has indicated that a high percentage of all such failures initiate at a well defined geometrical stress concentration. The effects of stress concentration under crash-pulse loading are therefore of primary interest to the seat designer. If either no load limiting or structurally integral load limiting is to be used, the effects of stress concentration are of urgent interest. If external load limiting is to be used, the stress concentration effects, while less urgent, are nevertheless important.

Theoretical analyses in the area of stress concentration effects are difficult for static loading and are not possible at the present state of the art for dynamic loading. Therefore, experimental testing is currently the only feasible alternative for studying stress concentration effects under dynamic loading conditions.

To provide a cursory insight into the stress concentration problem for aircraft seating under crash loading conditions, a limited experimental program was conducted. From data obtained in recent experimental aircraft crashes, the forces induced in aircraft seats under "typical" crash conditions exhibit rise times ranging from 0.5 to 50 milliseconds. The results described in the following paragraphs were obtained on a Hy-Ge high-load-rate machine so as to cover the load rise-time range associated with actual aircraft crashes. Details of the configuration and operation of the Hy-Ge machine are given in Reference 1.

TEST SPECIMENS USED

In designing the test specimens for this study, it was desired to duplicate actual dimensions and materials of aircraft seat stress concentrations as closely as possible. From a survey of actual aircraft seats, the specimens shown in Figures 135 and 136 were conceived, fabricated, and tested. All specimens were designed to have a static failure load of approximately 3200 pounds based on the net cross section. The theoretical stress concentration factors for all geometries used are presented in Table V.

Typical failures for each of the specimen types when dynamically tested to failure are shown in Figures 137 and 138.

EXPERIMENTAL RESULTS

Force versus deformation and energy absorption versus deformation data for the various types of specimens tested are shown in Figures 139 and 140. A comparison of energy absorbed prior to rupture for dynamic loading versus static loading is given in Table VI. Plots of the ratios of the dynamic ultimate loads to the static ultimate load for a specimen without stress raisers are shown in Figures 141 and 142. Also, a plot of total energy absorbed as a function of plastic loading rate is given in Figure 143.

CONCLUSIONS

Based on the results and data from the testing program described above, one may draw the following conclusions:

1. The energy per unit volume absorbed prior to failure by specimens without stress raisers was a function of the severity of the stress raiser and the magnitude of the cross-section nominal stress remote from the stress raiser. In one of the worst cases, the energy absorbed by a specimen was only about one-seventh the energy absorbed by smooth specimens with the same net cross-sectional area. This was true at all loading rates investigated.

2. The energy-absorption capacity prior to rupture is greater for higher loading rates than for static loading rates.

3. For both hole-type and fillet-type specimens, the ultimate rupture load is never as small as 80 percent of the ultimate rupture load of a specimen without stress raisers tested statically. At higher plastic loading rates, the ultimate rupture load increases, the ultimate load ratio becoming greater than 1.0.

4. From these studies, two basic seat design criteria associated with stress concentration may be defined: (1) ultimate rupture loads, and (2) energy-absorption capacity. Either or both criteria may be important, depending on the seat design; whether the seat is load limited externally, structurally-integrally load limited, or not load limited.

While the above conclusions are based on minimum data, they indicate that failure of a structural member containing geometrical discontinuities can occur at loads smaller than those predicted by theoretical analysis throughout the loading-rate range typical of aircraft crashes. Further, they seem to indicate that critical geometries exist; and if one designs outside the critical geometry range, significant weight savings may result. Also, the energy-absorption capacity is very sensitive to geometry, but does not seem to be a strong function of loading rate in the range of interest for aircraft crashes.

Obviously, the usefulness of such data depends greatly on whether or not the seat is integrally or externally load limited. Additional investigation of these matters is suggested for future work in providing useful design information.

COMPARISON OF THE EFFECTS OF STATIC VERSUS DYNAMIC LOADING ON SEAT COMPONENTS

GENERAL

In order to determine the energy-absorbing and ultimate load capacities of a typical aircraft seat, the analysis must necessarily be based upon a study of the component parts.

That load-deflection relationships can be greatly changed by varying the rate of straining is now well known. Experimental observations of these properties are not always consistent, however, being strongly influenced by such primary factors as material, geometrical shape of the cross section, presence or absence of discontinuities (both macroscopic and microscopic), length, and slenderness ration.

TEST SPECIMENS USED

As a result of these considerations, static and dynamic tests were performed on actual components of the seat leg assemblies of two types of commercial aircraft passenger seats, i. e., one of welded tubular steel construction and the other of riveted formed sheet aluminum construction.

BRIEF DESCRIPTION OF TESTS

The test performed on each component was designed to simulate crash-type loading and to insure repeatability of end conditions from static to dynamic. The desired results of these tests included:

1. Determination of whether rate of loading was important in fixing the load-deflection characteristics of seat structures.
2. Acquisition of realistic input data for computer simulation.

Each of the following was considered to be a fundamental type of test:

1. Axial tension load on the rear legs.
2. Axial compression load on the front legs.
3. Lateral bending load on legs.

EXPERIMENTAL RESULTS

The dynamic and static average load versus deflection data for the tubular steel and the sheet aluminum leg assembly components are shown for each of the fundamental tests in Figures 144, 145, and 146. Figure 147 shows the load-deflection relation for the forward-loaded composite leg assembly tests.

CONCLUSIONS

Based on the results and data from the testing program described above, one may draw the following conclusions:

1. There are no significant differences in the load-deflection

characteristics of components tested statically and those tested dynamically when the time to reach peak load is 0.03 second.

2. These tests indicate that these commercial airline seats qualify under the appropriate strength requirements, but that the failures occurred suddenly with very little energy absorption. These seats thus perform poorly on the basis of the load-limiting concept, which requires that the maximum load be sustained during relatively large deflections.

OVERALL SEAT DESIGN CONCEPTS AND RECOMMENDATIONS FOR RESISTANCE TO CRASH-PULSE LOADING

In the course of analyzing the data and performing feasibility studies associated with this project, there have emerged certain ideas and concepts which represent a somewhat subjective evaluation of the results thus far obtained. While no originality is claimed for the ideas, it may be useful to summarize the more pertinent observations.

STRENGTH AND DEFLECTION OF SEAT LEG TIEDOWN CONNECTIONS

Design requirements for the seat leg tiedown connections include both a strength requirement and a rotational displacement capability. This is especially true for the aft seat legs. The tensile and shear strength requirements of the connection are determined by the maximum anticipated forces on the seat, governed by a load limiter, if present. Conceptual designs of possible arrangements are depicted in Figures 133, 134, and 148.

The accommodation to rotational displacements may be necessitated by either of two considerations: (1) if a structurally integral energy-absorbing deformation of seat structure were included in the basic seat design, large rotations would occur at the floor tiedown; (2) even for a nominally rigid seat design, floor buckling or floor distortions may require a relative rotation of the seat leg with respect to the floor plane. Conceptual designs of these approaches have been previously discussed and are illustrated in Figures 133, 134, and 148.

STRENGTH OF SEAT IN FORE-AFT DIRECTION

To maximize the seat strength-to-weight ratio in the fore-aft direction, an external load limiter and high strength-to-weight-ratio materials in structural members might be used. Ductility requirements for seat structural components that are not required to deform appreciably under the crash-induced loads need not be high, perhaps less than 5 percent elongation in 2 inches. This suggests the use of materials usually excluded because of low ductility. It should again be emphasized that the use of low-ductility high-strength materials is made possible due to the use of an external load limiter.

Further, primary structure should, where possible, be designed to avoid flexural or torsional loading. Placing members in axial tension or compression or transverse shear provides the greatest structural efficiency. In compression members, the slenderness ratio should be made sufficiently

small that the material strength properties are largely exploited prior to buckling. Furthermore, the seat structure should be as free of geometrical discontinuities as possible. The design should approach a single formed structure with no joints, holes or severe changes in section size. The concept of using a single tube properly bent to form the entire primary structure is worthy of consideration. Clamping around members rather than bolting or riveting through members is to be encouraged in all parts of the primary structure.

STRENGTH OF SEAT IN LATERAL DIRECTION

Seats in current use rely largely on moment-resisting connections at the top of the seat leg assemblies to provide lateral seat strength. This is generally ineffectual. An increase in the lateral connection moment strength to the required level would probably be costly in weight. The introduction of a simple lateral truss design appears to be more efficient. A further efficiency would be achieved if the bracing against lateral seat collapse were also to serve a primary structural function for the fore-aft strength requirement. One suggested structural configuration to provide resistance to lateral collapse in an efficient manner is shown in Figure 149.

STRENGTH OF SEAT IN TORSION ABOUT A VERTICAL AXIS

Most three-passenger seats in current use offer low resistance to the torsional collapse mode described by torsional seat rotation about a vertical axis. In most instances the seat is more likely to collapse with

two passengers seated in adjacent seats, i.e., when the seat is loaded eccentrically, than if fully loaded. Since the torsional collapse mode entails a "warping" of the leg assemblies due to a rotation of the seat pan about the vertical axis with respect to the floor, a three-dimensional truss with resistance to lateral displacements would most effectively resist torsion about a vertical axis. Consequently, the recommendations and comments made in the preceding paragraph for lateral seat strength would apply equally well to torsional strength.

SEAT PAN STRENGTH

In designing the seat pan for occupant support and retention in the vertical direction, use may be made of the concept of membrane loading. Since flexural stresses are nonuniform over the thickness of a laterally loaded member while membrane stresses are uniform, the utilization of membrane loading should provide a more efficient use of material. An optimum configuration based on membrane loading may be arrived at from a consideration of membrane equilibrium. A flexible membrane support, such as a net, offers many favorable properties, principally high strength-to-weight ratio and adaptability to the supporting rigid frame. The seat net concept is demonstrated in Figure 149.

STRENGTH AND POSITION OF FRONT TUBE

The front cross tube in current aircraft seats is located at the seat pan level. Front tube failures have occurred frequently under the action of a

severe vertical component of crash-induced acceleration. These failures have been due in large measure to direct application of load from the occupant's thighs. Therefore, it is recommended that the front cross tube be lowered enough to avoid direct contact with the occupant. The primary function of the front cross tube would then be to provide only lateral strength and stability. The concept of a relocated front cross tube is demonstrated in Figure 149.

ATTENUATION OF VERTICAL FORCES AND ACCELERATIONS

To avoid spinal and other injuries to the passenger, the vertical acceleration must be attenuated to levels consistent with human tolerance. This may be accomplished effectively through the use of "cushions", extensible load-limiting seat pan, load-limiting seat legs, or a combination of these. The use of "tempered nylon" or other synthetic fibers that exhibit small elastic deformation prior to large plastic yielding might be suitable for a load-limiting seat pan. A combination of crushable seat cushion and load-limiting seat pan is suggested in the conceptual design illustrated in Figure 149. The crushable material would also act as a load spreader and provide some degree of passenger protection from direct contact with minor obstructions.

ATTENUATION OF FORE-AFT FORCES AND ACCELERATIONS

A rigid seat rigidly secured to the floor structure may give rise to a serious dynamic overshoot of the passenger mass, in the presence of a

fore-aft horizontal acceleration pulse. Such a dynamic overshoot imposes a design penalty in the form of increased fore-aft longitudinal strength requirements for the seat. Moreover, the occupant may not be able to tolerate the high acceleration levels associated with this dynamic overshoot.

Consequently, fore-aft attentuation of acceleration forces is recommended as a fundamental improvement in seat design. This attenuation may be accomplished either through an energy-absorbing deformation of the seat structure iteself, that is, structurally integral load limiting, or through the use of an external load-limiting device which permits the seat to translate rigidly while the load is limited externally. Both concepts have been investigated in this study and each has attendant advantges, as described earlier. Structurally integral load limiting does not require additional devices; however, allowance must be made for a collapse mode without rupture of the tiedown chain. This requires the use of highly ductile materials at all points of potential deformation. Further, the loads on the seat structure are not well defined. On the other hand, the rigid-structure externally load-limited seat permits the use of lower ductility, very high strength materials and well defined design loads. Moreover, the externally load-limited seat can provide any reasonable magnitude of stroke, as there is no collapse mechanism which limits the stroke. The concept of combining the external load limiter with the seat tiedown connection is also a weight-saving possibility. The seat of Figure 149 illustrates the concept

of the externally load-limited rigid seat.

SEAT BACK, FOOD TRAY, AND ARM REST REQUIREMENTS

In designing a seat for crashworthiness, the designer must consider modifications compatible with operational requirements, in particular the need for occupant comfort, as well as safety requirements. The seat structure must provide a base for an adjustable seat back and for arm rests. A head injury problem is associated with impacts against the aft end of the arm rest on the next seat forward. General conclusions regarding suitable arm rest design are embodied schematically in Figure 150. The major arm rest support, and perhaps the entire support, should be near the forward end of the arm rest. This concept permits construction of an arm rest cantilevered rearward. If the arm rest skeleton is of a ductile metal with the proper yield point, a head impact on the free aft end of this cantilever will cause it to bend plastically, effectively dissipating the impact energy without producing serious head injury. The aft end of the arm rest should be of a generally rounded shape with no exposed metal. Further, the metal skeleton under the padding should be free of sharp edges and local stiff regions. The padding itself should probably be a semirigid plastic foam to act as a load spreader for the head. To minimize head decelerations, the combined characteristics of the padding and arm rest structure should be analyzed by a technique comparable to that outlined in the head impact study in Chapter 4.

Looking at the food tray problem, one may observe that there are at least seven fundamental possibilities for location of a food tray. These include locations on the floor, ceiling, side wall, seat back, beneath the seat, in the arm rest, or remote stowage. Due to the use of the tray for functions other than food service, for example, use as a desk, remote stowage is thought to be undesirable. Due to the requirement of variable pitch seating, any location separate from the seat, such as on the floor, ceiling, or wall, is probably impractical. The general conclusion is that the tray should probably be attached locally to the seat structure. If this conclusion is accepted,several possible configurations suggest themselves. These include locations in or on the seat back, under the seat, or in the arm rest. To illustrate some of the more promising configurations, a few of the concepts are shown in Figures 151 through 156.

Other configurations can and have been conceived. The general conclusion is that the stowage location should be out of the zone of possible head impact. Arm-rest stowage, under-seat stowage, or possibly lower-seat-back stowage are all worth serious study.

One further important concept is that tray latching devices must be capable of retaining the food tray in the stowed position under impact acceleration environments of crash severity. A serious study to insure properly latched trays under crash conditions is of great importance.

The problem of head injury is dealt with in depth in Chapter 4 as a separate study. If the food tray if removed from the seat back, it will be possible to prevent head injury by appropriate foam padding on the seat back for crashes up to a certain level of severity. Beyond this level of severity, padding alone becomes impractical due to the high head velocities generated by the crash pulse, and the only feasible measures apparent today are either the use of shoulder harness or the use of aft-facing seats.

SHOULDER HARNESS AND AFT-FACING SEATS

Renewed consideration should be given to both the use of a shoulder harness and the use of aft-facing seats. Either measure serves to reduce significantly the total horizontal forces on the seat and accelerations and head velocity of the passenger, as was demonstrated in Chapter 2. These data are immediately applicable to military usage and may also be of interest in commercial applications for the future.

SEAT SPACING FLEXIBILITY

Additional operational requirements that must be met by any new crashworthy design include the need to provide variability in spacing and simple installation and removal of seats. The floor track load-limiter concept illustrated in Figure 127 can readily be made to meet these requirements. Moreover, this may be done in an efficient manner if the floor track member can be used as a basic airframe structural member, thus serving two functions. This concept is illustrated in Figure 149.

CHAPTER 4

HEAD IMPACT STUDY

GENERAL

From literature surveys made for the report "Crashworthiness Study for Passenger Seat Design (Phase I),"[1] head impact against local structures was found to be a primary cause of injury. To analyze effectively the problem of head impact, a simple numerical technique was developed to investigate the magnitudes of the forces and accelerations to which the head is subjected when impacting a "crushable foam" protective cushion at some prescribed initial impact velocity. This technique has been extended and written into a computer program, so that the effect of impact of the head, from the standpoint of human tolerance, could be assessed for various foam compositions and original foam thicknesses.

The extended analysis is based upon the development of time-dependent relationships for (1) the head velocity and (2) the head deceleration relative to the seat back. Specific limitations are then imposed on the initial head velocity and on the relative head deceleration. The limiting value of initial head velocity is that value of initial velocity which will result in the cushion being crushed to some preselected maximum value of strain. This is dependent upon the foam properties. The restriction on head deceleration is defined by human tolerance limitations. This is a function

of pulse duration and average head deceleration. In combination, however, these limitations define a maximum initial velocity curve as a function of original foam thickness, above which absence of concussion* is doubtful, regardless of foam characteristics. By staying within the safe region, as illustrated in Figures 157, 158, and 159, aircraft seat designers can, using this technique, select suitable foam materials and determine the most efficient initial thickness, that is, a foam having the least thickness for a given (prespecified) maximum strain.

COMPUTER PROGRAM

The computer program was written to allow the actual dynamic stress-strain curve for a crushable material to be approximated by any one of several mathematically describable curves, shown in Figure 160. Pertinent computer input data, in addition to material properties, include the projected head area, the head weight, the initial head velocity, and the ratio of the effective head mass to the actual head mass. This ratio is referred to as the head mass parameter, k, in later sections of this report. The head mass parameter is an arbitrary, but critical, number used to describe the extent to which a percentage of the weights of the body and arms may be added to that of the head to increase penetration into the foam. The concept is analogous to the calculation of shock forces in an

*The tolerance curve used in this study was established by Gurdjian and associates at Wayne State University and is based on concussion limits given in References 2 and 3.

impact of a weight on a spring when the spring is considered as having some mass. When selecting a value for k, the shear strength of the neck must be considered. A reasonable value of k probably would fall between 1.0 and 2.0, and this range has been used in the numerical analysis presented here.

As output information, the dynamic force on the head is computed from a knowledge of the foam characteristics and the rate of change of head area with respect to normal head displacement into the foam. Having the relation between the force on the head and the foam penetration, as well as the knowledge of a sufficient number of boundary conditions, the maximum head displacement (or foam deformation), the relative head velocity, and the relative head deceleration, all as functions of time, are computed and printed out.

DISCUSSION OF RESULTS

Determination of the head deceleration pulse duration, τ, according to this analysis, employed the assumption that the deceleration versus time curve terminated at the same instant that the relative head velocity became zero; that is, the deceleration dropped instantaneously from a maximum to zero at time τ. Several computed acceleration-time curves are shown in Figure 161. The damping characteristics and elastic properties of facial tissue, as well as those of the foam cushion, preclude this occurrence in actual practice. The head deceleration does not become zero

instantaneously, but is reduced over some finite interval of time. The rate of reduction of head deceleration depends largely upon the rebound characteristics of the foam material. Experiments performed by Turnbow[4] and by Shield and Covington[5] to determine the dynamic properties of rigid foams revealed that foams can be found for which this rebound energy is a small percentage (in some cases less than 5 percent) of the total energy absorbed for strains of 70 to 80 percent. This means that the finite interval of time required in reducing the deceleration to zero from a maximum will be short with respect to the total time in reducing the initial velocity to zero.

Furthermore, the human tolerance data reported by Gurdjian,[2] Lissner,[3] and Haley and Turnbow[6] were admittedly approximate in nature. Nevertheless, it is felt that their results are as good as any available and that these results provide a reasonable envelope of human tolerance to which the results of the head impact computer program can be compared.

Finally, the deceleration pulse duration, using most practical foam materials, will be of sufficient duration to place the operating point under the human tolerance curve in a region where small changes in pulse duration have little or no effect on the tolerance level.

For these reasons, small inaccuracies in computed pulse duration will not have a significant effect on the evaluation and selection of a particular foam and original thickness.

For purposes of comparison of results, the ratio of maximum allowable stress to dynamic yield stress was kept constant in four of the five foam materials analyzed. Foam 1 (from Reference 4) and foam 5 (from Reference 5) in Table VII are real foams, whereas foams 2, 3, and 4 are hypothetical, yet realistic, foams. The material characteristics are given in Table VII.

The desirable property of these foams, and of any applicable foam, is that their stress-strain curves have a horizontal plateau throughout a large range of strain, say 5 percent to 70 percent.

Original cushion thicknesses of 2, 4, 6, and 8 inches and initial head velocities from 120 to 720 inches per second were used to compute the maximum foam deformation, the head velocity and head decelerations, all as functions of time, as well as the average head deceleration over the interval and pulse duration.

The curves plotted from the computer results provide information for the most severe impact condition, that is, for a perfectly rigid seat back. Plastic deformation of the framework behind the foam pad will tend to reduce the severity of the decelerative forces transmitted to the head while increasing the pulse duration; except for lack of time this could easily have been included in the present program. Since the seat can approach the nearly rigid state under some conditions, for instance, certain tubular

steel seats in the breakover position, design under the assumed rigid condition seems reasonable.

The curves in Figures 162 through 166 give an overall perspective of the impact event. The two prominent asymptotic lines indicate the human tolerance limits. Any head impact for which the actual average head deceleration lies above the lower line will, in all probability, result in the passenger's becoming unconscious or seriously injured, thus presenting at least a hazard to evacuation.

A description of these curves is best done in an example. As entry conditions, choose the head mass parameter, k, equal to 1.5 and the initial cushion thickness equal to 6.0 inches. Using Figure 164, note that there are three groups of original foam thickness curves (each group containing 2-, 4-, and 6-inch lines). Each group corresponds to one of the head mass parameters, 1.0, 1.5, or 2.0, shown along the bottom of the graph. For a foam having the stress-strain curve and the projected head area-penetration curve shown at the top of the figure, the relative velocity of the head at the instant of impact cannot exceed approximately 347 inches per second; that is, the velocity corresponding to the point at which the 6-inch thickness line for k = 1.5 crosses the line corresponding to the human tolerance limit based on average acceleration of a triangular pulse (lower curve). At this point, the average head deceleration is 62G and the pulse duration is 13.6 milliseconds.

If, for k = 1.5, an original foam thickness of 2.0 inches has been chosen instead of 6.0 inches, the initial head impact velocity could not exceed approximately 197 inches per second, that is, the velocity at the point "x" on the 2.0-inch line. The average head deceleration at this point is 43G and the pulse duration is 12 milliseconds.

In using the curves in Figures 162 through 166, it is important to understand that the lines of constant initial thickness cannot be extrapolated to higher initial velocities. The reason for this is that there is a limiting initial velocity above which a particular foam of given thickness cannot absorb sufficient energy to stop the head within the specified strain limitations. This value was fixed at 0.80 in this study.

Interpolation between lines of constant impact velocity, initial thickness, and maximum penetration is allowable, as it also is between head mass parameters for a given foam thickness.

Lines of uniform foam penetration could have been drawn to assist in the selection of an optimum original thickness, but for clarity they were omitted. Had these lines been drawn, it would be apparent that the most effective use of the foam occurs when the foam strain becomes a maximum just at the limit of human tolerance. This can be shown in a more direct manner.

In Figures 162 through 166, the strain limit (represented by the "x" at the

upper end of the original thickness curves) for the various original thicknesses is seen to correspond to definite initial velocities. In addition, the points at which the human tolerance line crosses the thickness lines correspond to distinct values of initial velocities. These points describe limitations on the initial velocity, the former corresponding to maximum strain and the latter to human tolerance. On a graph of limiting initial velocity and original thickness, these limiting conditions occur as a pair of intersecting lines. The lines are plotted in Figures 157 and 158. Operation in the region below the human tolerance line and to the right of the maximum strain line in each graph is considered safe. To obtain the most effective use of the foam and still maintain a minimum original foam thickness, a value for the original foam thickness near the intersection of the two lines should be selected.

The intersection points of the human tolerance and strain limit lines, that is, the points defining the optimum cushion thickness for the different conditions, were plotted on a graph against the corresponding limiting head impact velocities. The result was that one smooth curve could be drawn through all the points, as shown in Figure 159. This curve, then, is an invariant for the specified maximum strain and human tolerance limits, and it defines a limiting velocity above which concussion is probable. The curve appears to vary only with original thickness, being independent of the foam characteristics and effective head mass.

This does not mean that the foam characteristics are an unimportant consideration in the design of a protective cushion. By careful study it can be seen that variation of the properties of the material and/or the head mass parameter will cause the point of operation in Figure 159 to move along the curve. Conversely, if it is desired to operate at a specific point on the curve, then for a given head mass parameter, the stress-strain characteristics of the foam are fixed.

Design curves were drawn to reduce the labor of employing this technique and to present the results in a straightforward manner. The final result is shown for a group of typical rigid foam materials in Figure 167. As an example of the use of this curve, suppose that separate tests on anthropomorphic dummies, cadavers, and animals have shown that it is reasonable to select a head mass parameter, k, equal to 1.5. The seat design requires that the original thickness of the protective cushion be 2.75 inches. Enter the graph in Figure 167 at the bottom at 2.75 inches and move up along this line of constant thickness until it intersects the k = 1.5 line. The maximum head impact velocity (from the upper scale corresponding to this point) is 300 inches per second. The dynamic yield stress of the foam used must be 32 pounds per square inch.

Only two requirements are necessary to use these curves for design. The first is that the stress-strain curve be similar in shape to those used to derive the results from which Figure 167 was plotted. It has been shown

by comparison that the foam properties used in the computations are realistic. Second, an estimate must be made of the effective head mass. This also has been discussed, and it is felt that a suitable estimate for design purposes can be made.

COMPARISON OF RESULTS WITH THE ANALYTICALLY CALCULATED HEAD VELOCITIES

A study of the results obtained from the computer program described in Chapter 1 for calculating the dynamic response of the seat-passenger system when subjected to various input acceleration pulses shows that the maximum head velocity for the models studied (that is, with and without simulated muscle tension and seat damping, also without restraint by a shoulder harness) can become exceedingly large, that is, greater than 800 inches per second in many cases.

The program, in its present state, neglects the probability of contact of any part of the simulated passenger with any other structure, such as the seat immediately ahead. Such contact would serve as a retardant to the motion of the head, thus reducing its velocity.

Assuming that the head would contact the back of the preceding seat, a locus of likely impact points was determined. By studying the head velocity-time curves and head displacement-time data, it was found that the head velocity at the point at which the head might normally contact the back of the preceding seat is only about 85 to 90 percent of the maximum

head velocity. Comparing the maximum head velocities thus computed for various pulses (see, for example, Figure 50) with the allowable head velocities for the various foams as given in Figures 162 through 166, it is apparent that a cushion of reasonable thickness cannot be designed using these materials to restrict the average head deceleration to a value within the range of human tolerance. This is an important observation. In effect, it requires that, in order to maintain a level of survivability, at least one of the two following conditions must be satisfied:

1. The head velocity must not be allowed to attain such high relative values as 800 inches per second. Velocity attenuation through the use of an external device such as a shoulder harness is essential.
2. The seat back structure must be capable of withstanding large deformations under the influence of forces of such magnitude as to keep the head deceleration in the desired range. Proper selection of a suitable cushion material is desirable to distribute the force uniformly on the head, but the cushion alone cannot be depended upon to supply complete head protection.

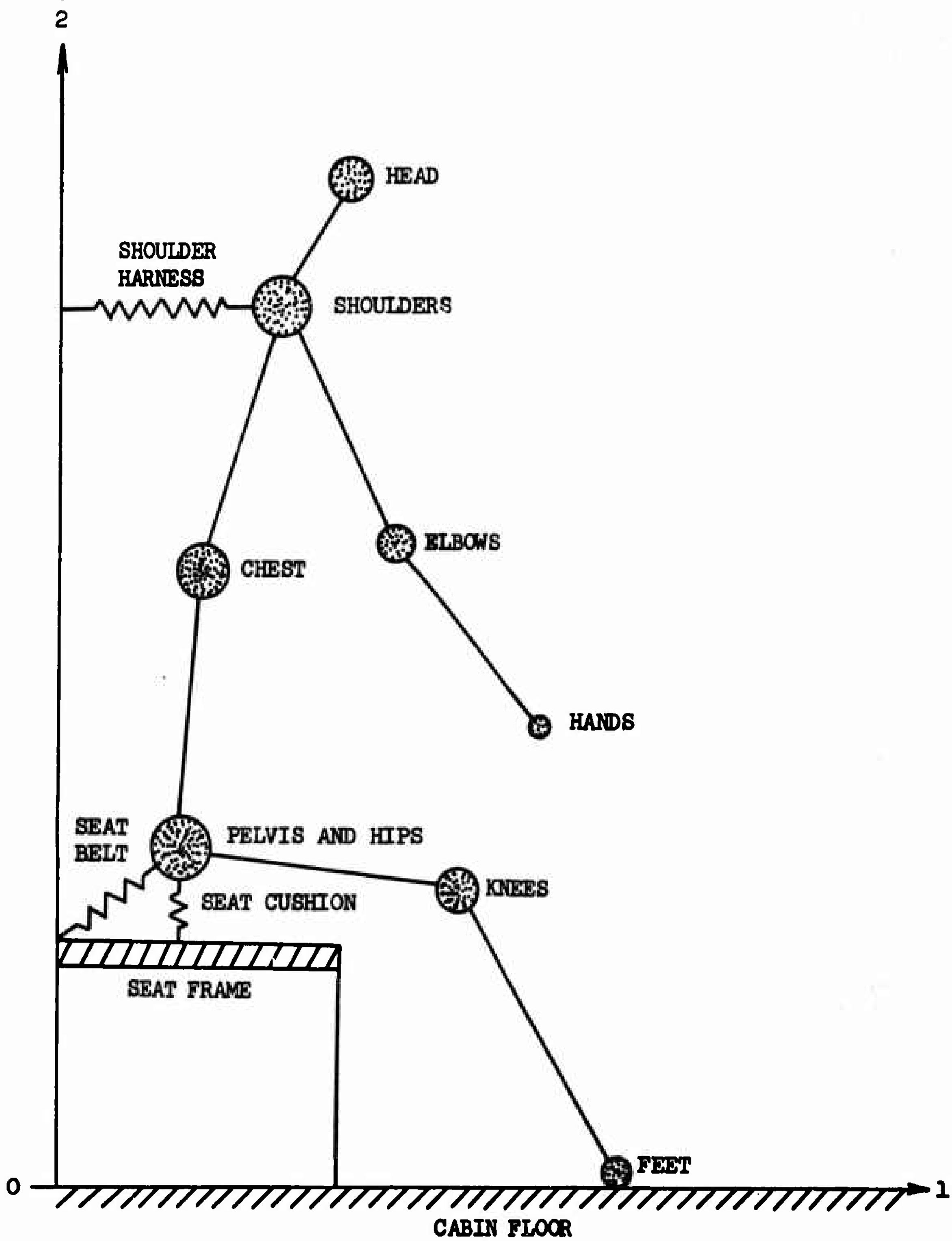

Figure 1. Mathematical Model.

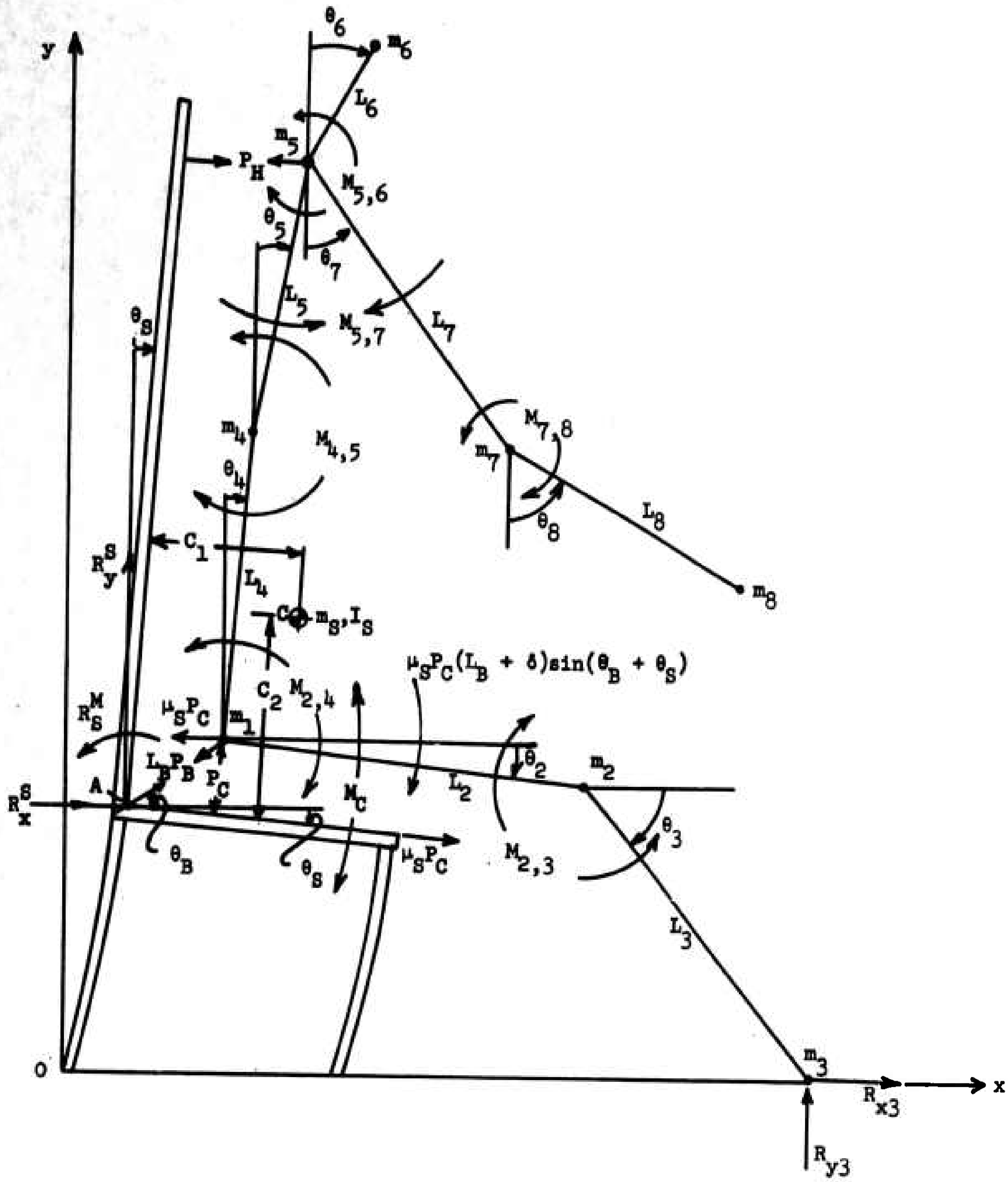

Figure 2. Free-Body Diagram of Passenger and Seat.

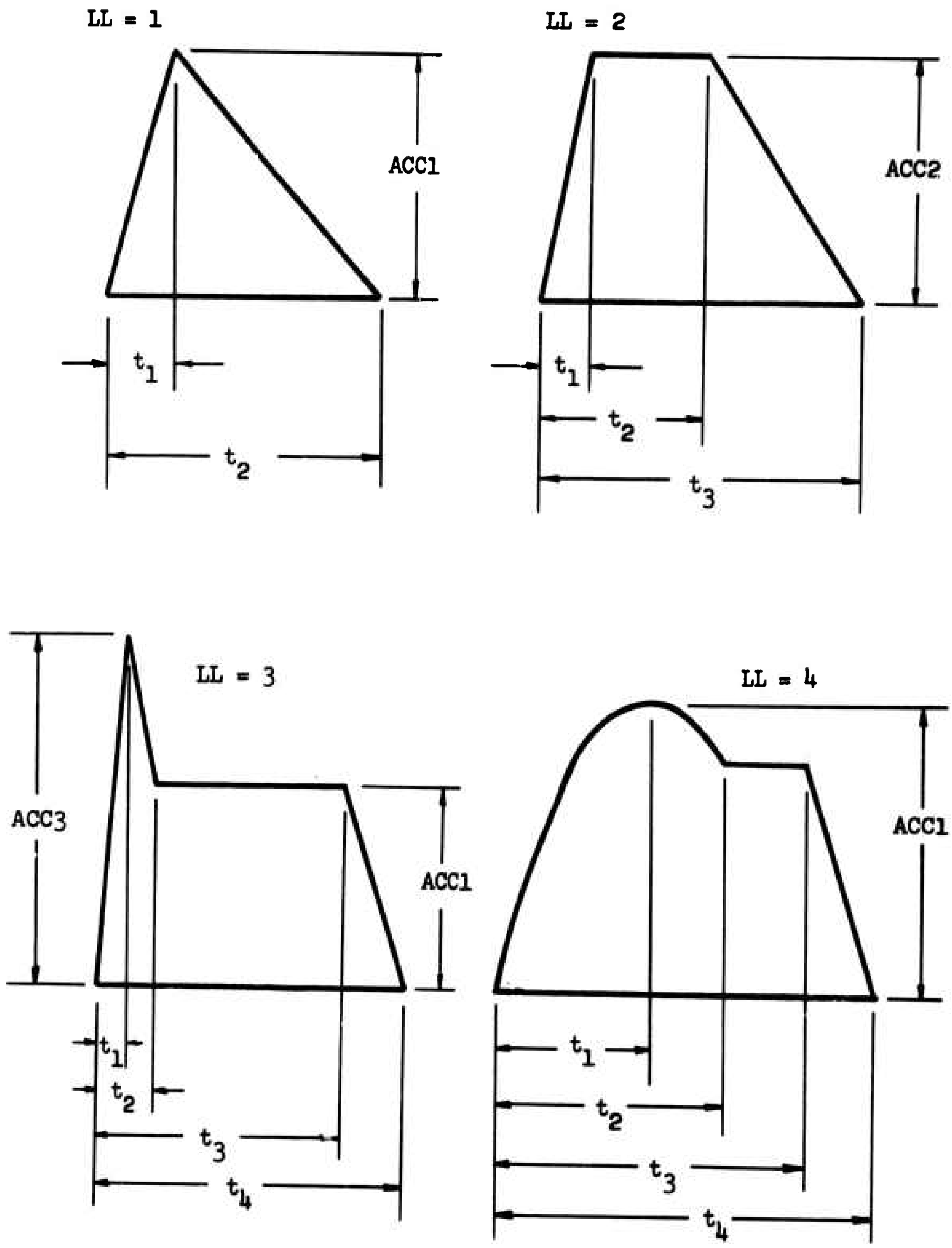

Figure 3. Acceleration Pulses Coded for Use in the Computer Study.

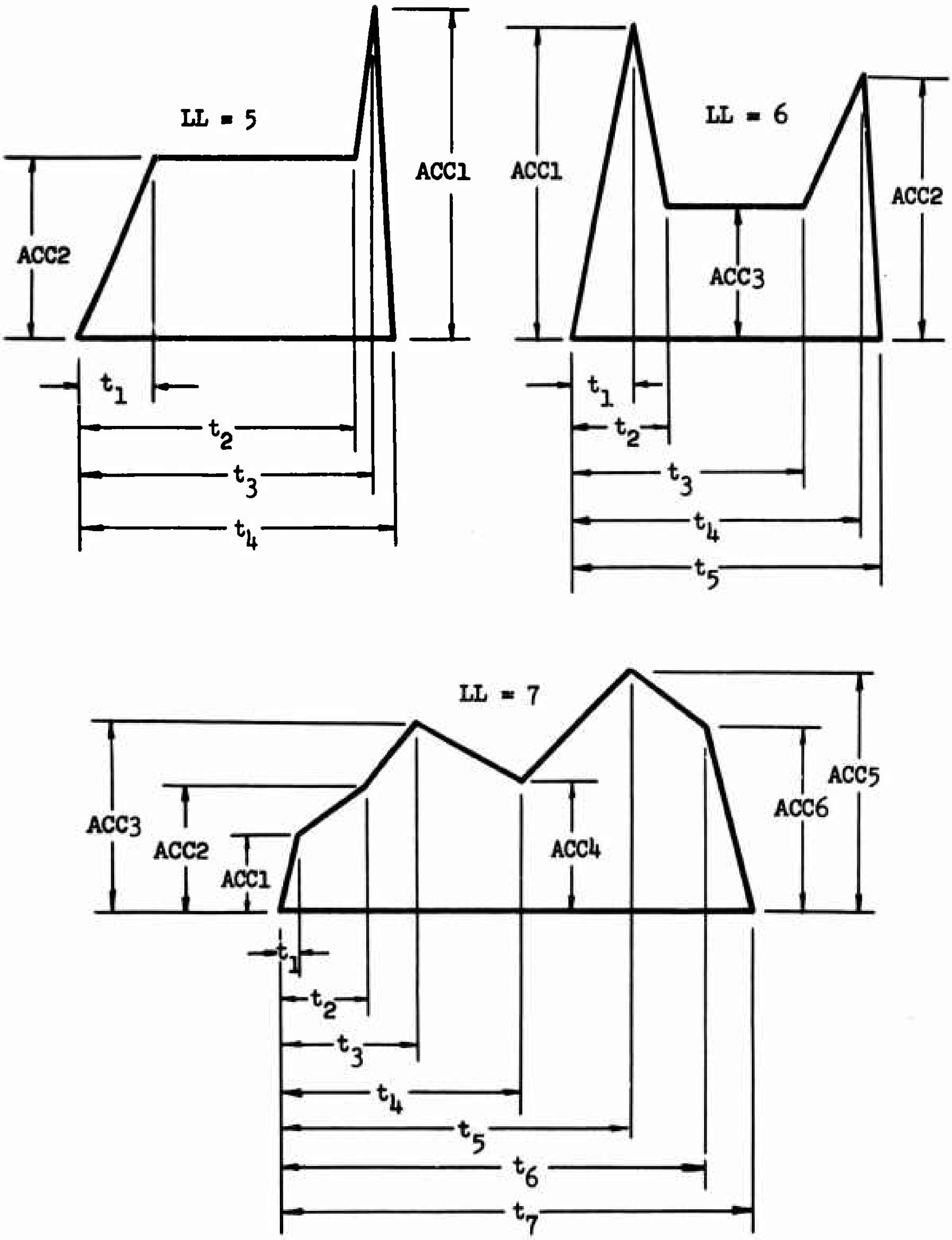

Figure 3 (contd.). Acceleration Pulses Coded for Use in the Computer Study.

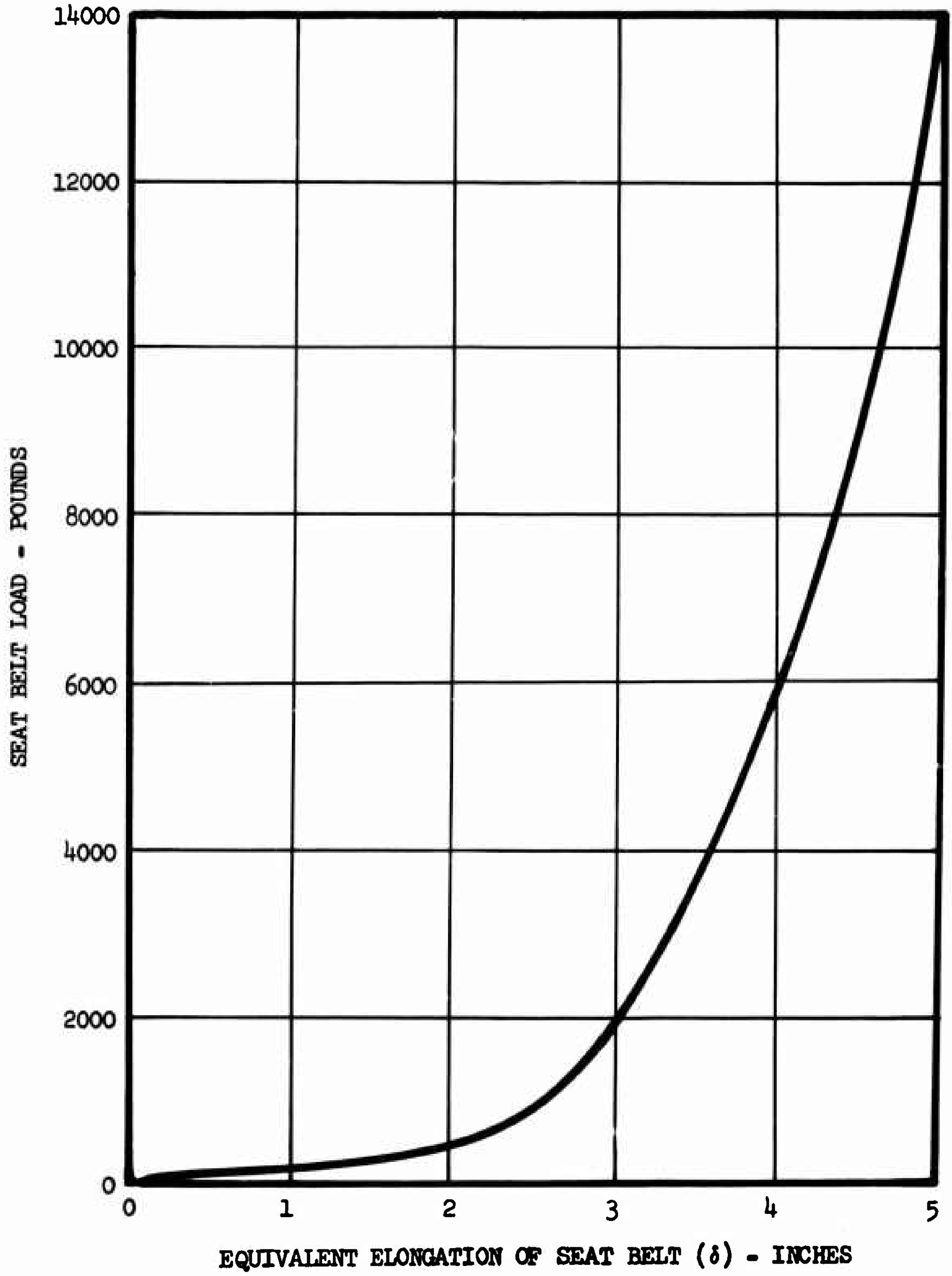

Figure 4. Load Versus Elongation Characteristics of the "Typical" Navy Seat Belt Used in All Calculations. (The effect of the human abdomen is included in the curve. The curve shown does not include the "rate effect", $k_{B5}\dot{\delta}$ (see Equation 18).)

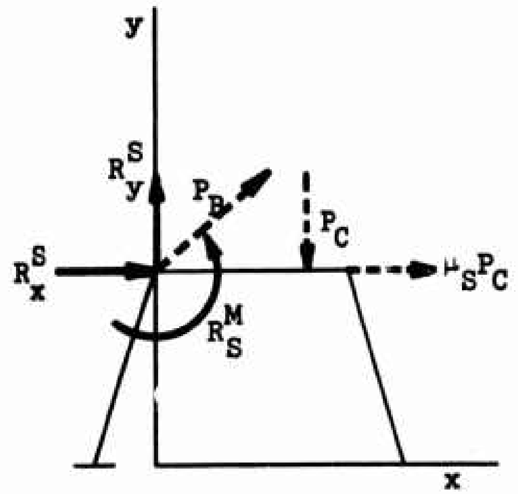

Figure 5. Seat Loads (P_B, P_C, $\mu_S P_C$) and Reactions (R_x^S, R_y^S, R_S^M).

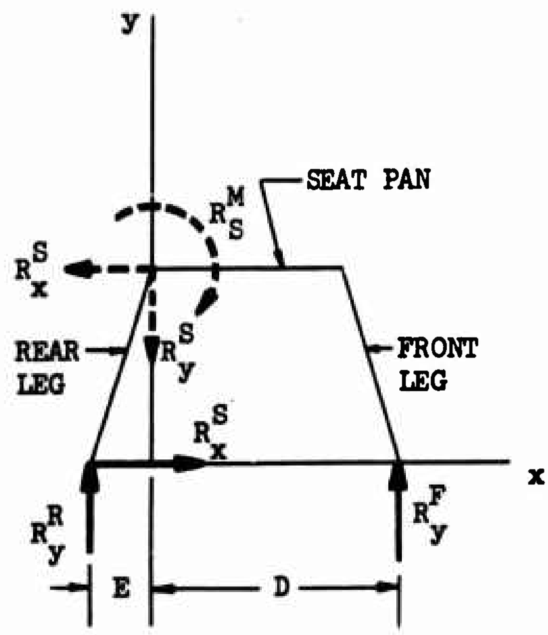

Figure 6 Seat Loads and Floor Reactions.

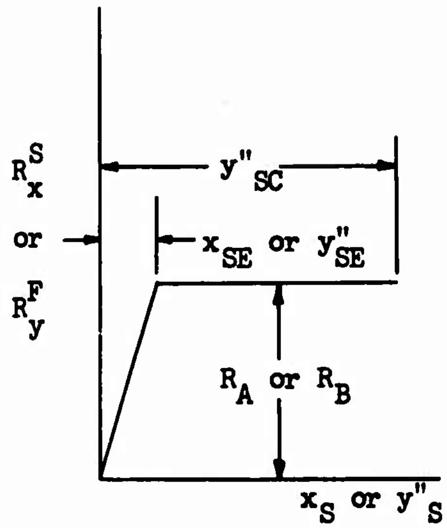

Figure 7. Assumed Load-Deflection Curve for Reactions R_x^S and R_y^F.

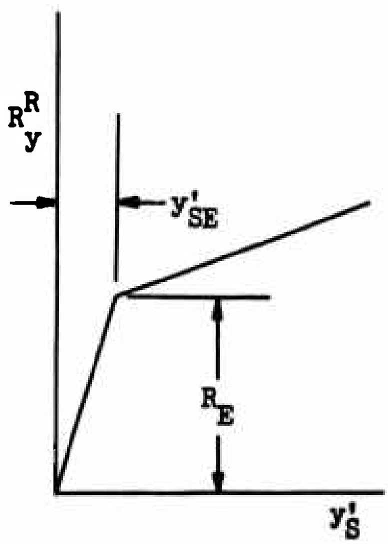

Figure 8. Assumed Load-Deflection Curve for Reaction R_y^R.

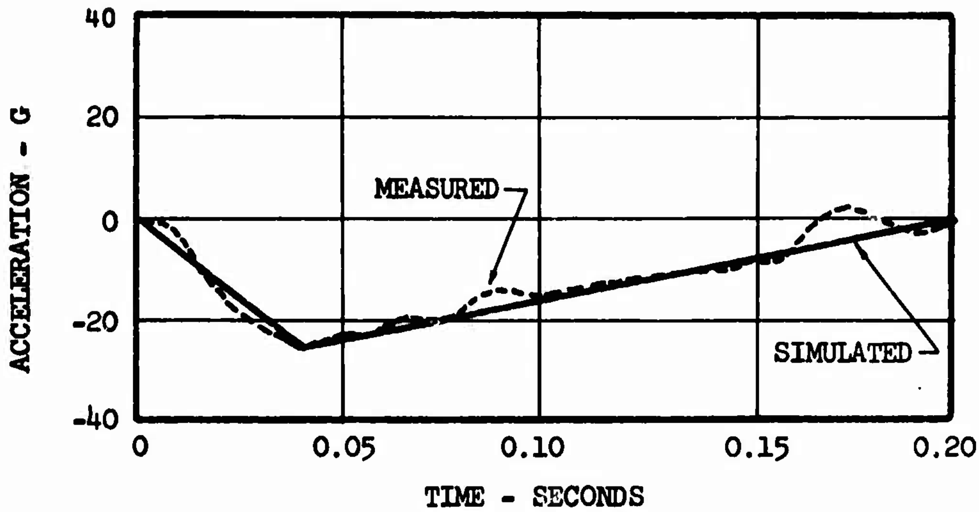

Figure 9. Simulated and Measured Longitudinal Sled Acceleration.

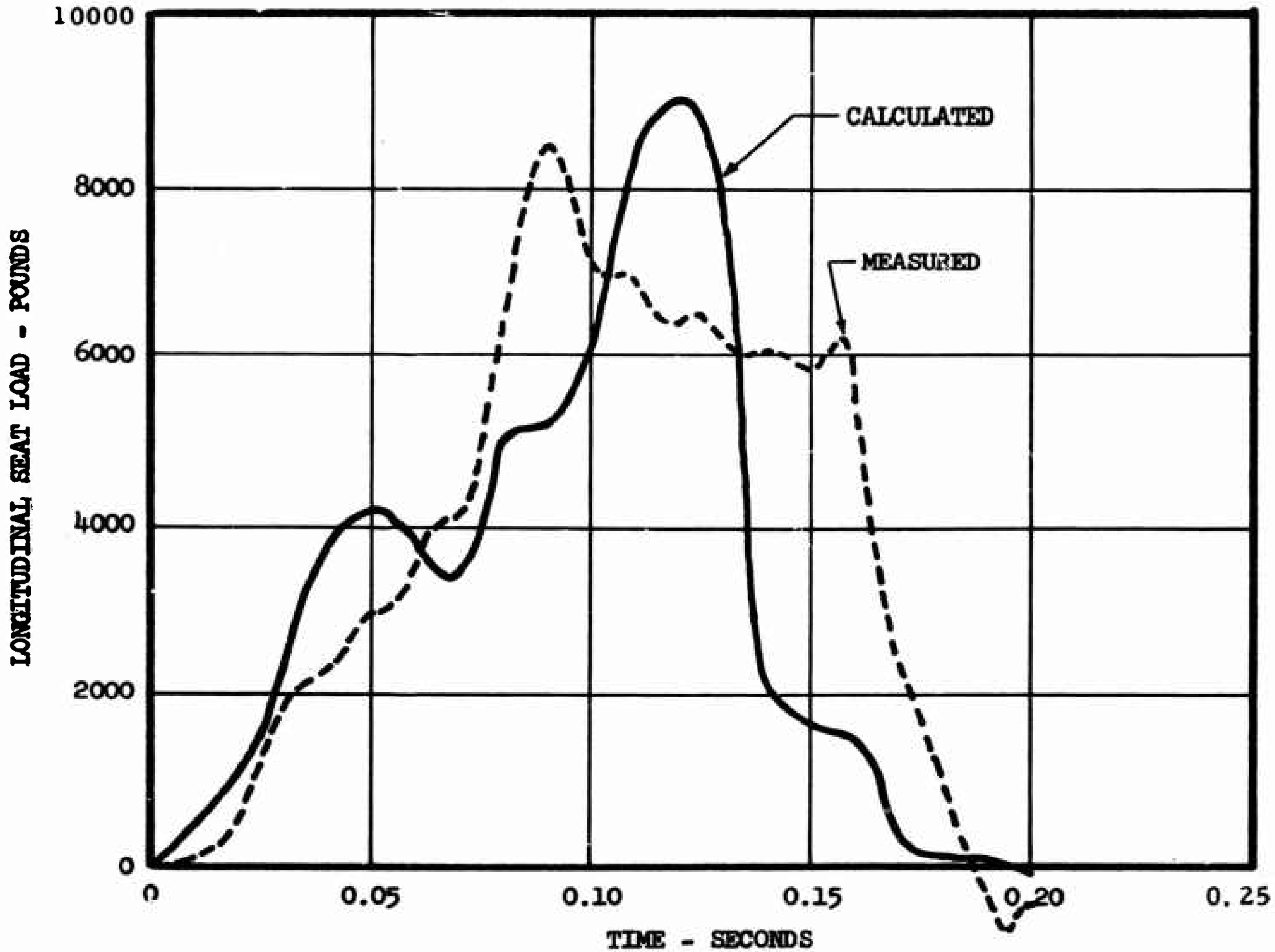

Figure 10. Calculated and Measured Longitudinal Load Versus Time.

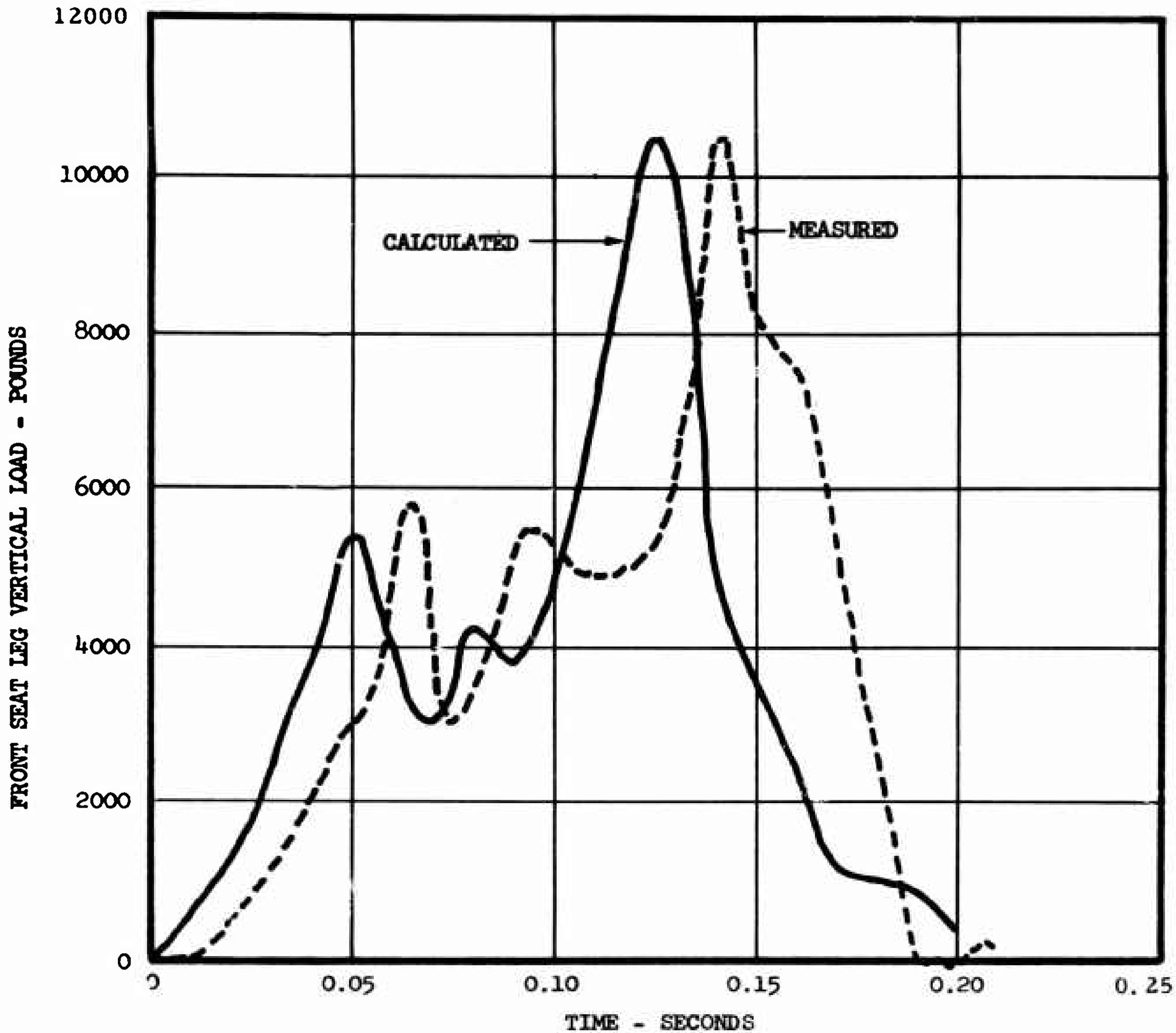

Figure 11. Calculated and Measured Front Leg Vertical Load Versus Time.

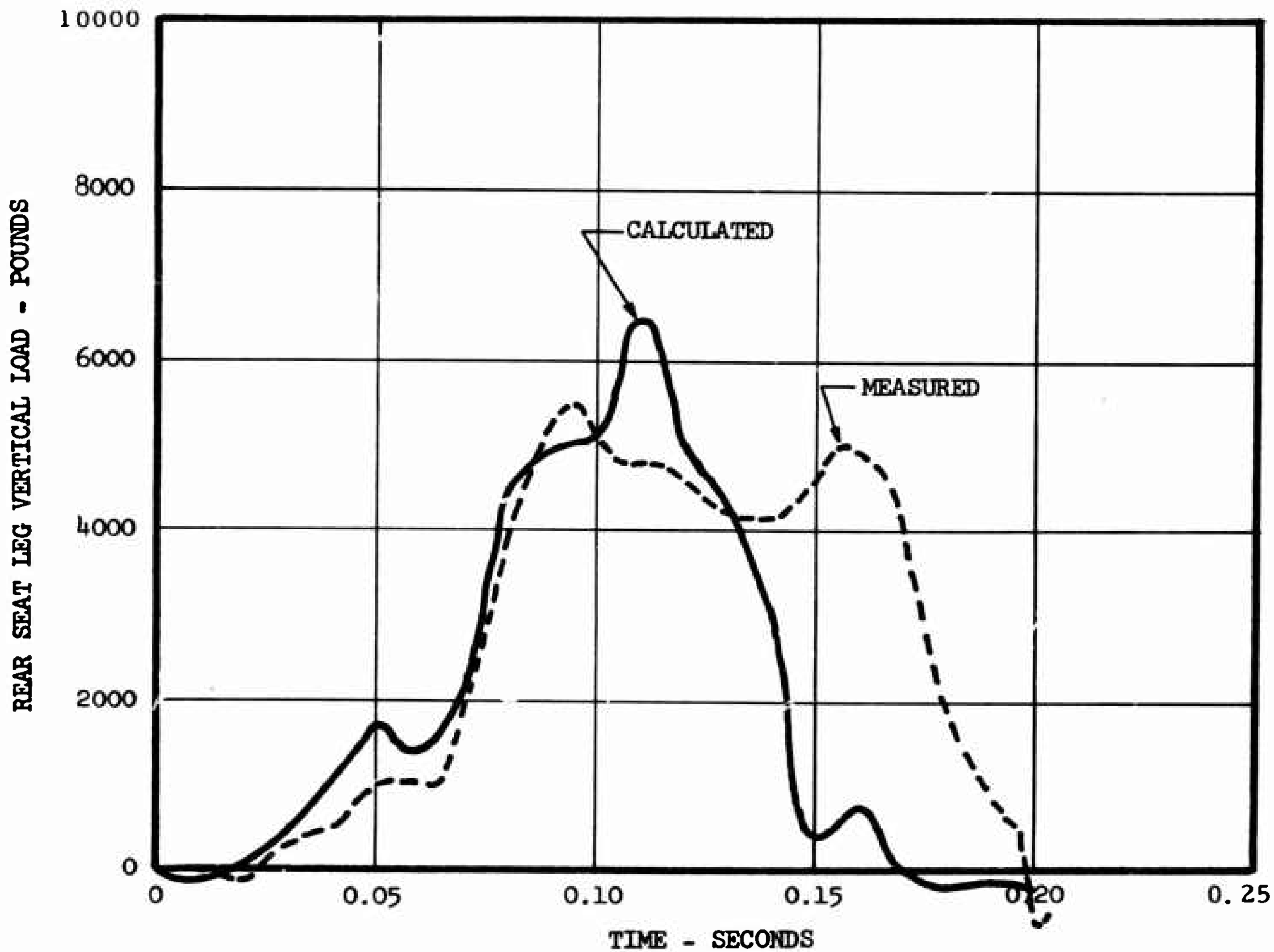

Figure 12. Calculated and Measured Rear Leg Vertical Load Versus Time.

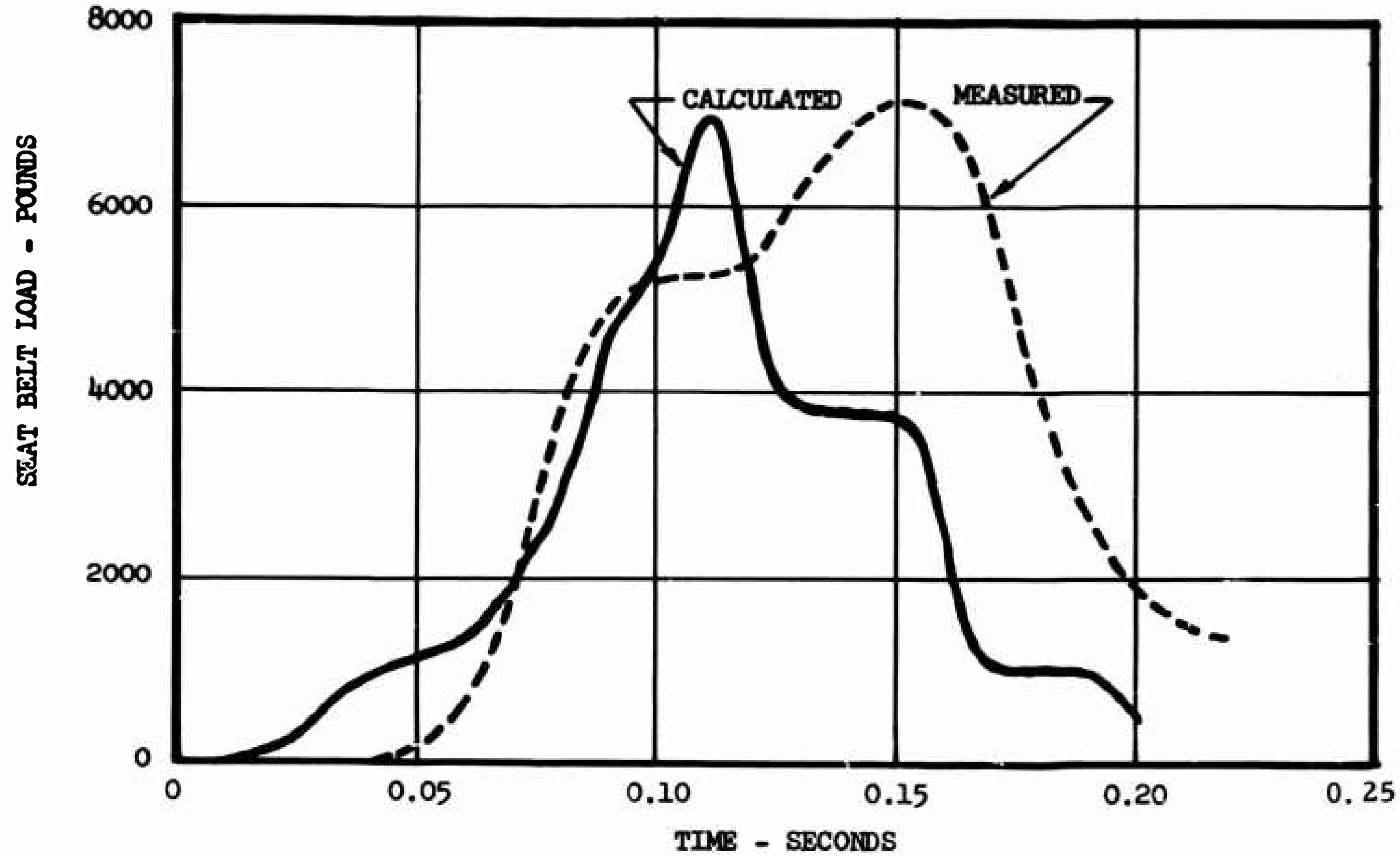

Figure 13. Calculated and Measured Seat Belt Load Versus Time.

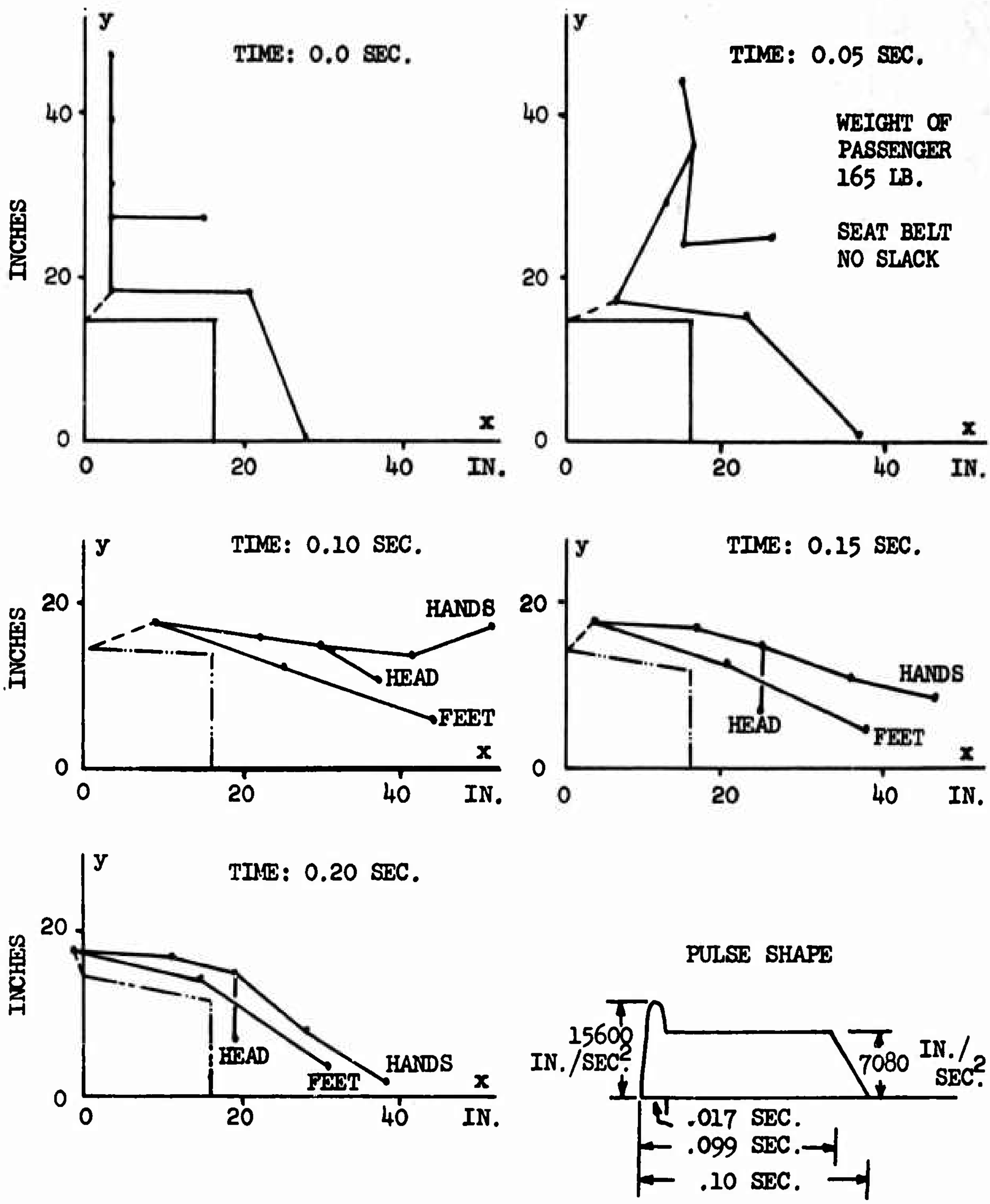

Figure 14. Displacement Response of Passenger to Trapezoidal Pulse of 0.10 Second With Sinusoidal Spike. $A_y/A_x = 0.20$.

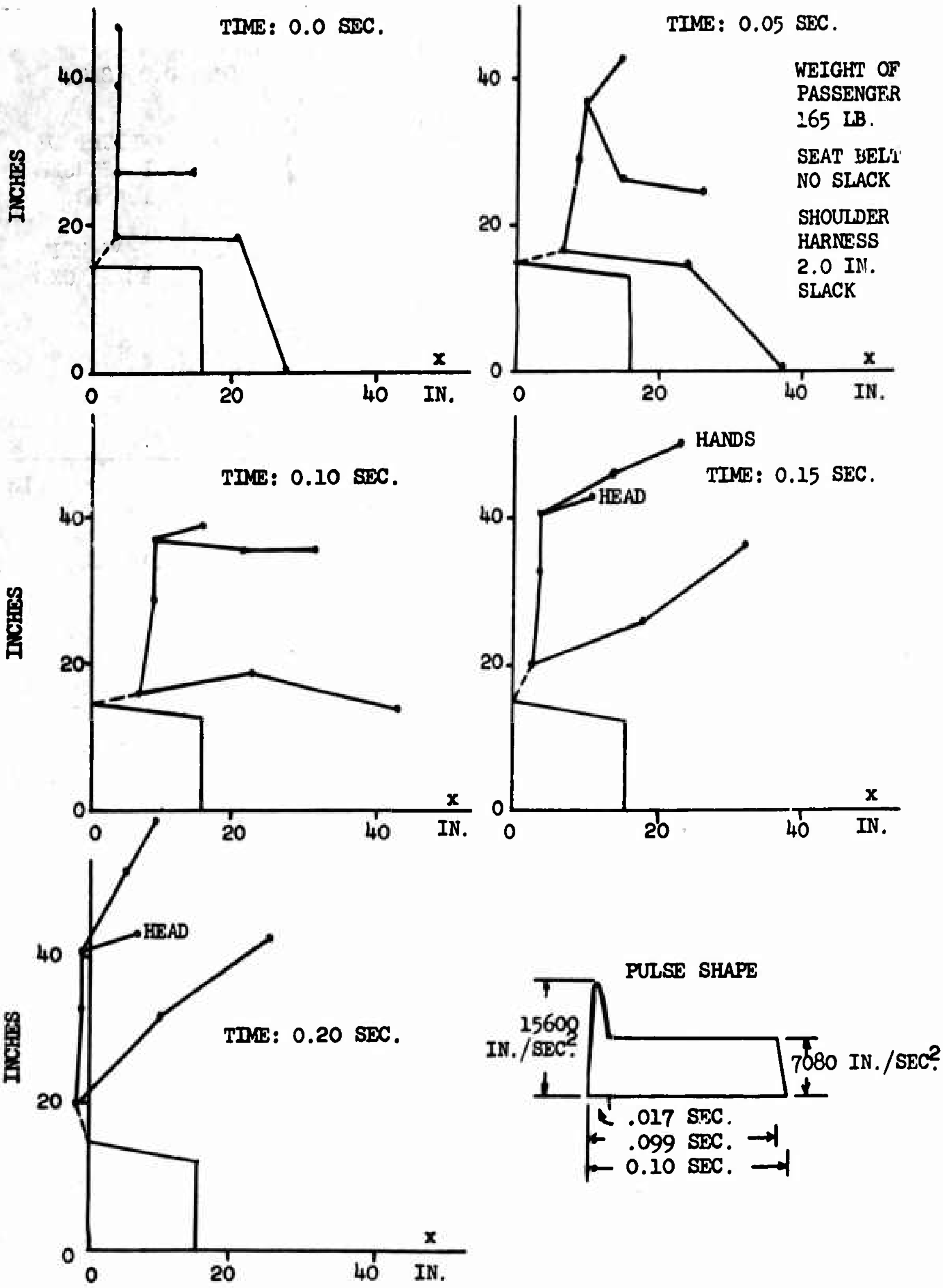

Figure 15. Displacement Response of Passenger to Trapezoidal Pulse of 0.10 Second With Sinusoidal Spike. $A_y/A_x = 0.20$.

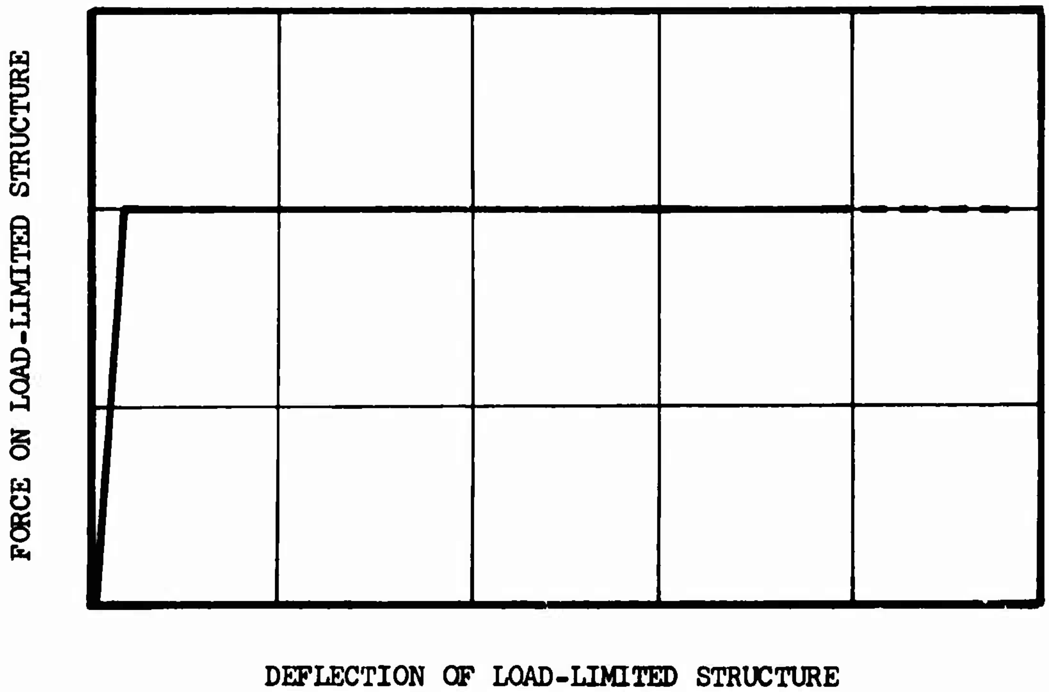

Figure 16. Ideal Relation Between Force and Deflection in a Load-Limited Structure.

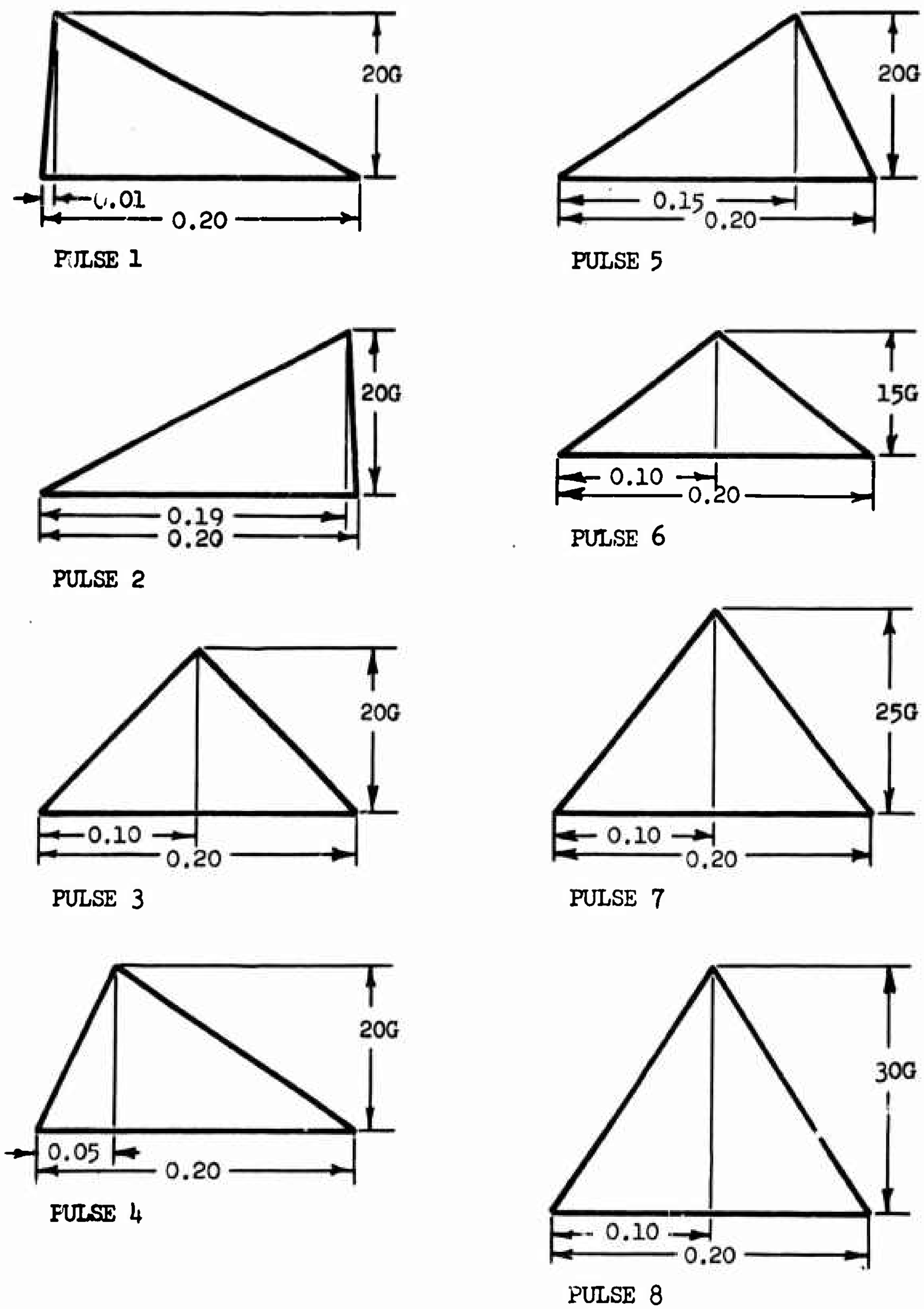

Figure 17. Initial Selection of Pulses for Use in the Study of the Response of Seat-Passenger Systems to Impulsive Loading.

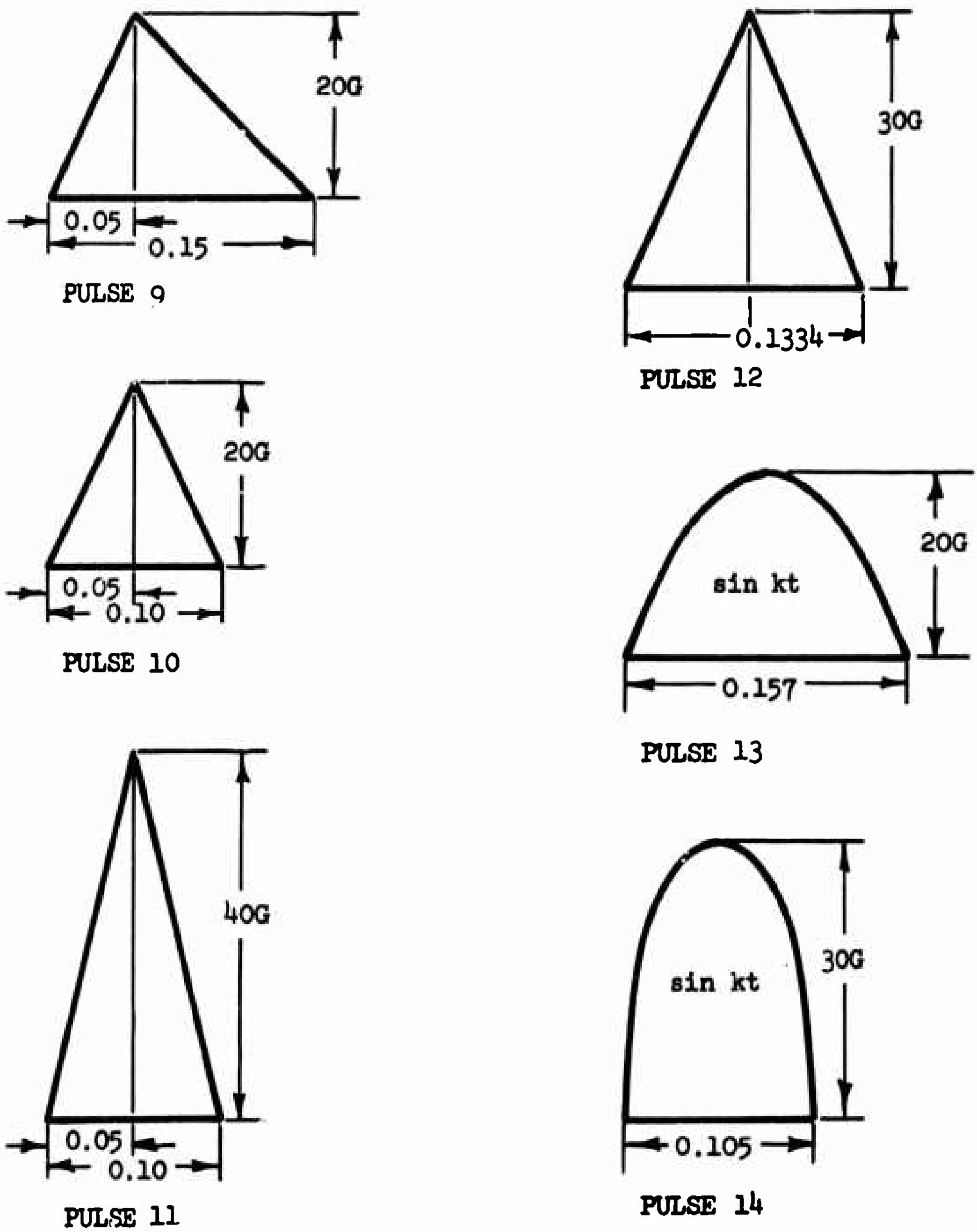

Figure 17 (contd.). Initial Selection of Pulses for Use in the Study of the Response of Seat-Passenger Systems to Impulsive Loading.

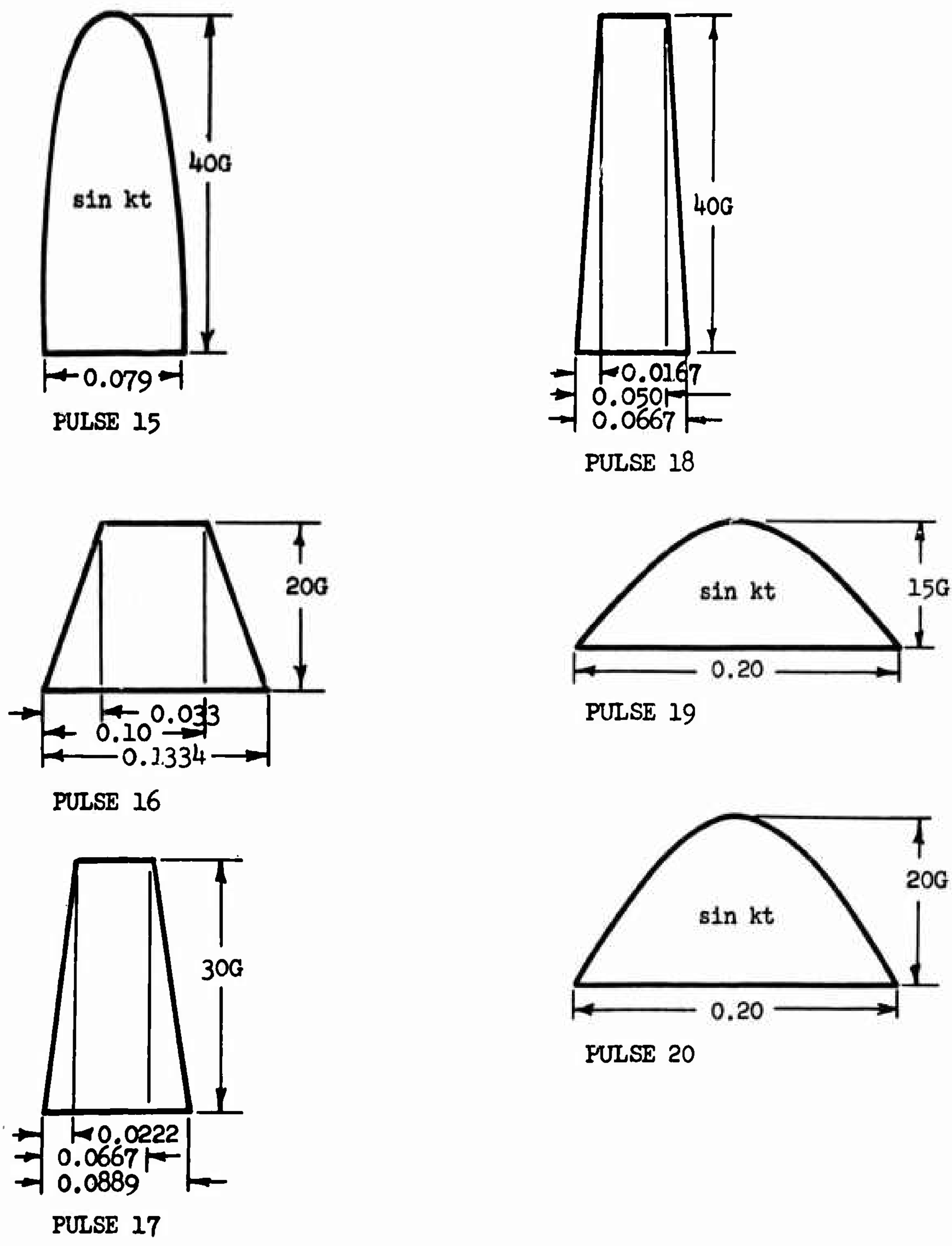

Figure 17 (contd.). Initial Selection of Pulses for Use in the Study of the Response of Seat-Passenger Systems to Impulsive Loading.

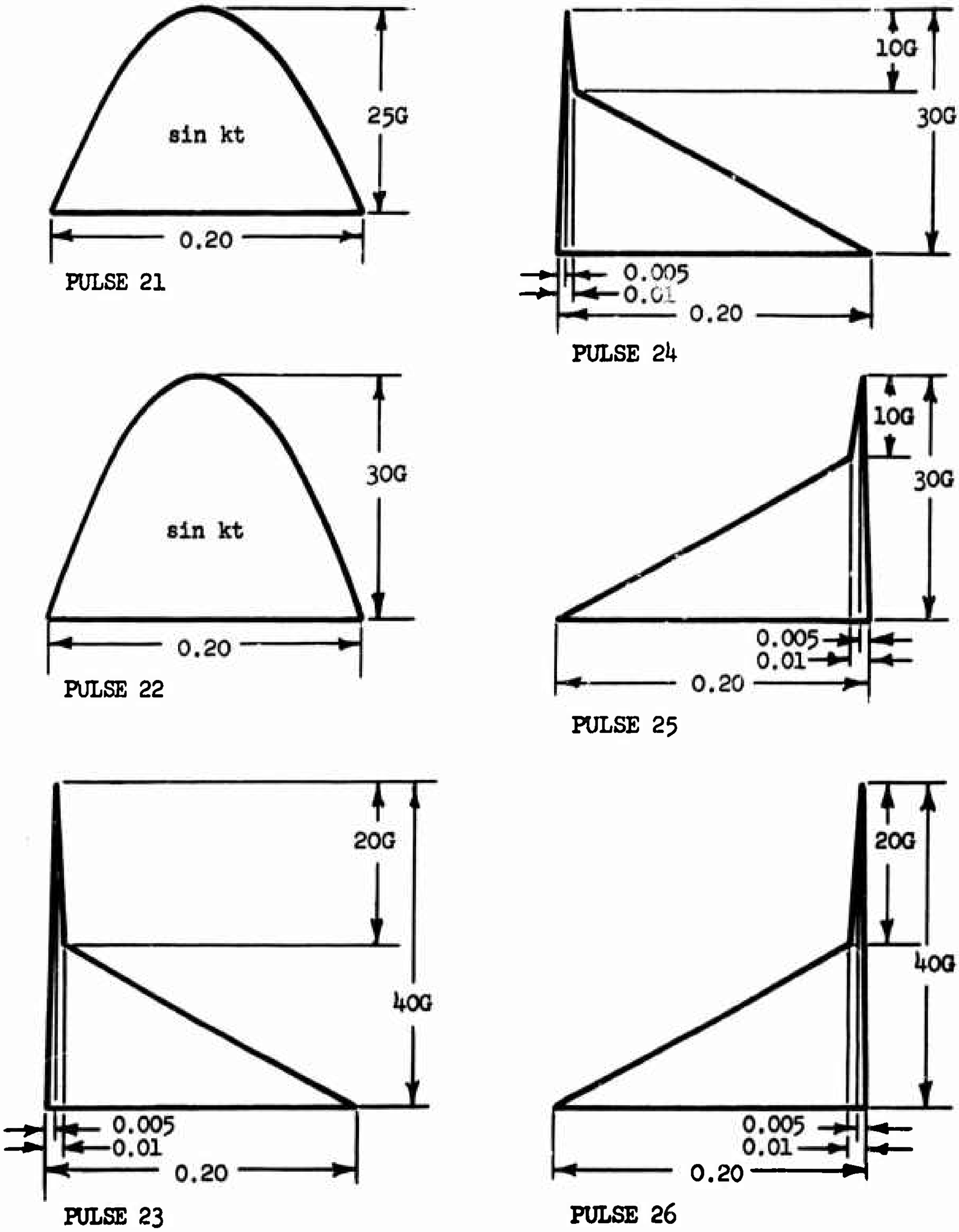

Figure 17 (contd.). Initial Selection of Pulses for Use in the Study of the Response of Seat-Passenger Systems to Impulsive Loading.

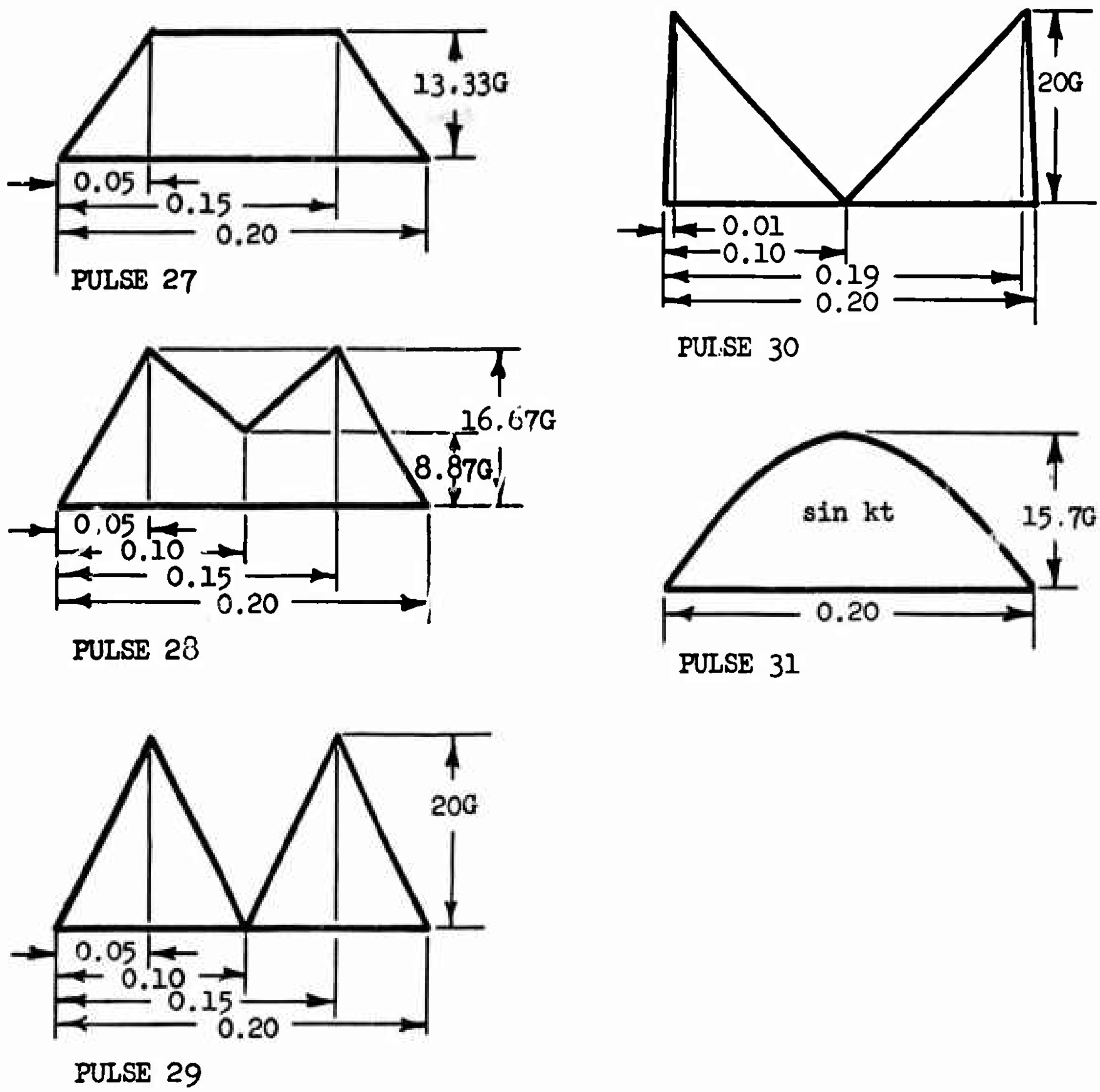

Figure 17 (contd.). Initial Selection of Pulses for Use in the Study of the Response of Seat-Passenger Systems to Impulsive Loading.

Figures 18 through 26

Design Variables as Functions of Time for Triangular Crash Pulses

(See p. 39)

Pulse 1

Pulse 2

Pulse 3

Pulse 4

Pulse 5

(For pulse shapes see Figure 17)

Seat Belt	Typical (see Figure 4)
Passenger Weight	187 pounds
Load-Limiter Setting	3396, 5660, and 7924 pounds
Ratio of Vertical to Horizontal Acceleration	0.2
Additional Input Conditions	See Table II, column A

Caution:

While qualitative trends and comparisons may be dependably observed in the results presented, quantitative values should be used with caution. Due to changes and improvements in the computer program during preparation of the curves, current best estimates may differ somewhat from the data presented. For example, see Appendix III, page 285.

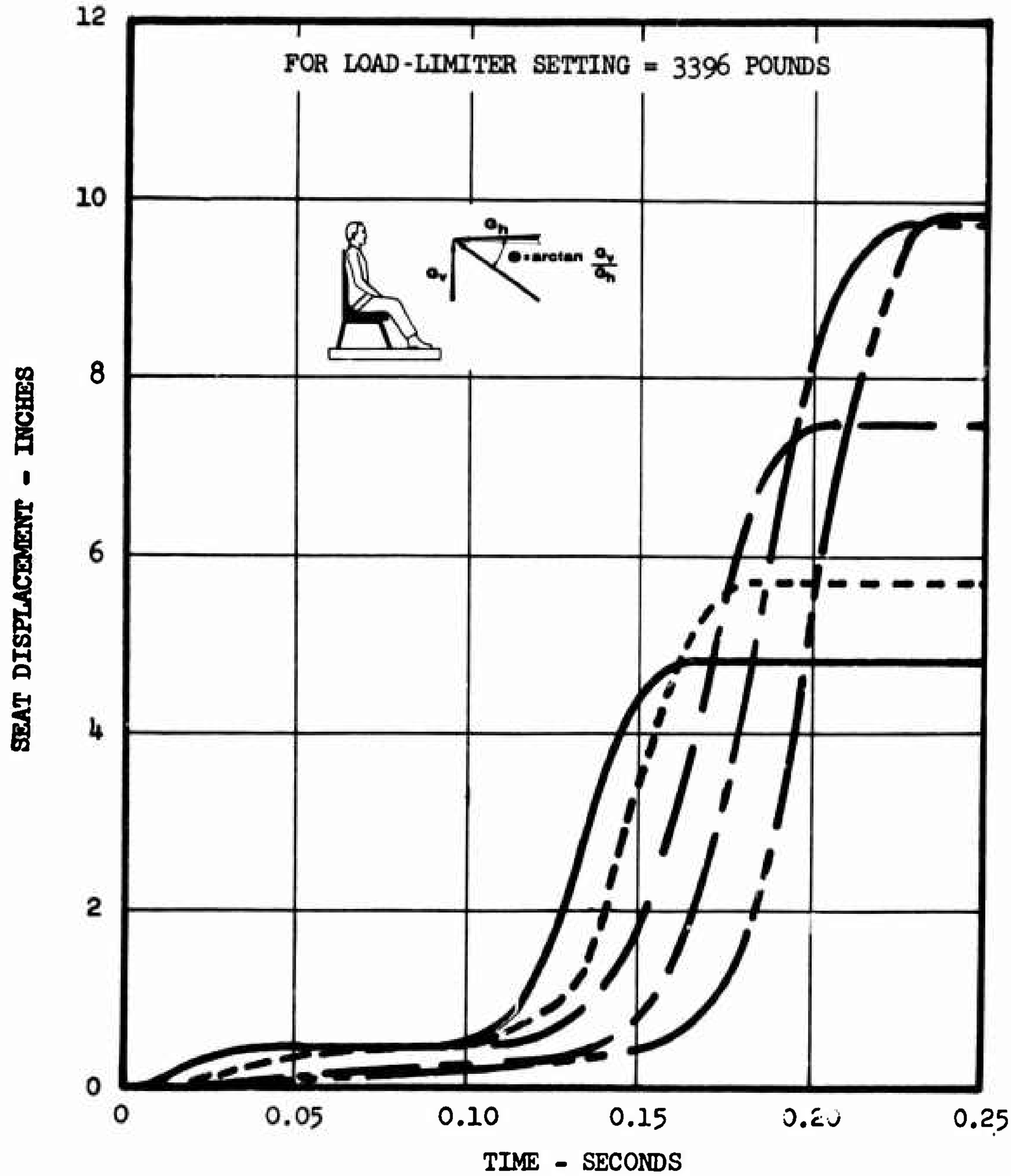

Figure 18. Seat Displacement Versus Time.

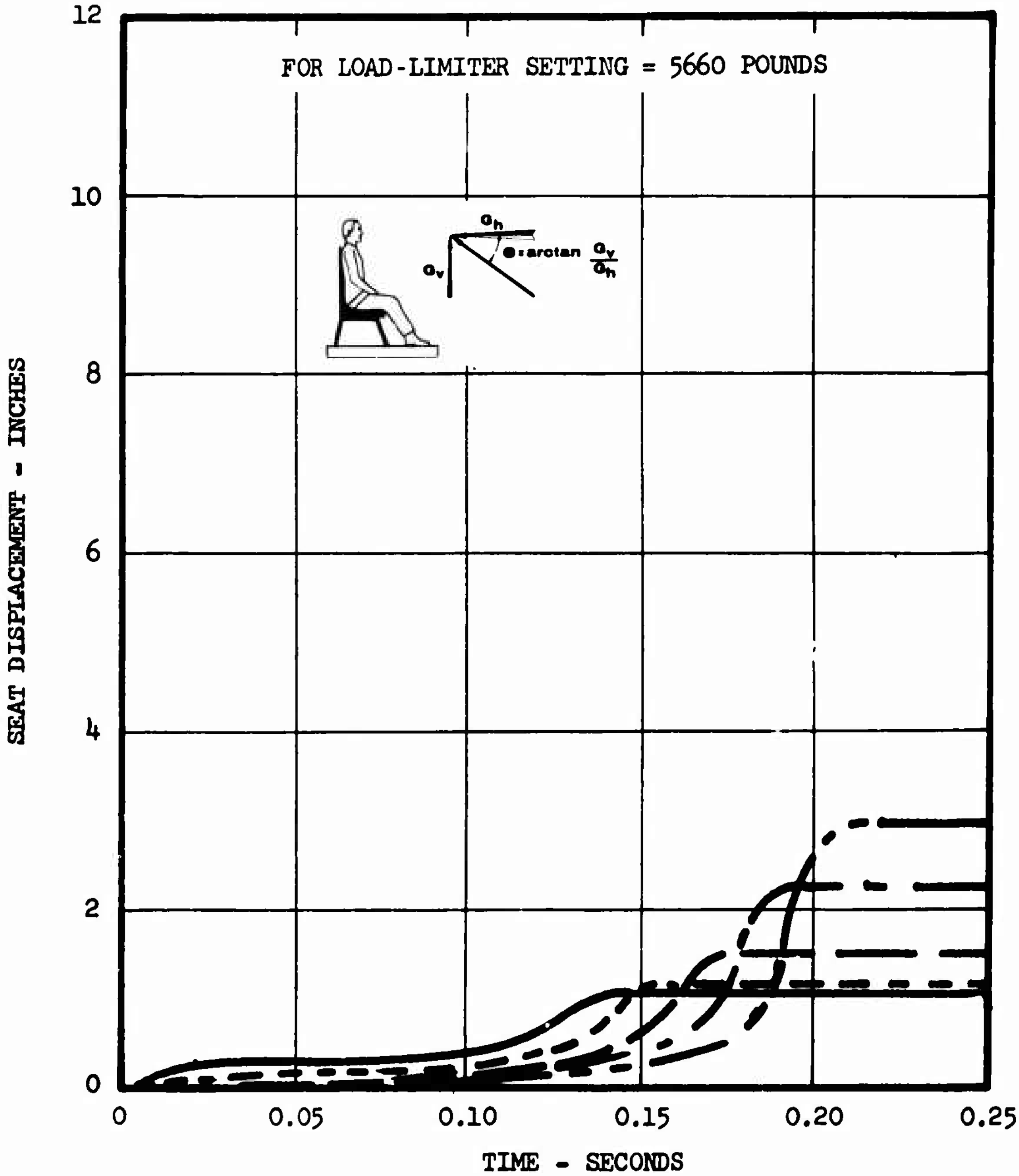

Figure 19. Seat Displacement Versus Time.

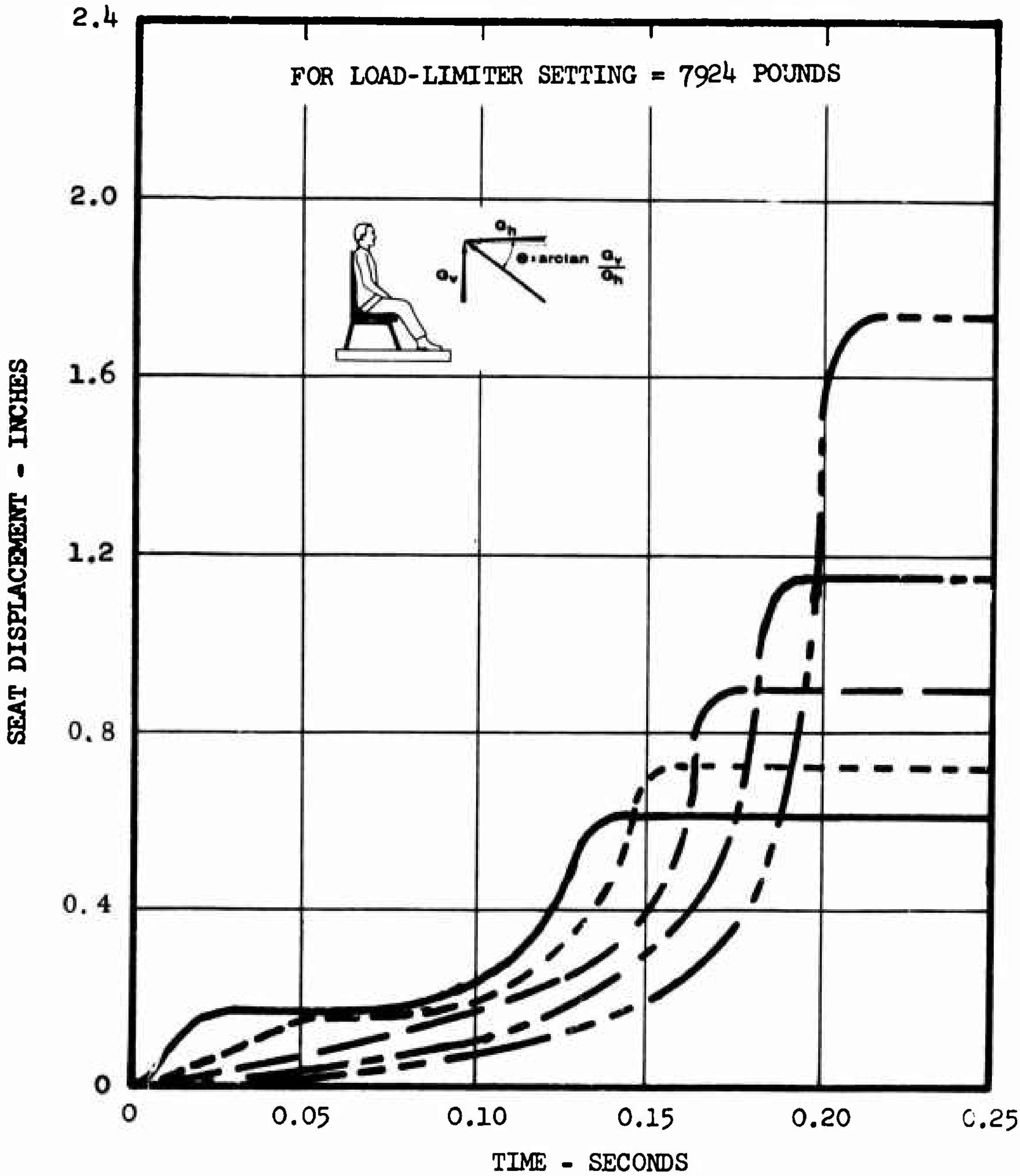

Figure 20. Seat Displacement Versus Time.

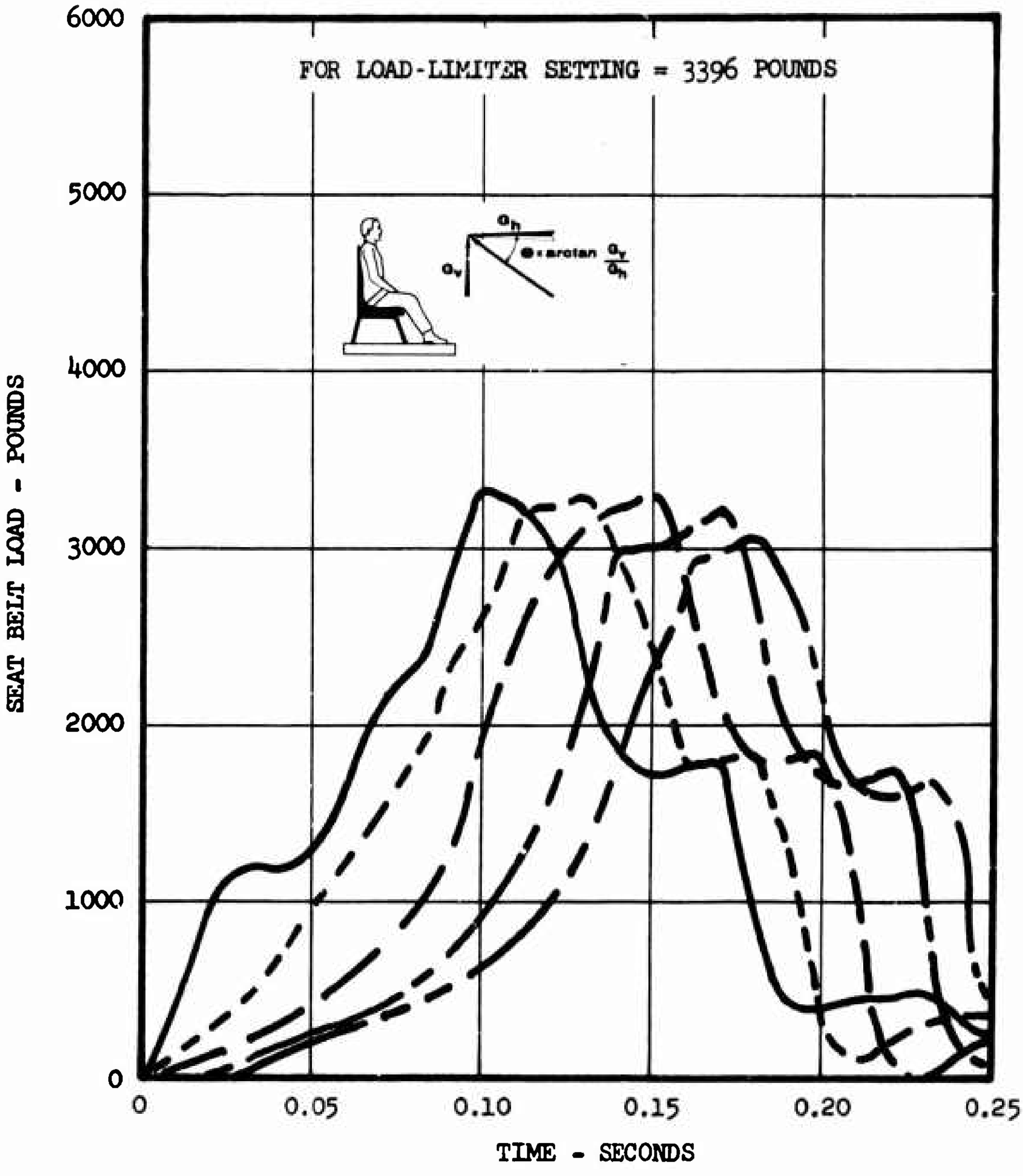

Figure 21. Seat Belt Load Versus Time.

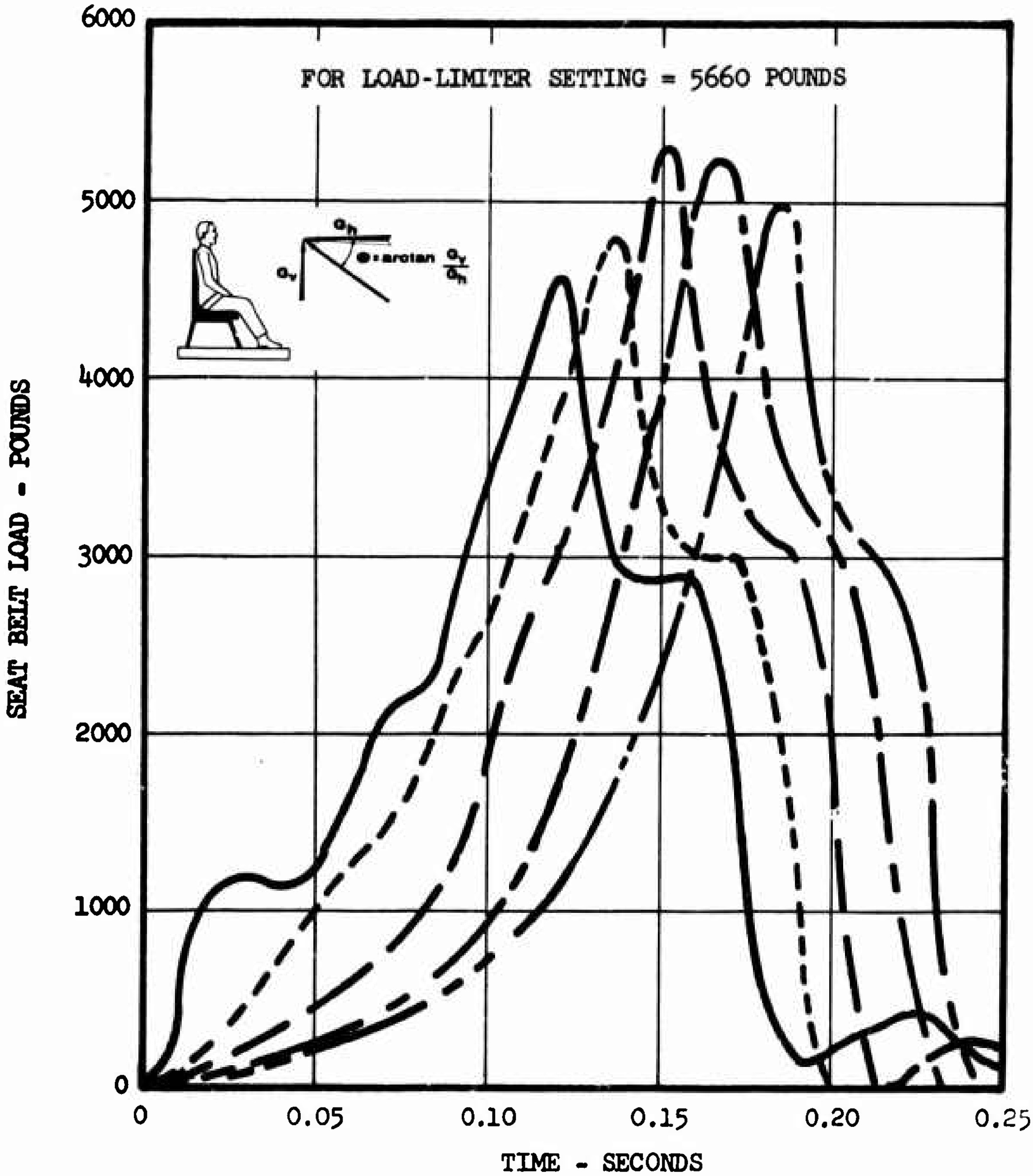

Figure 22. Seat Belt Load Versus Time.

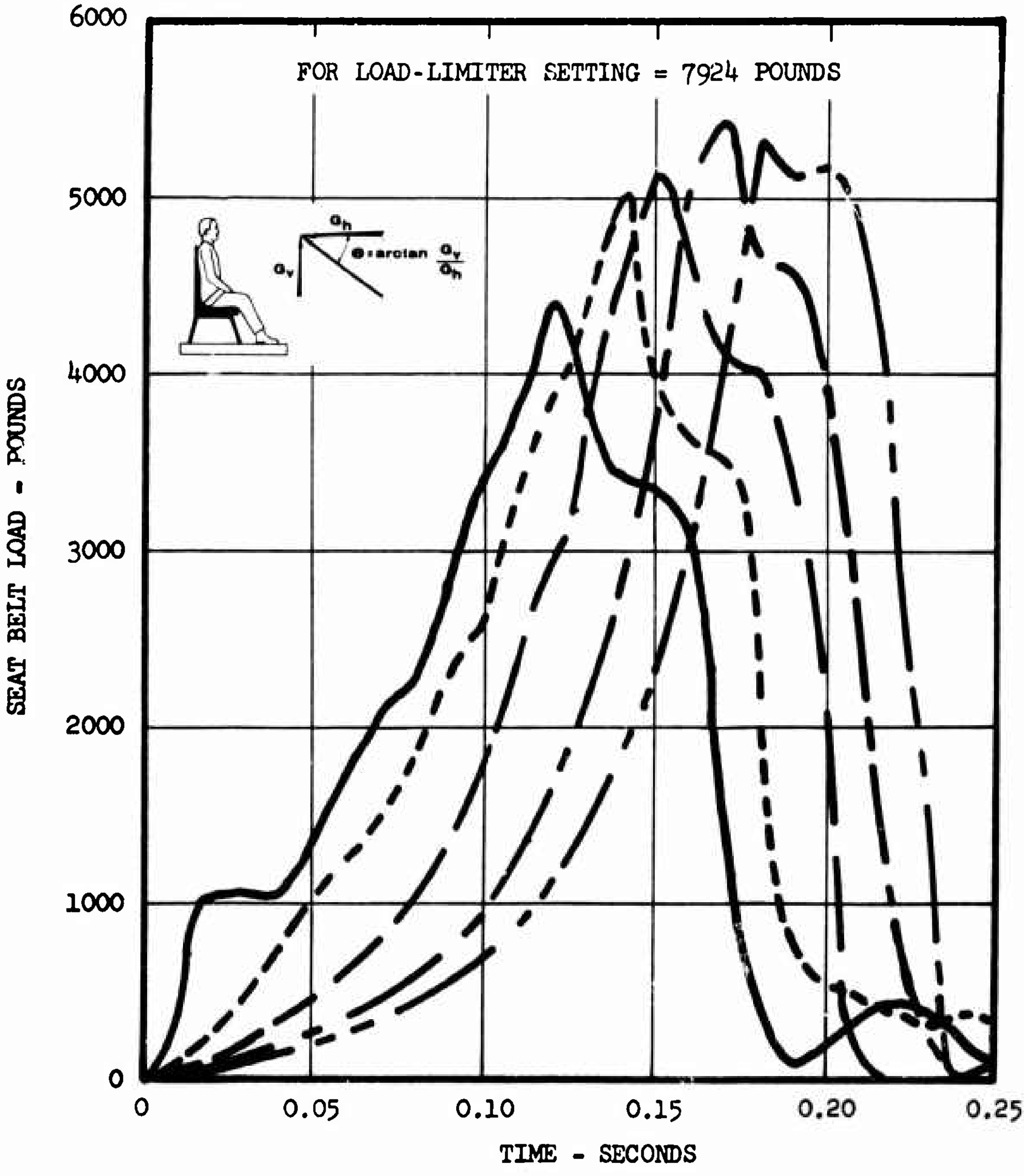

Figure 23. Seat Belt Load Versus Time.

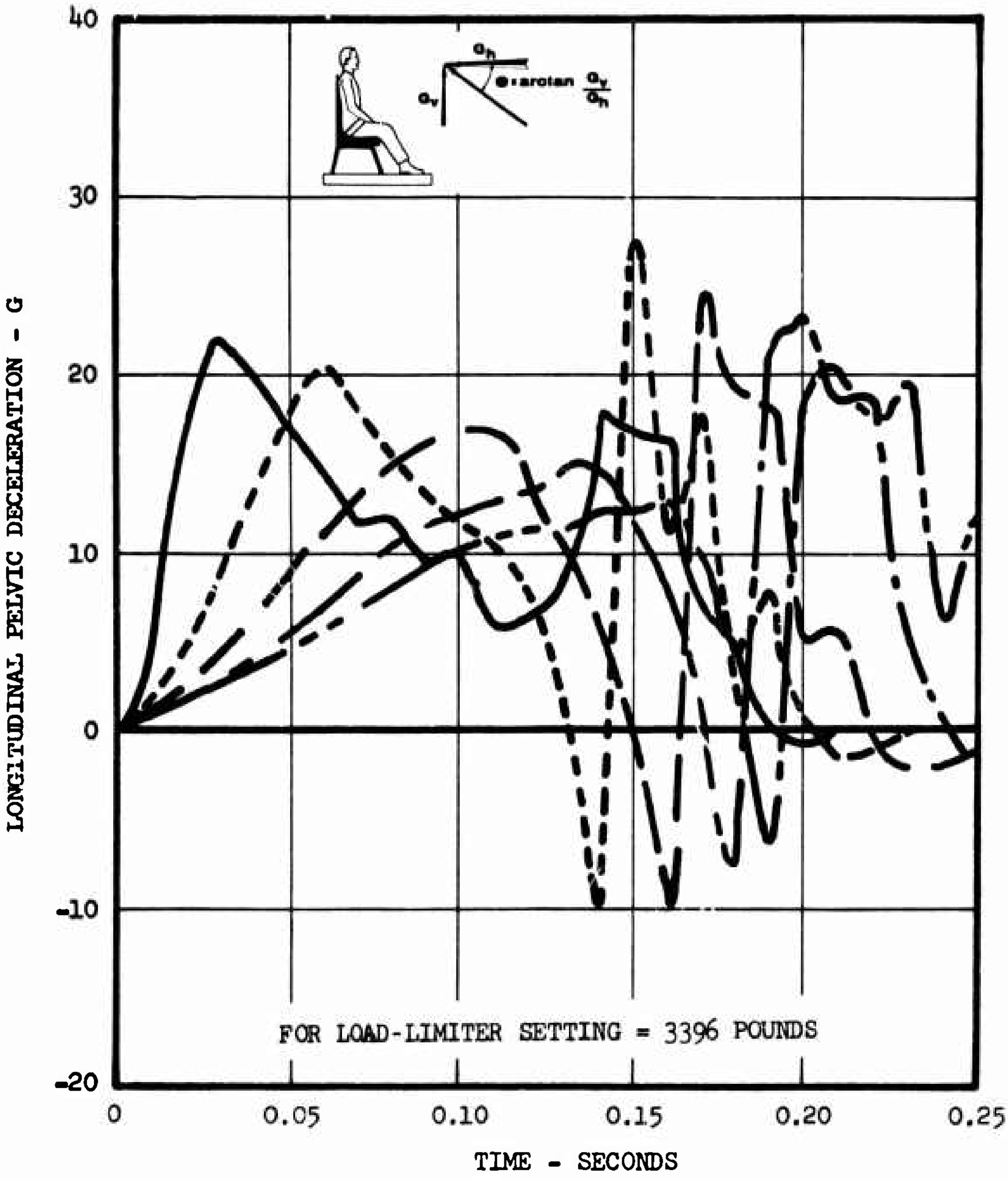

Figure 24. Longitudinal Pelvic Deceleration Versus Time.

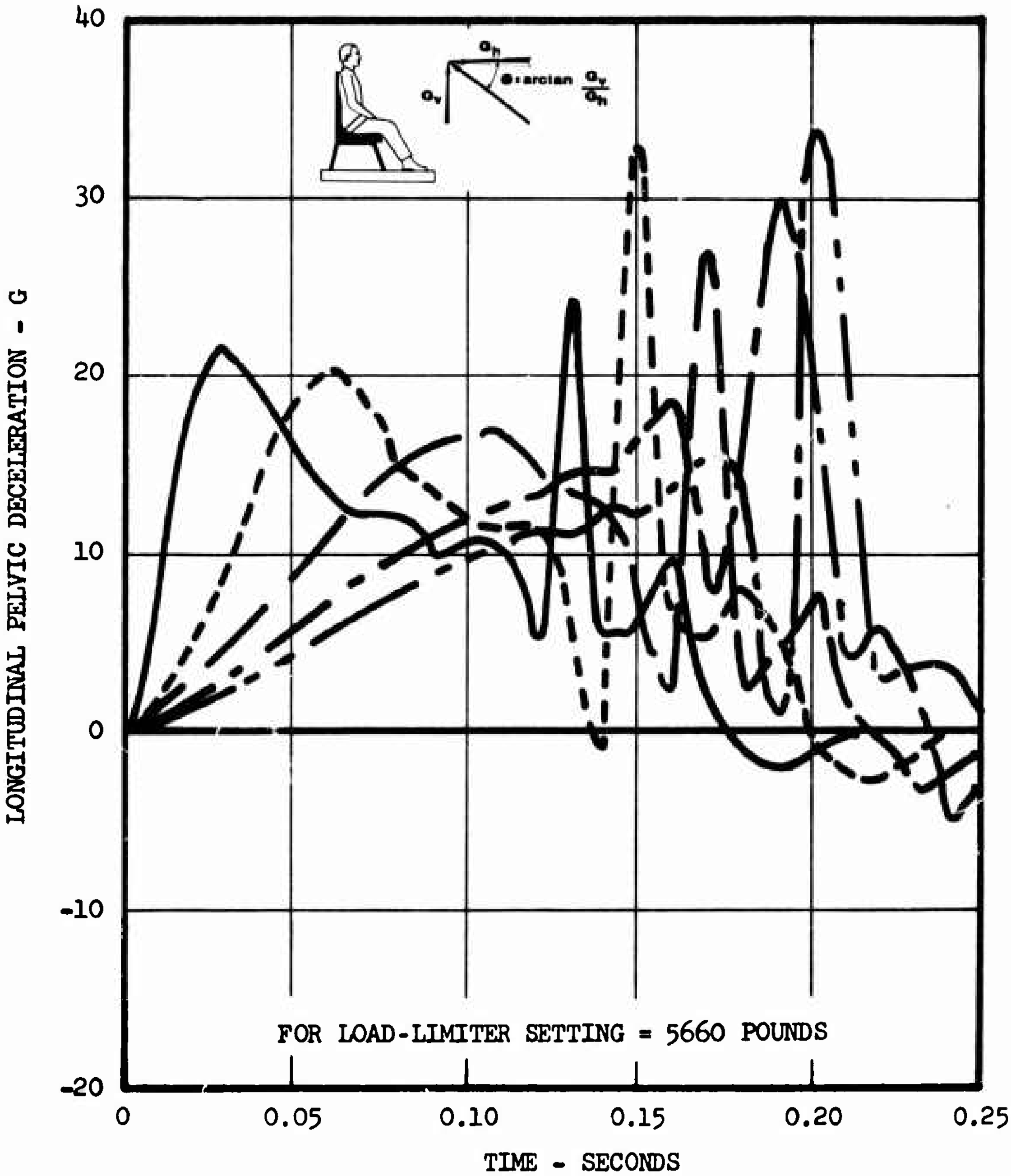

Figure 25. Longitudinal Pelvic Deceleration Versus Time.

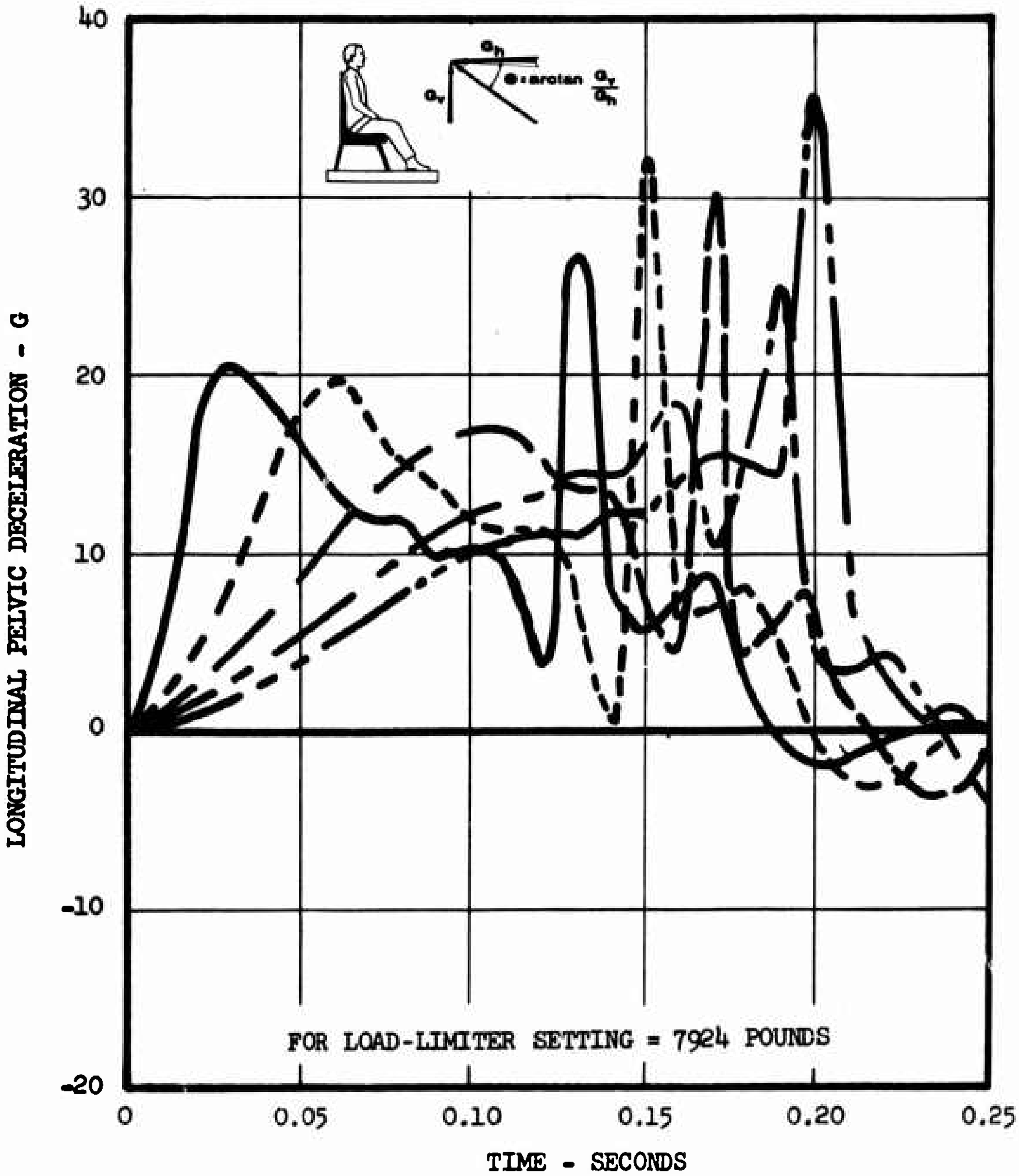

Figure 26. Longitudinal Pelvic Deceleration Versus Time.

Figures 27 through 34

Design Variables as Functions of Time for Trapezoidal Crash Pulses

(See p. 40)

Pulse 3	————————————
Pulse 16	- - - - - - - - - - - - - -
Pulse 18*	— — — — — —

(For pulse shapes see Figure 17)

Seat Belt	Typical (see Figure 4)
Passenger Weight	187 pounds
Load-Limiter Setting	5660 pounds
Ratio of Vertical to Horizontal Acceleration	0.2
Additional Input Conditions	See Table II, column B

Caution:
While qualitative trends and comparisons may be dependably observed in the results presented, quantitative values should be used with caution. Due to changes and improvements in the computer program during preparation of the curves, current best estimates may differ somewhat from the data presented. For example, see Appendix III, page 285.

*Seat damping coefficients are zero in computer program.

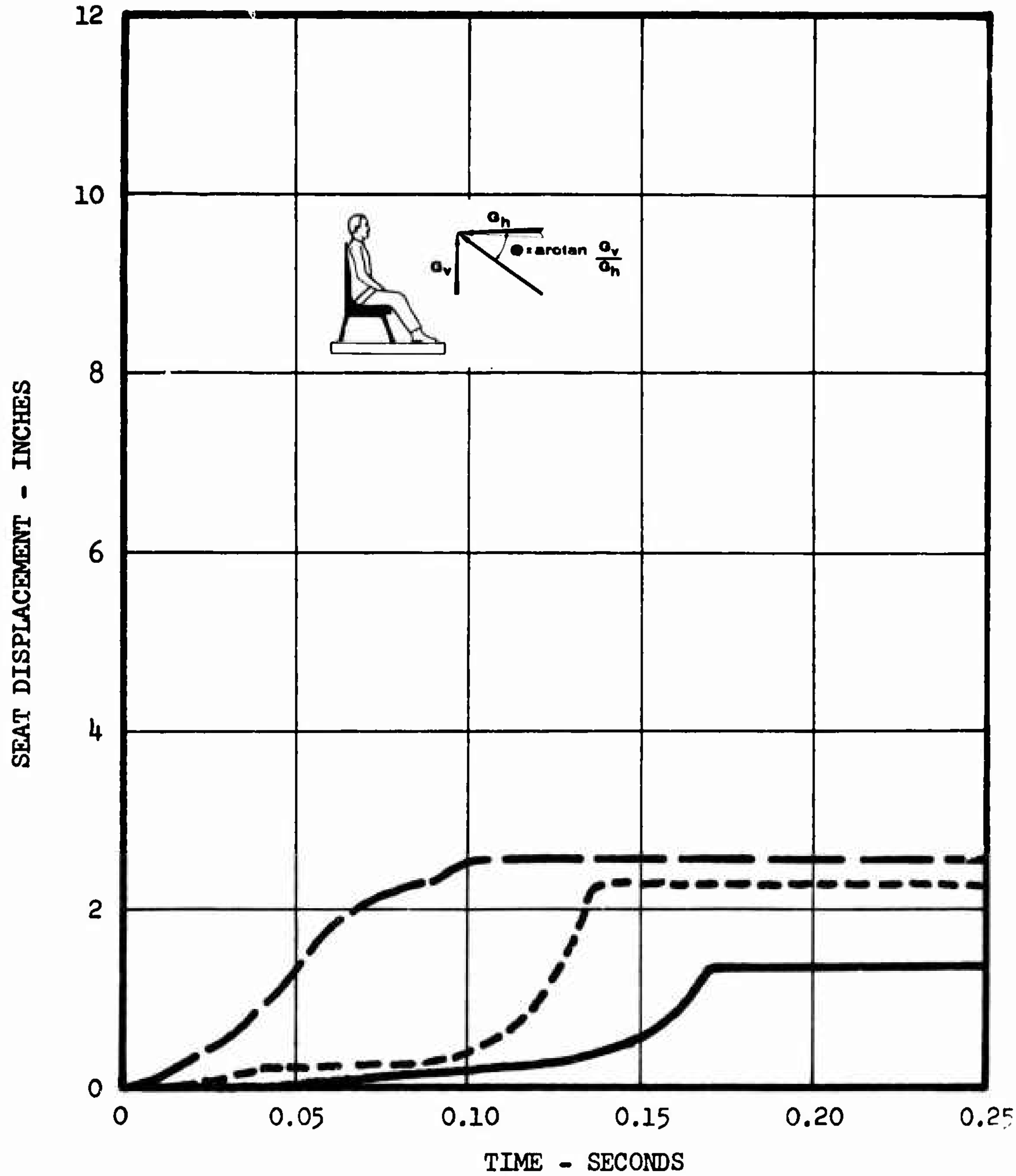

Figure 27. Seat Displacement Versus Time.

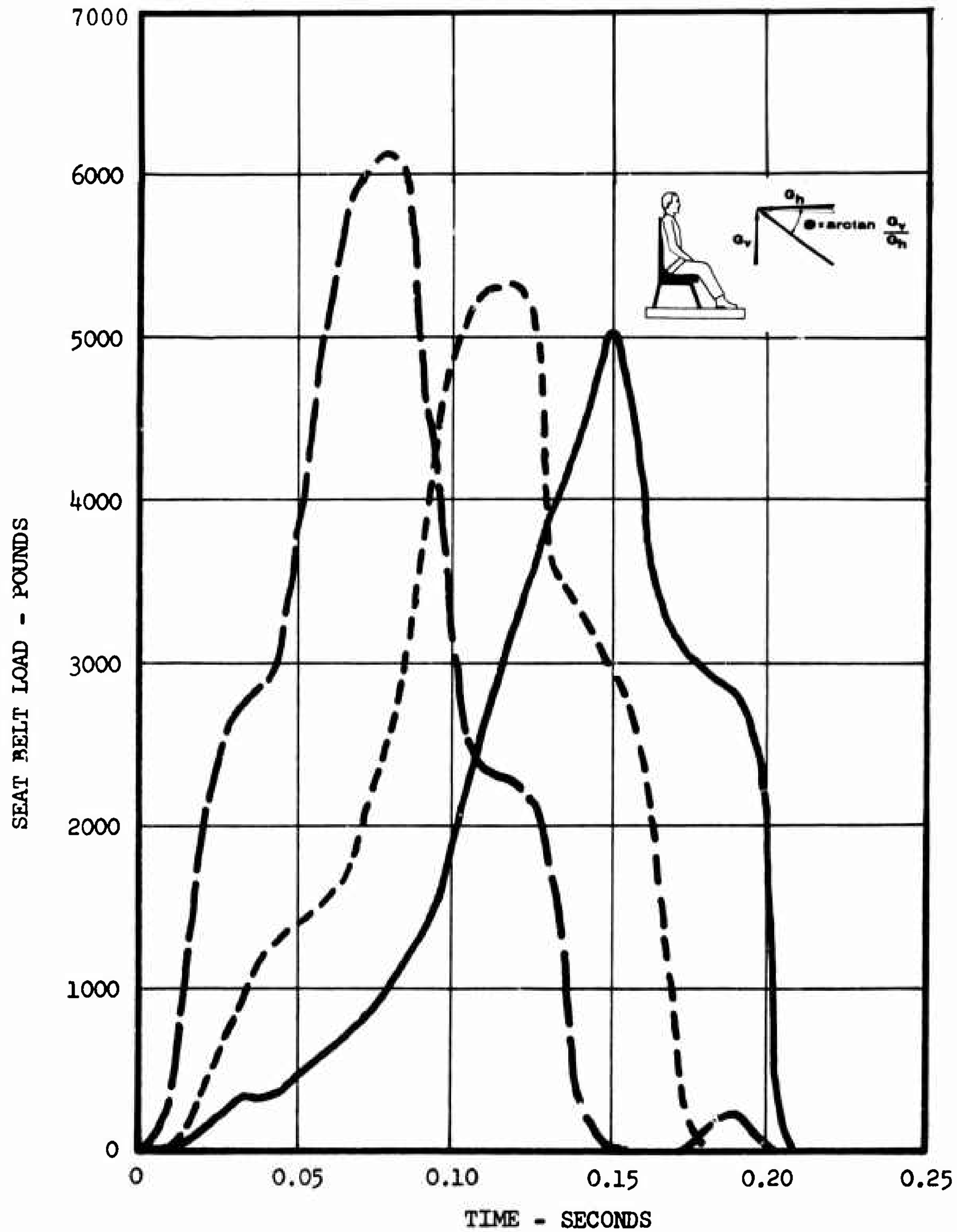

Figure 28. Seat Belt Load Versus Time.

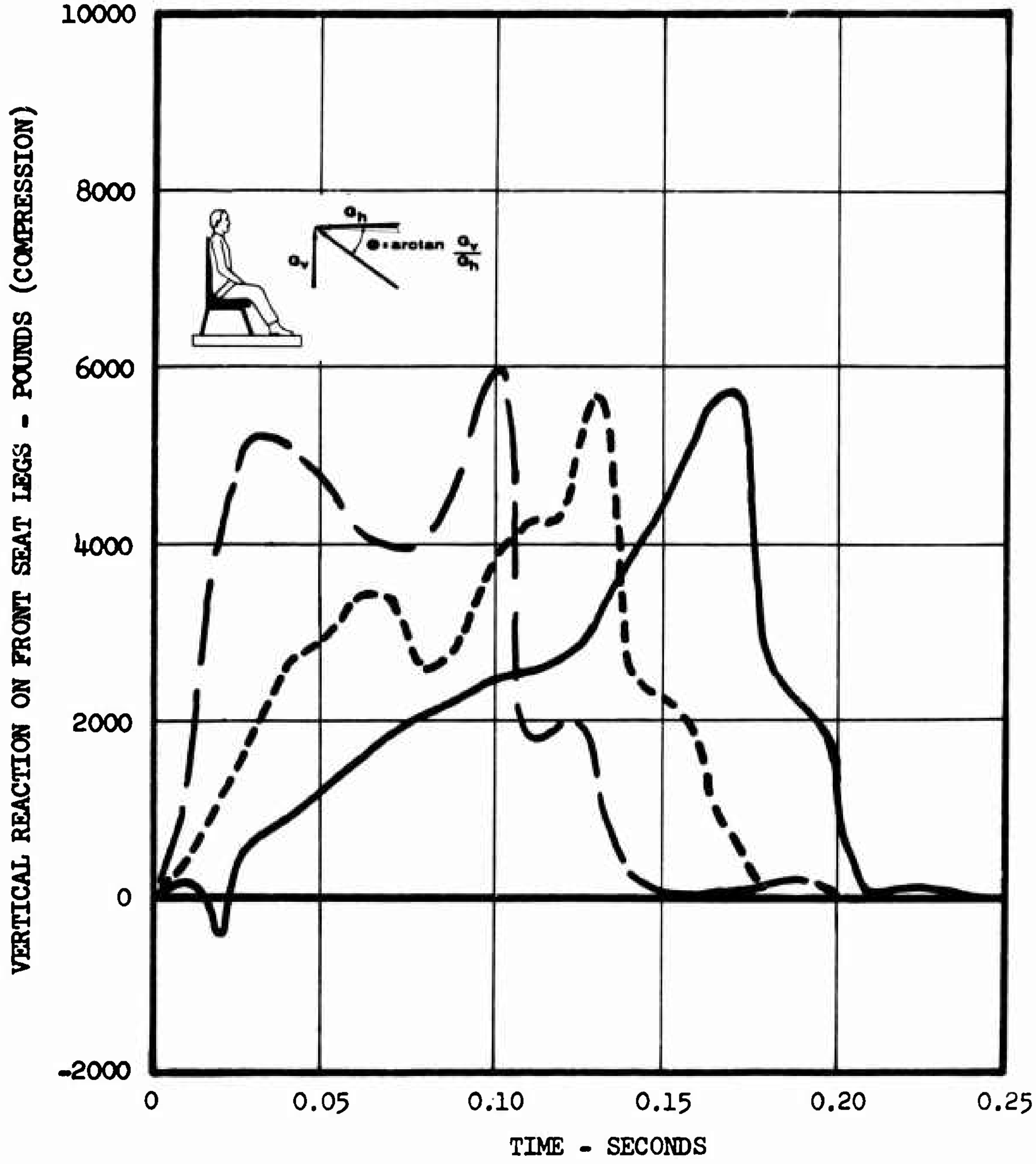

Figure 29. Vertical Reaction on Front Seat Legs Versus Time.

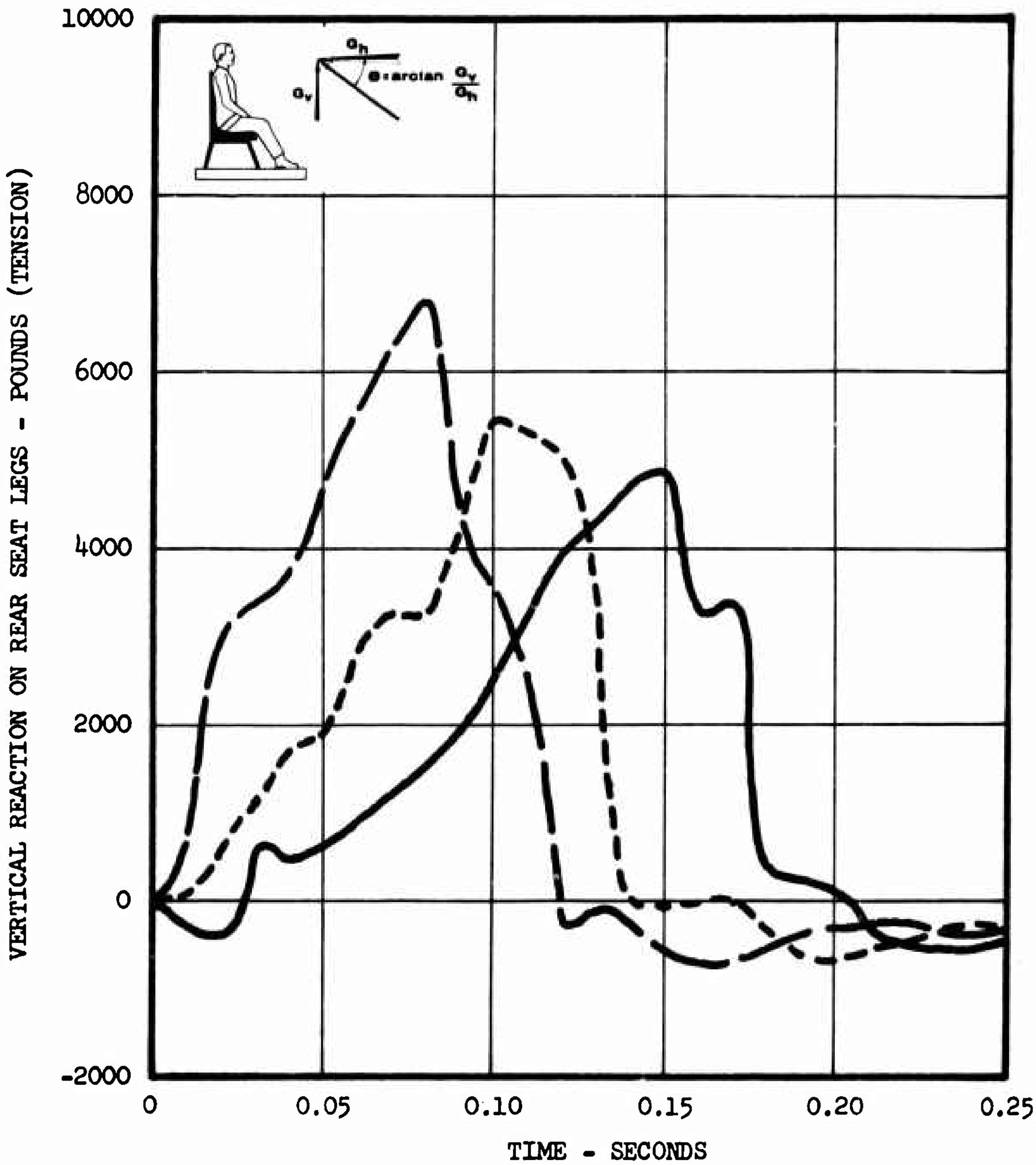

Figure 30. Vertical Reaction on Rear Seat Legs Versus Time.

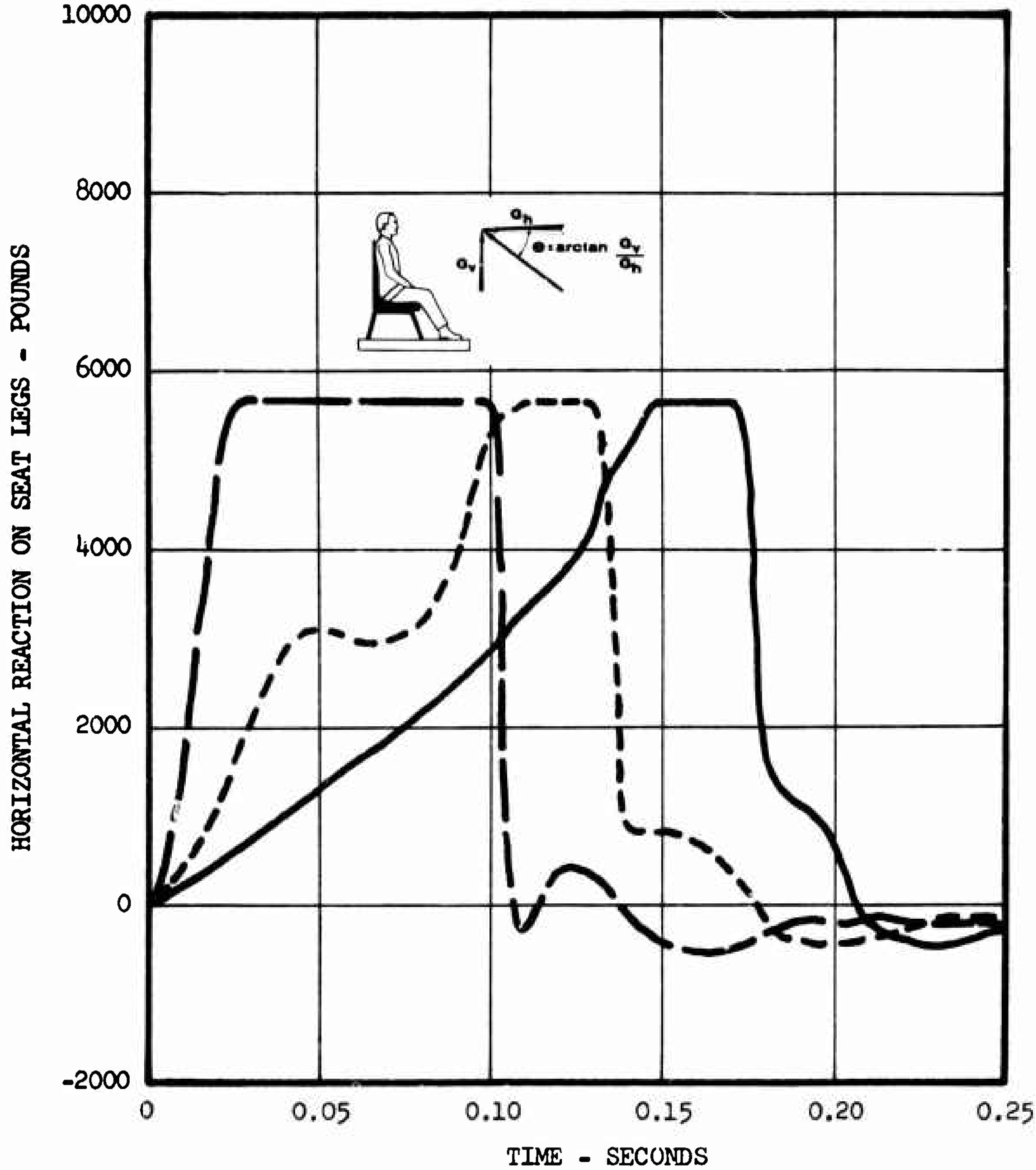

Figure 31. Horizontal Reaction on Seat Legs Versus Time.

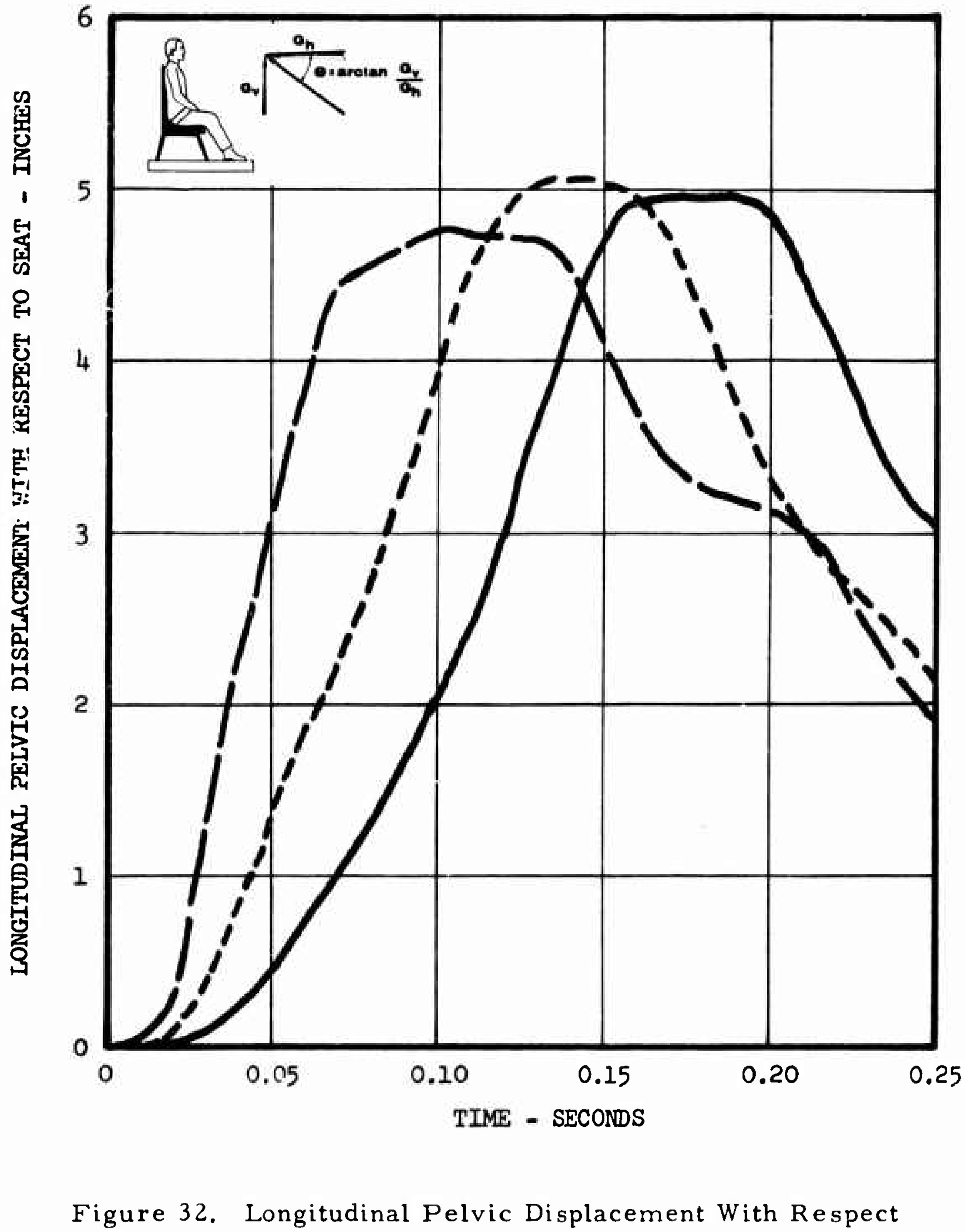

Figure 32. Longitudinal Pelvic Displacement With Respect to Seat Versus Time.

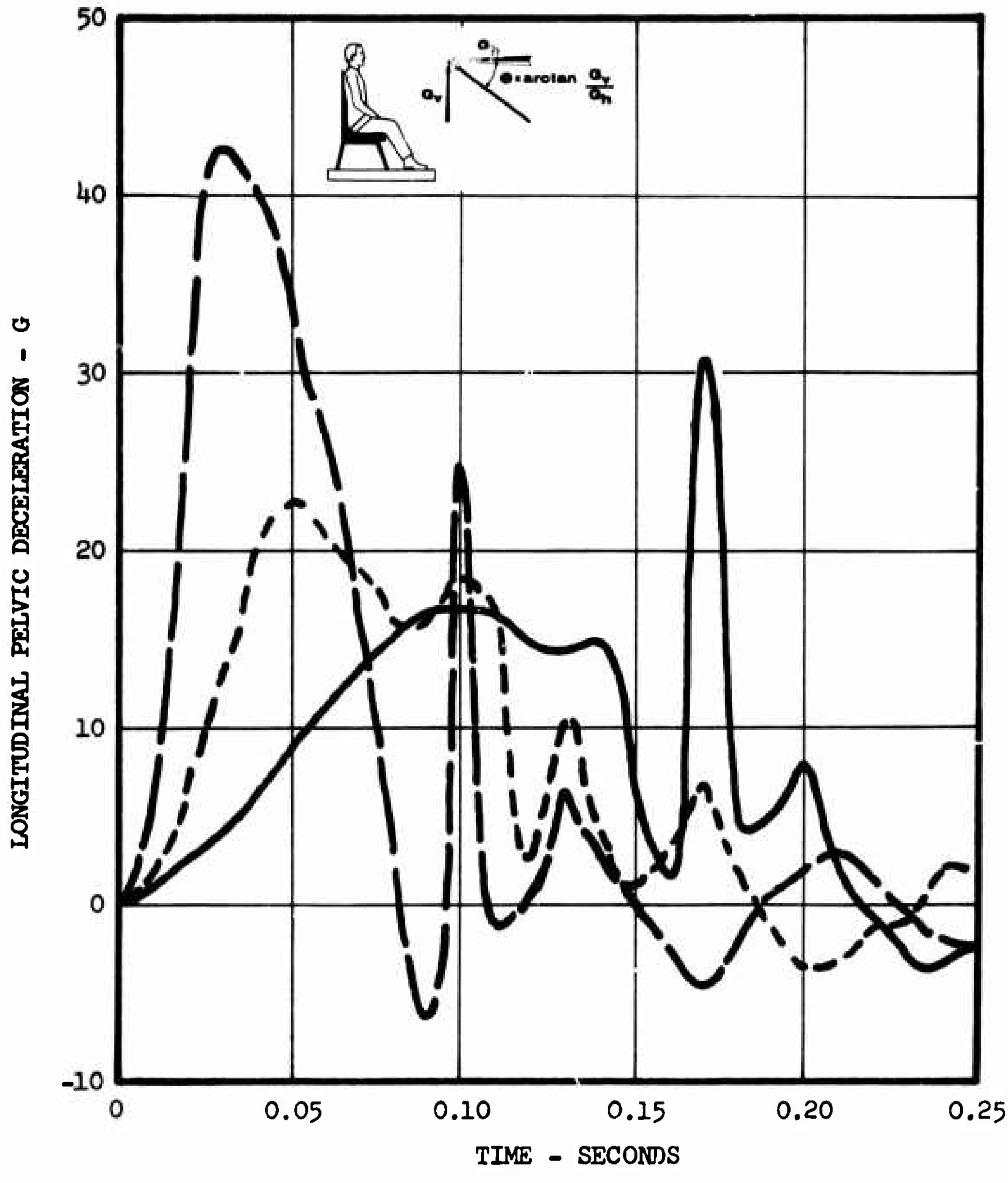

Figure 33. Longitudinal Pelvic Deceleration Versus Time.

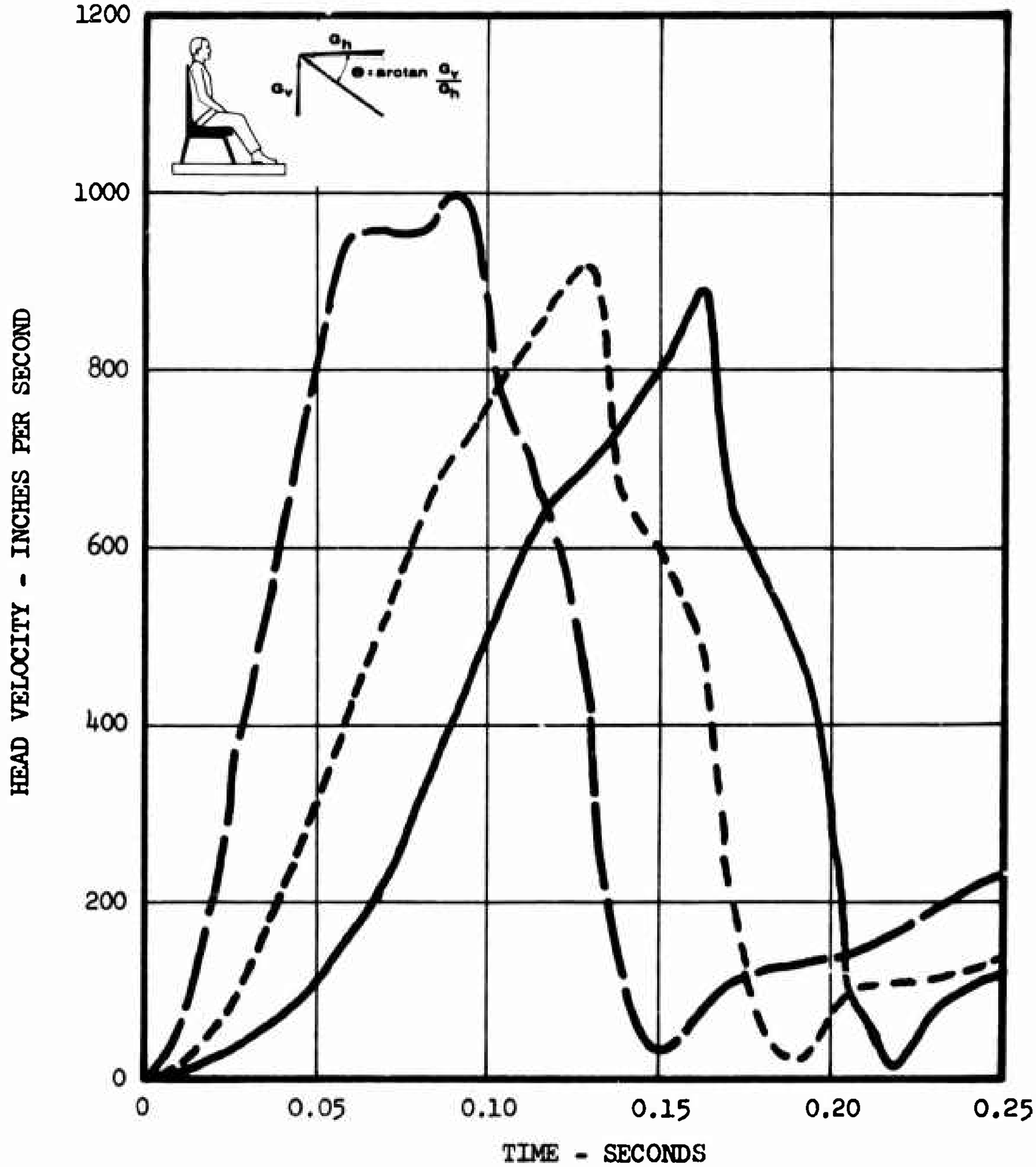

Figure 34. Head Velocity Versus Time.

Figures 35 through 42

Design Variables as Functions of Time for Sinusoidal Crash Pulses

(See p. 41)

Pulse 3	――――――――――――――
Pulse 13*	— — — — — —
Pulse 15*	- - - - - - - - - - - - - -

(For pulse shapes see Figure 17)

Seat Belt	Typical (see Figure 4)
Passenger Weight	187 pounds
Load-Limiter Setting	5660 pounds
Ratio of Vertical to Horizontal Acceleration	0.2
Additional Input Conditions	See Table II, column B

Caution:
While qualitative trends and comparisons may be dependably observed in the results presented, quantitative values should be used with caution. Due to changes and improvements in the computer program during preparation of the curves, current best estimates may differ somewhat from the data presented. For example, see Appendix III, page 285.

*Seat damping coefficients are zero in computer program.

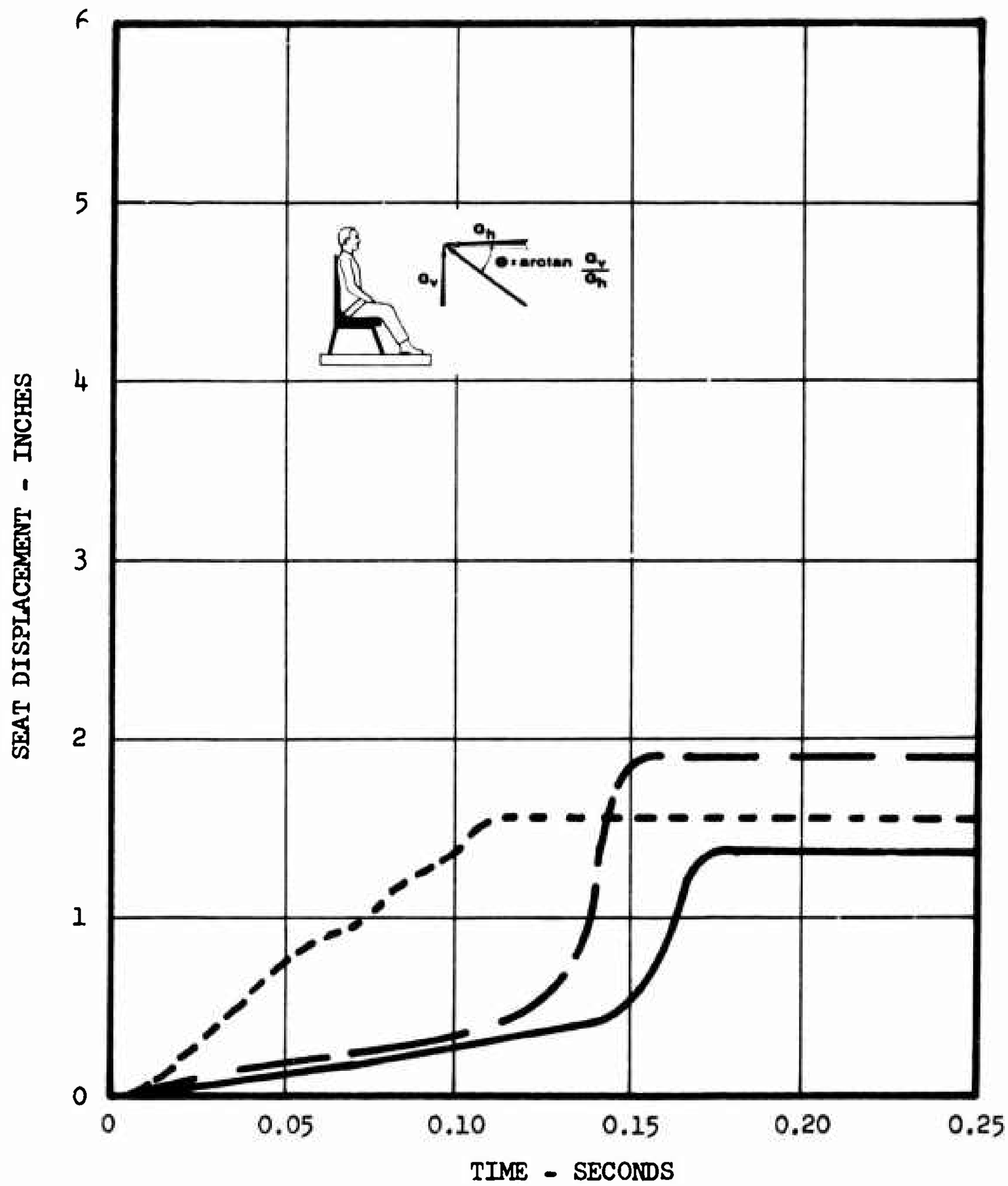

Figure 35. Seat Displacement Versus Time.

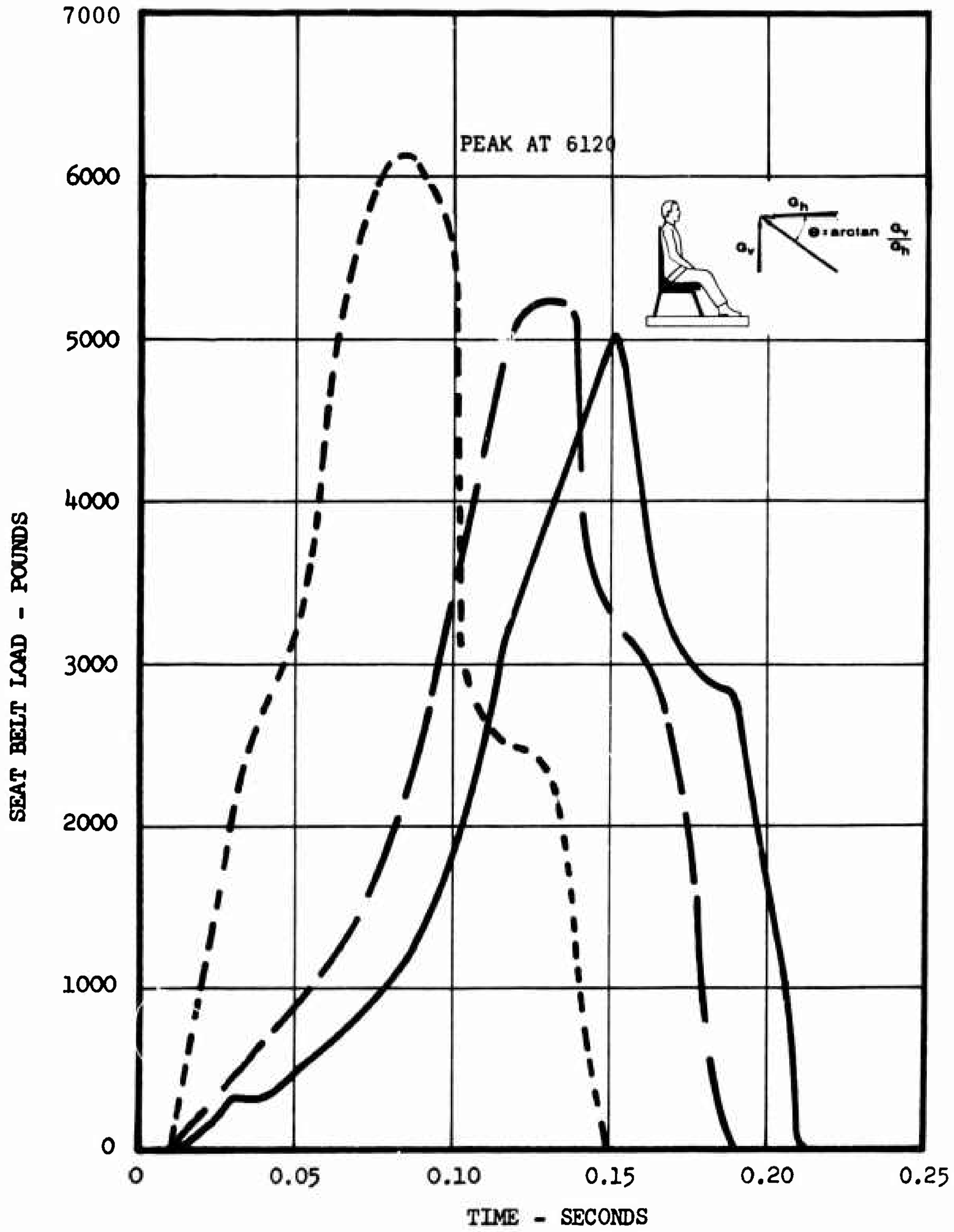

Figure 36. Seat Belt Load Versus Time.

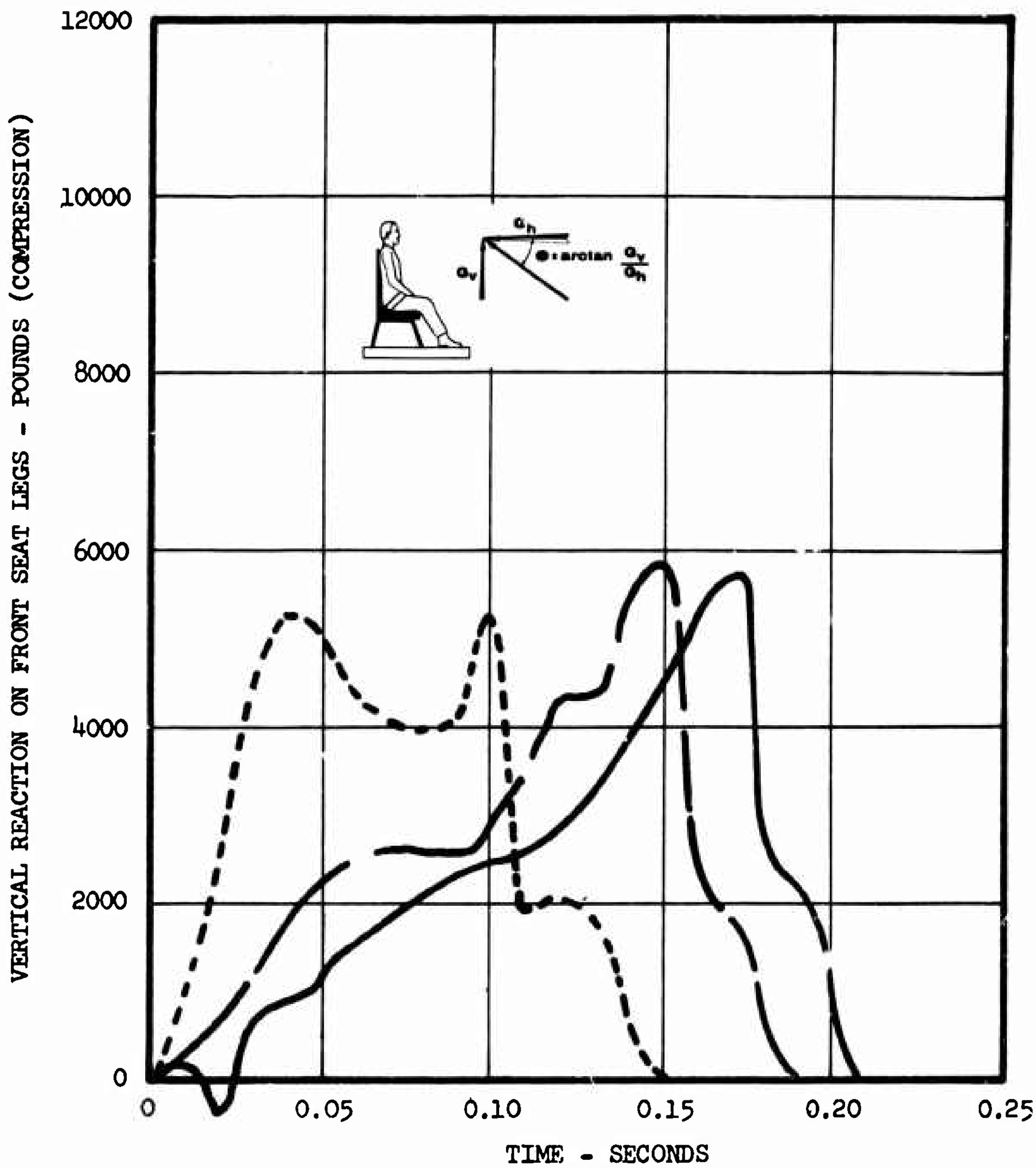

Figure 37. Vertical Reaction on Front Seat Legs Versus Time.

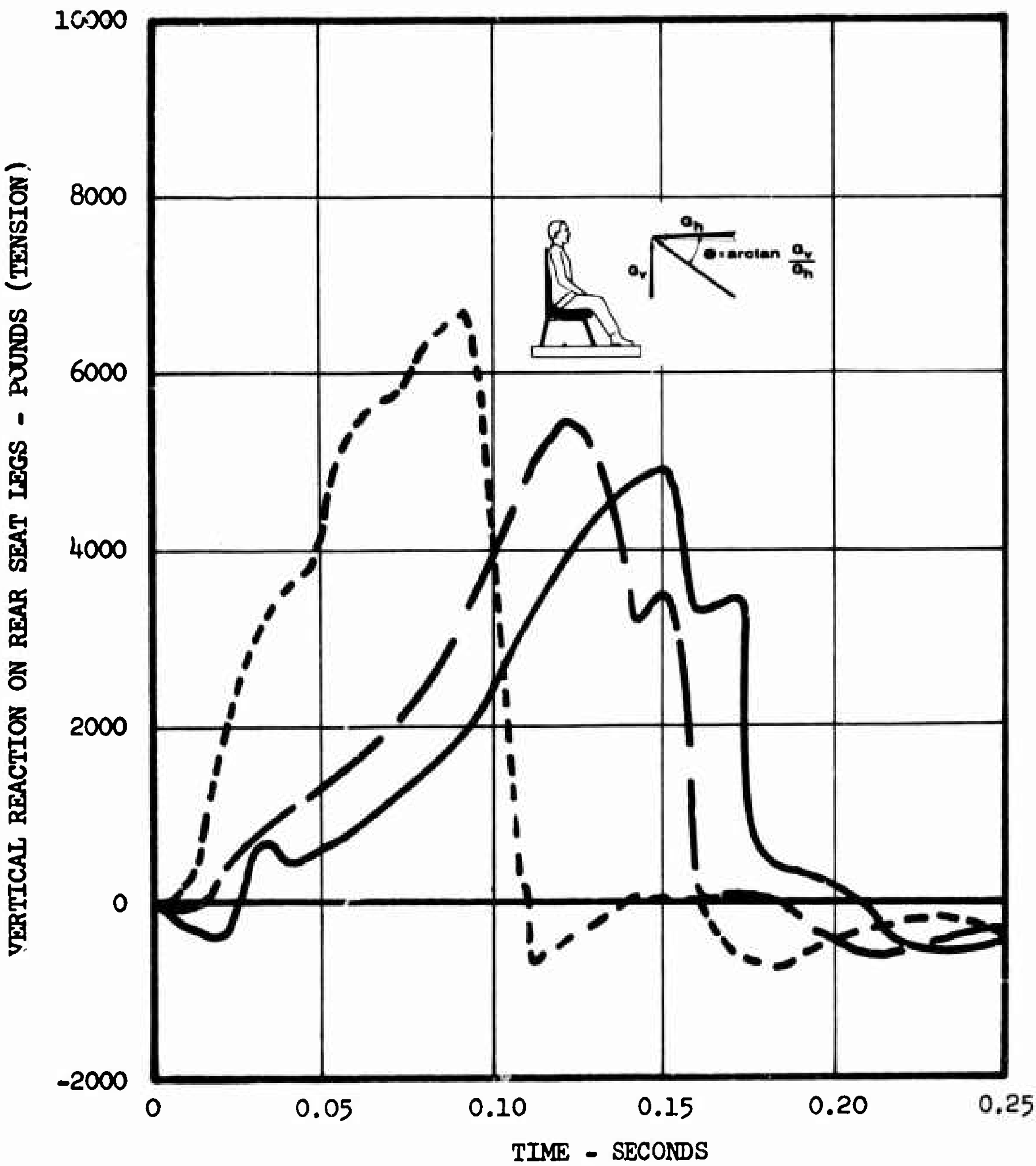

Figure 38. Vertical Reaction on Rear Seat Legs Versus Time.

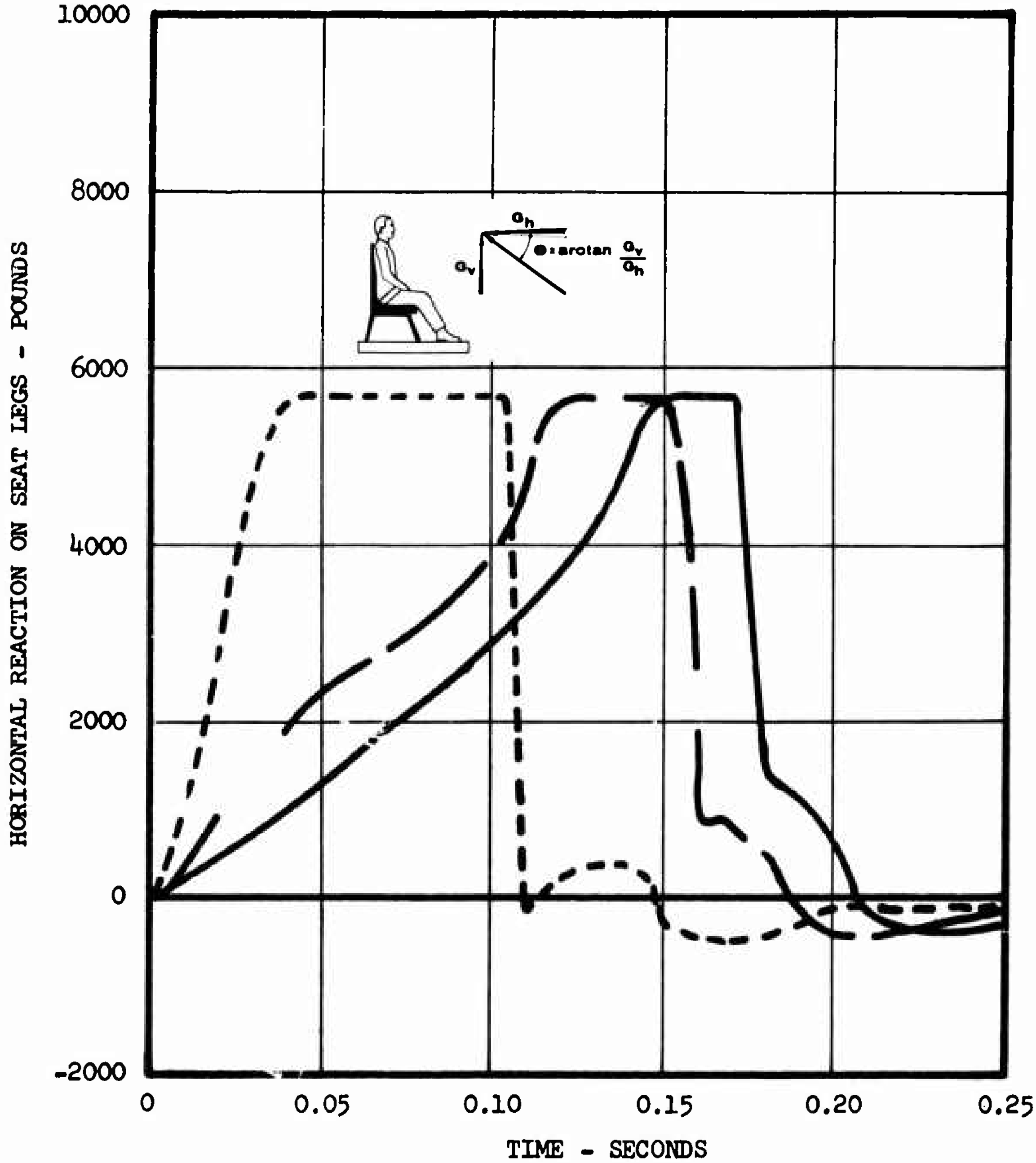

Figure 39. Horizontal Reaction on Seat Legs Versus Time.

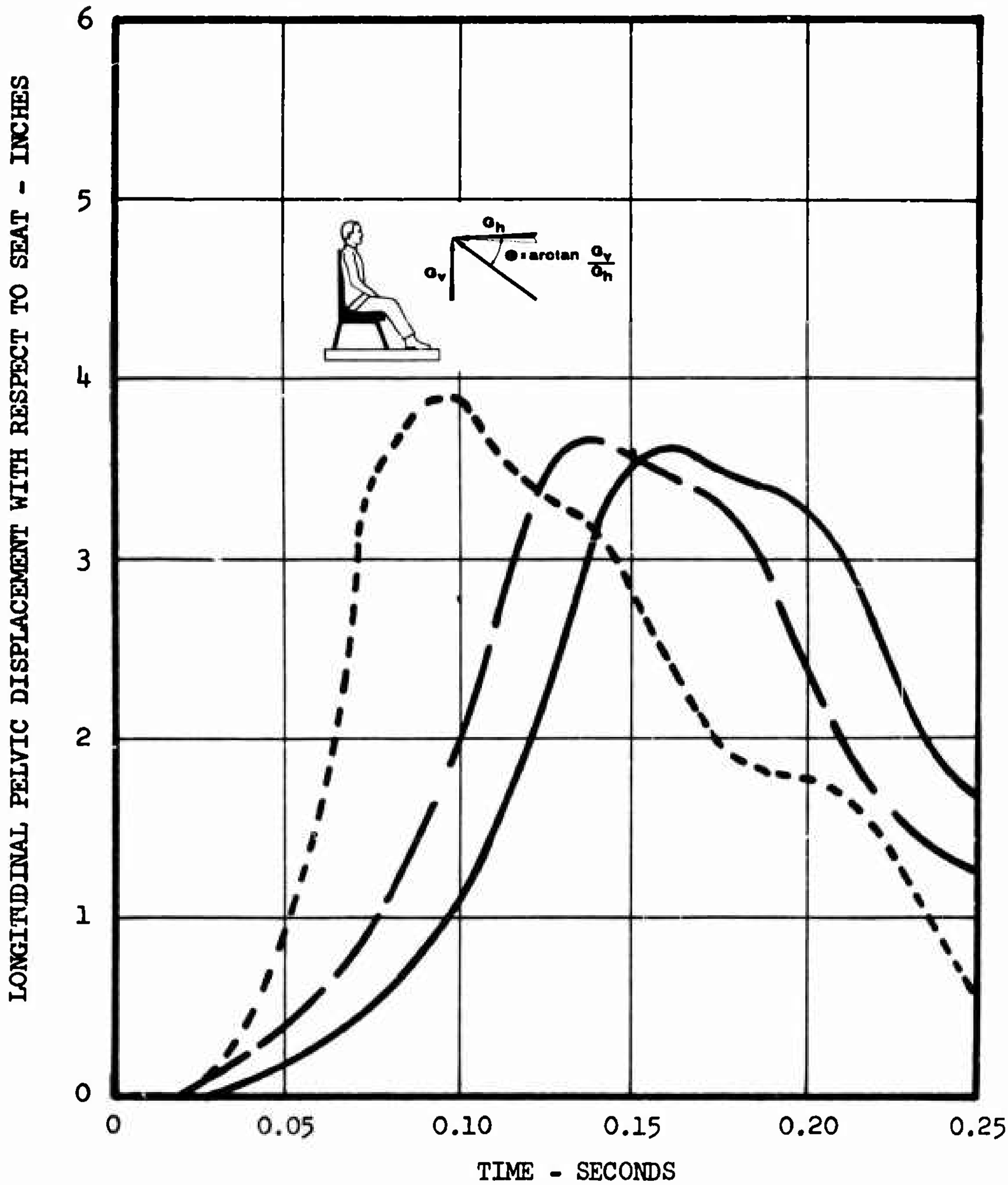

Figure 40. Longitudinal Pelvic Displacement With Respect to Seat Versus Time.

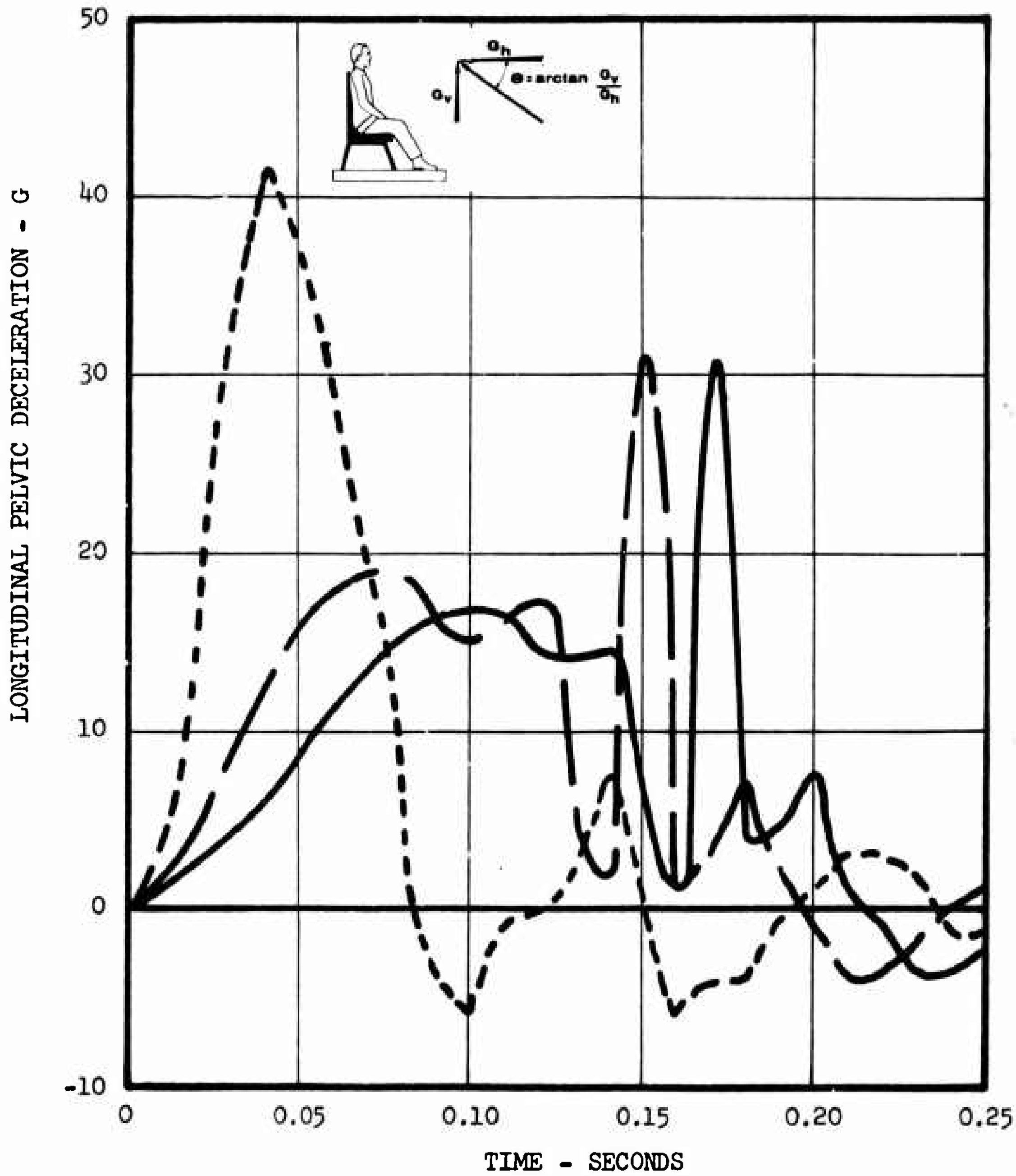

Figure 41. Longitudinal Pelvic Deceleration Versus Time.

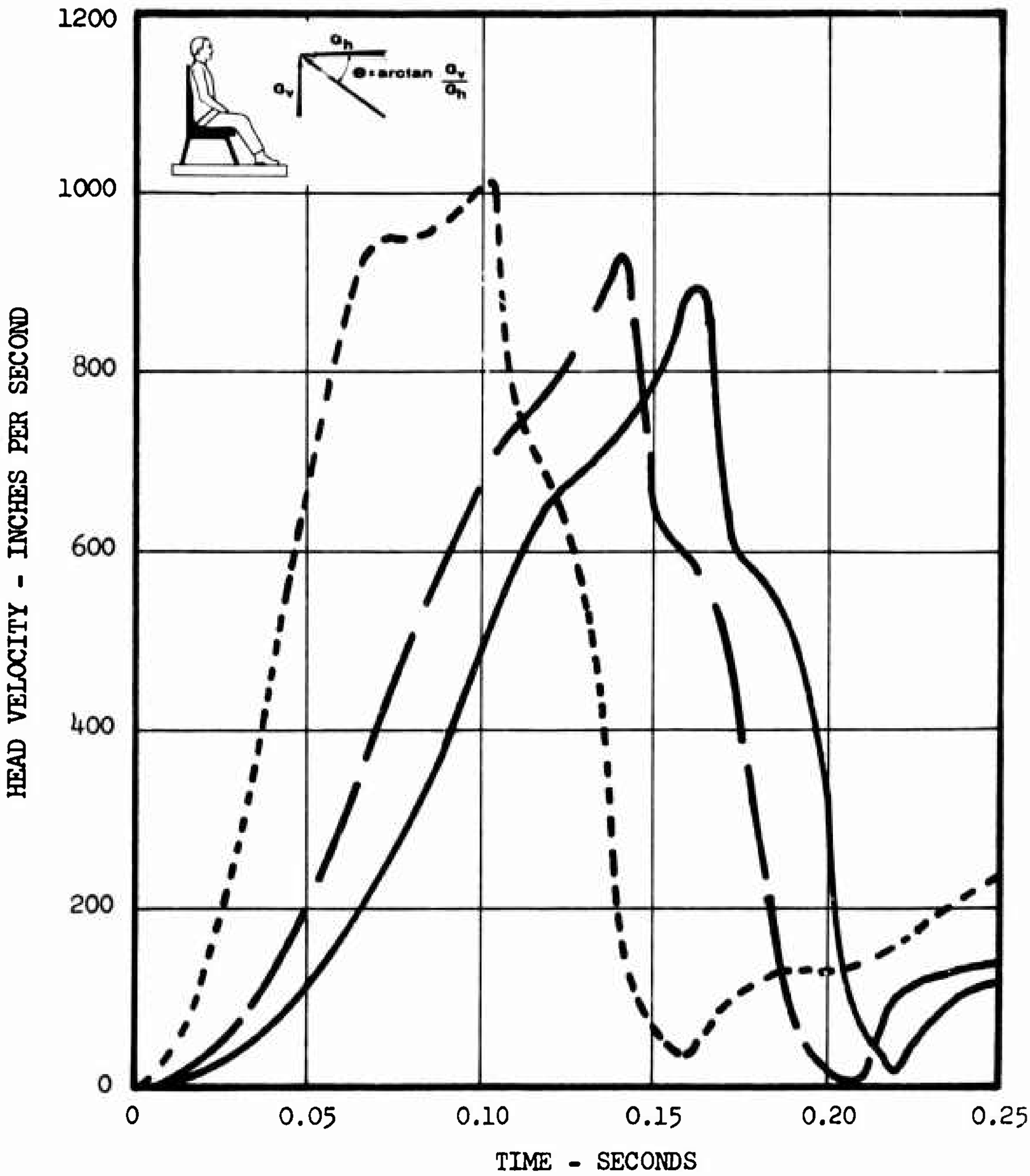

Figure 42. Head Velocity Versus Time.

Figures 43 through 50

Effects of Changing the Load-Limiter Setting

(See p. 42)

Pulse 1

Pulse 2

Pulse 3

Pulse 4

Pulse 5

(For pulse shapes see Figure 17)

Seat Belt	Typical (see Figure 4)
Passenger Weight	187 pounds
Ratio of Vertical to Horizontal Acceleration	0. 2
Additional Input Conditions	See Table II, column A

Caution:
While qualitative trends and comparisons may be dependably observed in the results presented, quantitative values should be used with caution. Due to changes and improvements in the computer program during preparation of the curves, current best estimates may differ somewhat from the data presented. For example, see Appendix III, page 285.

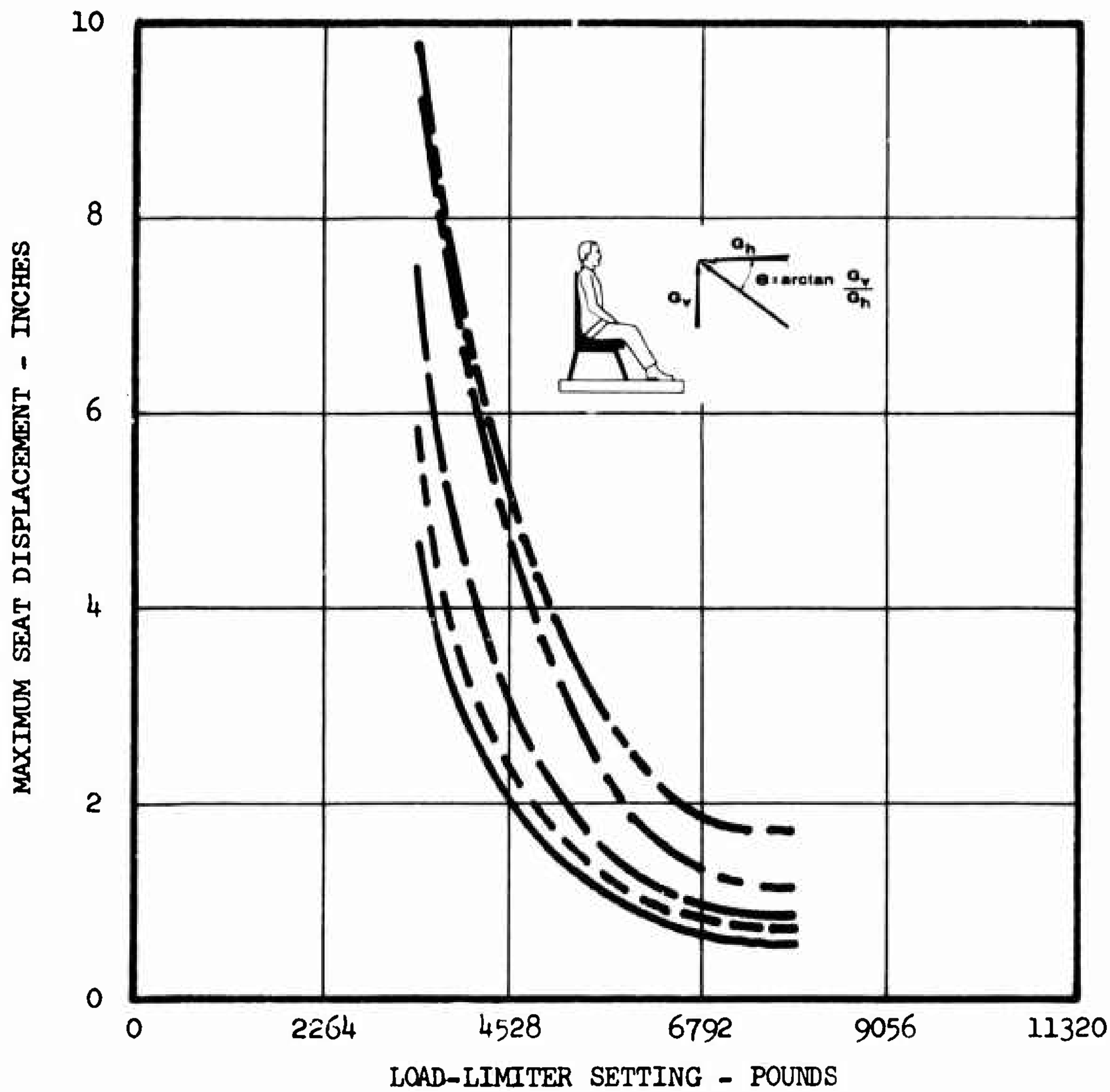

Figure 43. Maximum Seat Displacement Versus Load-Limiter Setting.

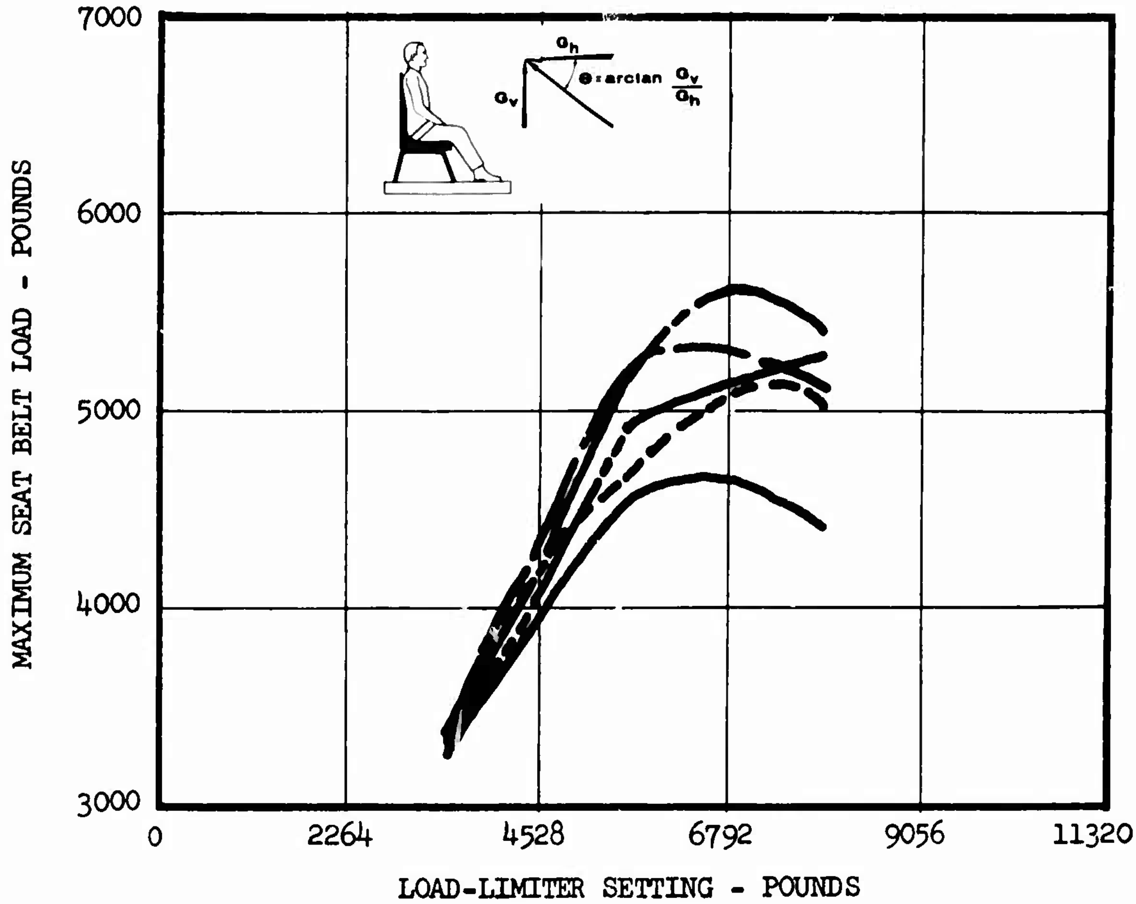

Figure 44. Maximum Seat Belt Load Versus Load-Limiter Setting.

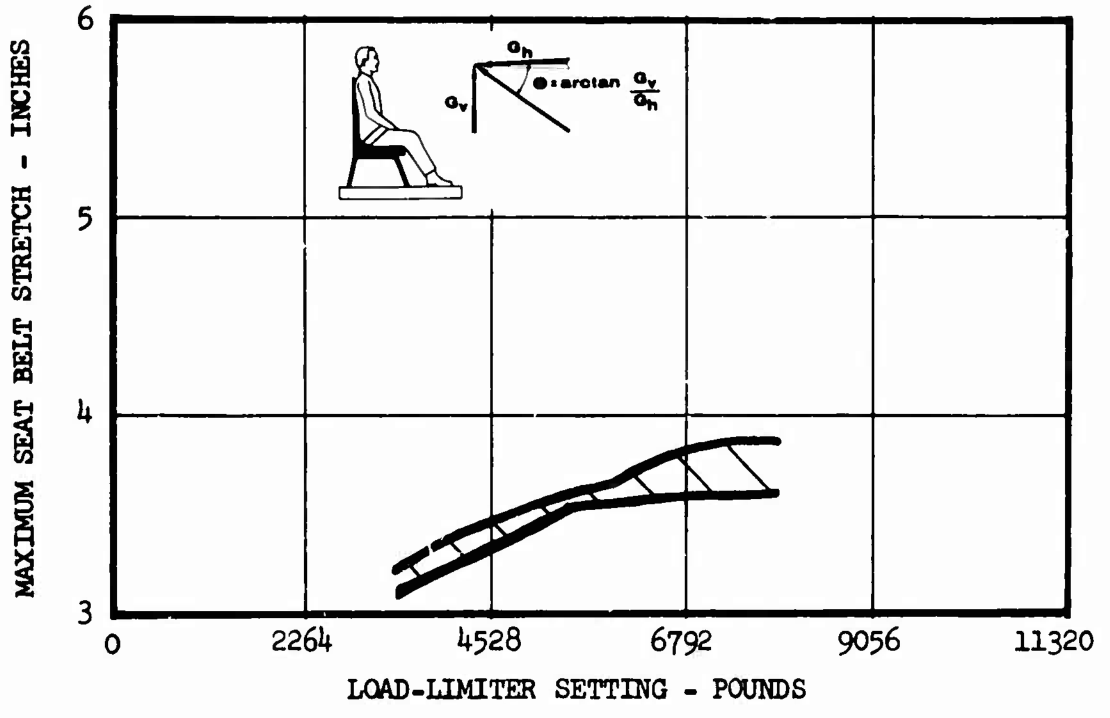

Figure 45. Maximum Seat Belt Stretch Versus Load-Limiter Setting.

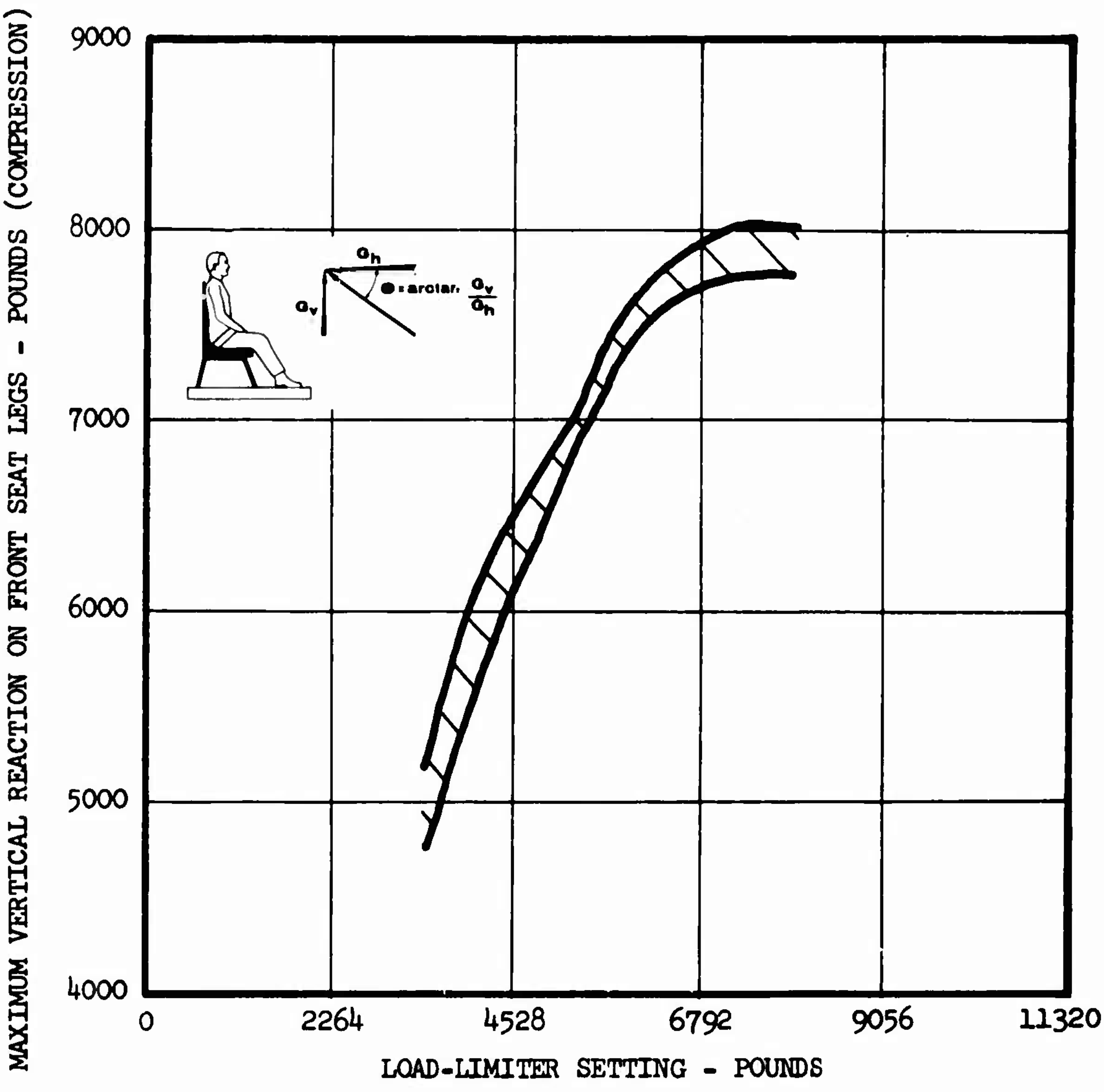

Figure 46. Maximum Vertical Reaction on Front Seat Legs Versus Load-Limiter Setting.

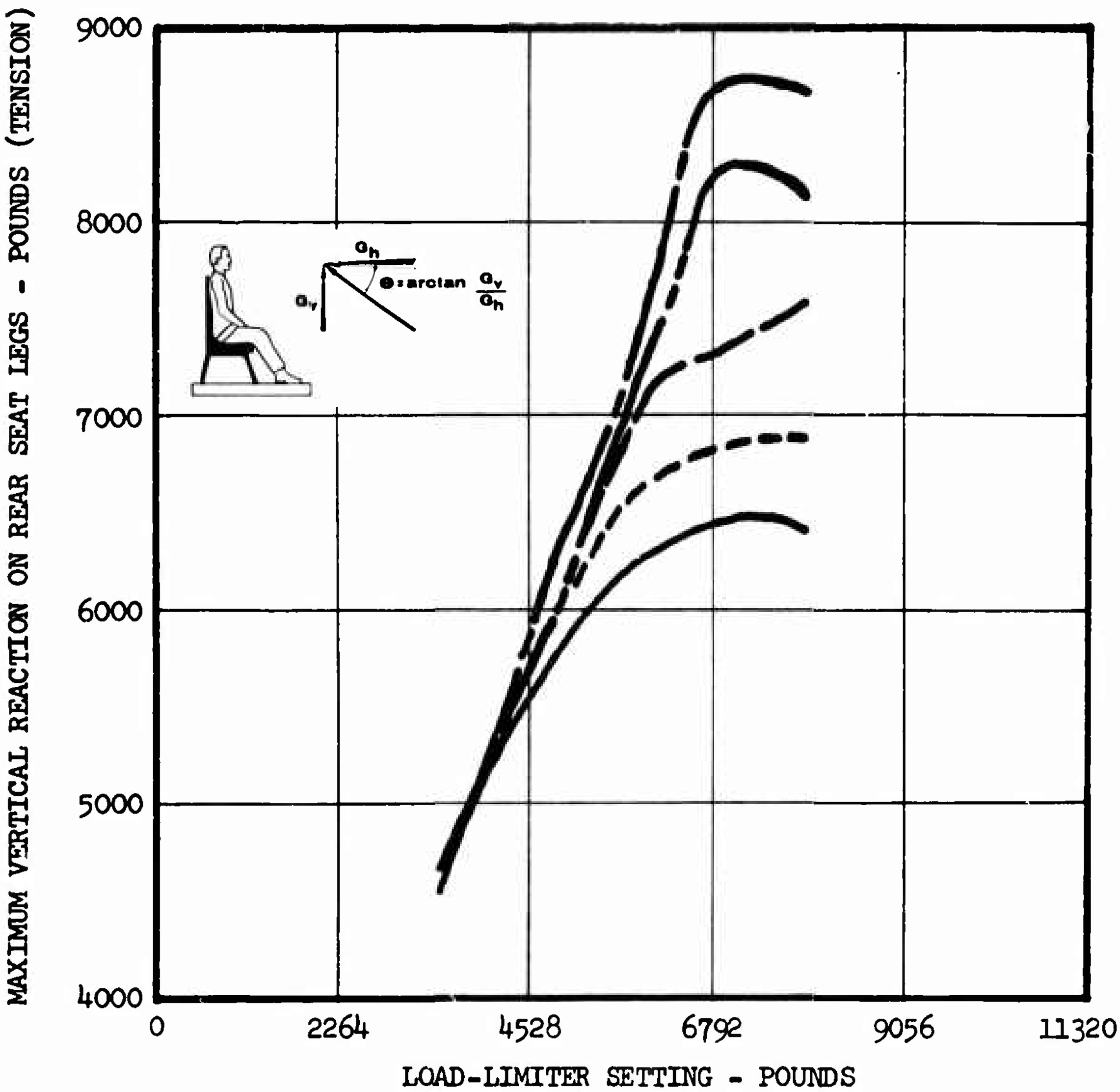

Figure 47. Maximum Vertical Reaction on Rear Seat Legs Versus Load-Limiter Setting.

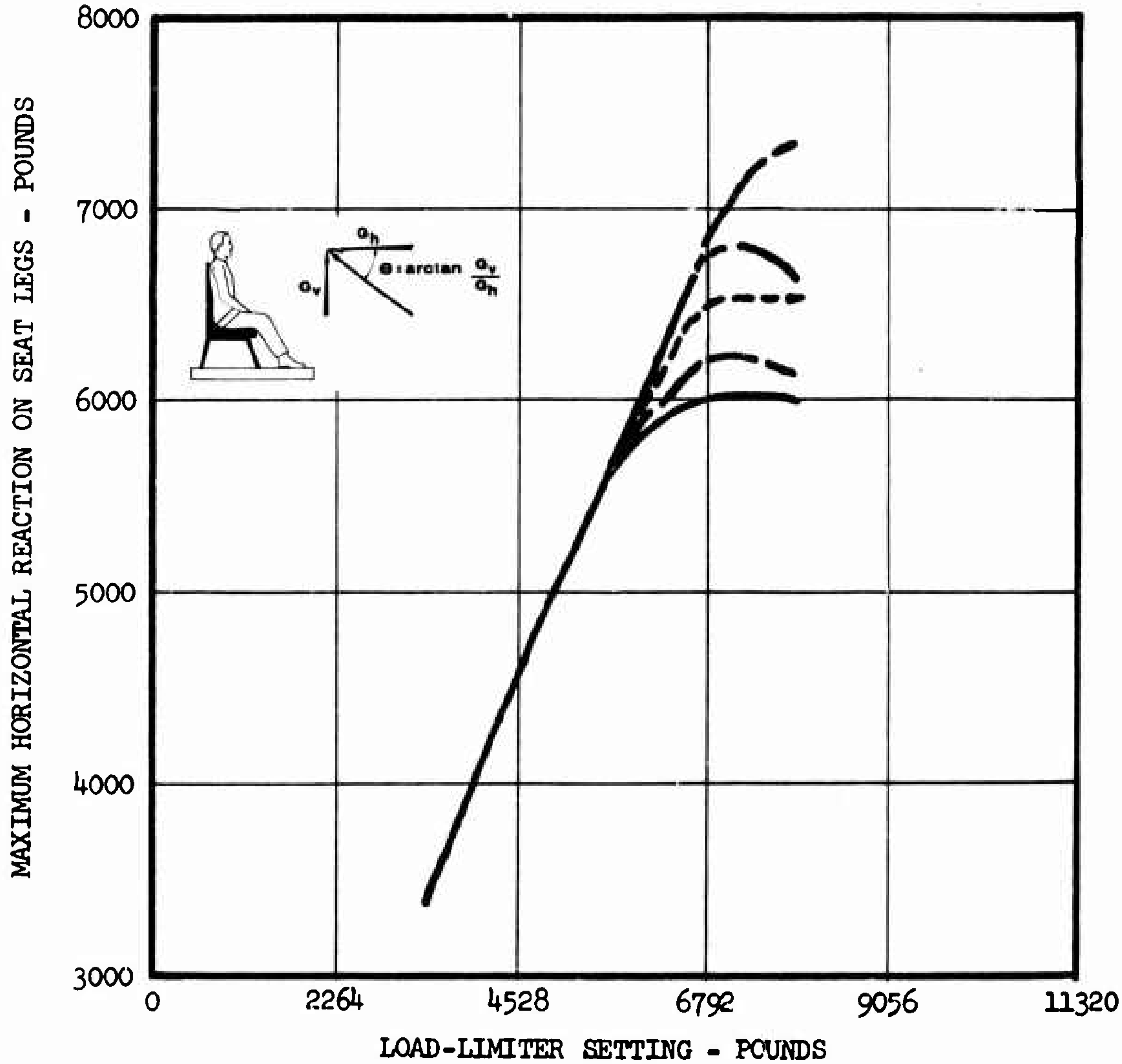

Figure 48. Maximum Horizontal Reaction on Seat Legs Versus Load-Limiter Setting.

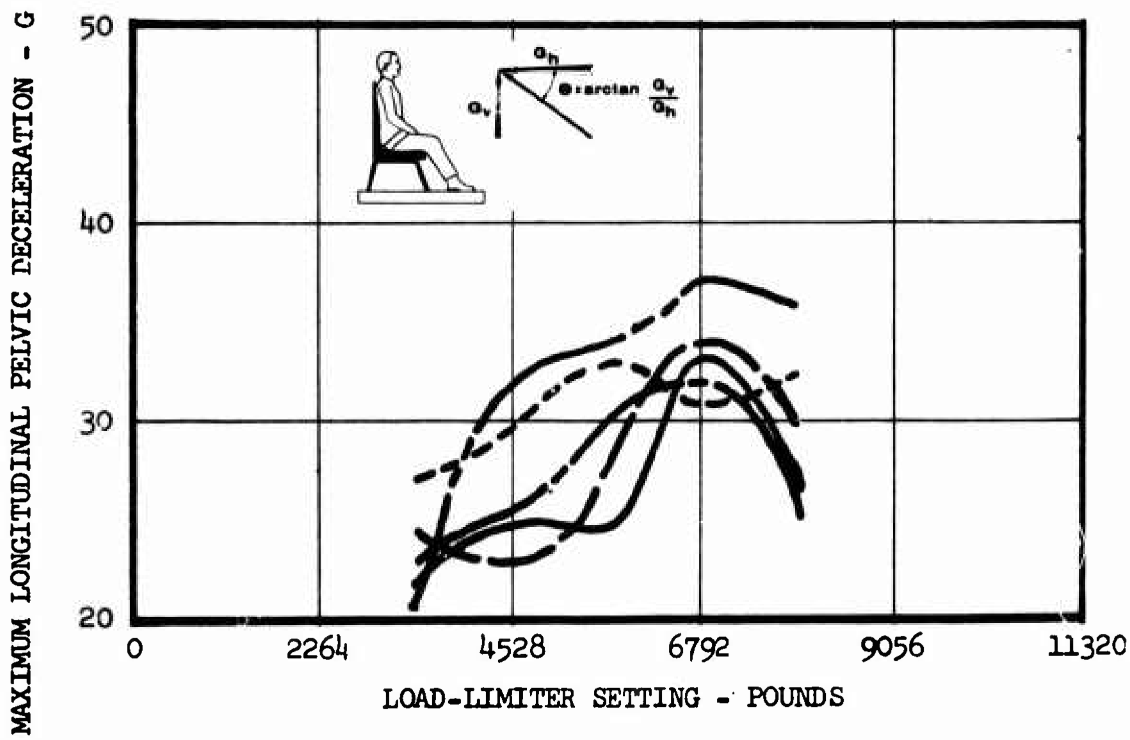

Figure 49. Maximum Longitudinal Pelvic Deceleration Versus Load-Limiter Setting.

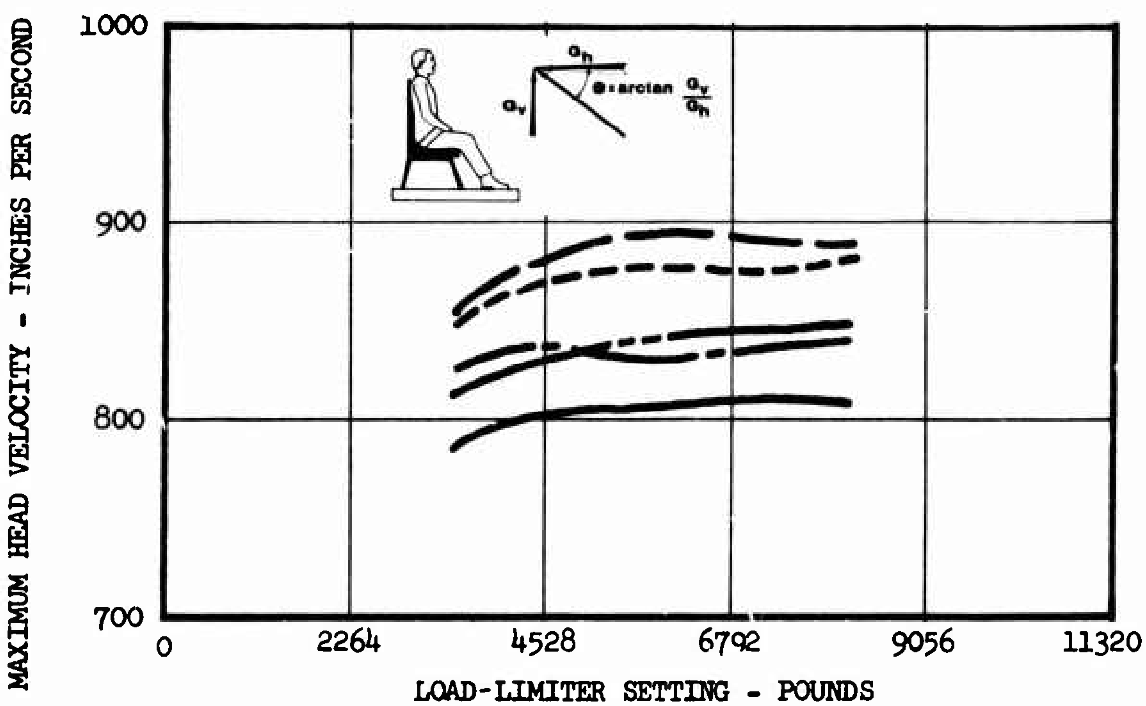

Figure 50. Maximum Head Velocity Versus Load-Limiter Setting.

Figures 51 through 58

Effects of Rise Time in Triangular Crash Pulses

(See p. 43)

Pulse	No. 3 (see Figure 17)
Seat Belt	Typical (see Figure 4)
Passenger Weight	187 pounds
Load-Limiter Setting	
3396 pounds (15G)	————————————
4528 pounds (20G)	——— - ——— - ———
5660 pounds (25G)	——— - - ——— - -
6792 pounds (30G)	—— —— —— —— —— —
7924 pounds (35G)	- - - - - - - - - - - - - -
Ratio of Vertical to Horizontal Acceleration	0.2
Additional Input Conditions	See Table II, column A

Caution:

While qualitative trends and comparisons may be dependably observed in the results presented, quantitative values should be used with caution. Due to changes and improvements in the computer program during preparation of the curves, current best estimates may differ somewhat from the data presented. For example, see Appendix III, page 285.

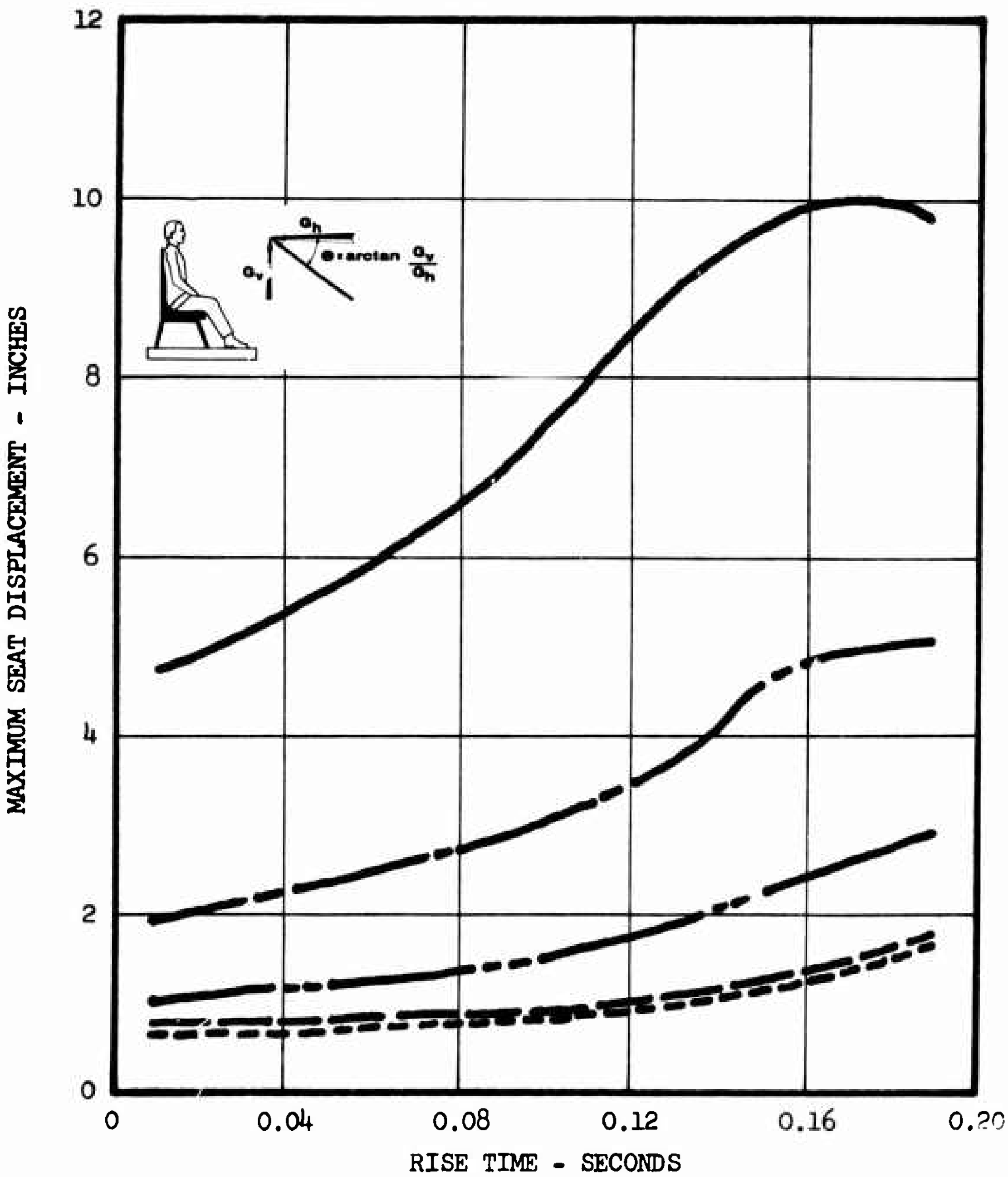

Figure 51. Maximum Seat Displacement Versus Rise Time.

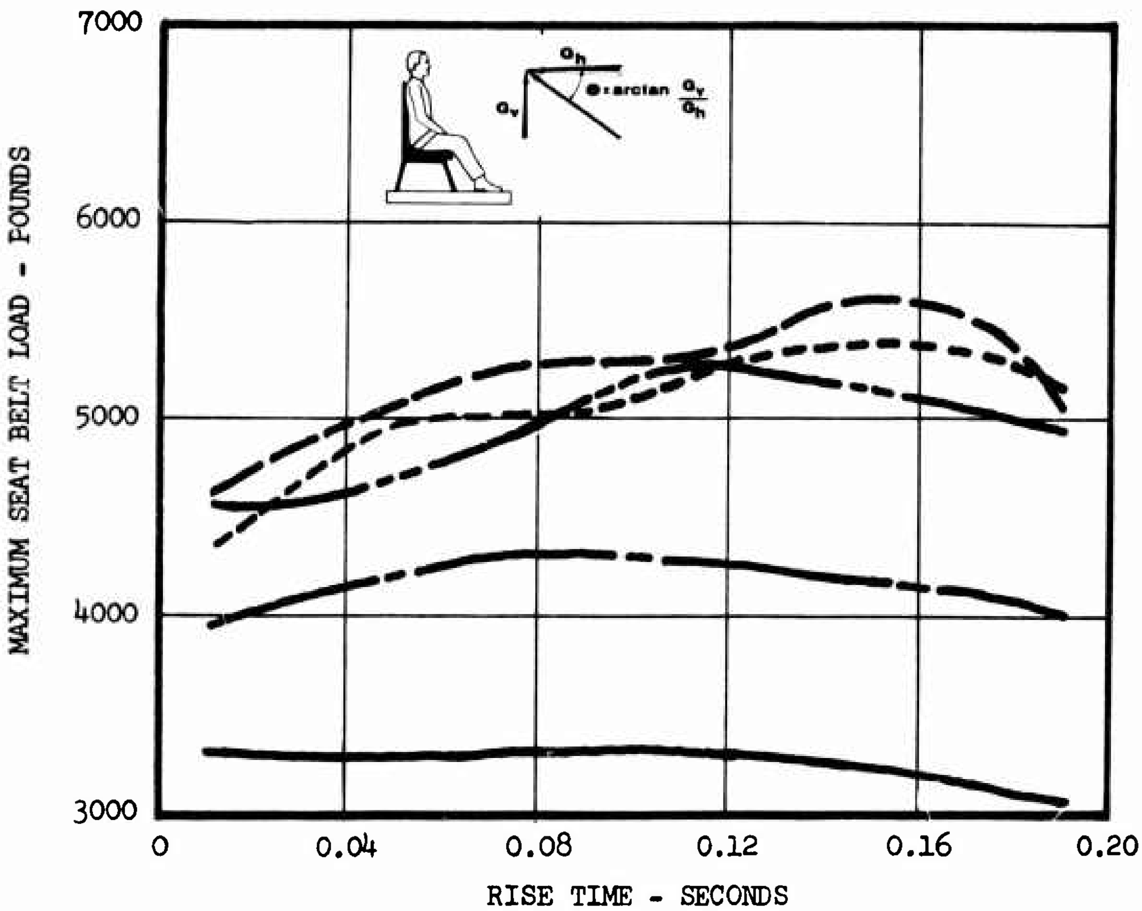

Figure 52. Maximum Seat Belt Load Versus Rise Time.

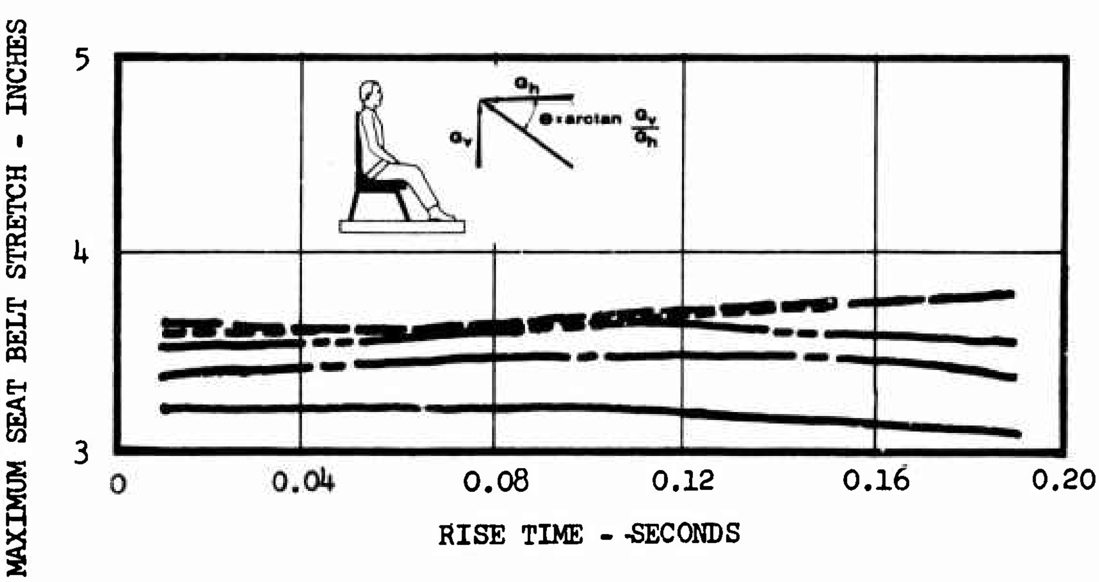

Figure 53. Maximum Seat Belt Stretch Versus Rise Time.

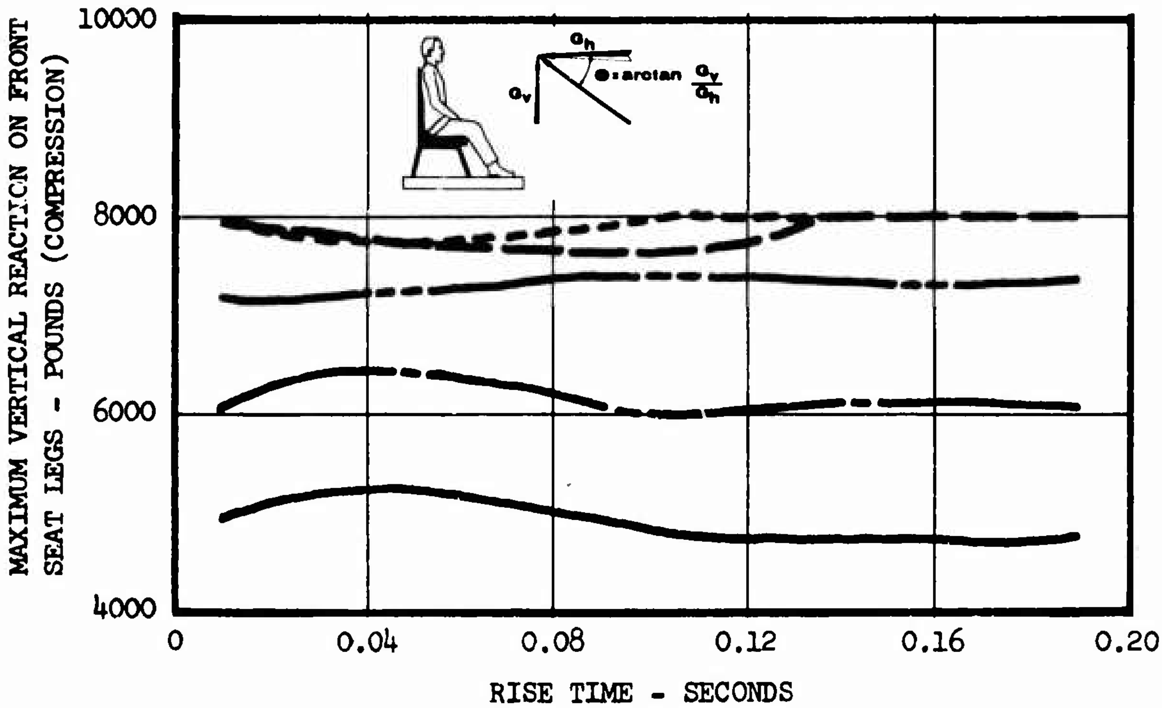

Figure 54. Maximum Vertical Reaction on Front Seat Legs Versus Rise Time.

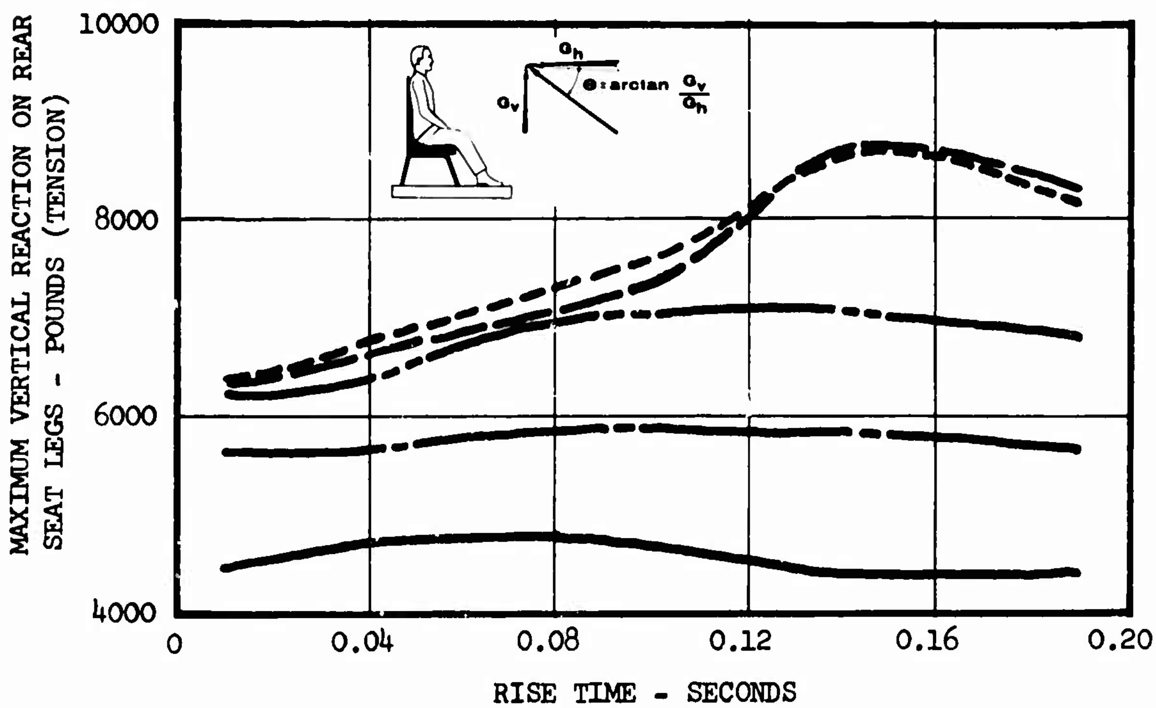

Figure 55. Maximum Vertical Reaction on Rear Seat Legs Versus Rise Time.

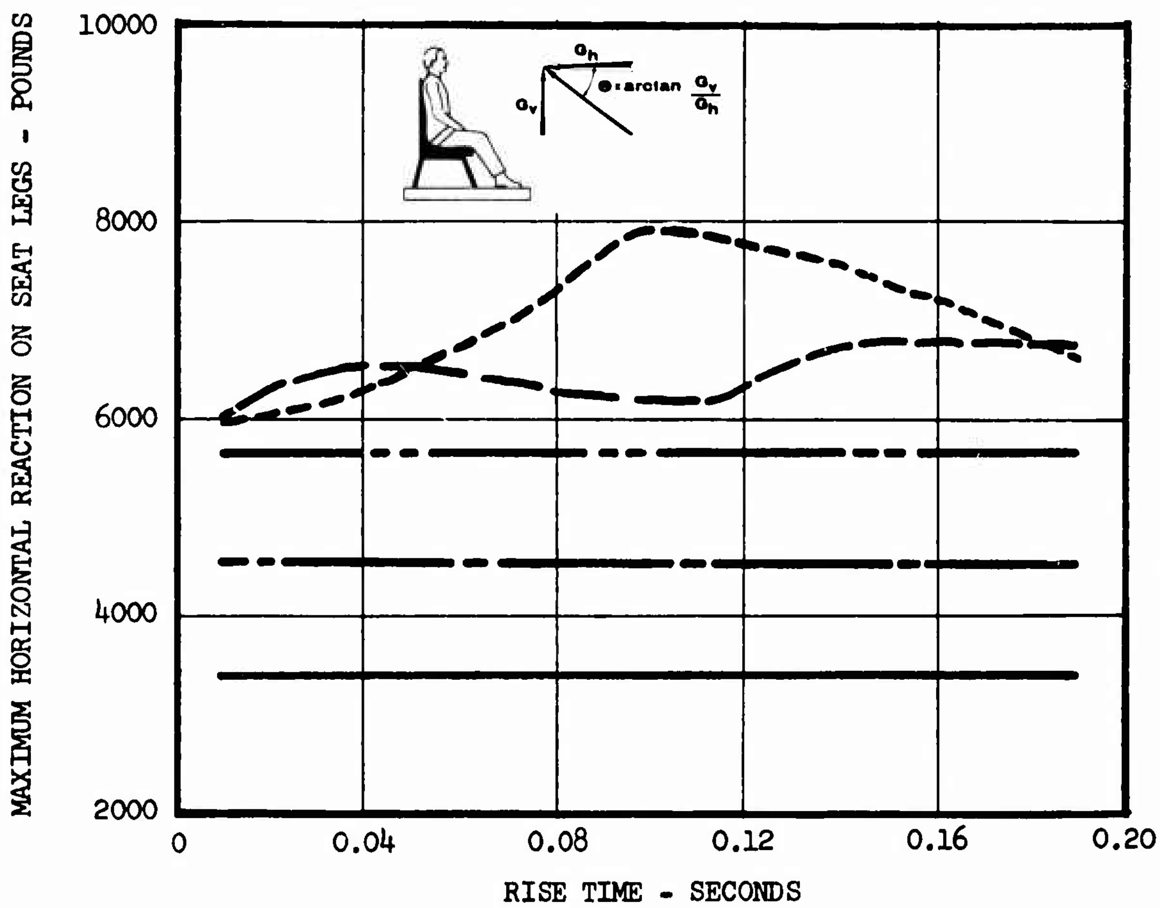

Figure 56. Maximum Horizontal Reaction on Seat Legs Versus Rise Time.

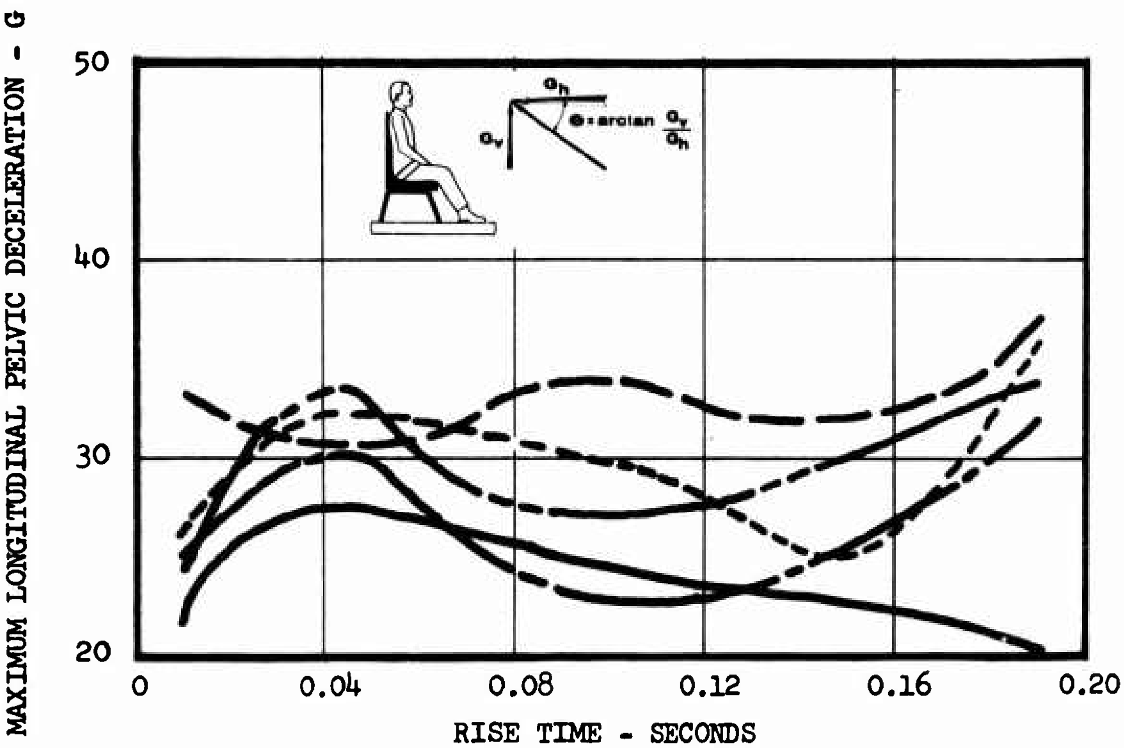

Figure 57. Maximum Longitudinal Pelvic Deceleration Versus Rise Time.

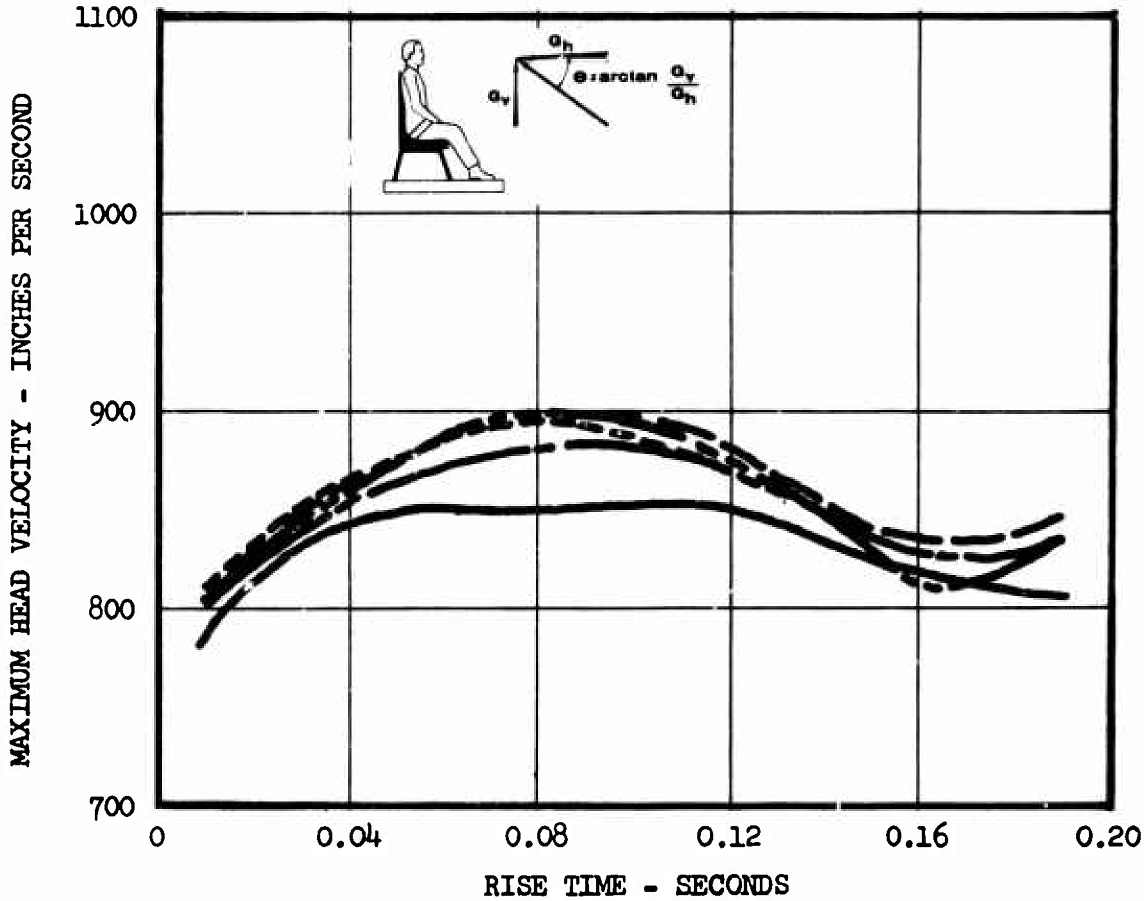

Figure 58. Maximum Head Velocity Versus Rise Time.

Figures 59 through 66

Effects of Changing the Peak Values of Triangular Crash Pulses

(See p. 44)

Pulse 3	————————
Pulse 11*	— — — — — —

(For pulse shapes see Figure 17)

Seat Belt	Typical (see Figure 4)
Passenger Weight	187 pounds
Load-Limiter Setting	5660 pounds
Ratio of Vertical to Horizontal Acceleration	0.2
Additional Input Conditions	See Table II, column B

Caution:
While qualitative trends and comparisons may be dependably observed in the results presented, quantitative values should be used with caution. Due to changes and improvements in the computer program during preparation of the curves, current best estimates may differ somewhat from the data presented. For example, see Appendix III, page 285.

*Seat damping coefficients are zero in computer program.

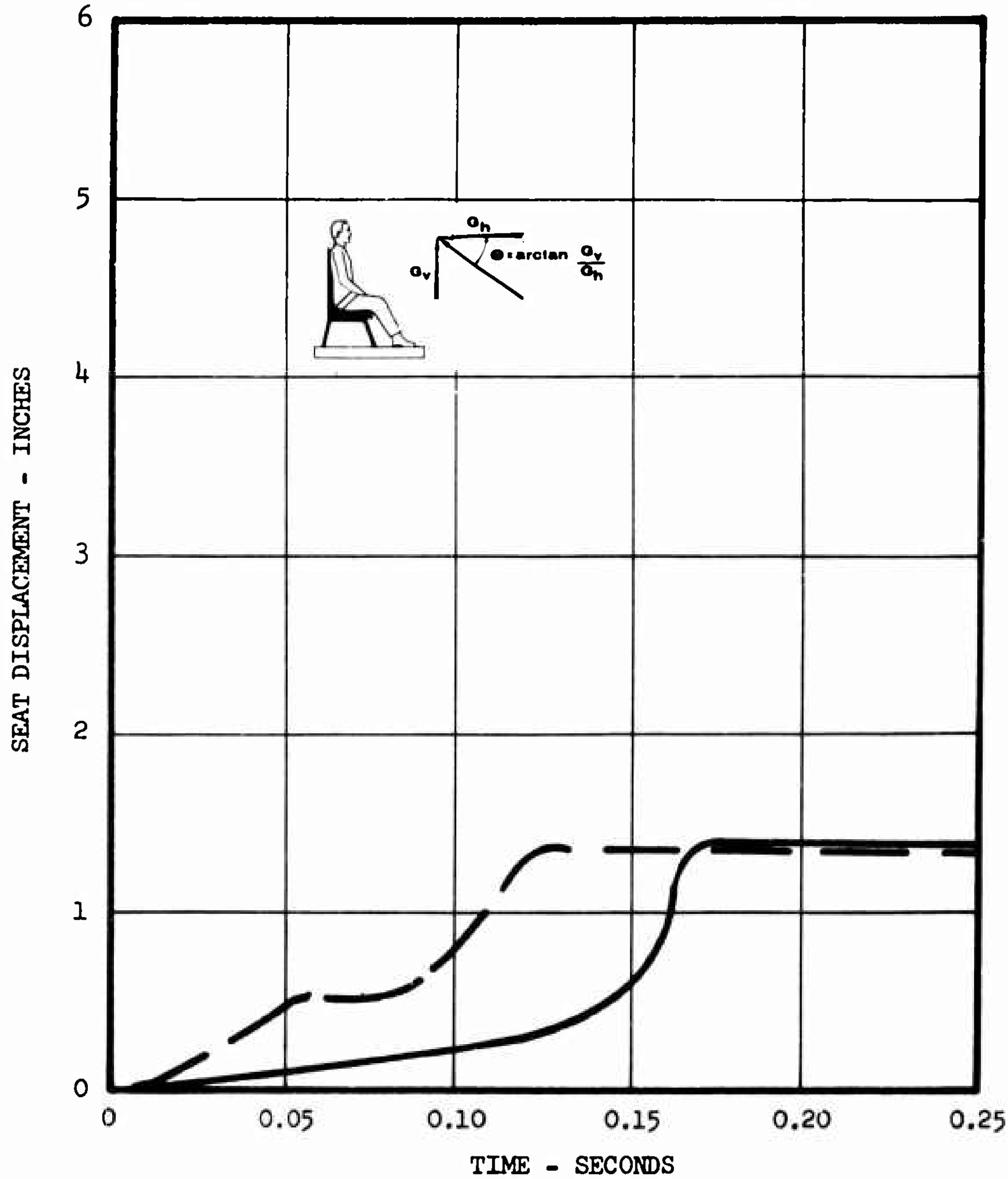

Figure 59. Seat Displacement Versus Time.

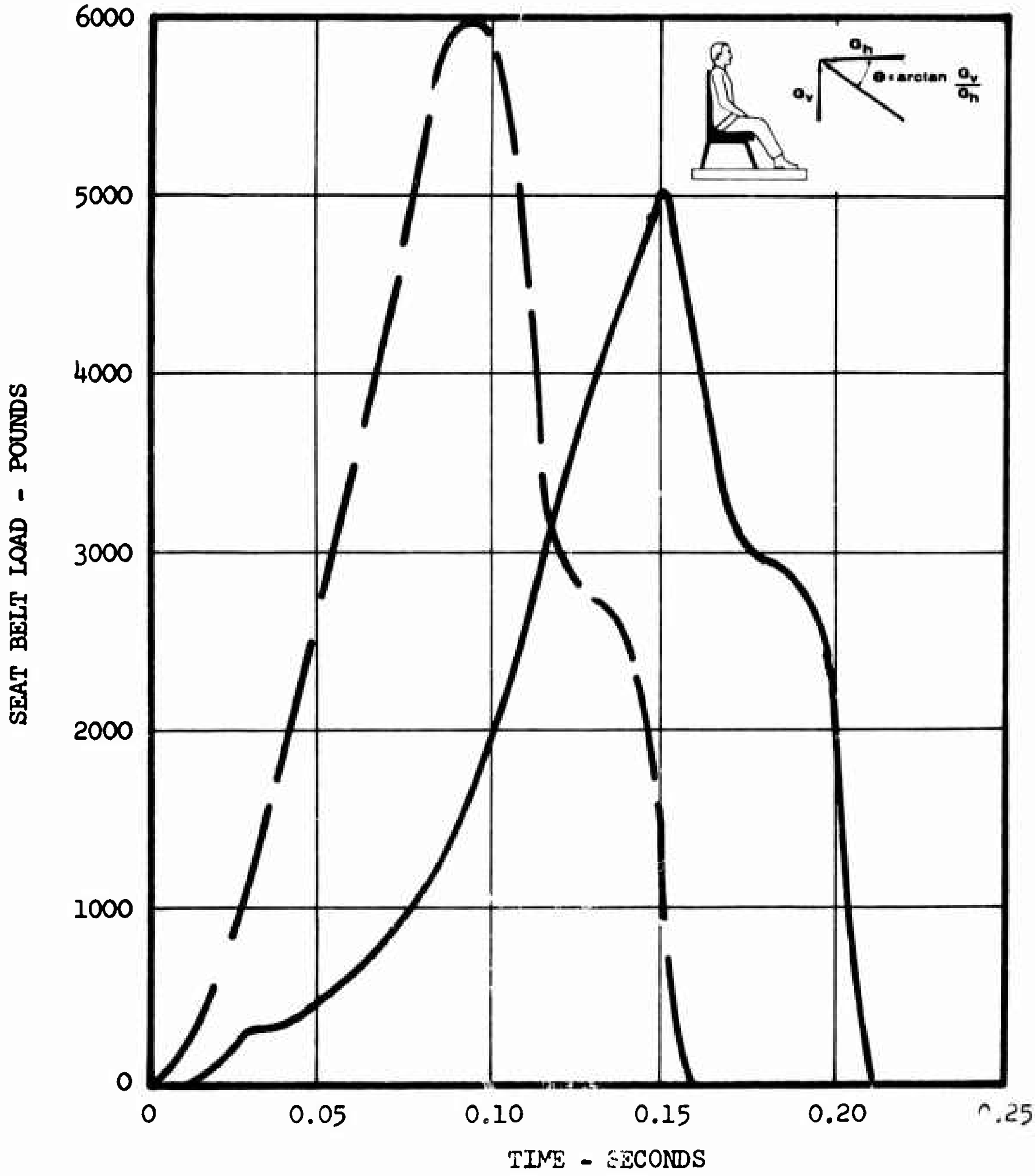

Figure 60. Seat Belt Load Versus Time.

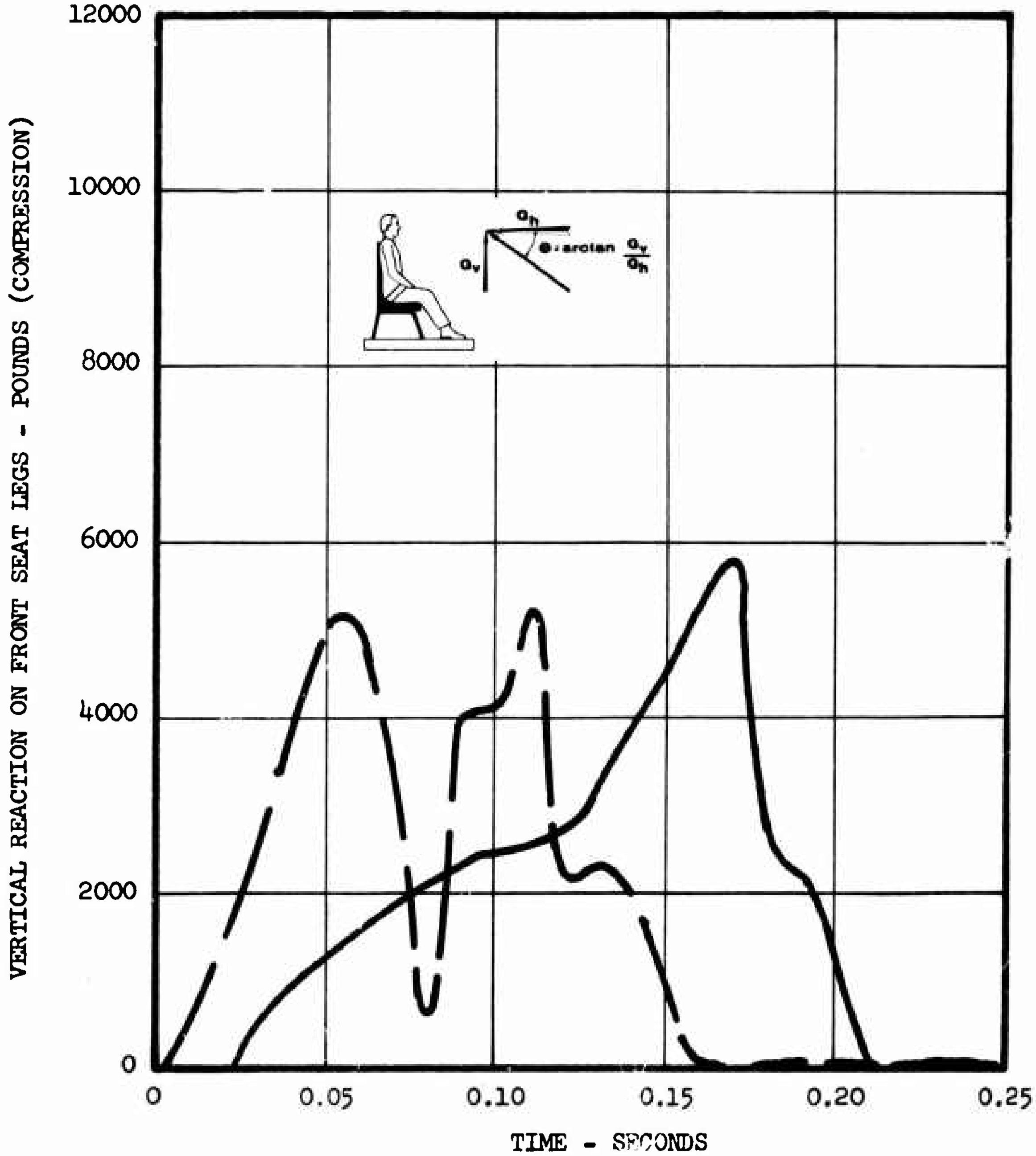

Figure 61. Vertical Reaction on Front Seat Legs Versus Time.

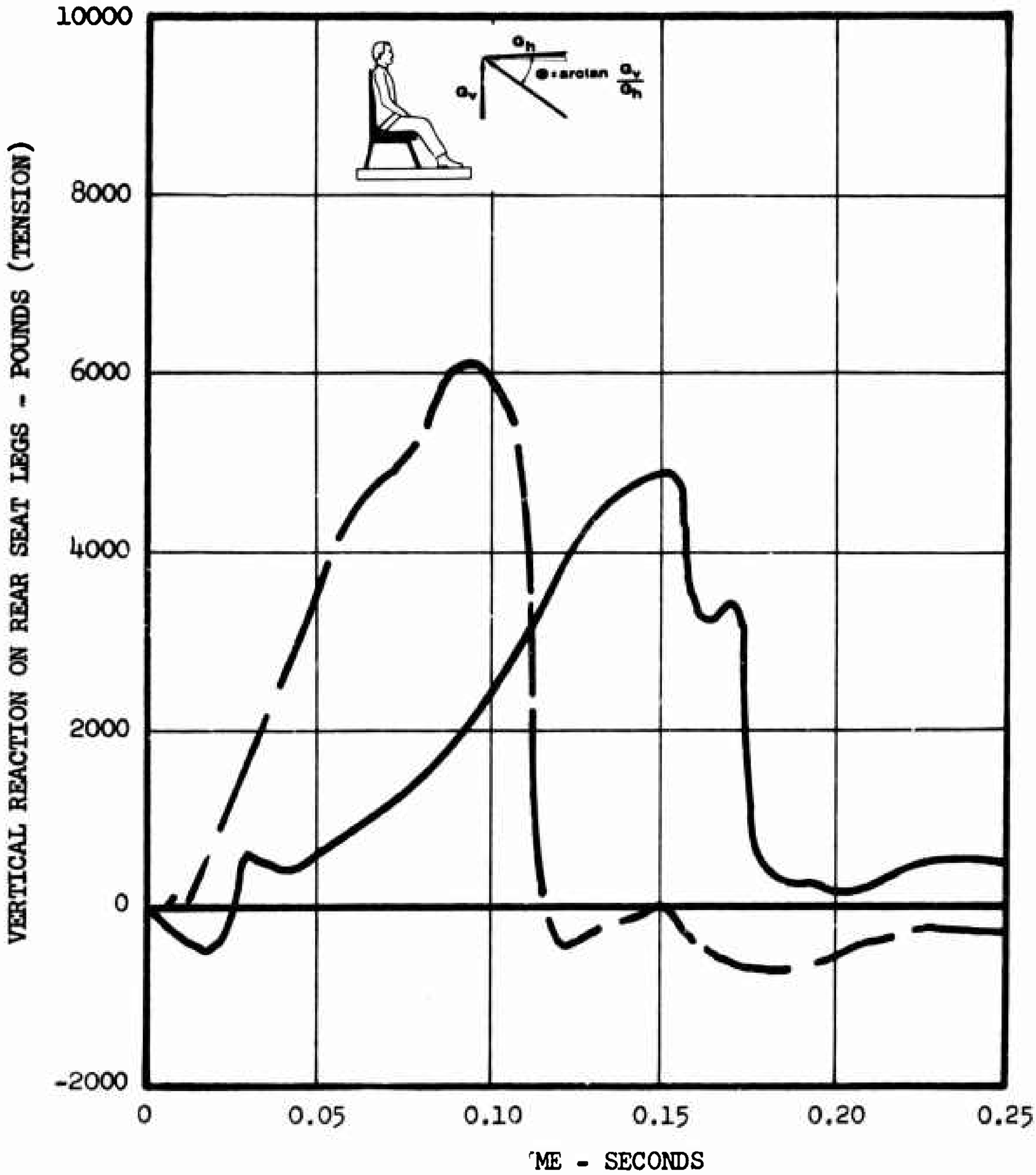

Figure 62. Vertical Reaction on Rear Seat Legs Versus Time.

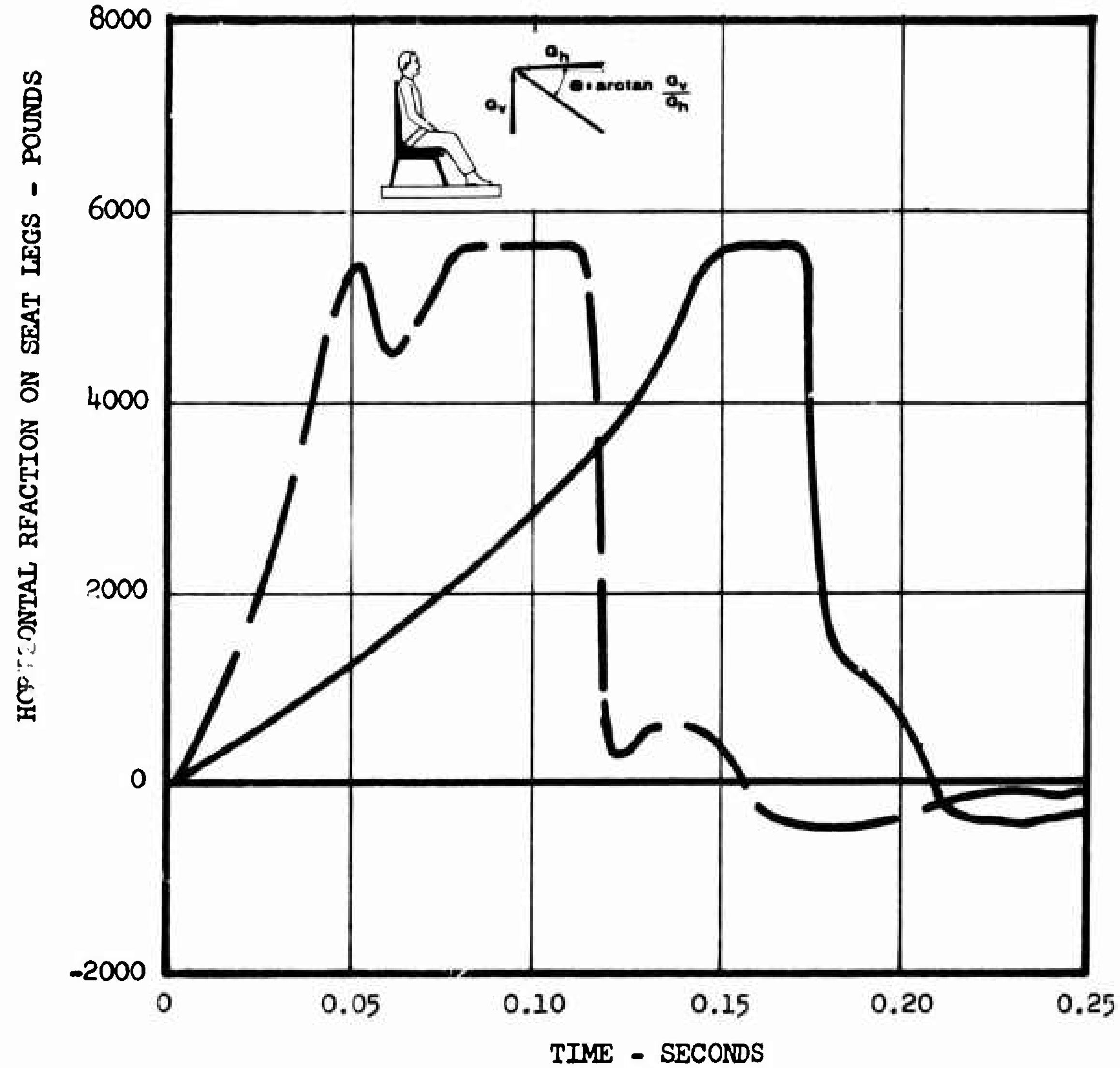

Figure 63. Horizontal Reaction on Seat Legs Versus Time.

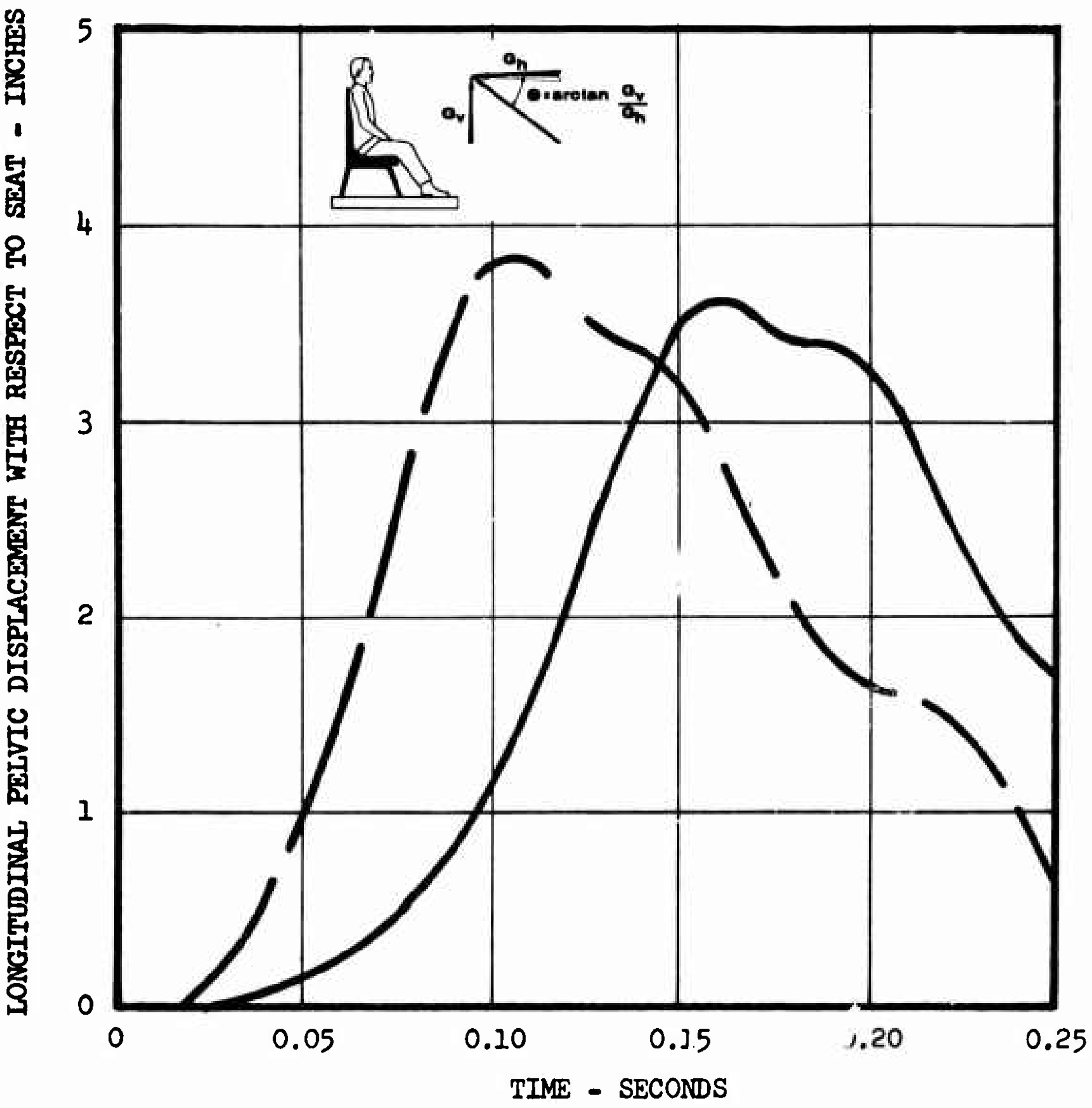

Figure 64. Longitudinal Pelvic Displacement With Respect to Seat Versus Time.

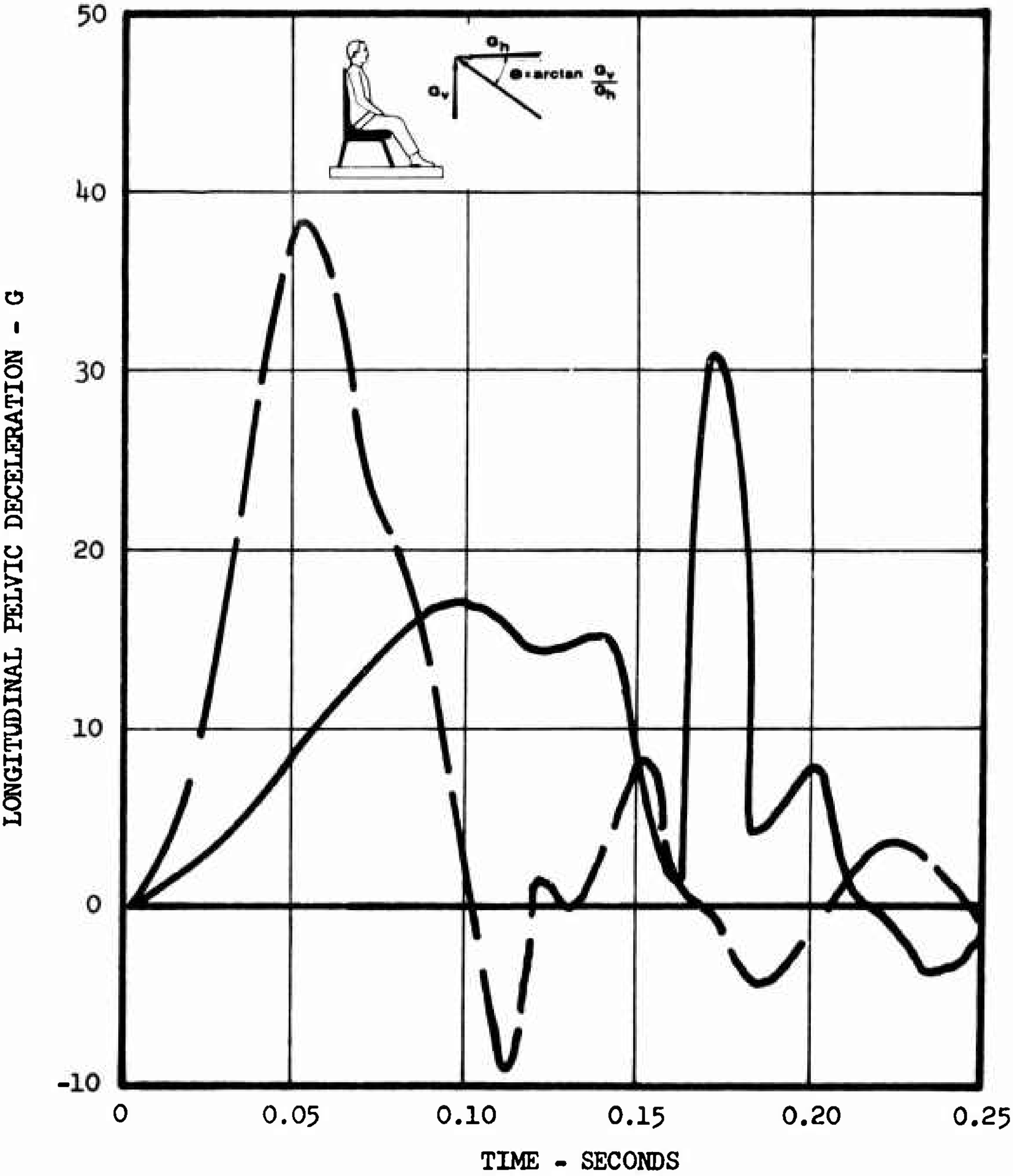

Figure 65. Longitudinal Pelvic Deceleration Versus Time.

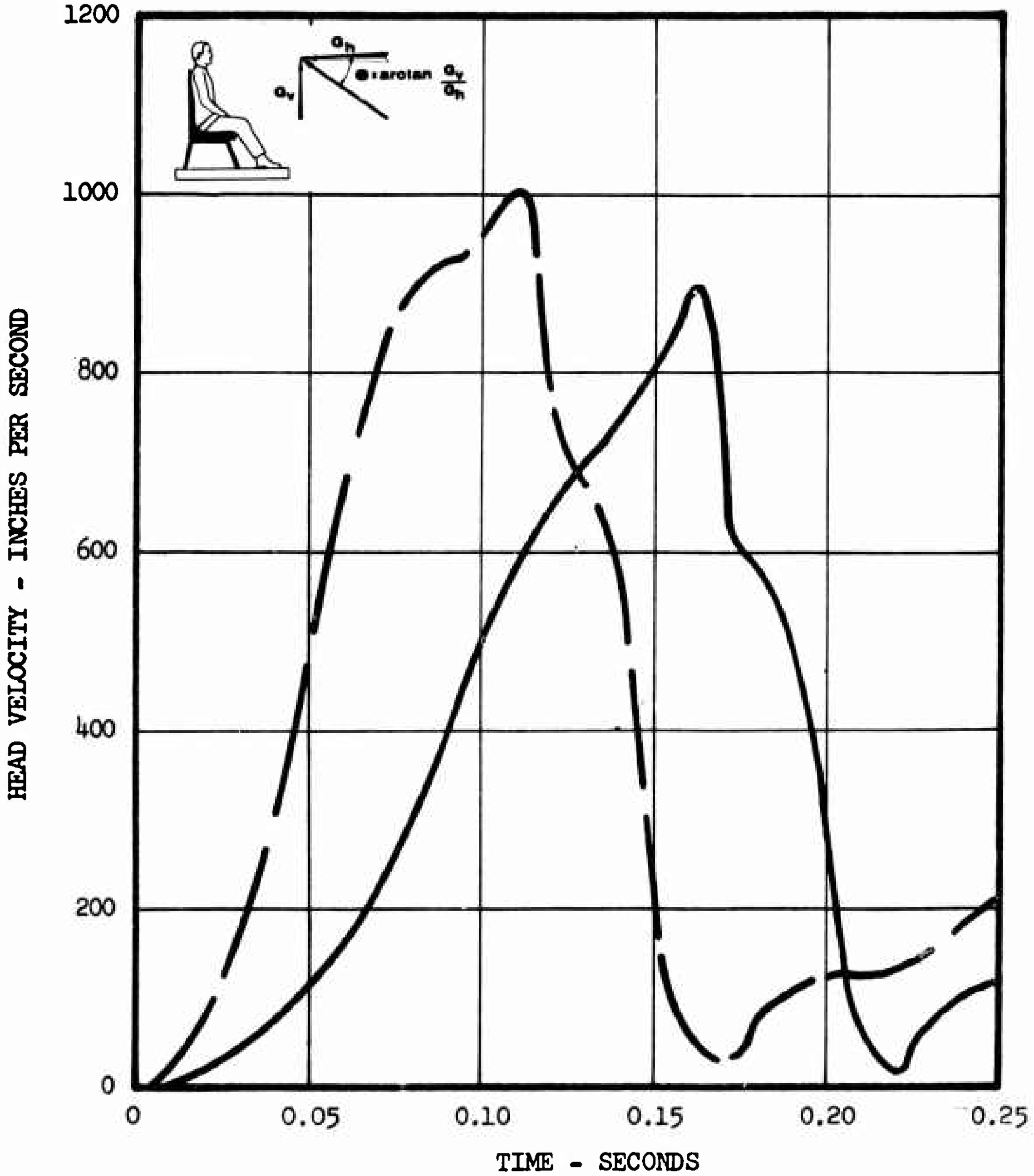

Figure 66. Head Velocity Versus Time.

Figures 67 through 74

Effects of Secondary Spikes in the Crash Pulse

(See p. 45)

Pulse 1

Pulse 2

Pulse 3

Pulse 23*

Pulse 26*

(For pulse shapes see Figure 17)

Seat Belt	Typical (see Figure 4)
Passenger Weight	187 pounds
Load-Limiter Setting	5660 pounds
Ratio of Vertical to Horizontal Acceleration	0. 2
Additional Input Conditions	See Table II, column B

Caution: While qualitative trends and comparisons may be dependably observed in the results presented, quantitative values should be used with caution. Due to changes and improvements in the computer program during preparation of the curves, current best estimates may differ somewhat from the data presented. For example, see Appendix III, page 285.

*Seat damping coefficients are zero in computer program.

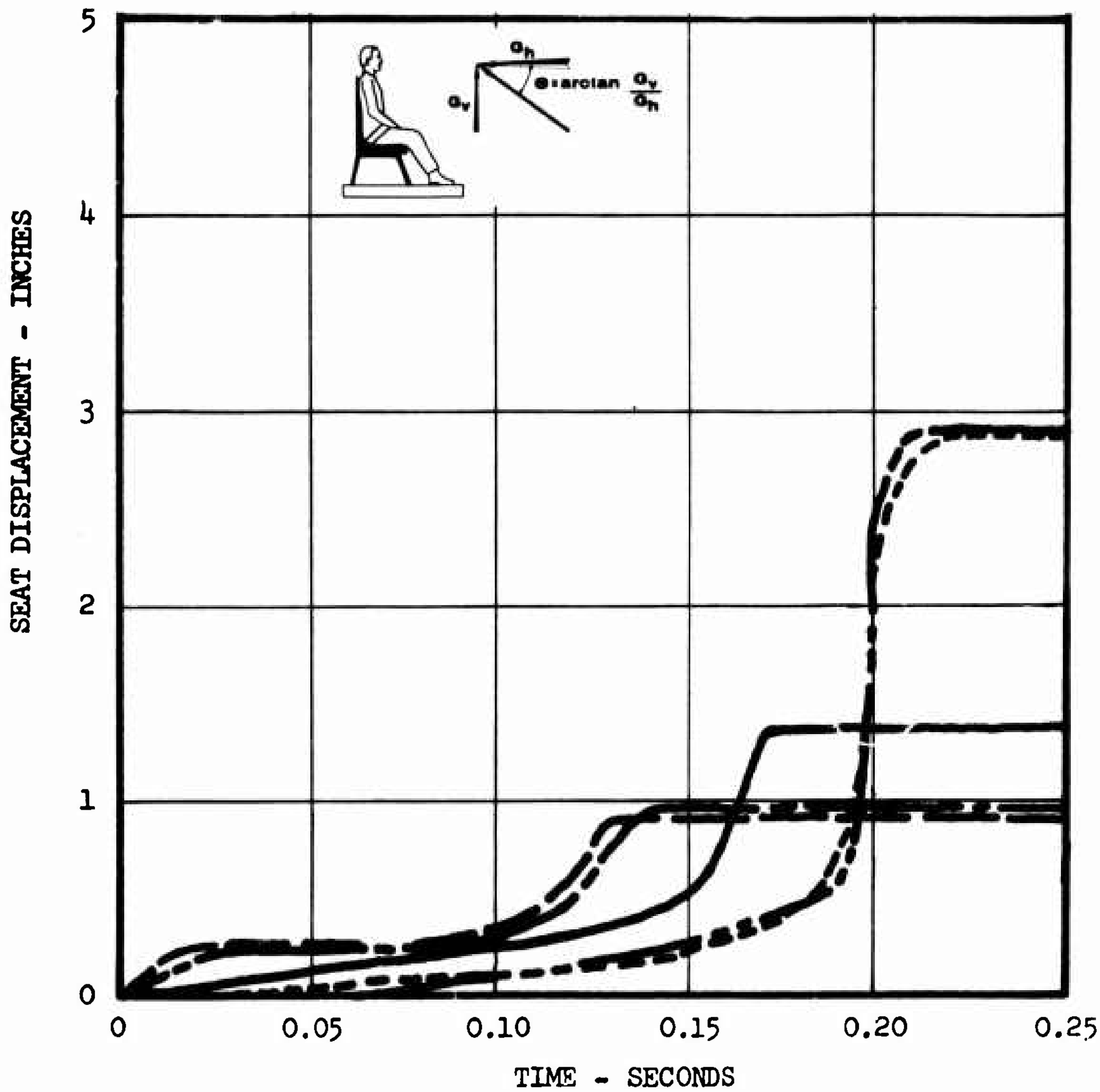

Figure 67. Seat Displacement Versus Time.

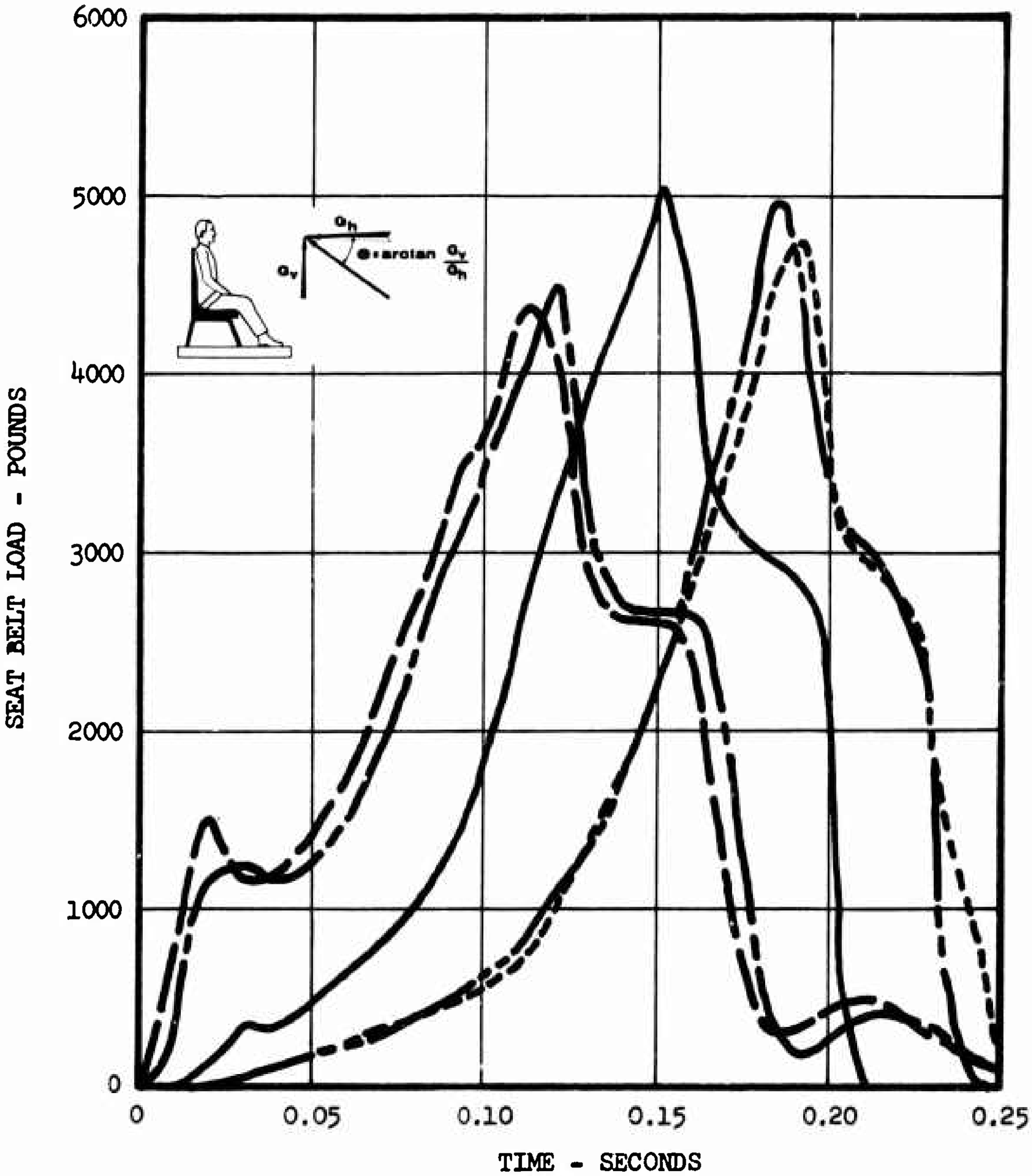

Figure 68. Seat Belt Load Versus Time.

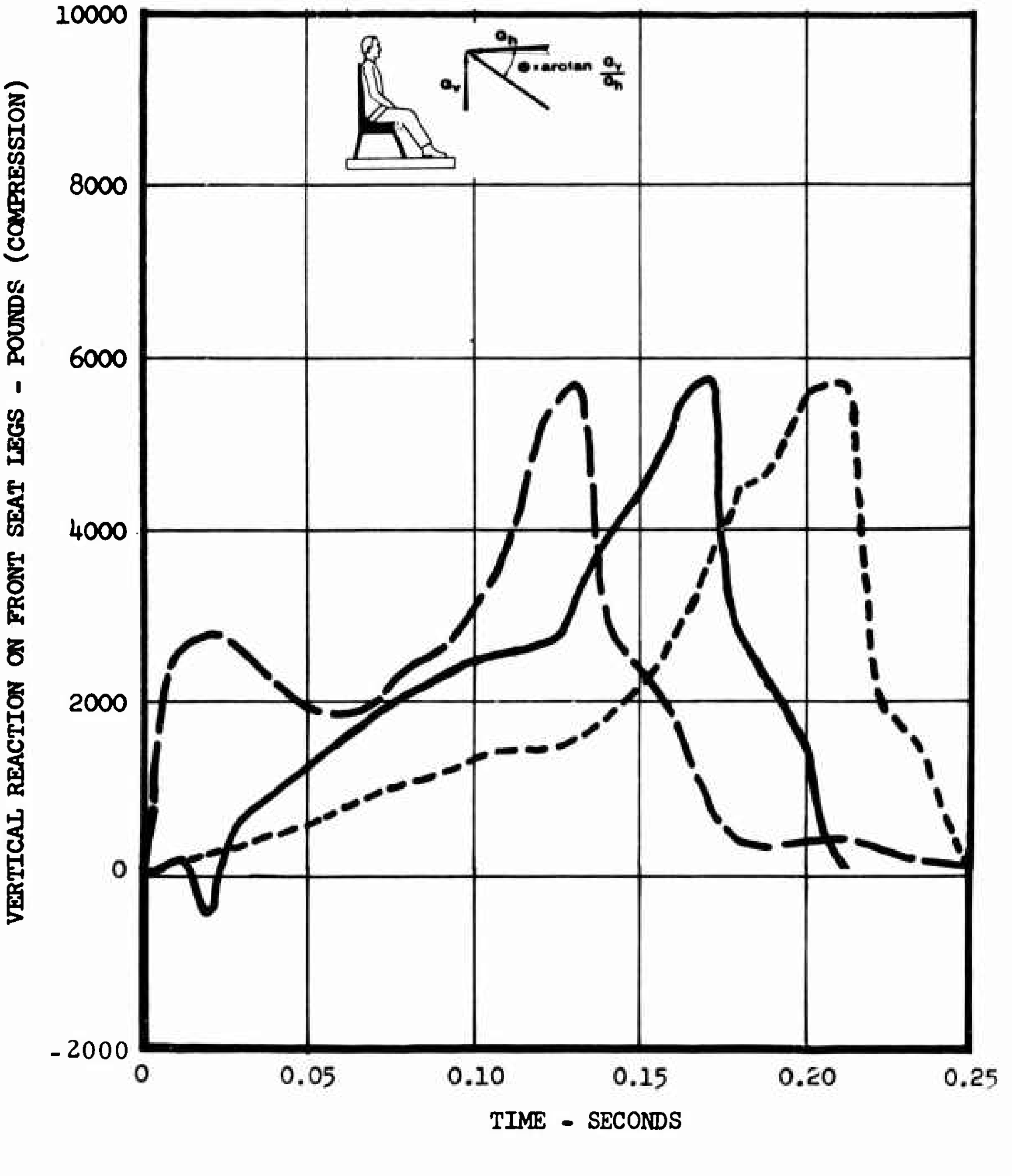

Figure 69. Vertical Reaction on Front Seat Legs Versus Time.

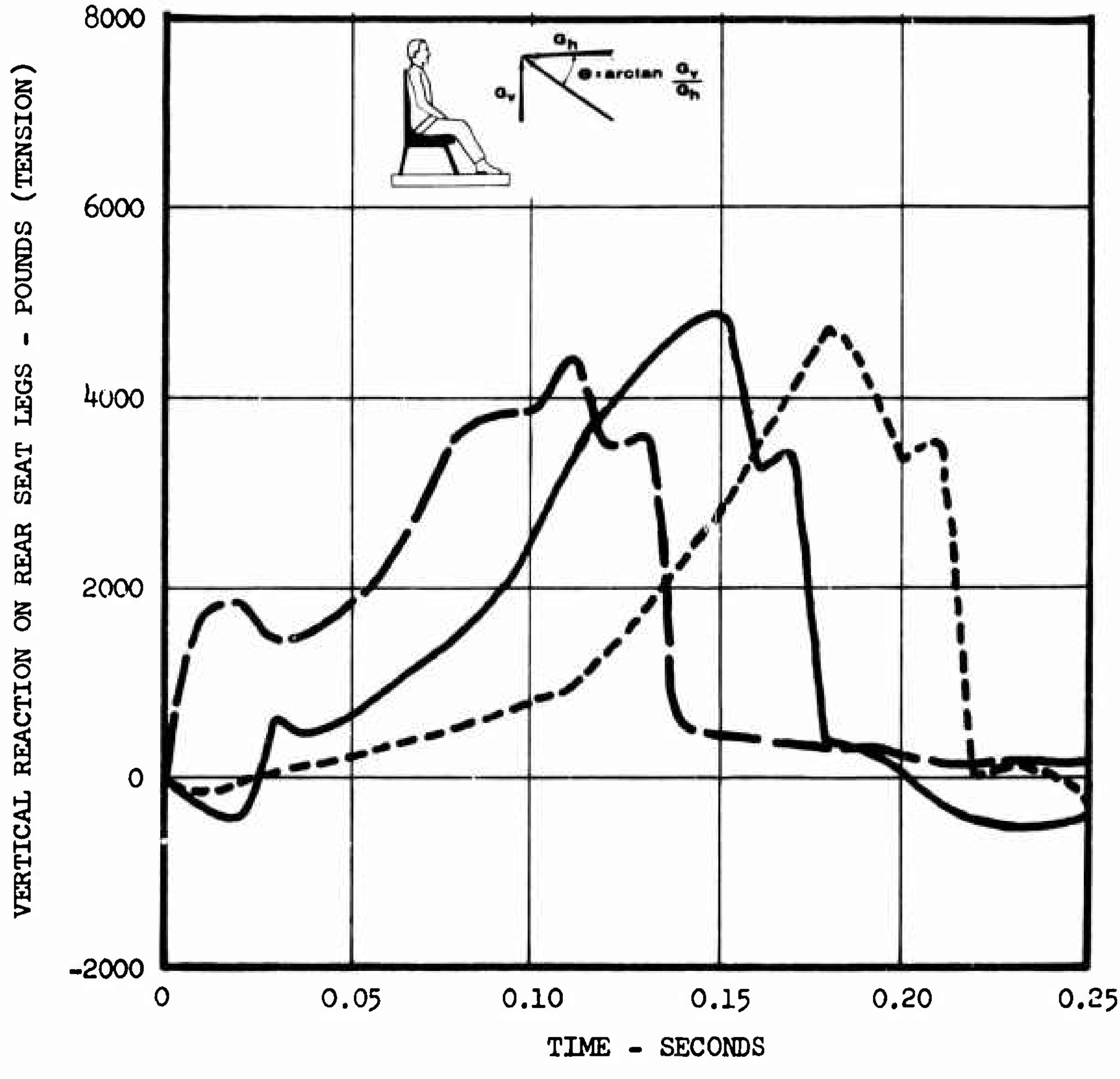

Figure 70. Vertical Reaction on Rear Seat Legs Versus Time.

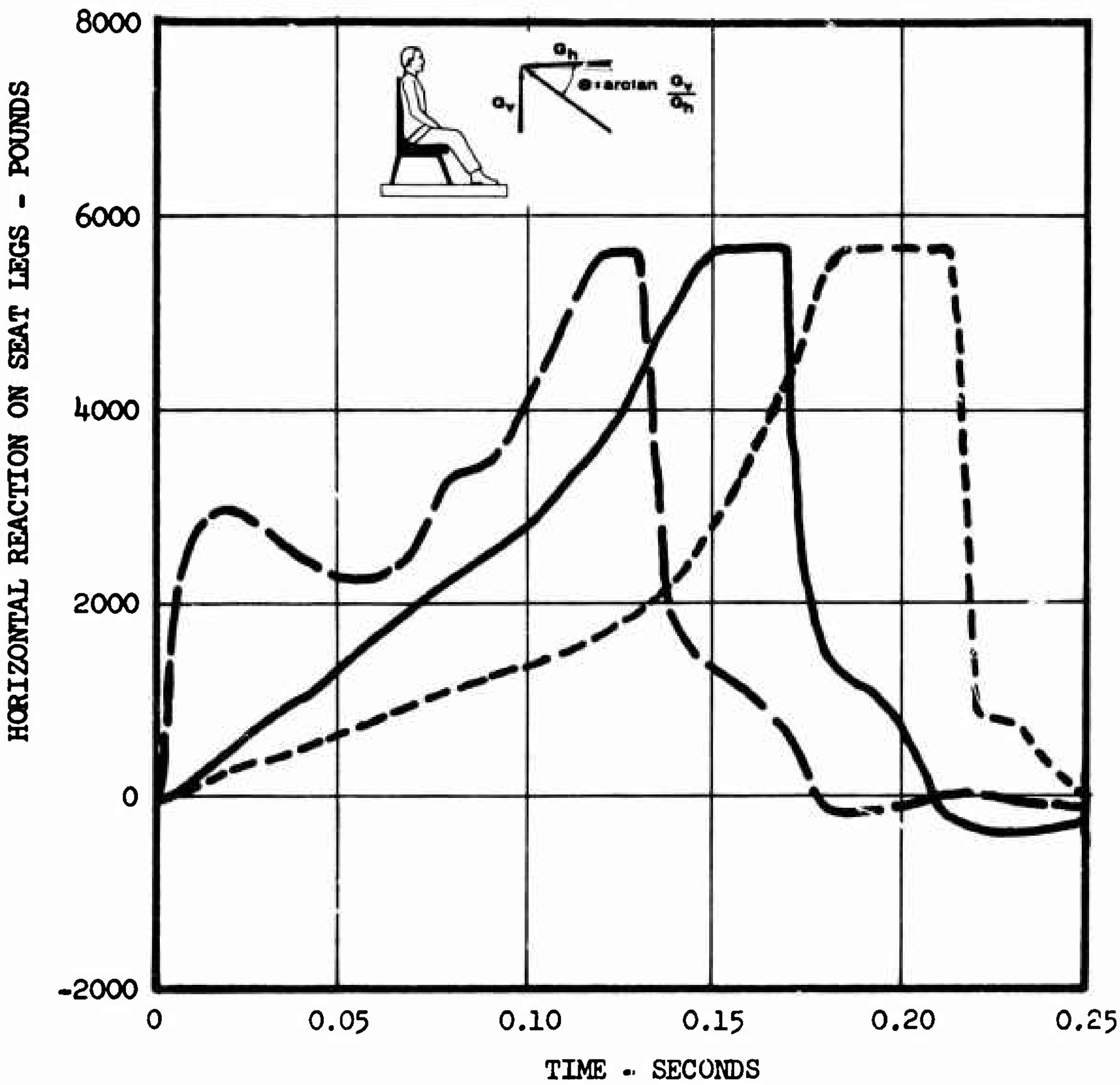

Figure 71. Horizontal Reaction on Seat Legs Versus Time.

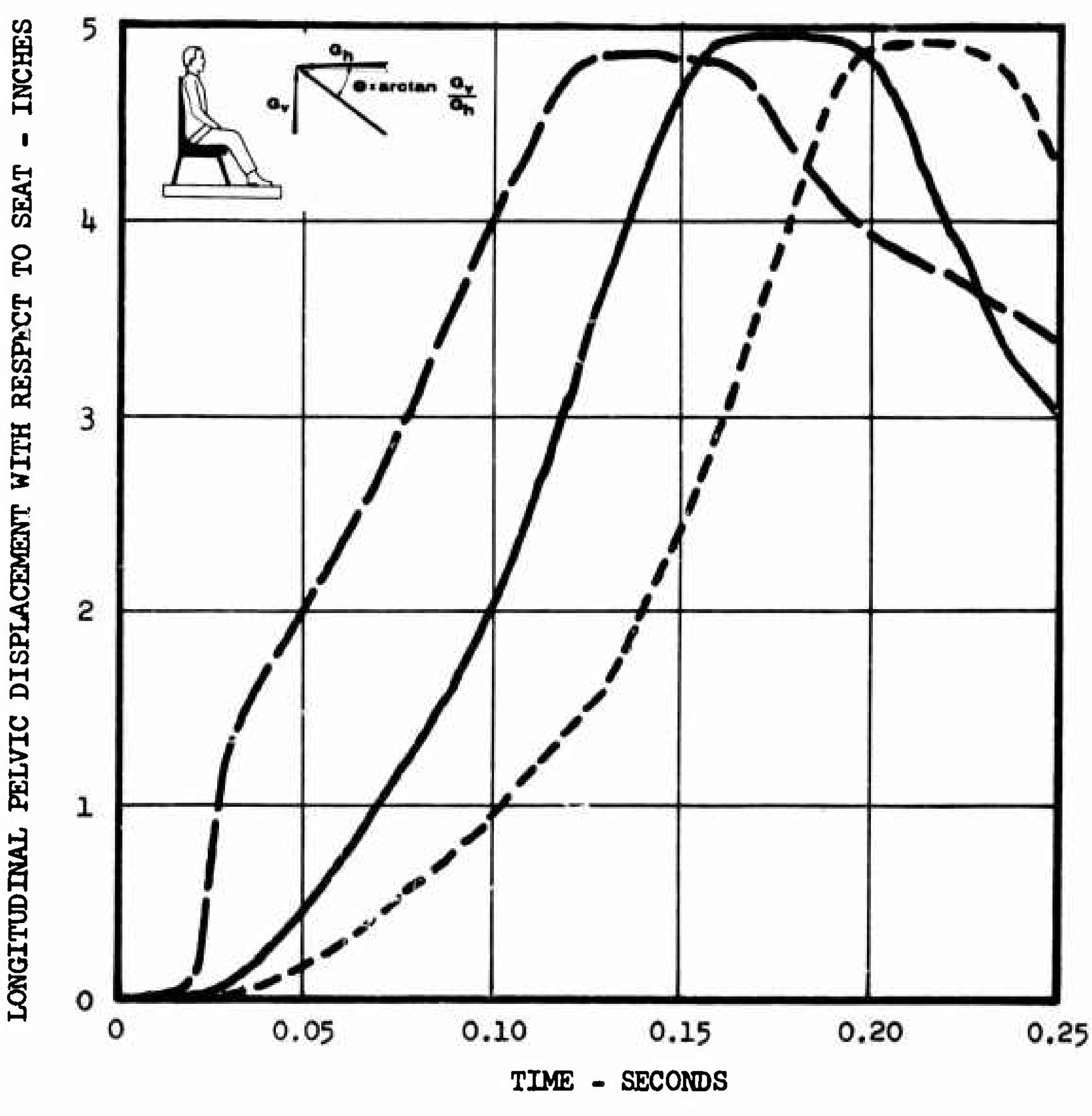

Figure 72. Longitudinal Pelvic Displacement With Respect to Seat Versus Time.

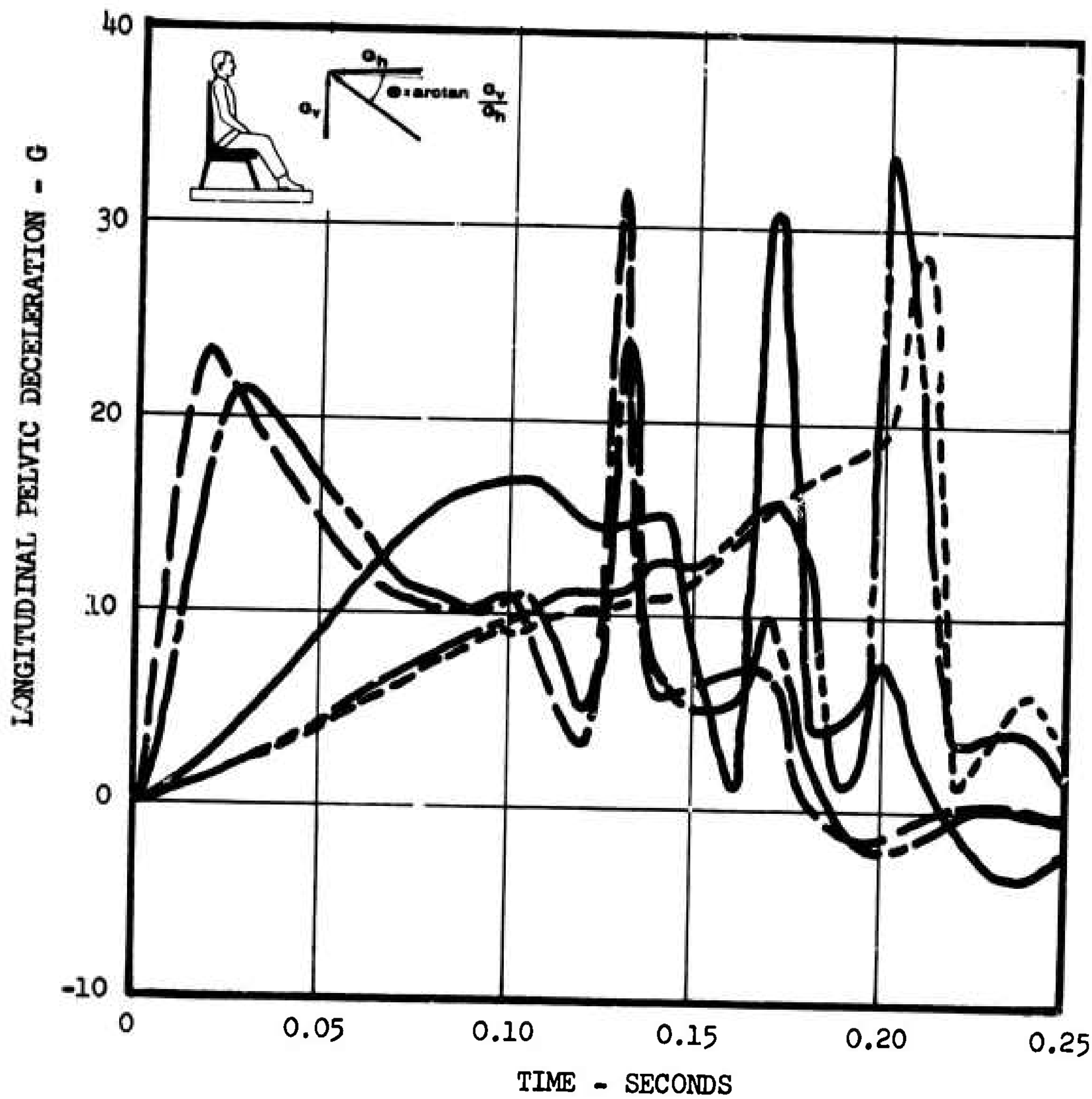

Figure 73. Longitudinal Pelvic Deceleration Versus Time.

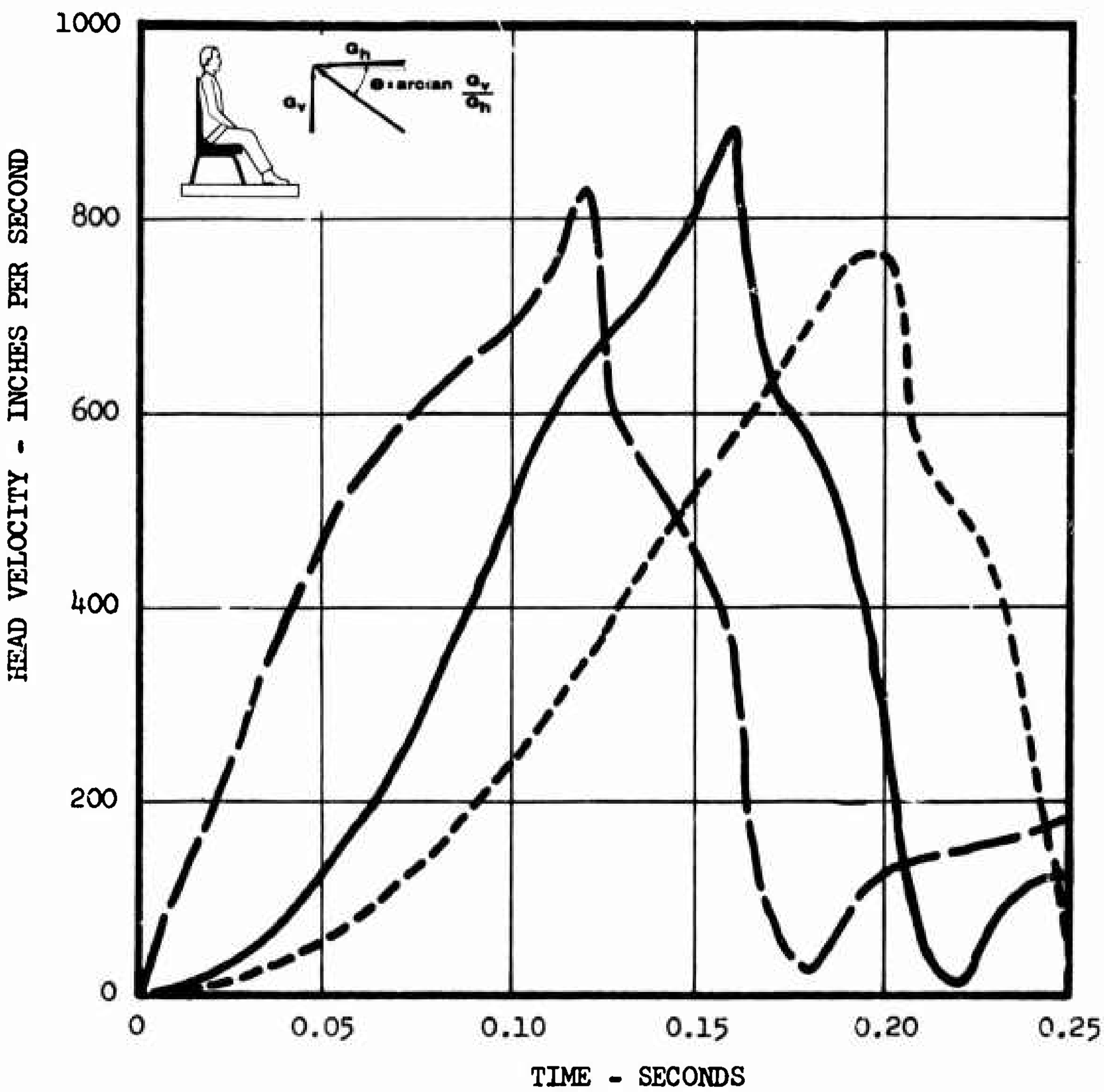

Figure 74. Head Velocity Versus Time.

Figures 75 through 82

Effects of Repeated Peaks in the Crash Pulse

(See p. 46)

Pulse 3

Pulse 29

Pulse 30

(For pulse shapes see Figure 17)

Seat Belt	Typical (see Figure 4)
Passenger Weight	187 pounds
Load-Limiter Setting	5660 pounds
Ratio of Vertical to Horizontal Acceleration	0. 2
Additional Input Conditions	See Table II, column B

Caution:
While qualitative trends and comparisons may be dependably observed in the results presented, quantitative values should be used with caution. Due to changes and improvements in the computer program during preparation of the curves, current best estimates may differ somewhat from the data presented. For example, see Appendix III, page 285.

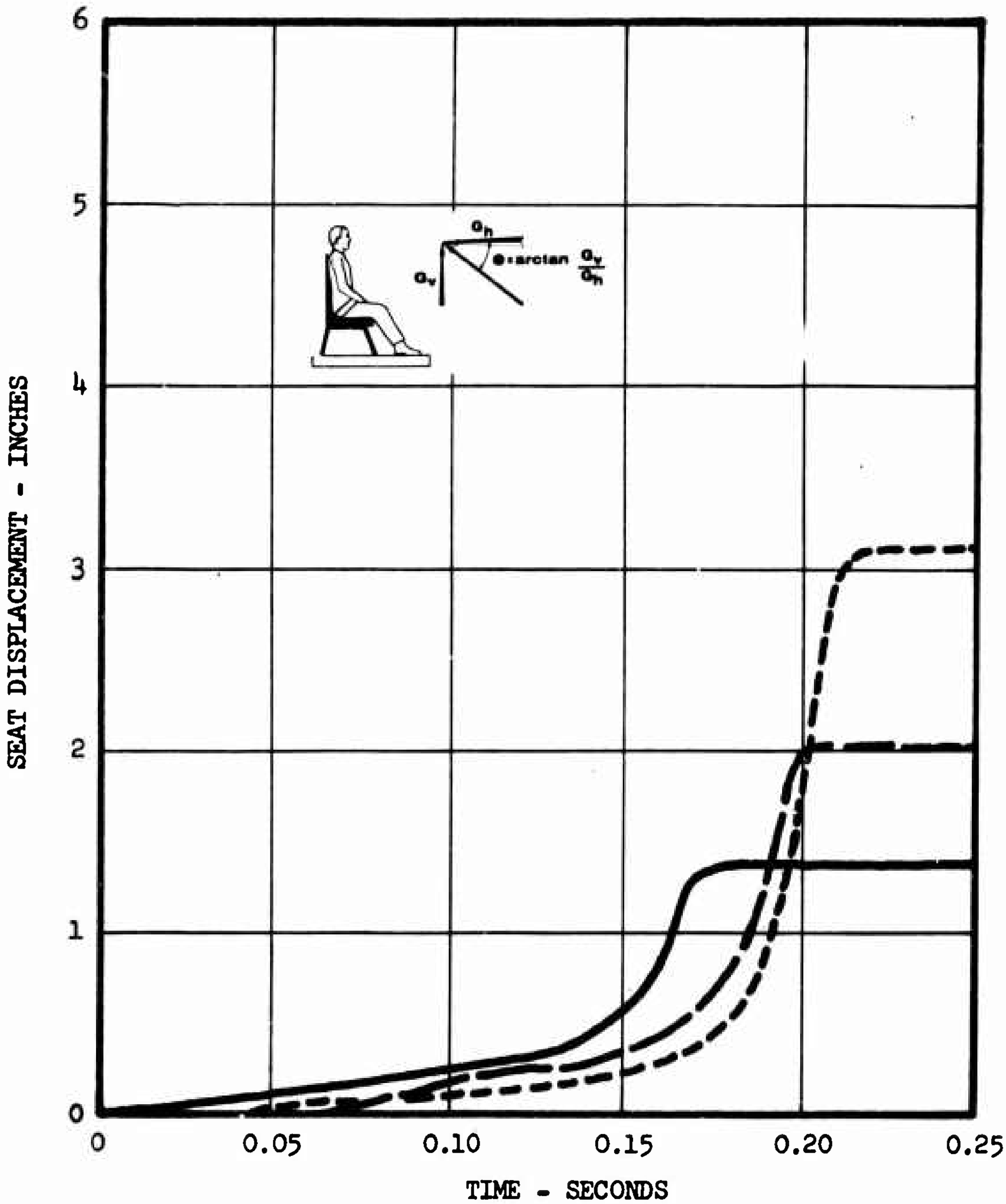

Figure 75. Seat Displacement Versus Time.

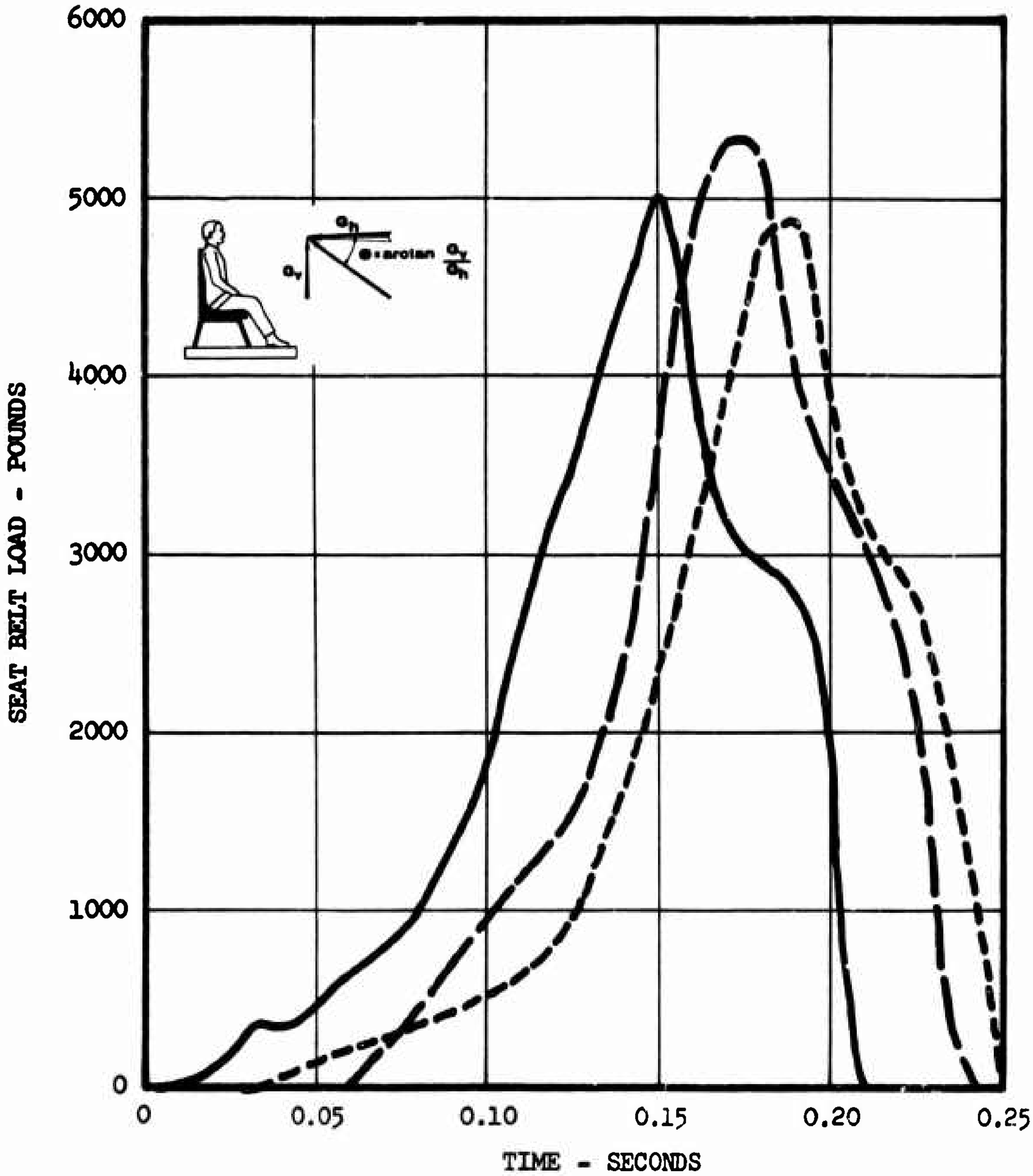

Figure 76. Seat Belt Load Versus Time.

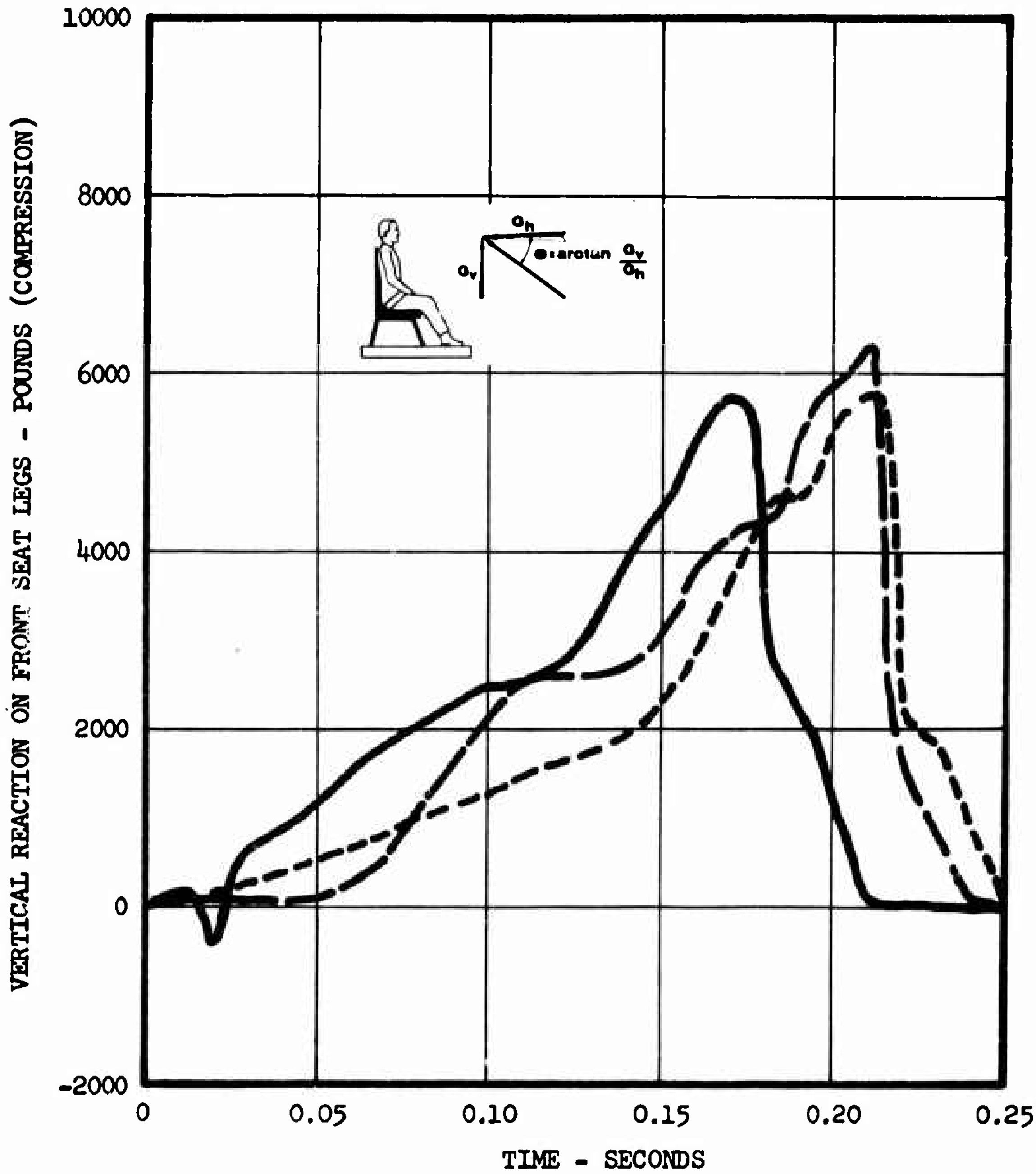

Figure 77. Vertical Reaction on Front Seat Legs Versus Time.

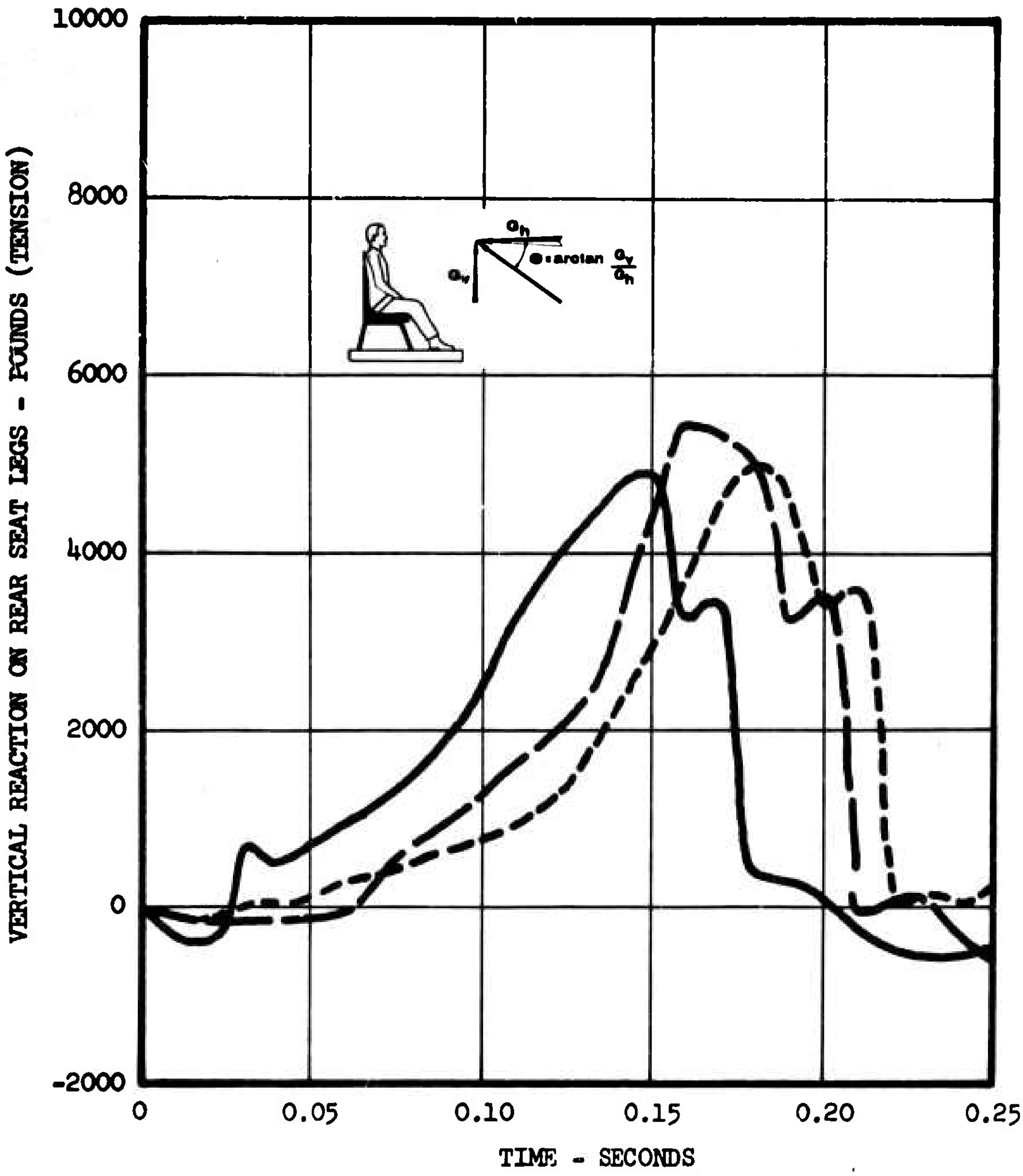

Figure 78. Vertical Reaction on Rear Seat Legs Versus Time.

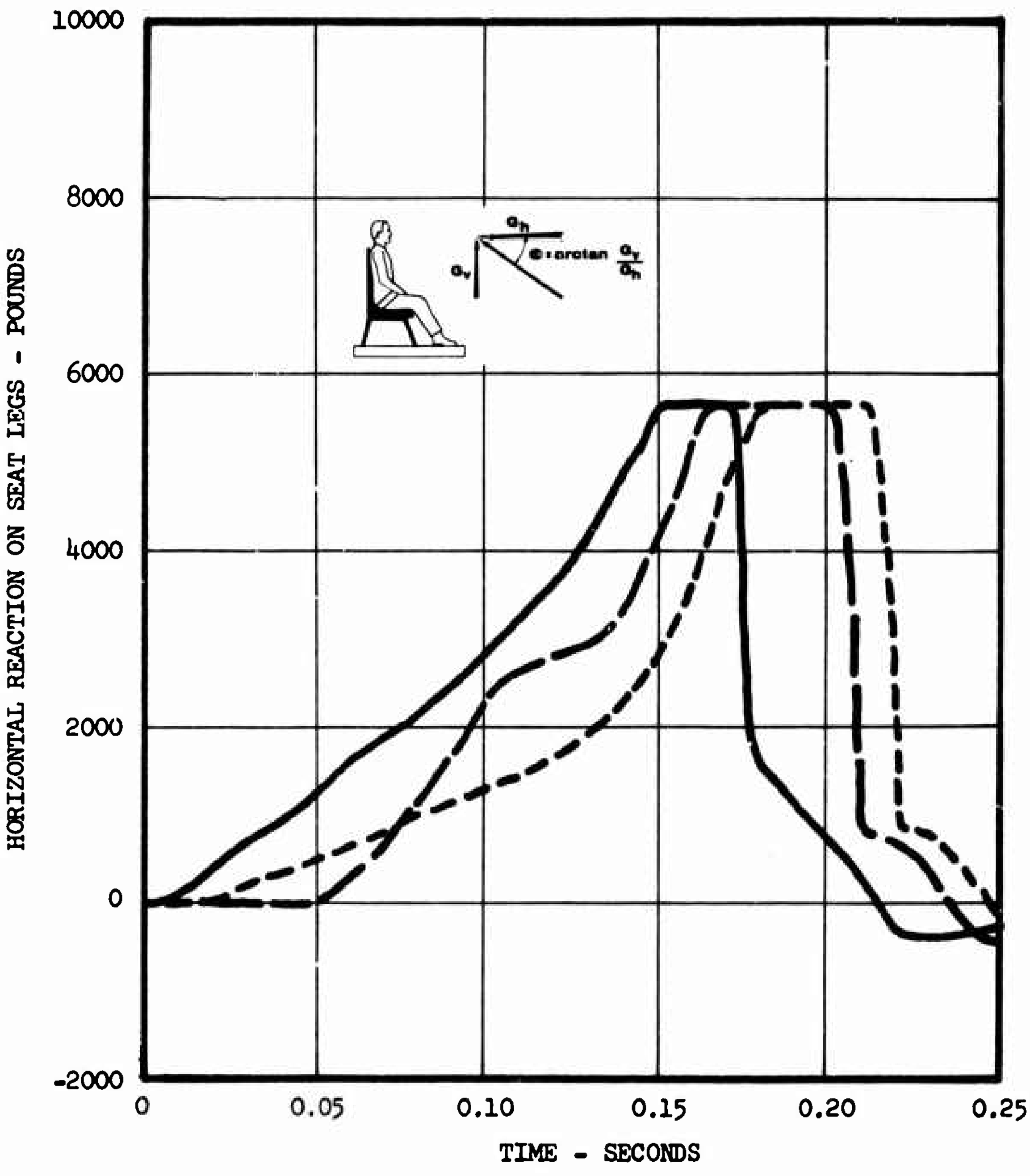

Figure 79. Horizontal Reaction on Seat Legs Versus Time.

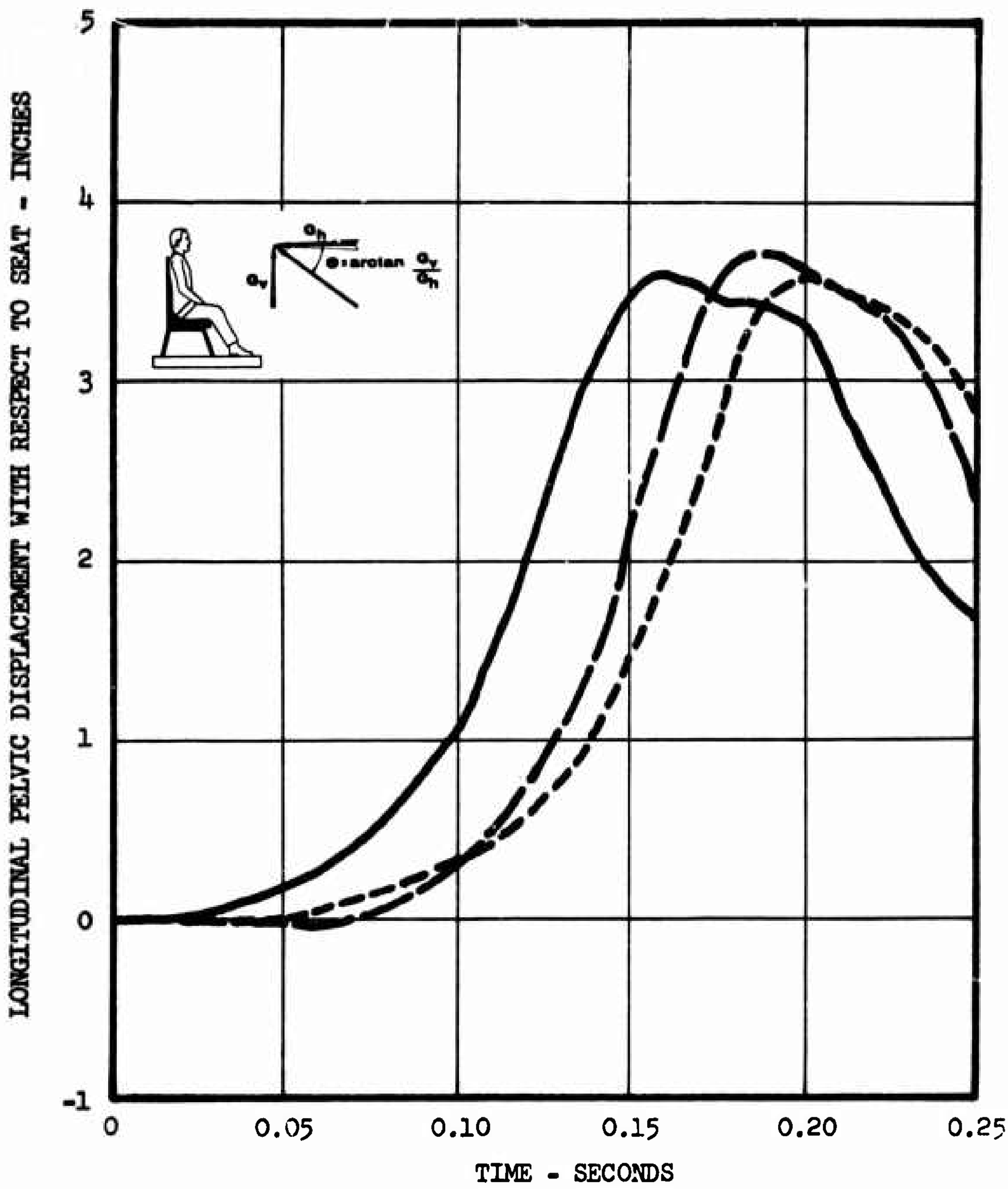

Figure 80. Longitudinal Pelvic Displacement With Respect to Seat Versus Time.

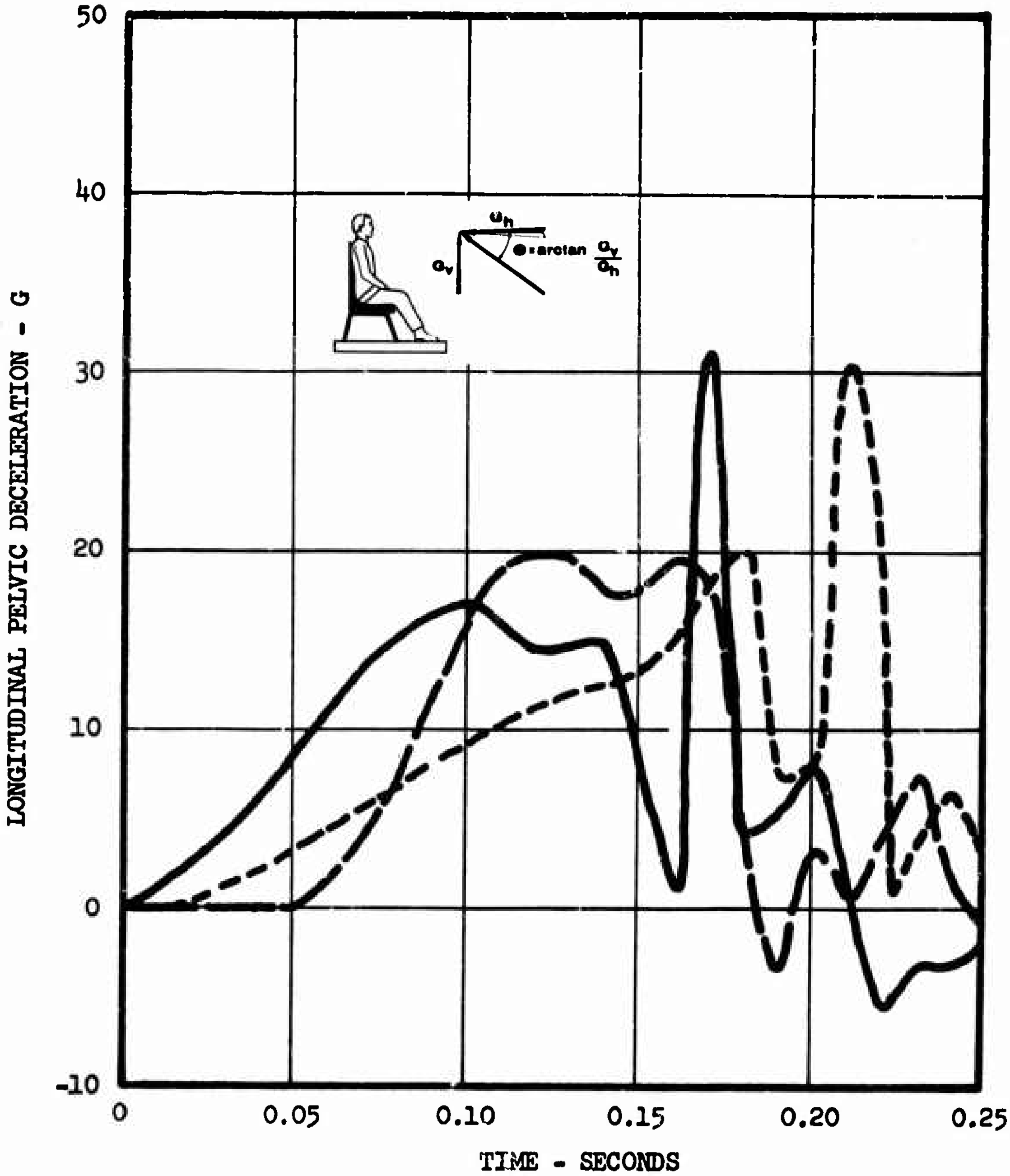

Figure 81. Longitudinal Pelvic Deceleration Versus Time.

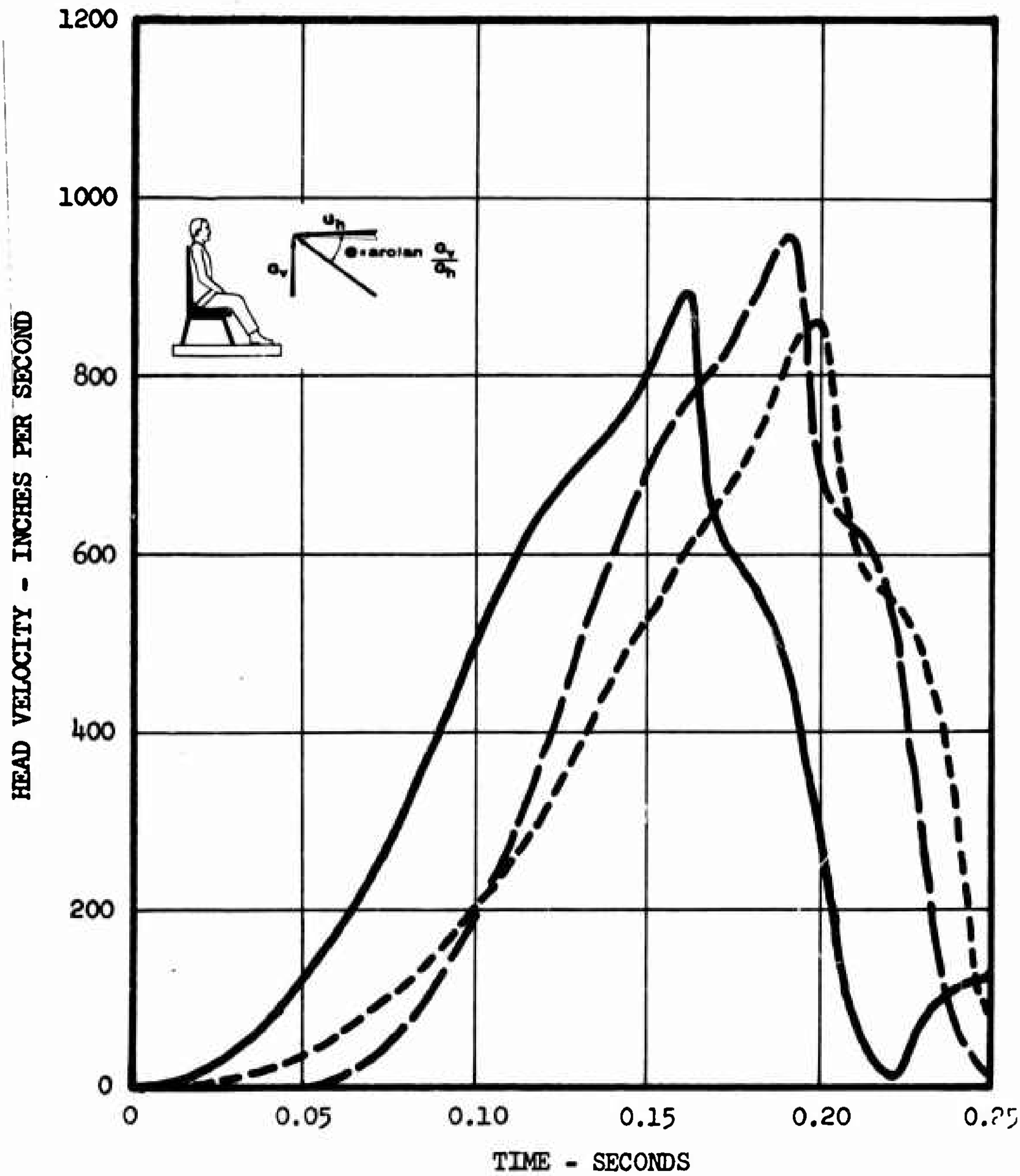

Figure 32. Head Velocity Versus Time.

Figures 83 through 90

Effects of Ratio of Vertical to Horizontal Acceleration Components on Seat

(See p. 46)

Pulse	No. 3* (see Figure 17)
Seat Belt	Typical (see Figure 4)
Passenger Weight	187 pounds
Load-Limiter Setting	5660 pounds

Ratio of Vertical to Horizontal Acceleration

$G_V/G_H = 0.0$	— — — — — —
$= 0.2$	————————————
$= 0.4$	- - - - - - - - - - - - - -

Additional Input Conditions	See Table II, column B

Caution:
While qualitative trends and comparisons may be dependably observed in the results presented, quantitative values should be used with caution. Due to changes and improvements in the computer program during preparation of the curves, current best estimates may differ somewhat from the data presented. For example, see Appendix III, page 285.

*Seat damping coefficients are zero in computer program.

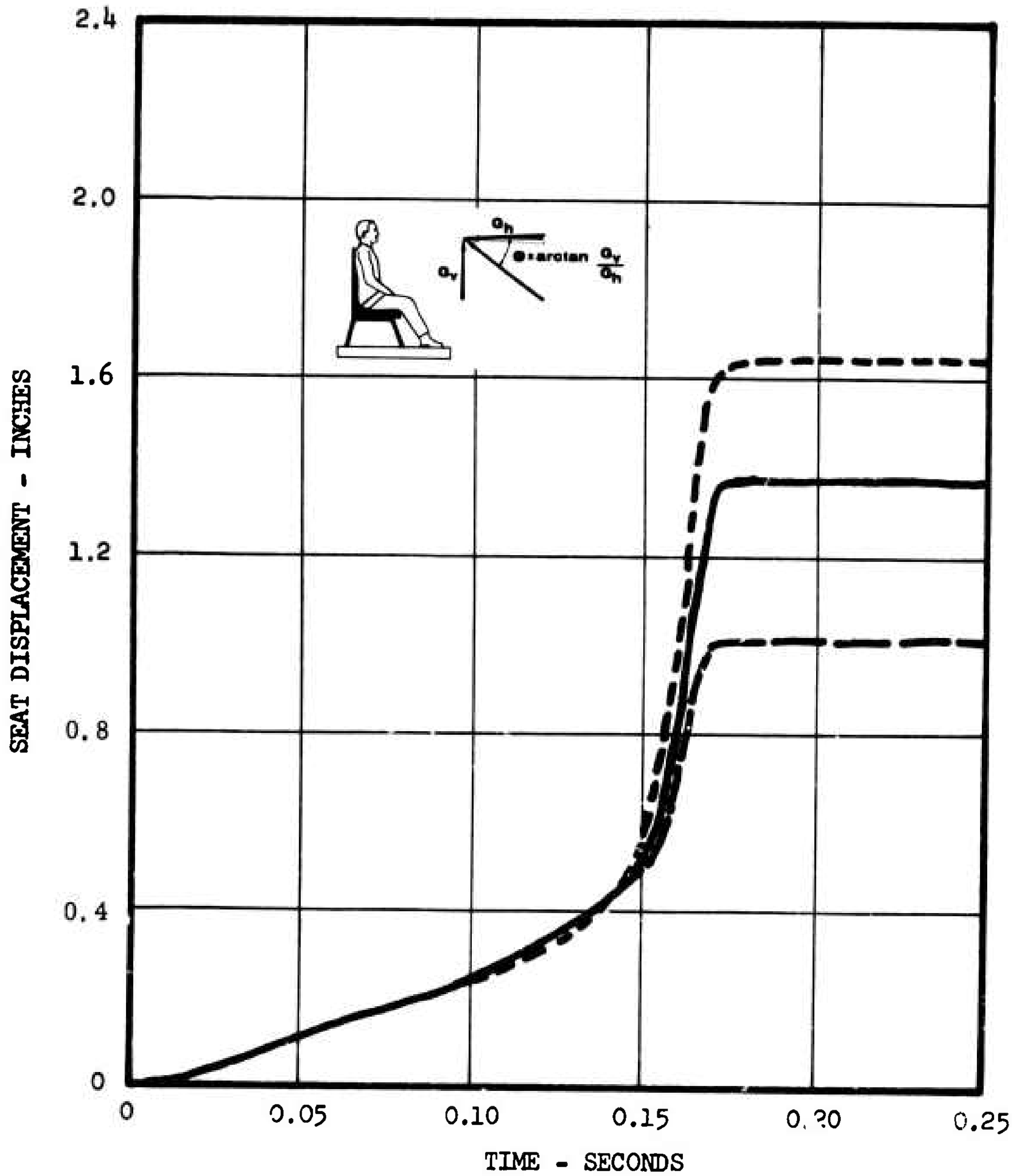

Figure 83. Seat Displacement Versus Time.

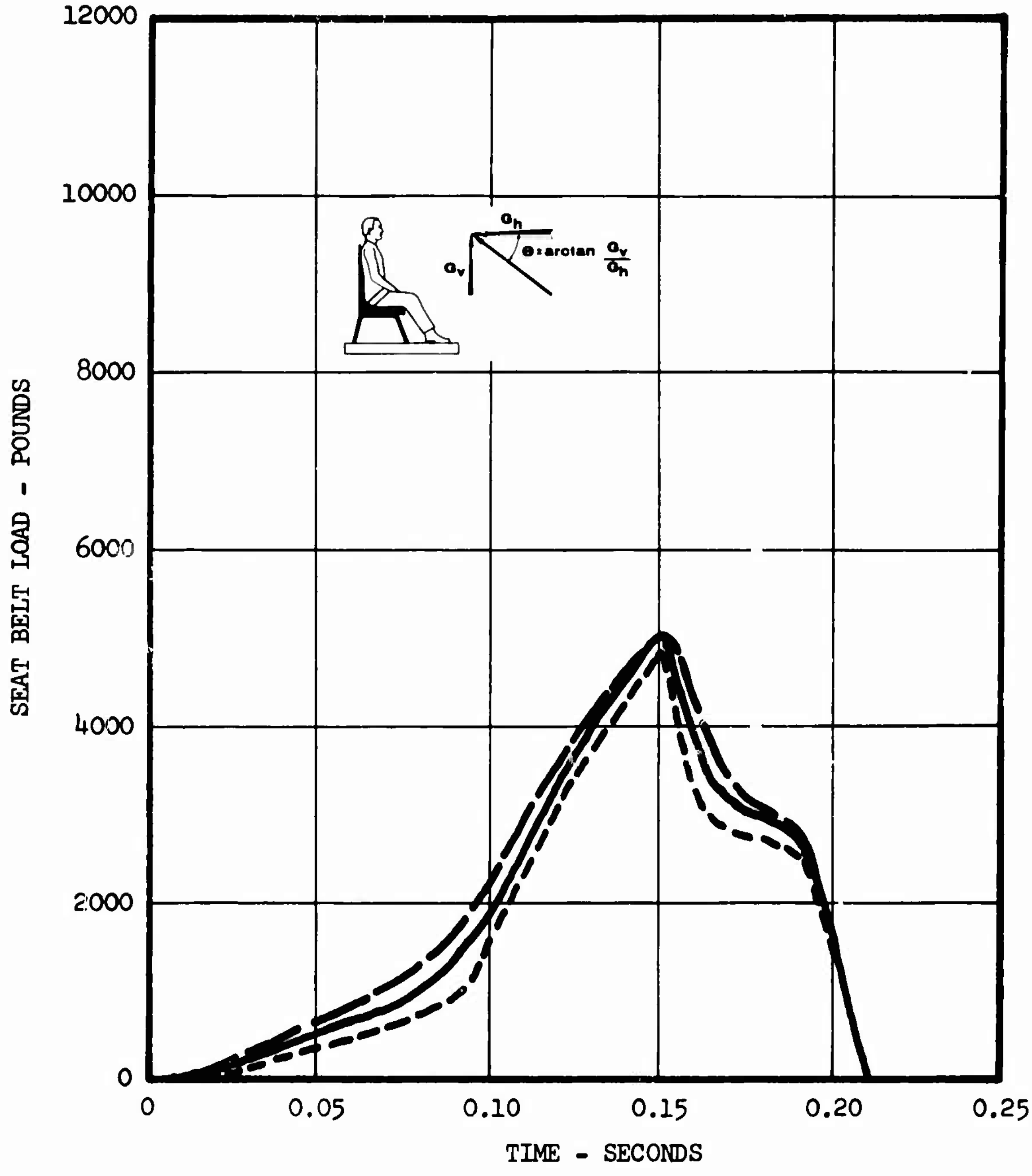

Figure 84. Seat Belt Load Versus Time.

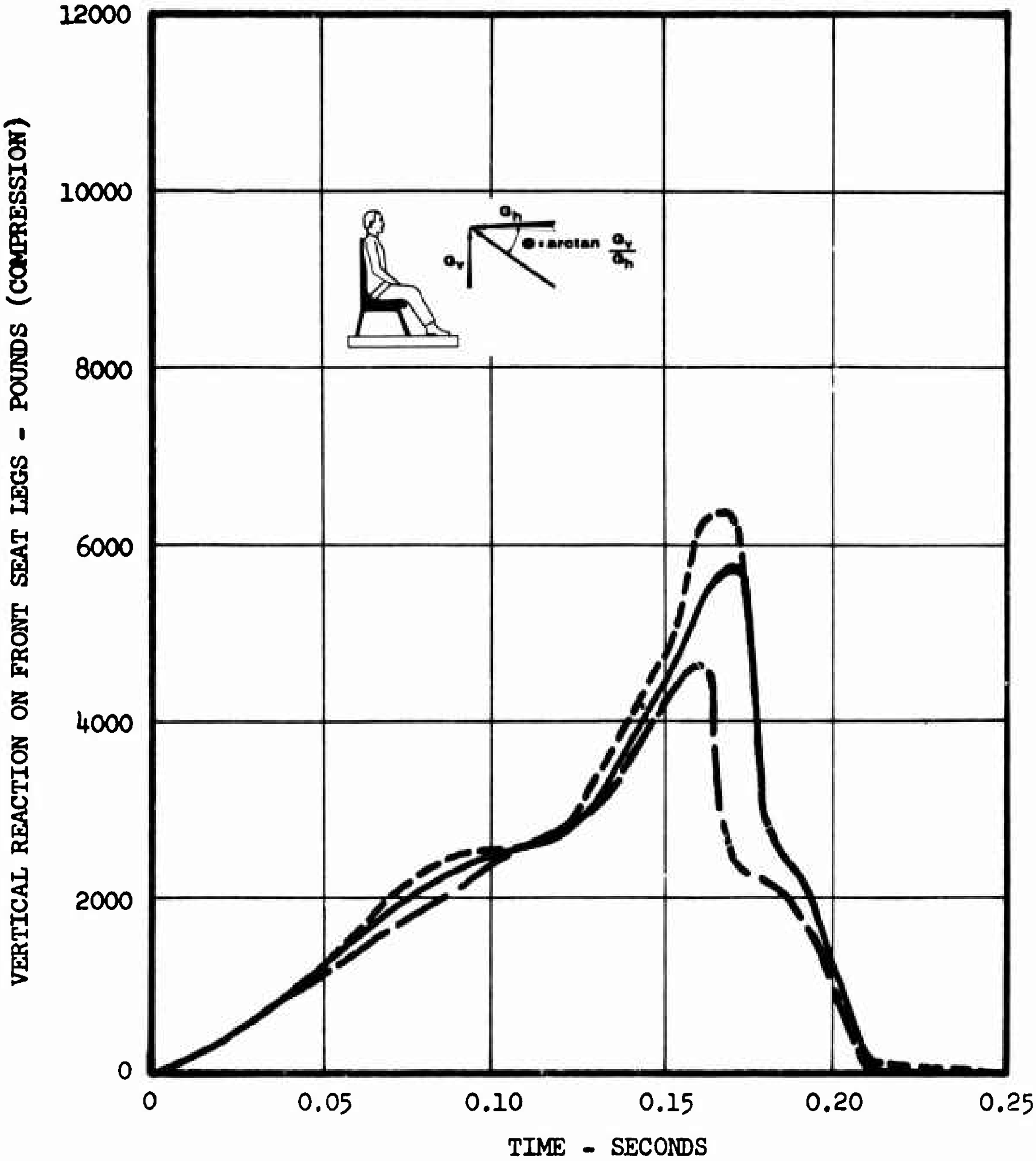

Figure 85. Vertical Reaction on Front Seat Legs Versus Time.

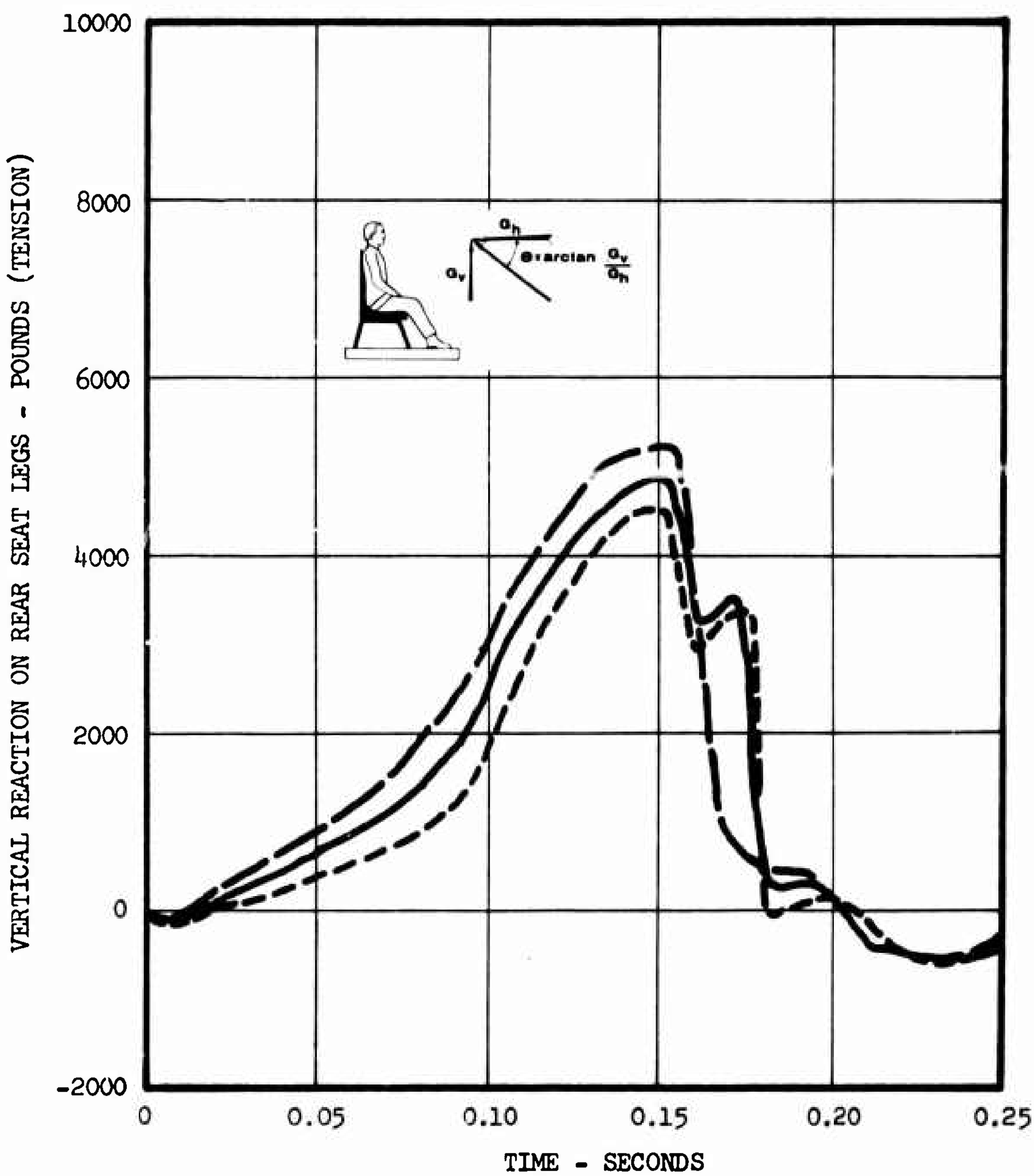

Figure 86. Vertical Reaction on Rear Seat Legs Versus Time.

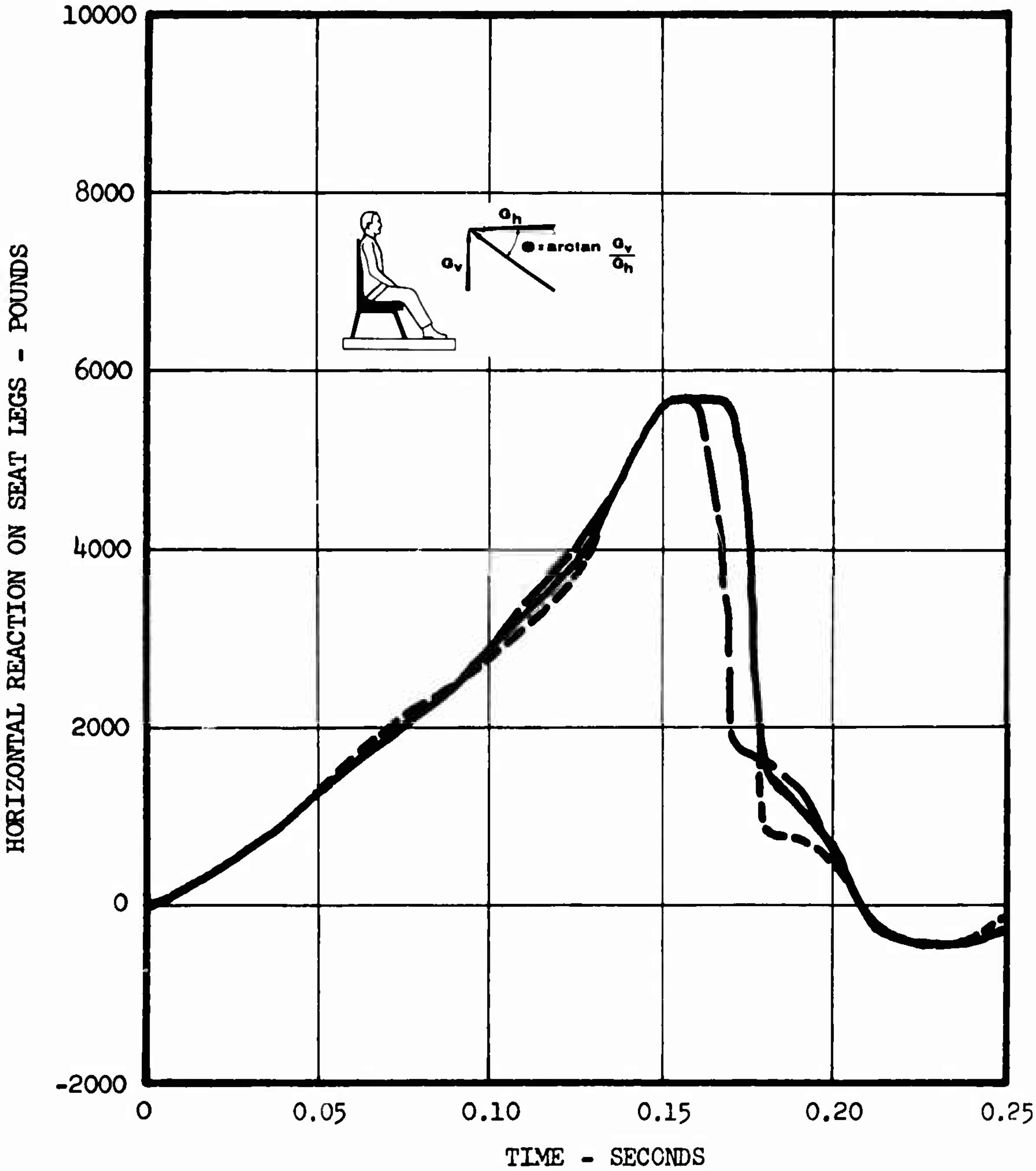

Figure 87. Horizontal Reaction on Seat Legs Versus Time.

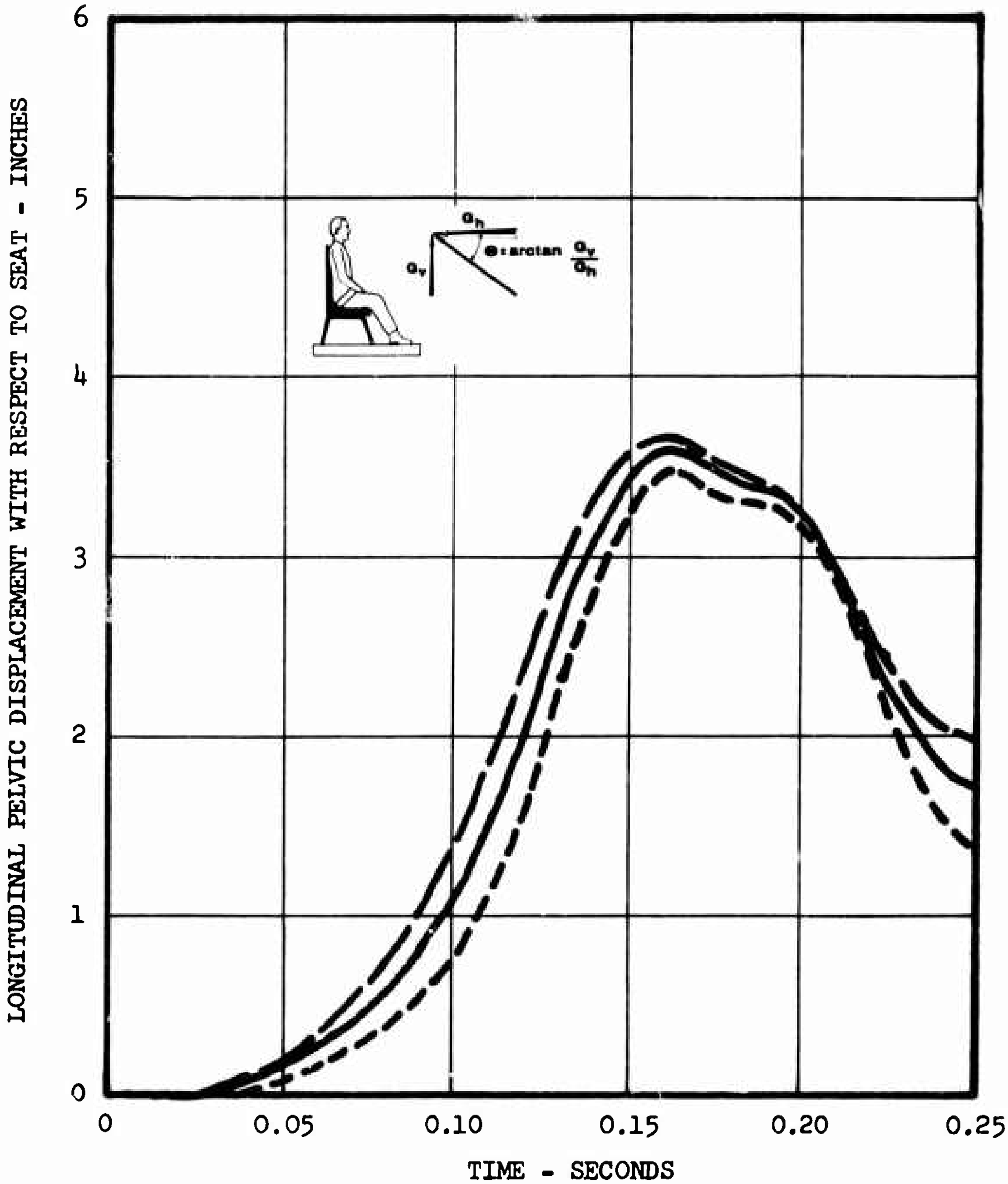

Figure 88. Longitudinal Pelvic Displacement With Respect to Seat Versus Time.

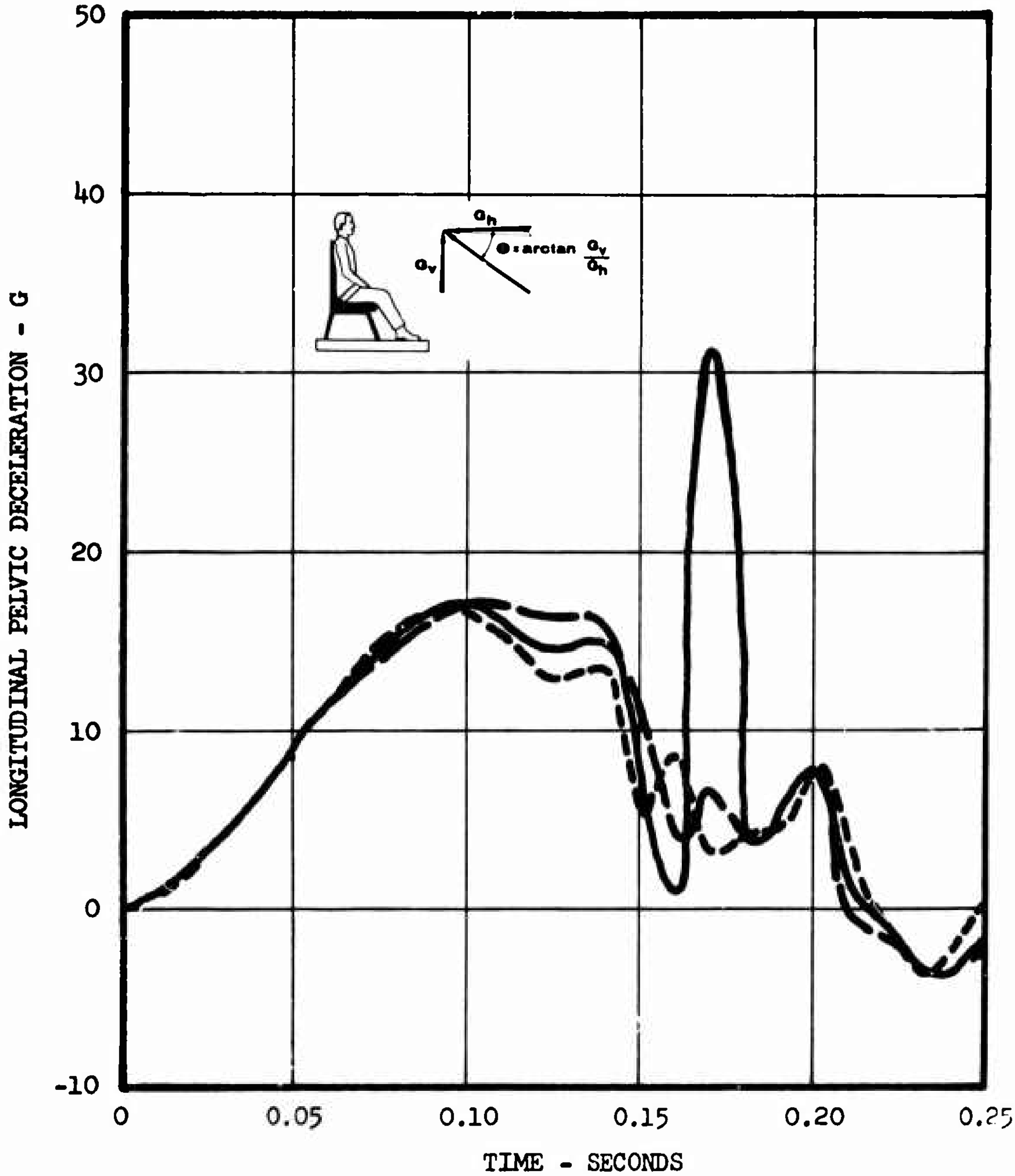

Figure 89. Longitudinal Pelvic Deceleration Versus Time.

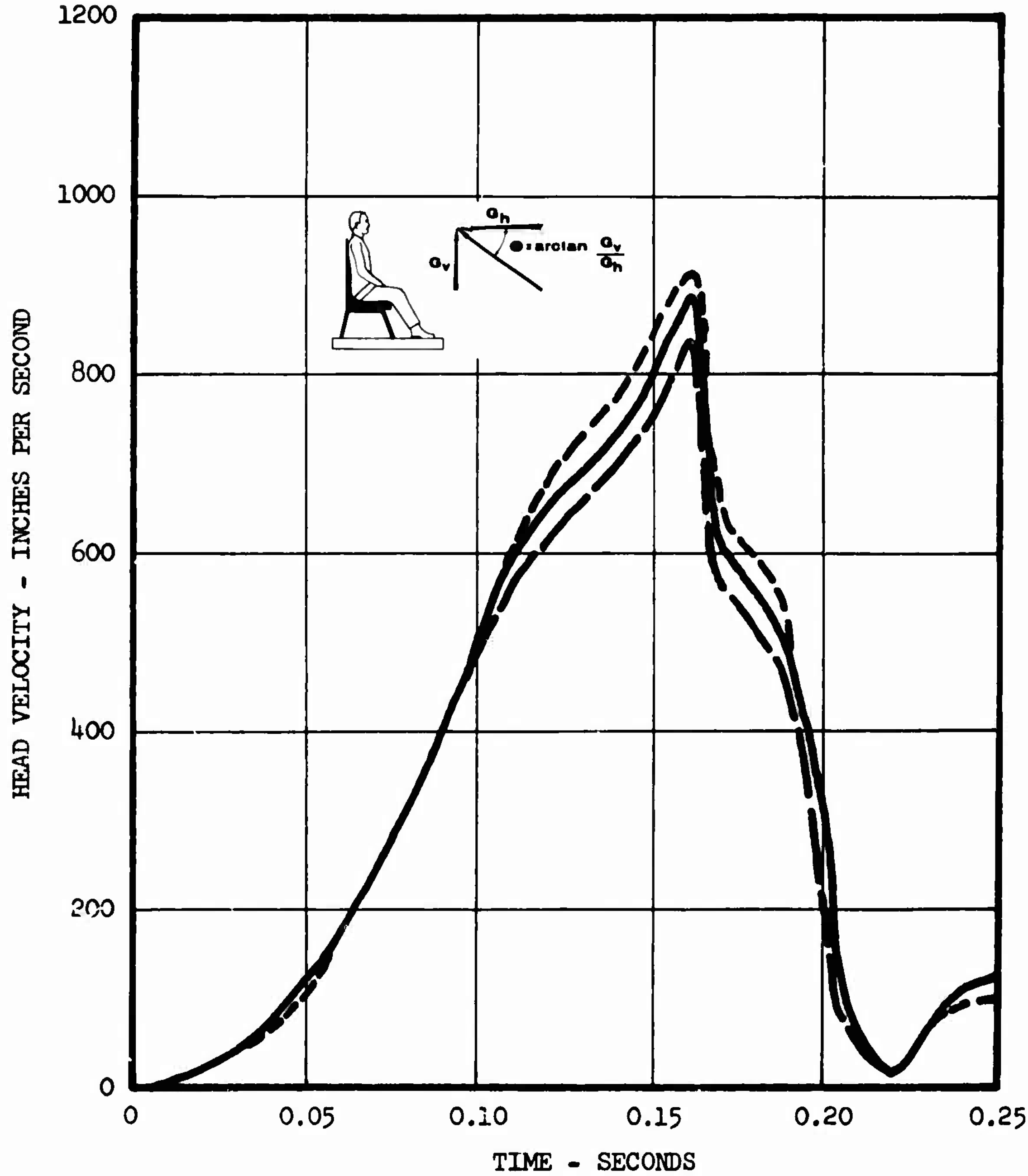

Figure 90. Head Velocity Versus Time.

Figures 91 through 98

Effects of Passenger Weight

(See p. 47)

Pulse	No. 3* (see Figure 17)
Seat Belt	Typical (see Figure 4)
Passenger Weight	
187 pounds	————————
100 pounds	— — — — — —
Load-Limiter Setting	5660 pounds
Ratio of Vertical to Horizontal Acceleration	0.2
Additional Input Conditions	See Table II
187-pound passenger	Column B
100-pound passenger	Column C

Caution: While qualitative trends and comparisons may be dependably observed in the results presented, quantitative values should be used with caution. Due to changes and improvements in the computer program during preparation of the curves, current best estimates may differ somewhat from the data presented. For example, see Appendix III, page 285.

*Seat damping coefficients are zero in computer program.

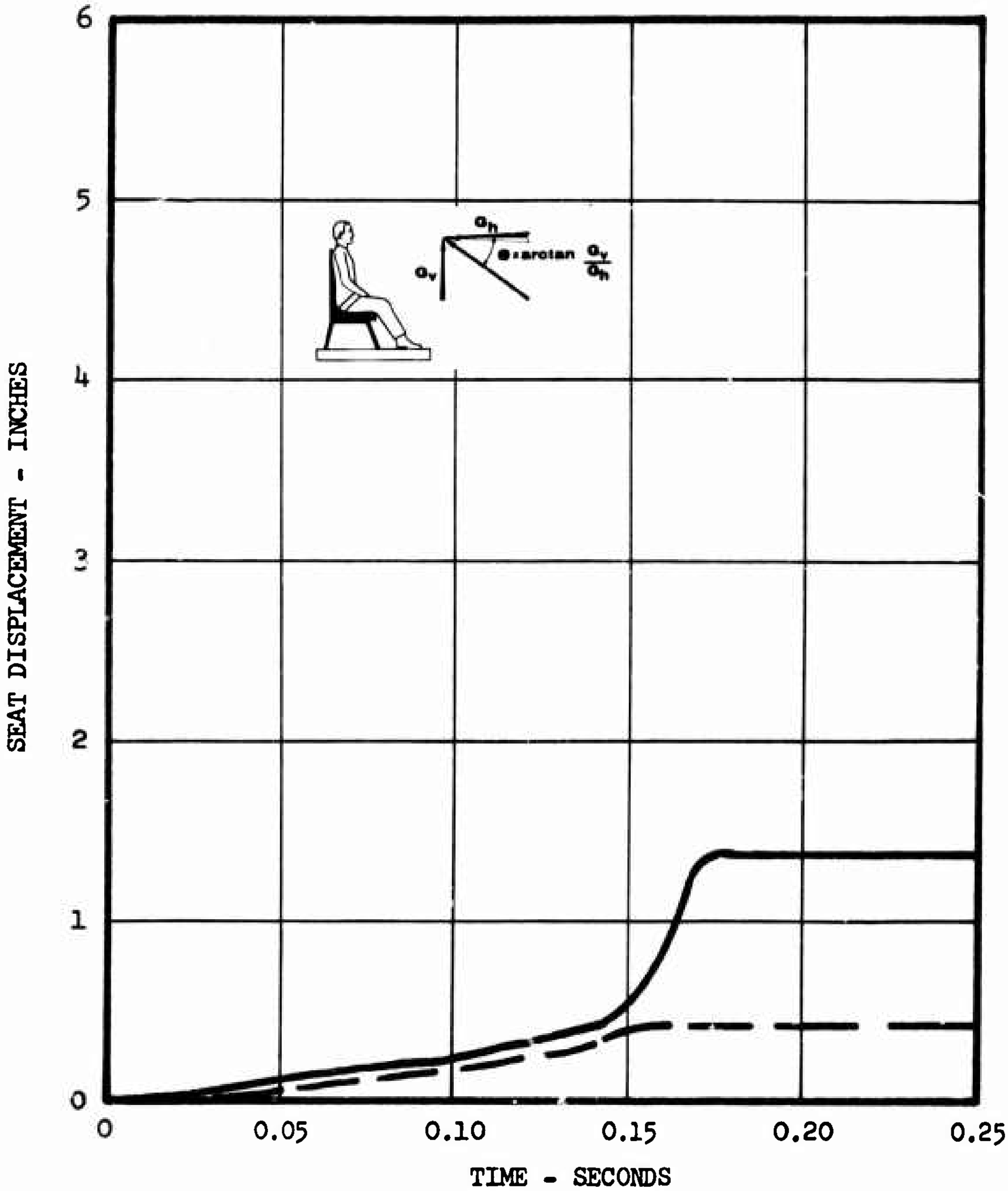

Figure 91. Seat Displacement Versus Time.

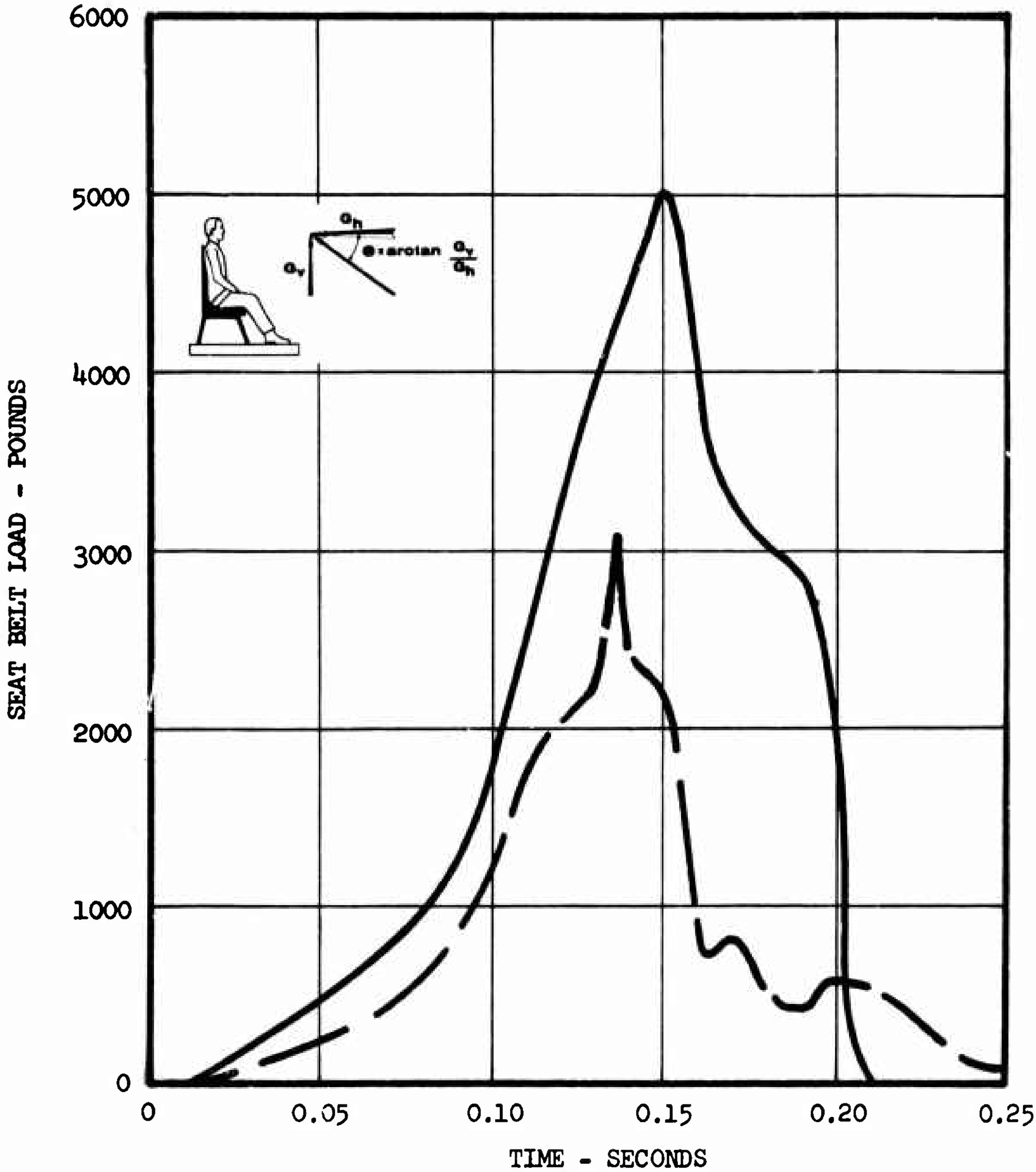

Figure 92. Seat Belt Load Versus Time.

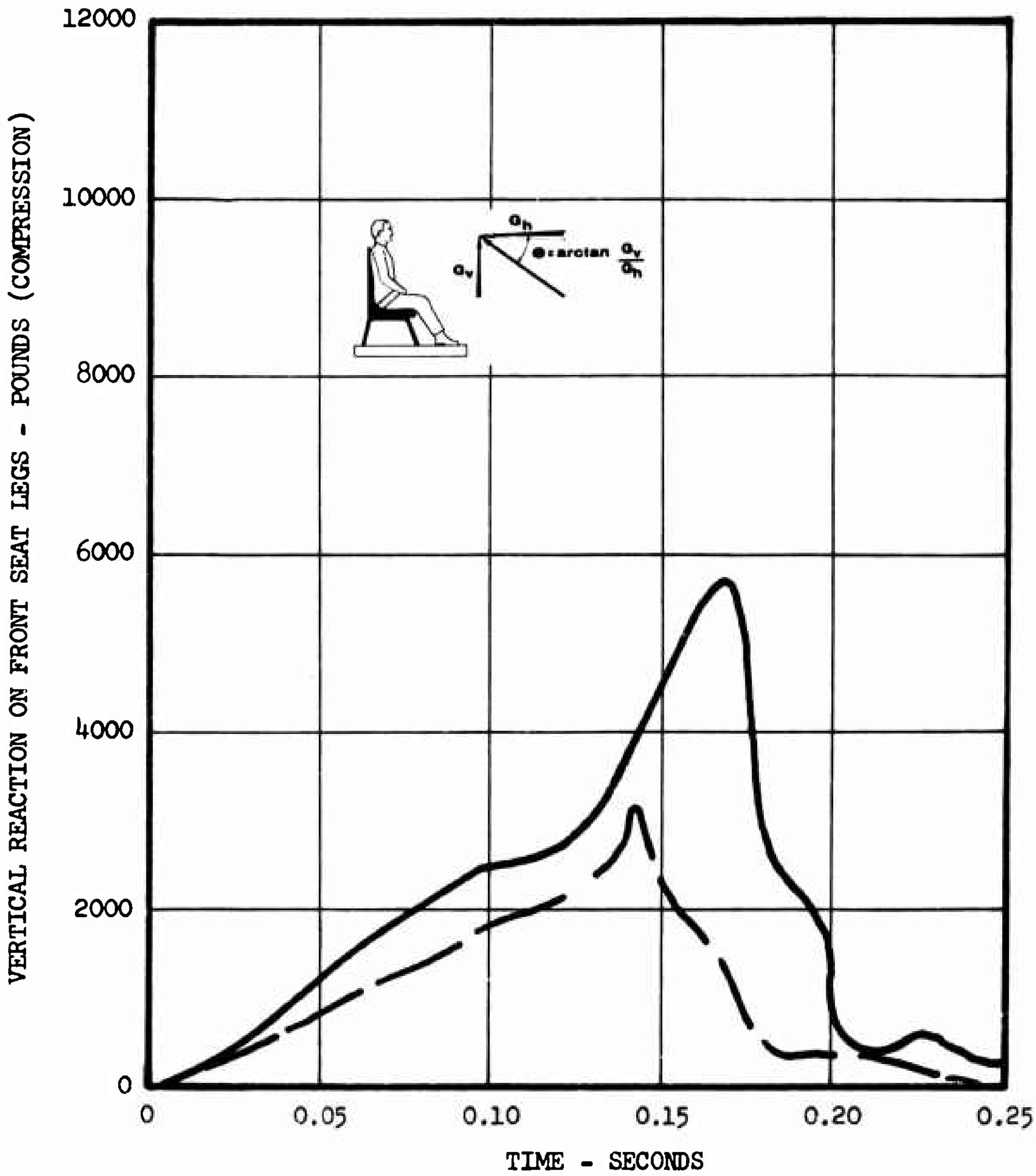

Figure 93. Vertical Reaction on Front Seat Legs Versus Time.

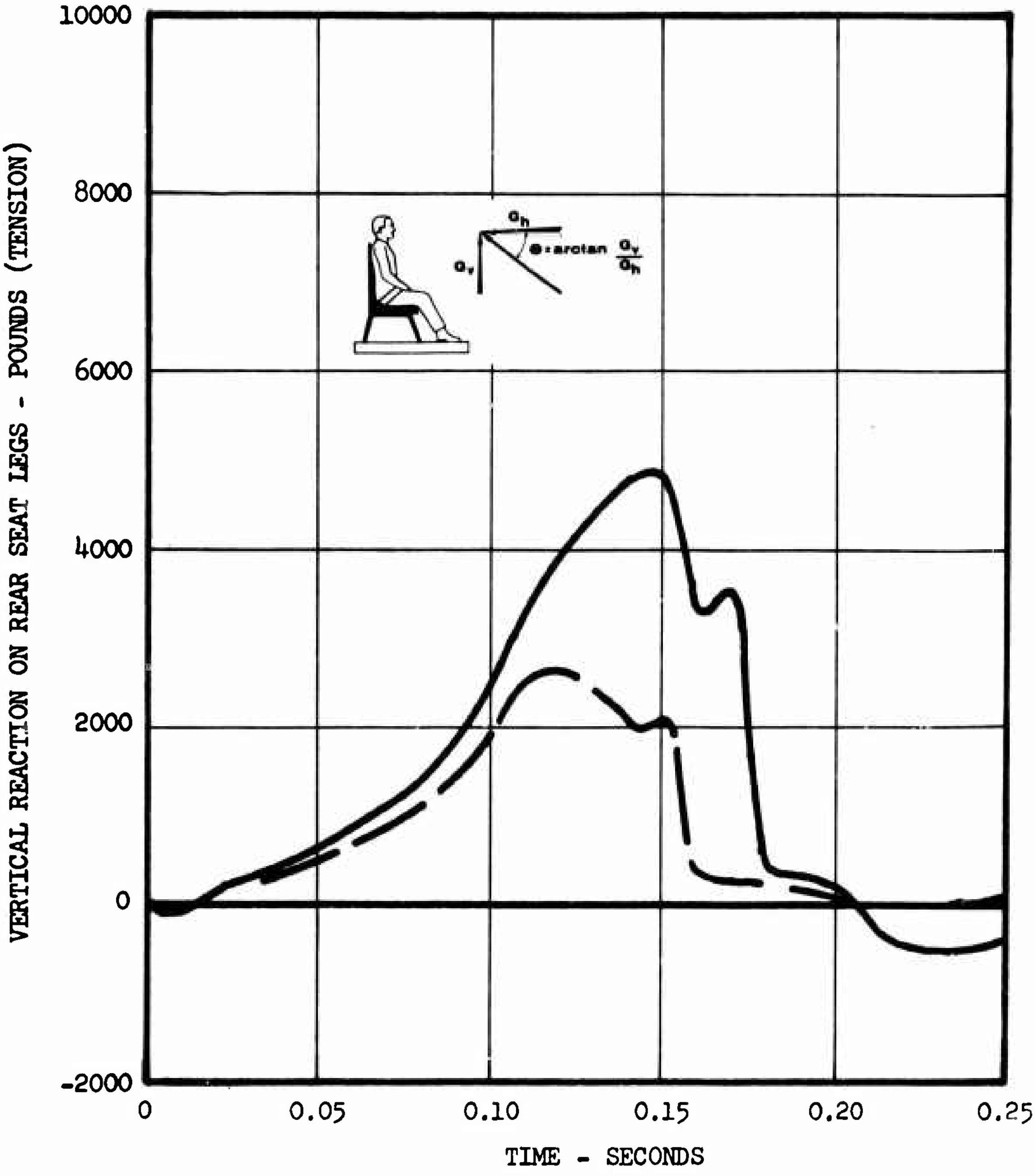

Figure 94. Vertical Reaction on Rear Set Legs Versus Time.

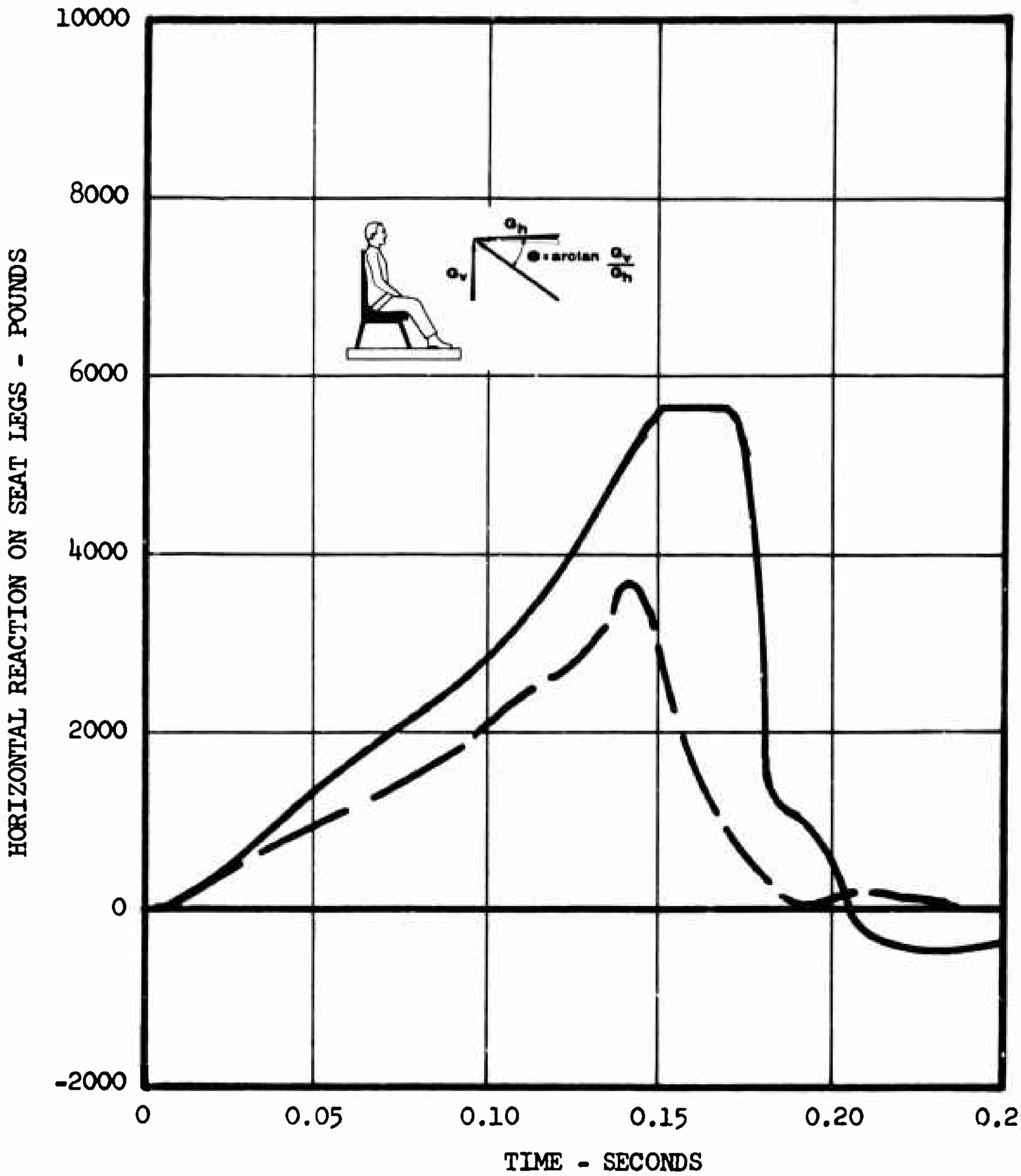

Figure 95. Horizontal Reaction on Seat Legs Versus Time.

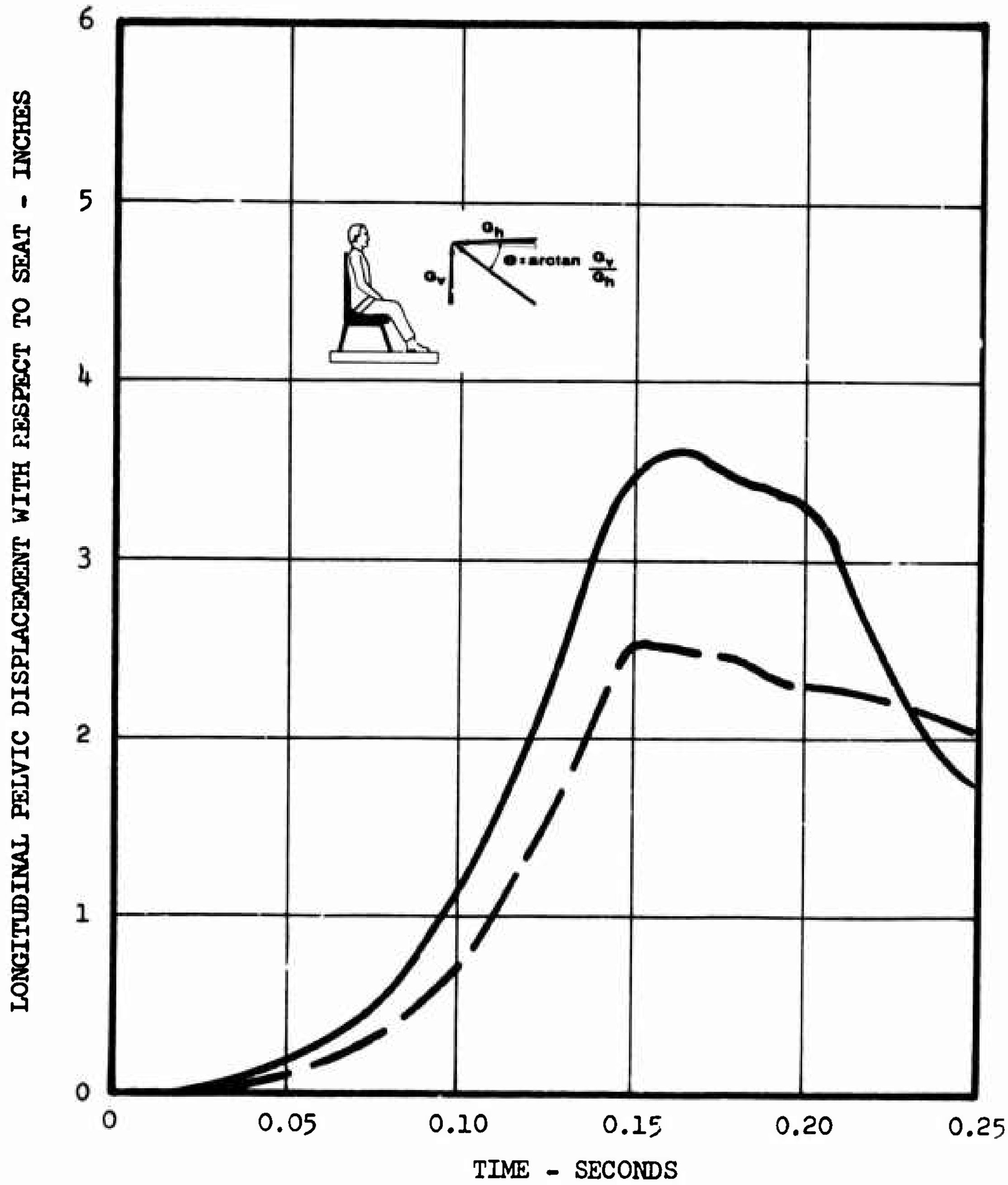

Figure 96. Longitudinal Pelvic Displacement With Respect to Seat Versus Time.

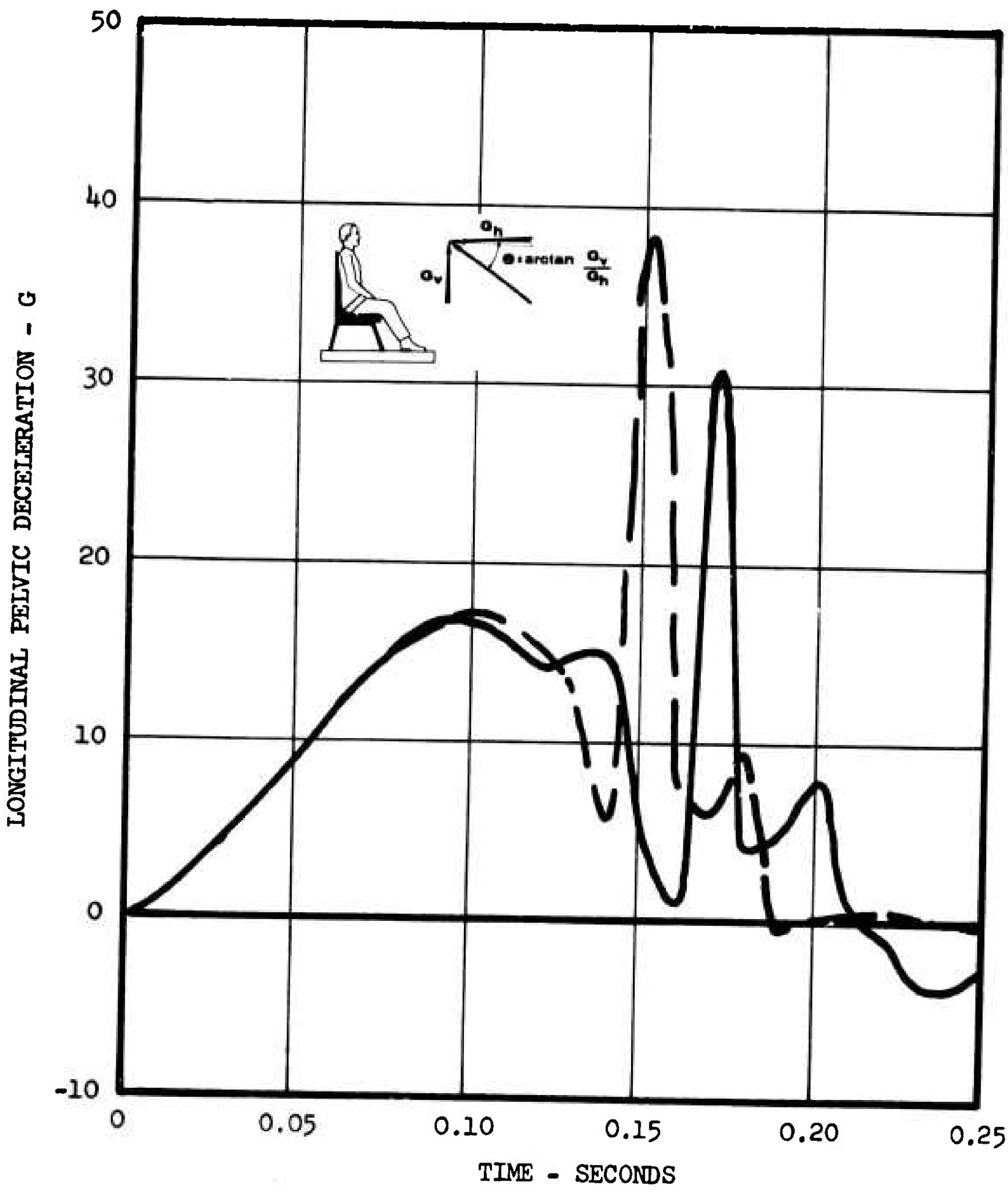

Figure 97. Longitudinal Pelvic Deceleration Versus Time.

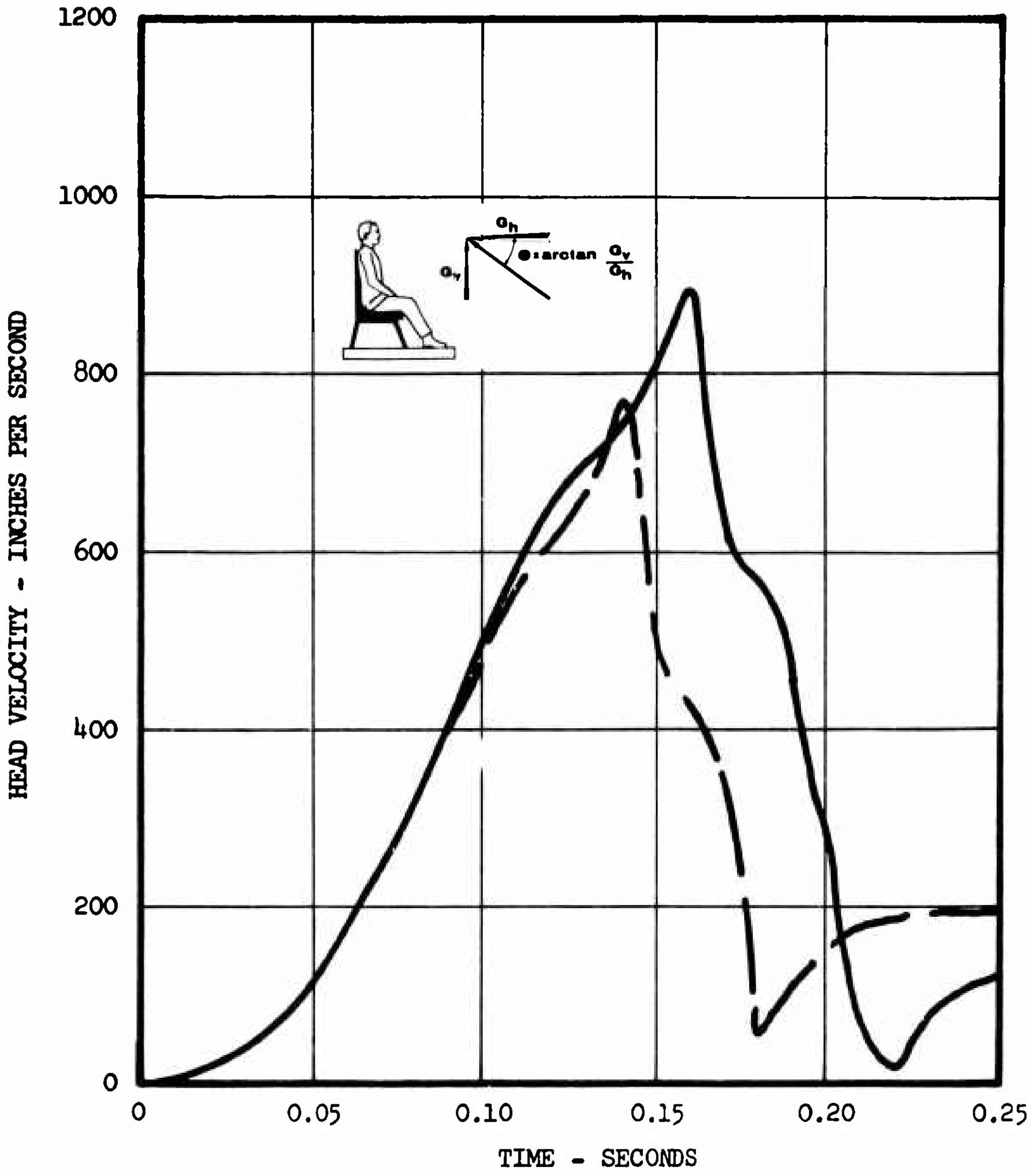

Figure 98. Head Velocity Versus Time.

Figures 99 through 106

Effects of Slack in the Seat Belt

(See p. 48)

Pulse	No. 1 (see Figure 17)
Seat Belt	Typical (see Figure 4)
Passenger Weight	187 pounds
Ratio of Vertical to Horizontal Acceleration	0. 2
Additional Input Conditions	See Table II, column A
No Seat Belt Slack	— — — — — —
2-Inch Seat Belt Slack	————————————
5-Inch Seat Belt Slack	——— – ——— – ———

Caution:
While qualitative trends and comparisons may be dependably observed in the results presented, quantitative values should be used with caution. Due to changes and improvements in the computer program during preparation of the curves, current best estimates may differ somewhat from the data presented. For example, see Appendix III, page 285.

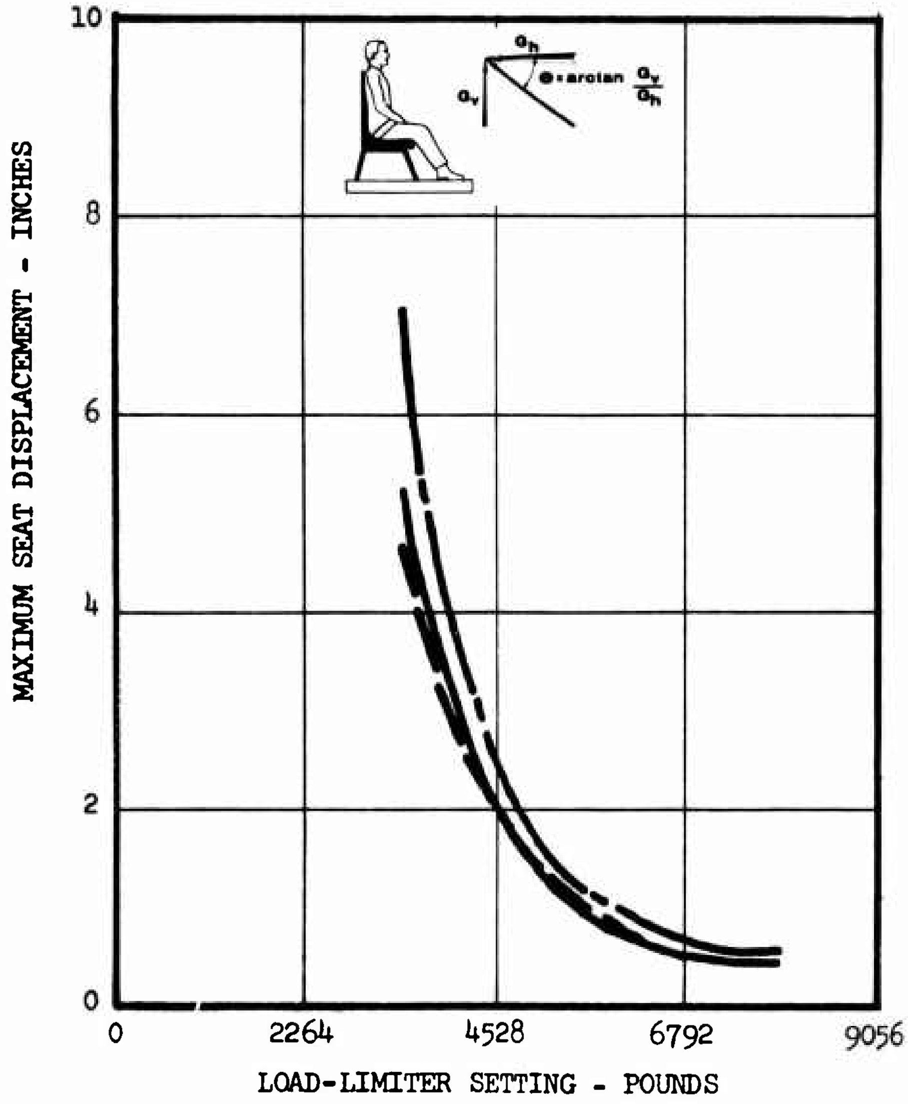

Figure 99. Maximum Seat Displacement Versus Load-Limiter Setting.

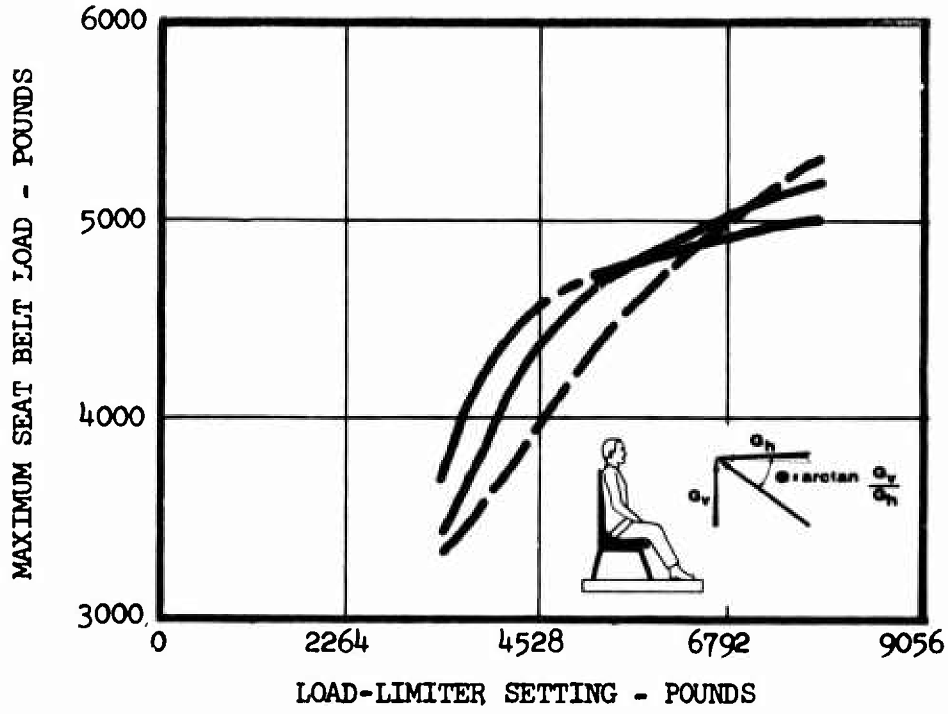

Figure 100. Maximum Seat Belt Load Versus Load-Limiter Setting.

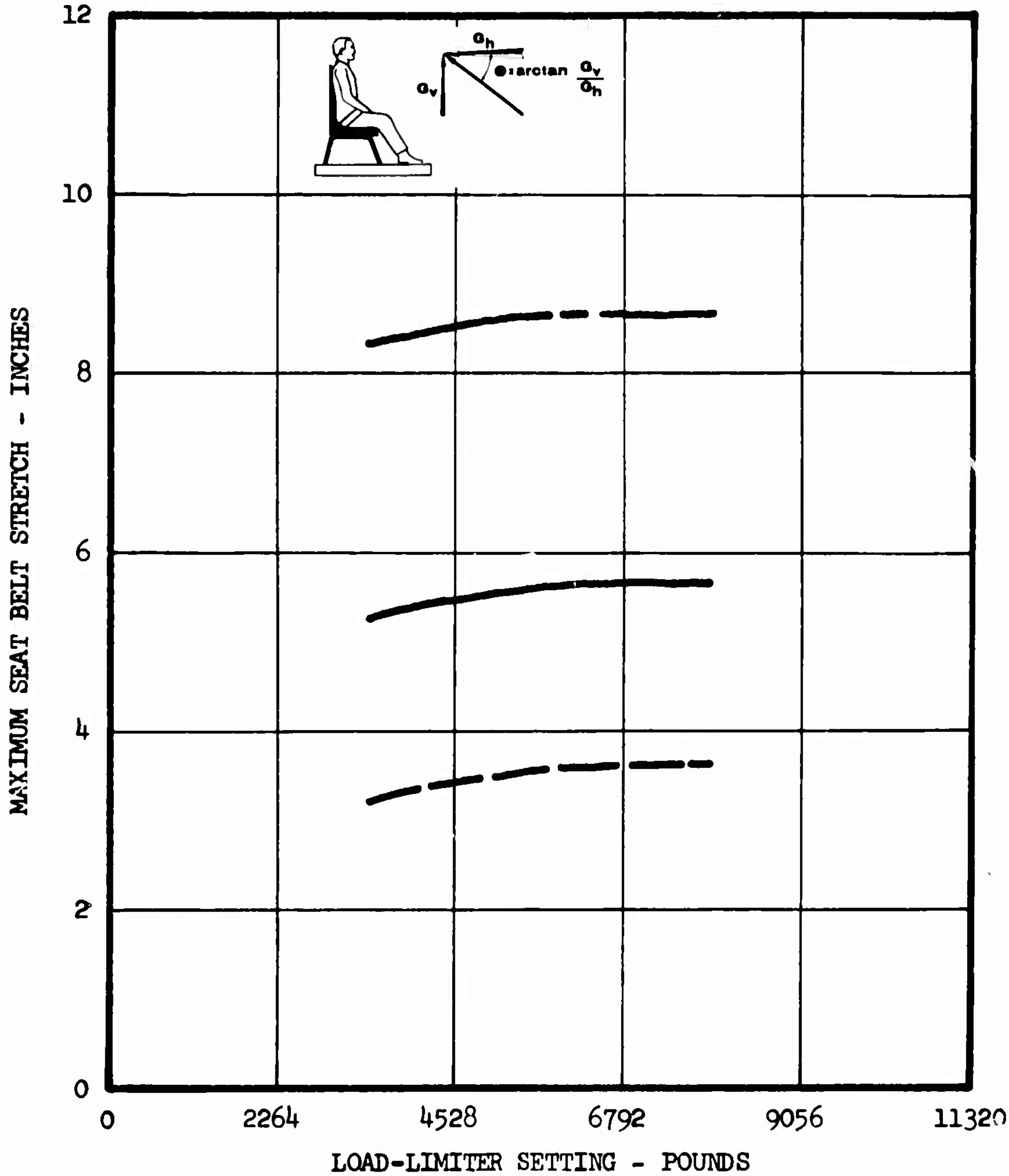

Figure 101. Maximum Seat Belt Stretch Versus Load-Limiter Setting.

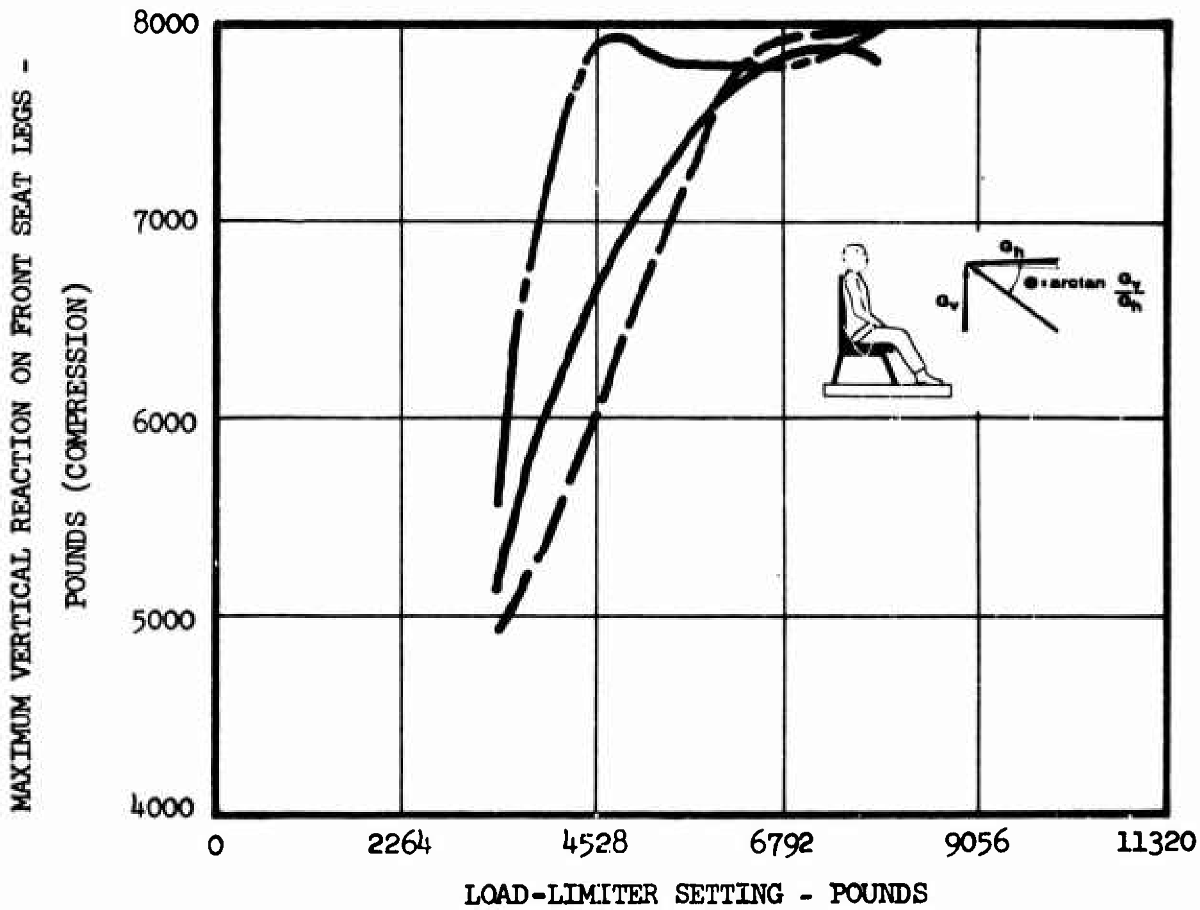

Figure 102. Maximum Vertical Reaction on Front Seat Legs Versus Load-Limiter Setting.

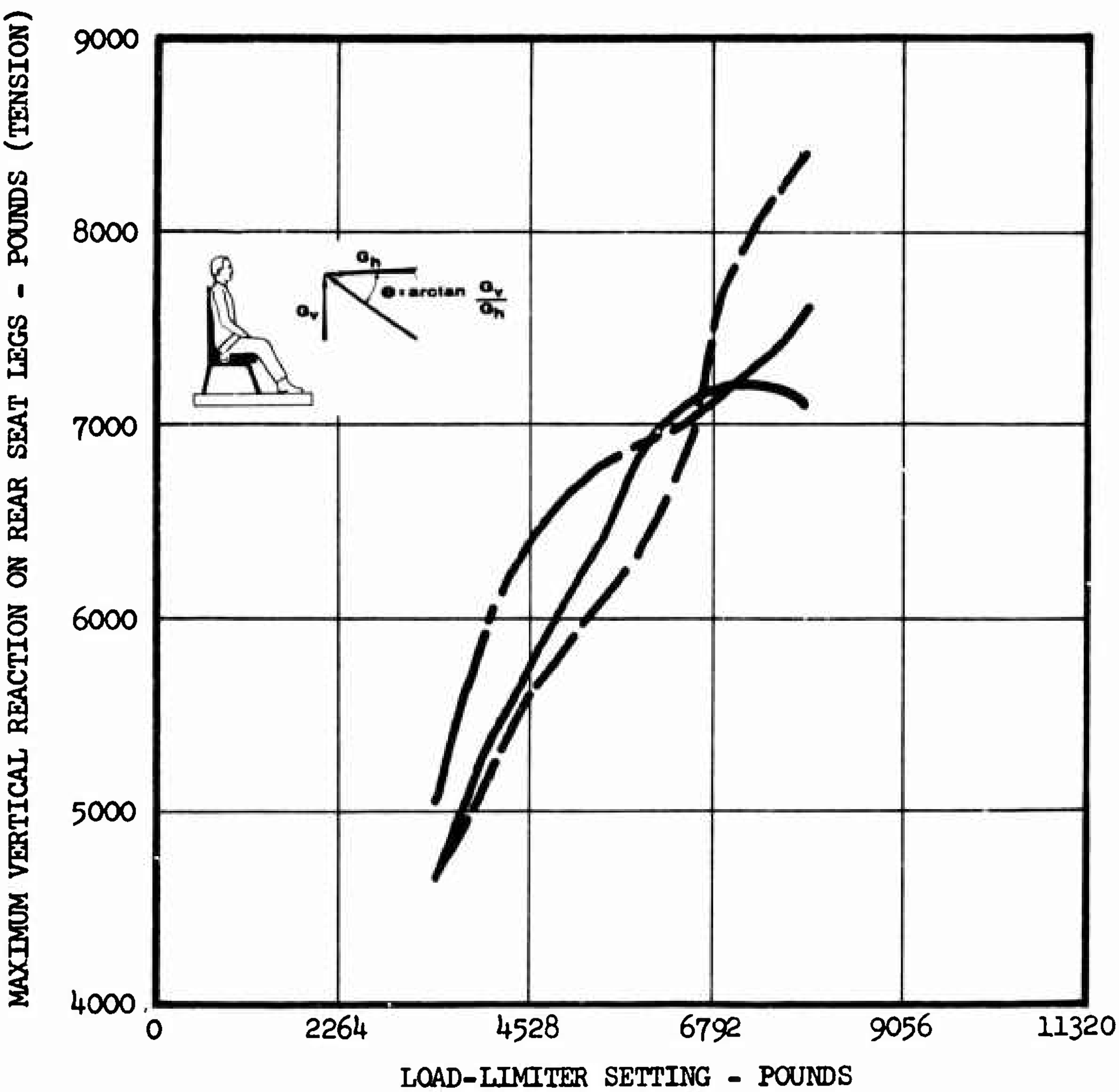

Figure 103. Maximum Vertical Reaction on Rear Seat Legs Versus Load-Limiter Setting.

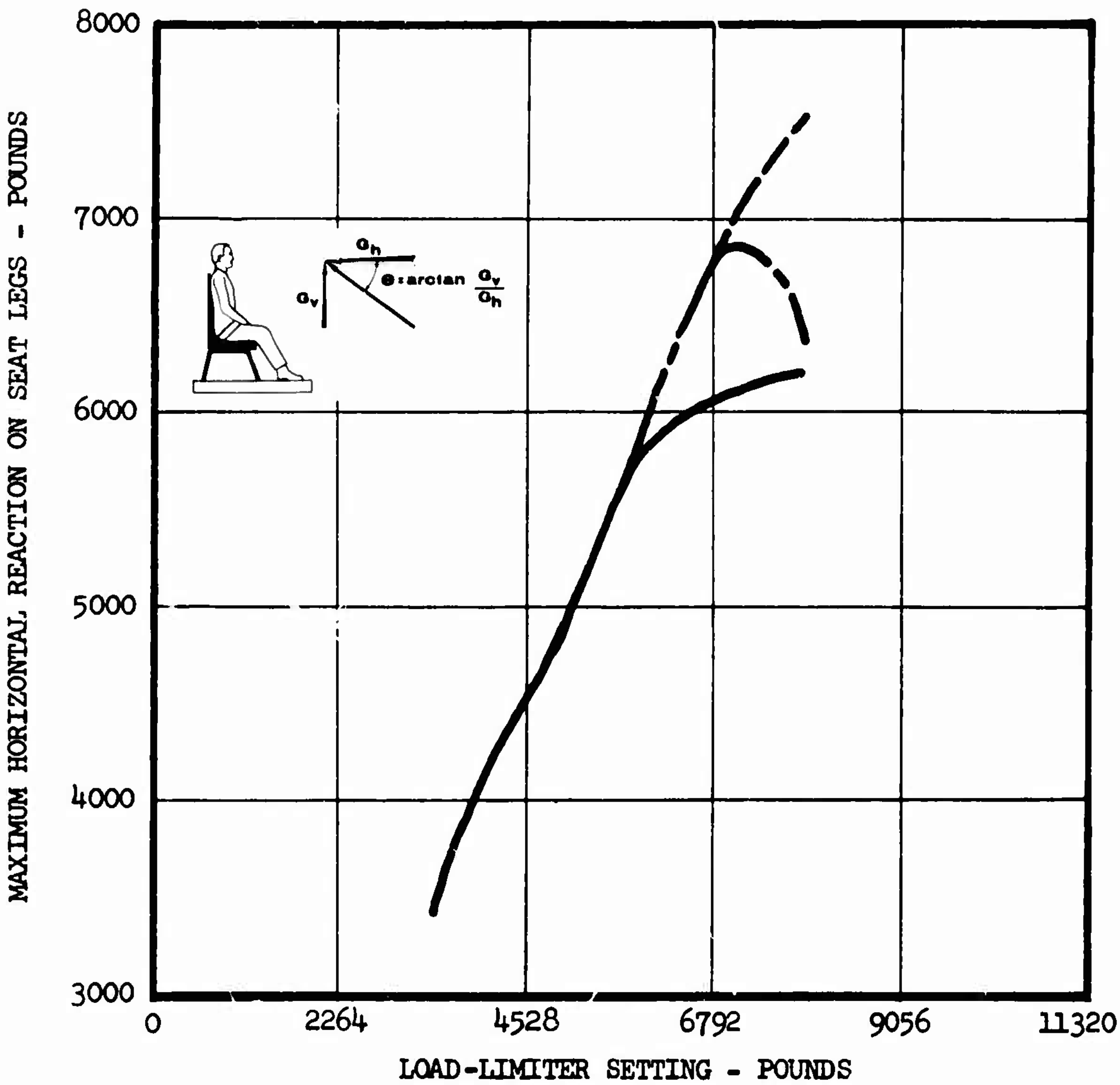

Figure 104. Maximum Horizontal Reaction on Seat Legs Versus Load-Limiter Setting.

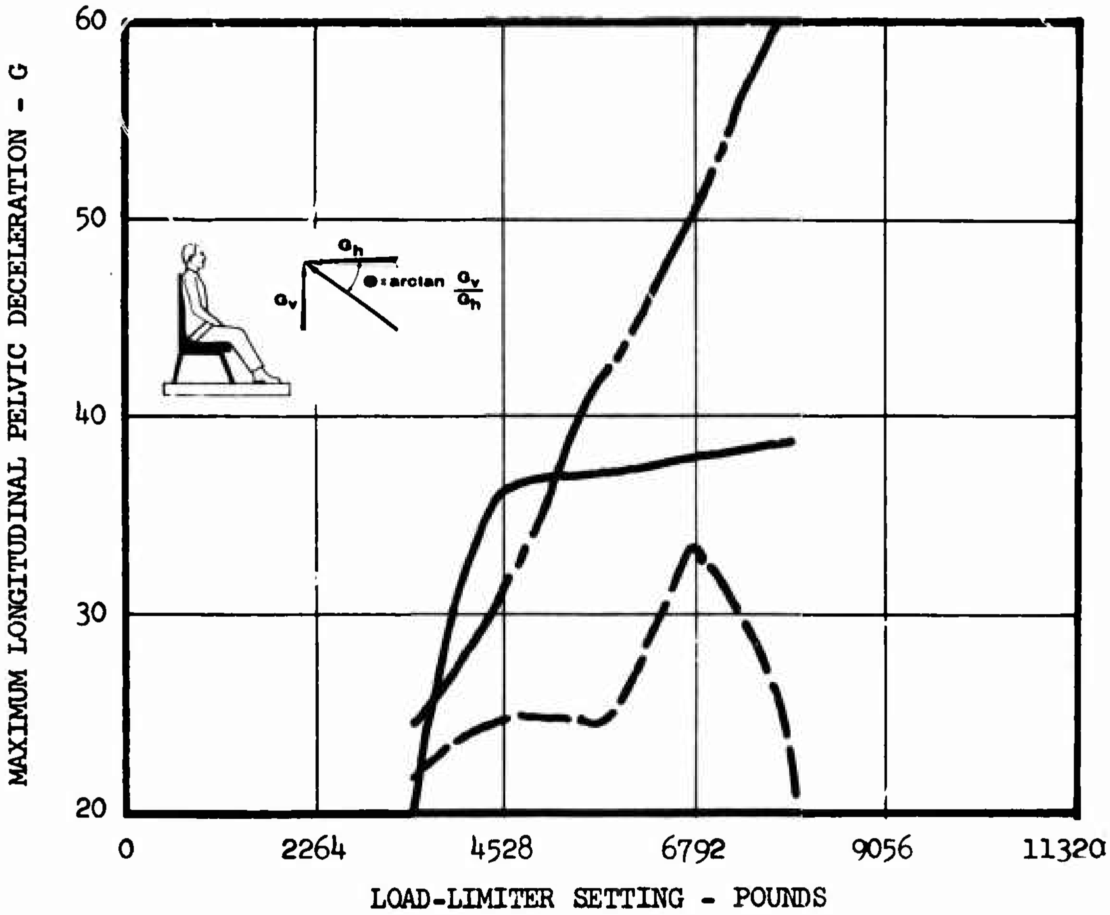

Figure 105. Maximum Longitudinal Pelvic Deceleration Versus Load-Limiter Setting.

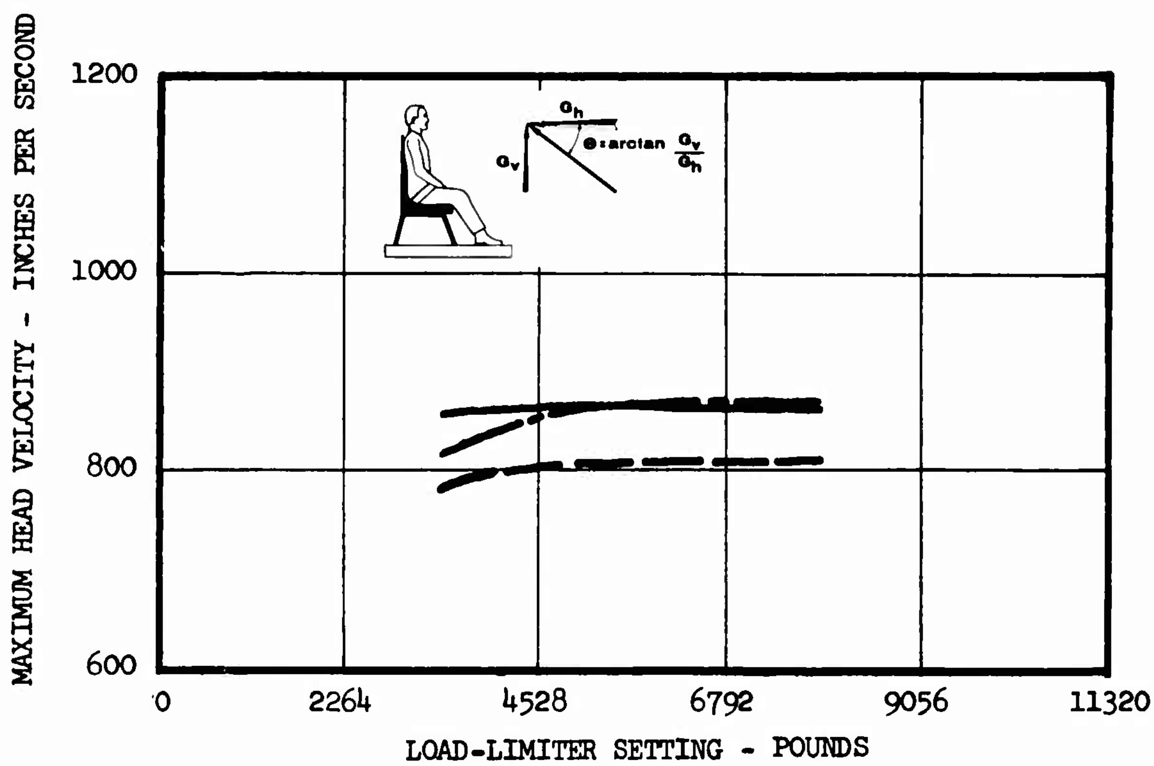

Figure 106. Maximum Head Velocity Versus Load-Limiter Setting.

Figures 107 through 114

Effects of Slack in the Seat Belt

(See p. 48)

Pulse	No. 1 (see Figure 17)
Seat Belt	Typical (see Figure 4)
Passenger Weight	187 pounds
Load-Limiter Setting	5660 pounds
Ratio of Vertical to Horizontal Acceleration	0. 2
Additional Input Conditions	See Table II, column A
No Seat Belt Slack	
2-Inch Seat Belt Slack	
5-Inch Seat Belt Slack	

Caution:
While qualitative trends and comparisons may be dependably observed in the results presented, quantitative values should be used with caution. Due to changes and improvements in the computer program during preparation of the curves, current best estimates may differ somewhat from the data presented. For example, see Appendix III, page 285.

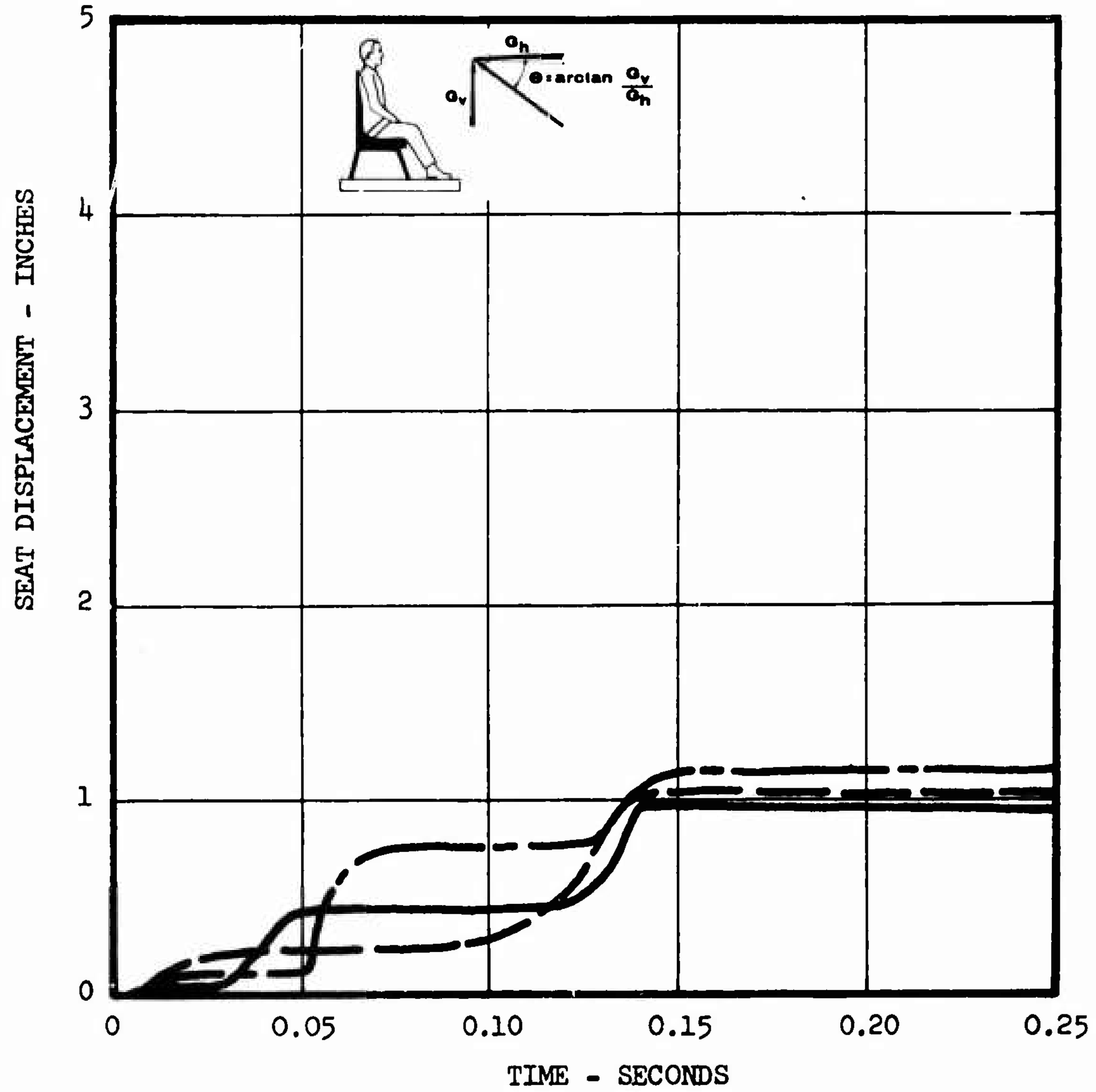

Figure 107. Seat Displacement Versus Time.

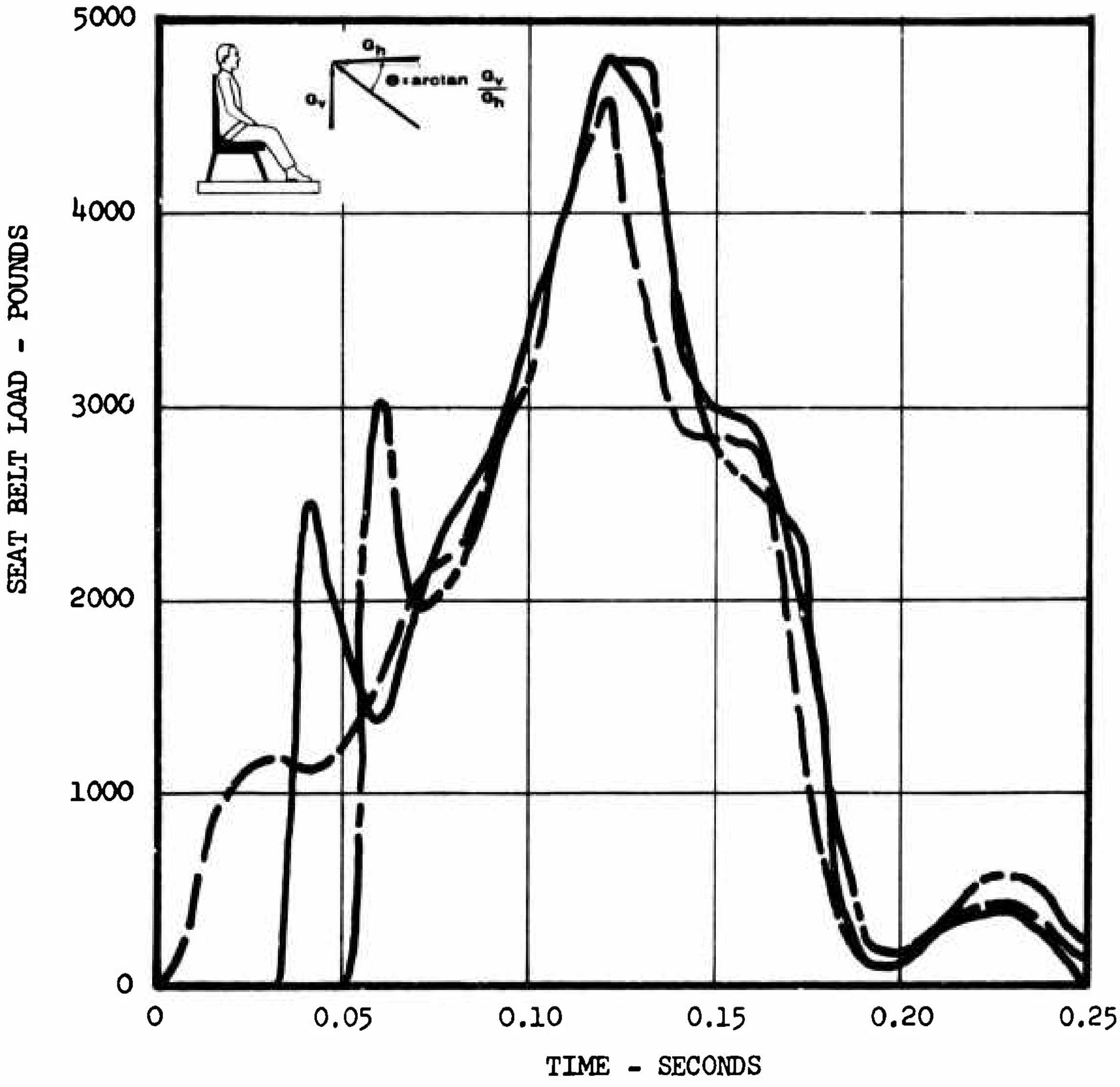

Figure 108. Seat Belt Load Versus Time.

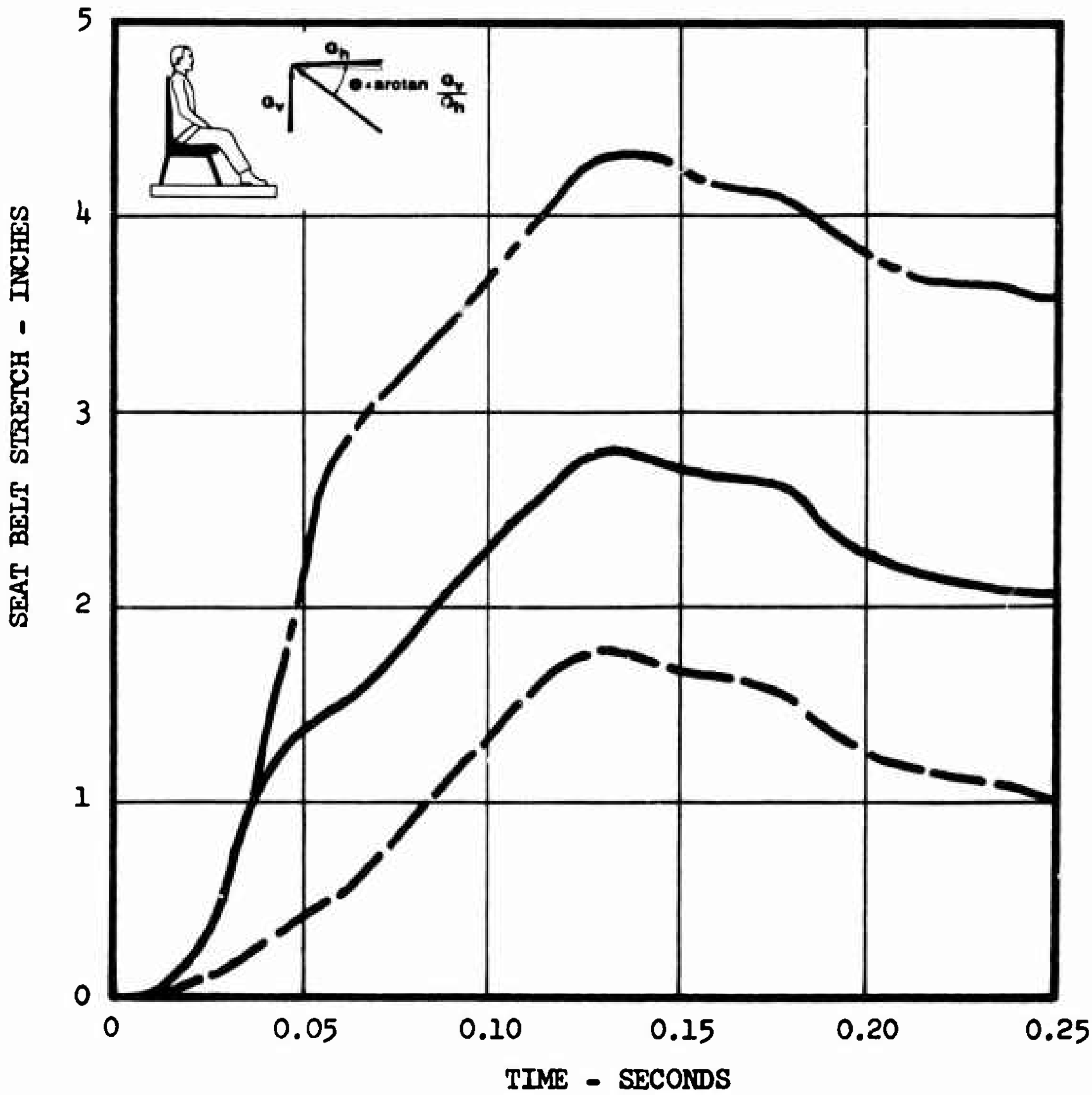

Figure 109. Seat Belt Stretch Versus Time.

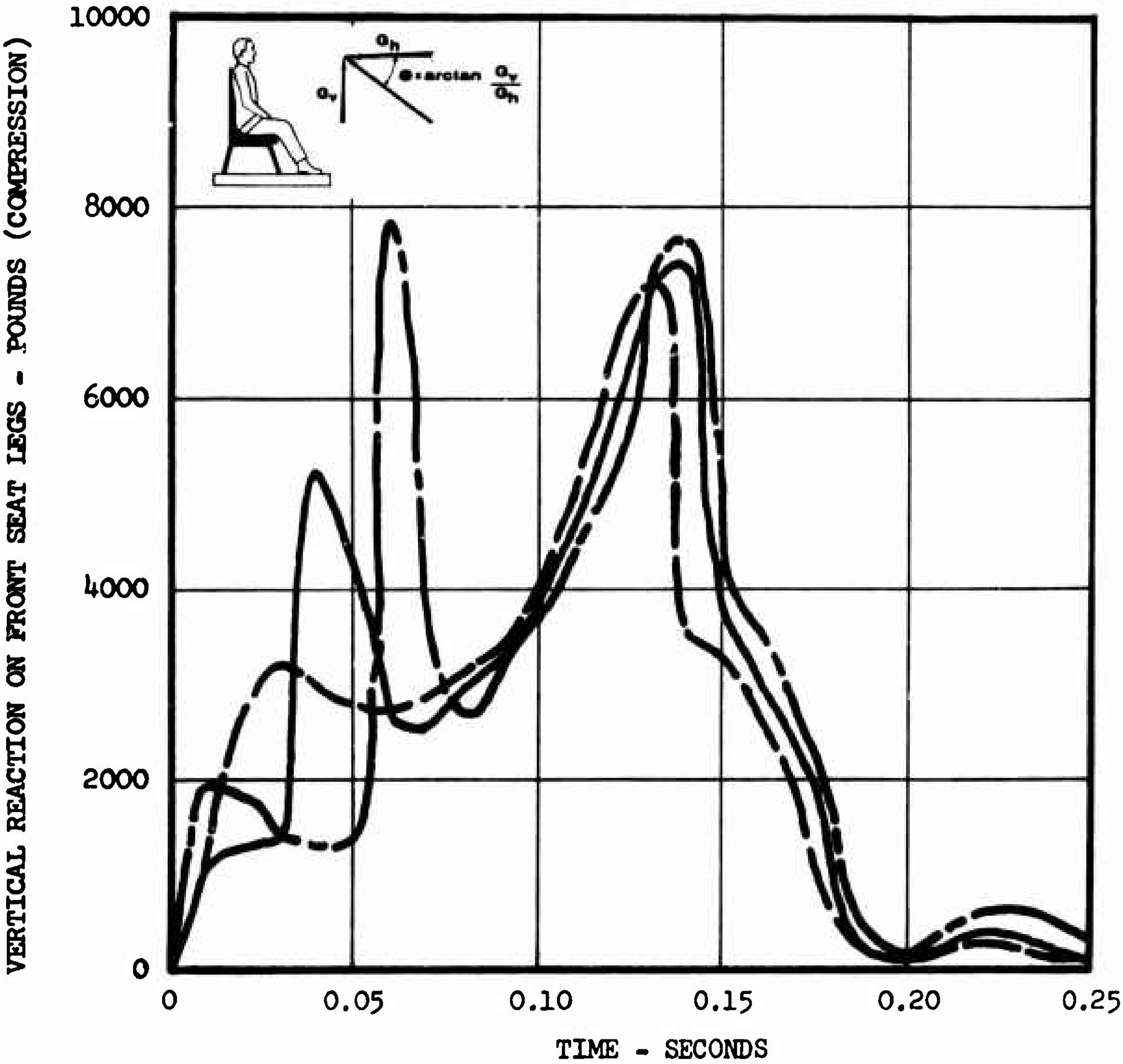

Figure 110. Vertical Reaction on Front Seat Legs Versus Time.

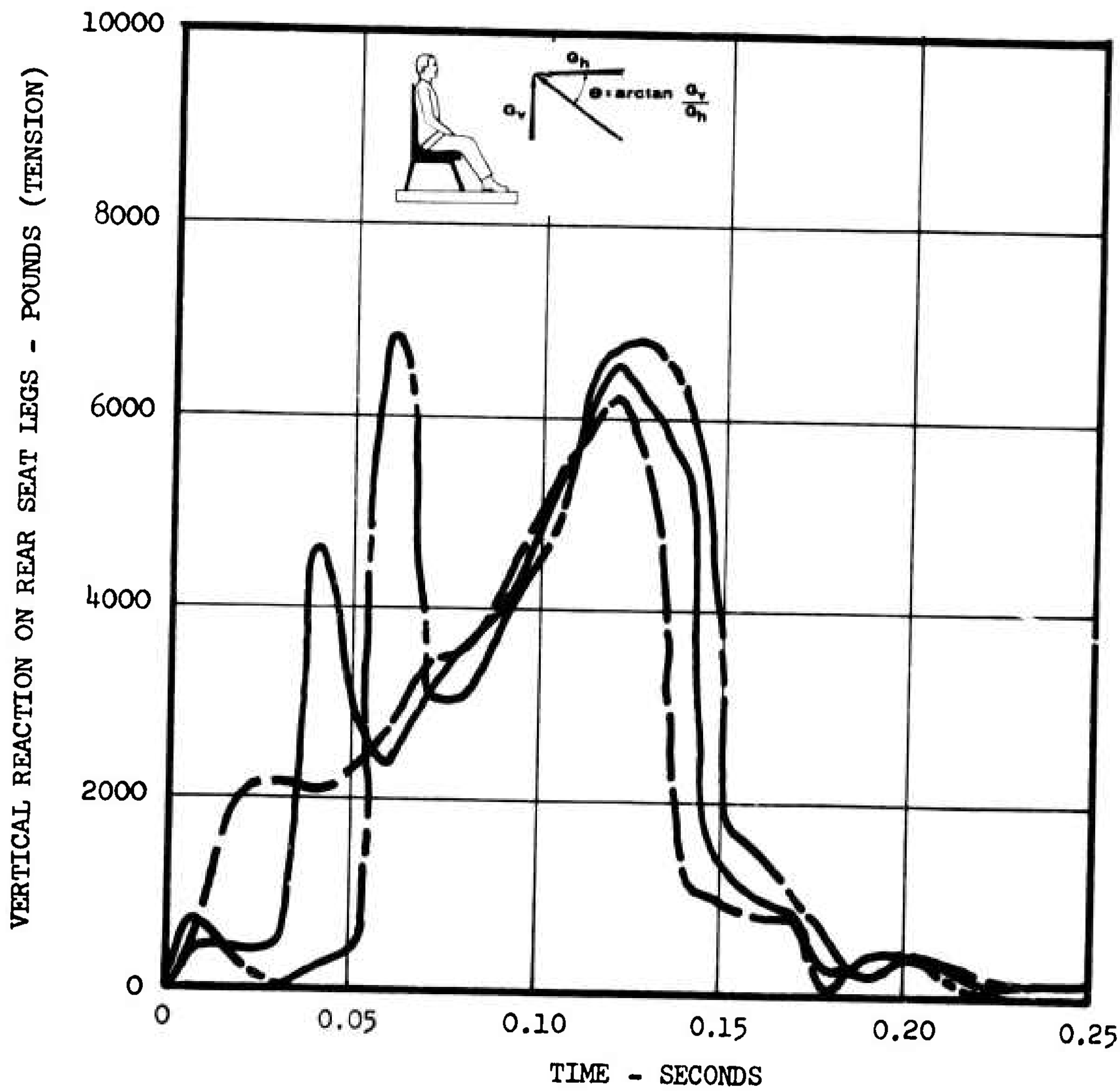

Figure 111. Vertical Reaction on Rear Seat Legs Versus Time.

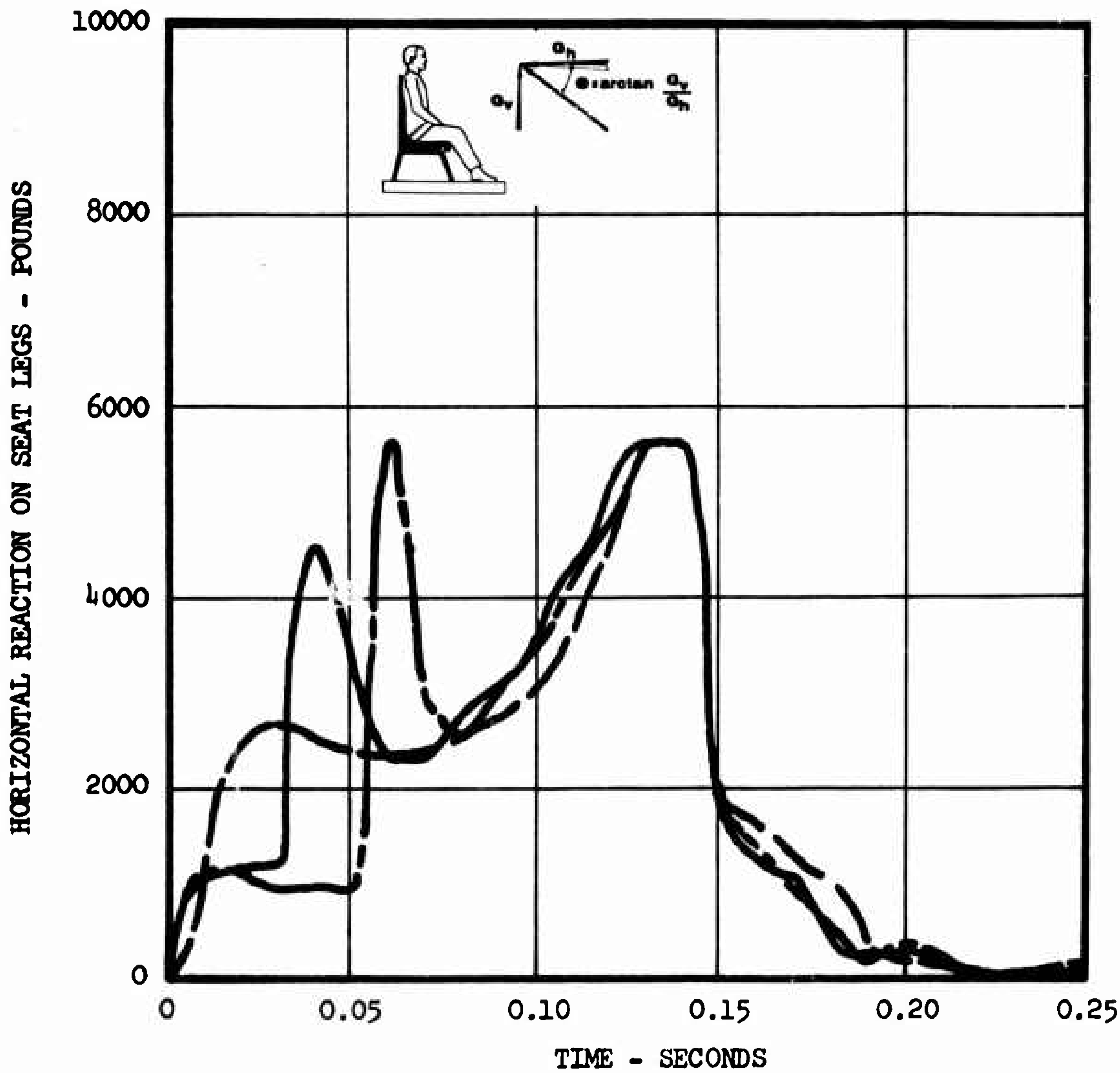

Figure 112. Horizontal Reaction on Seat Legs Versus Time.

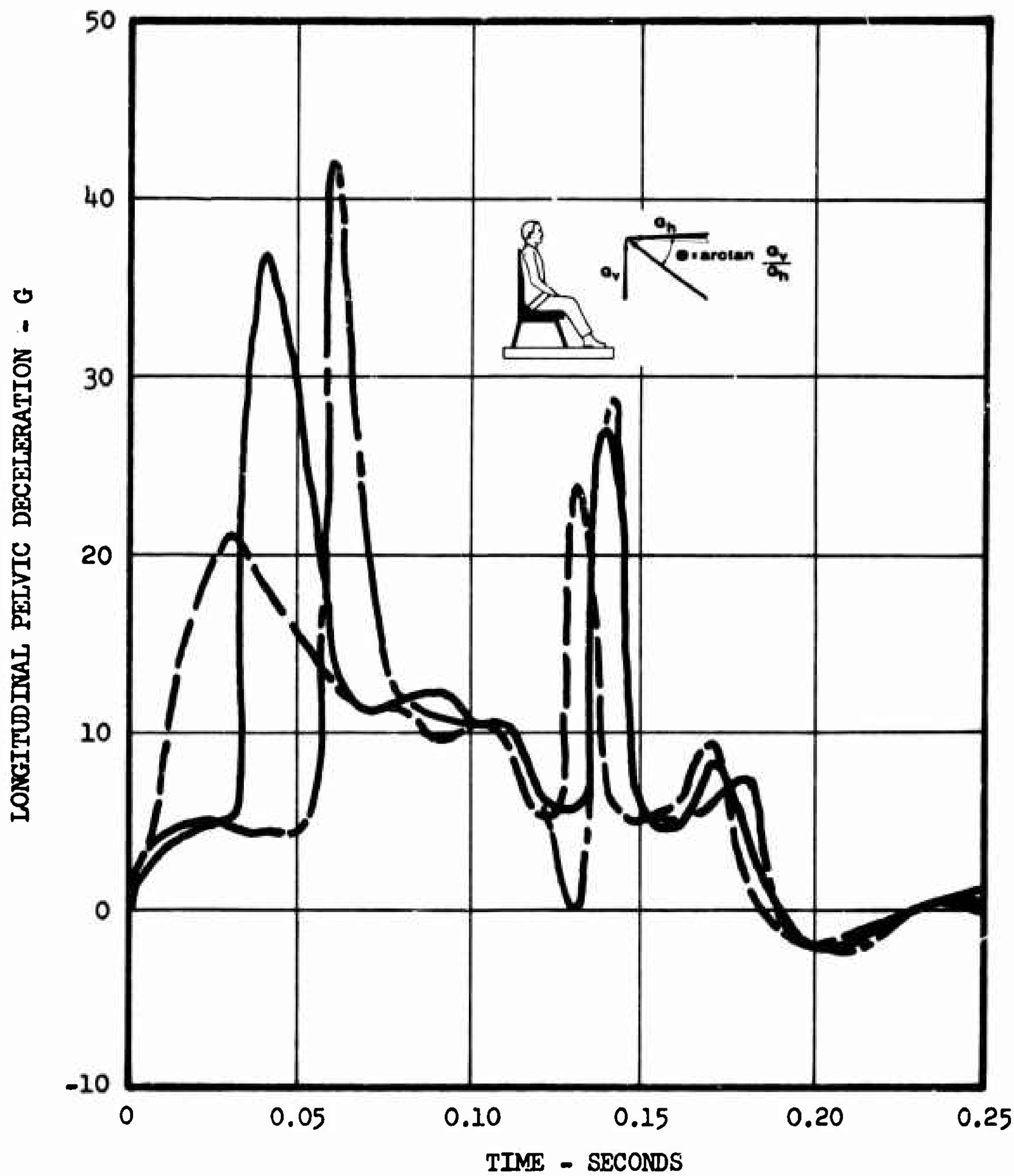

Figure 113. Longitudinal Pelvic Deceleration Versus Time.

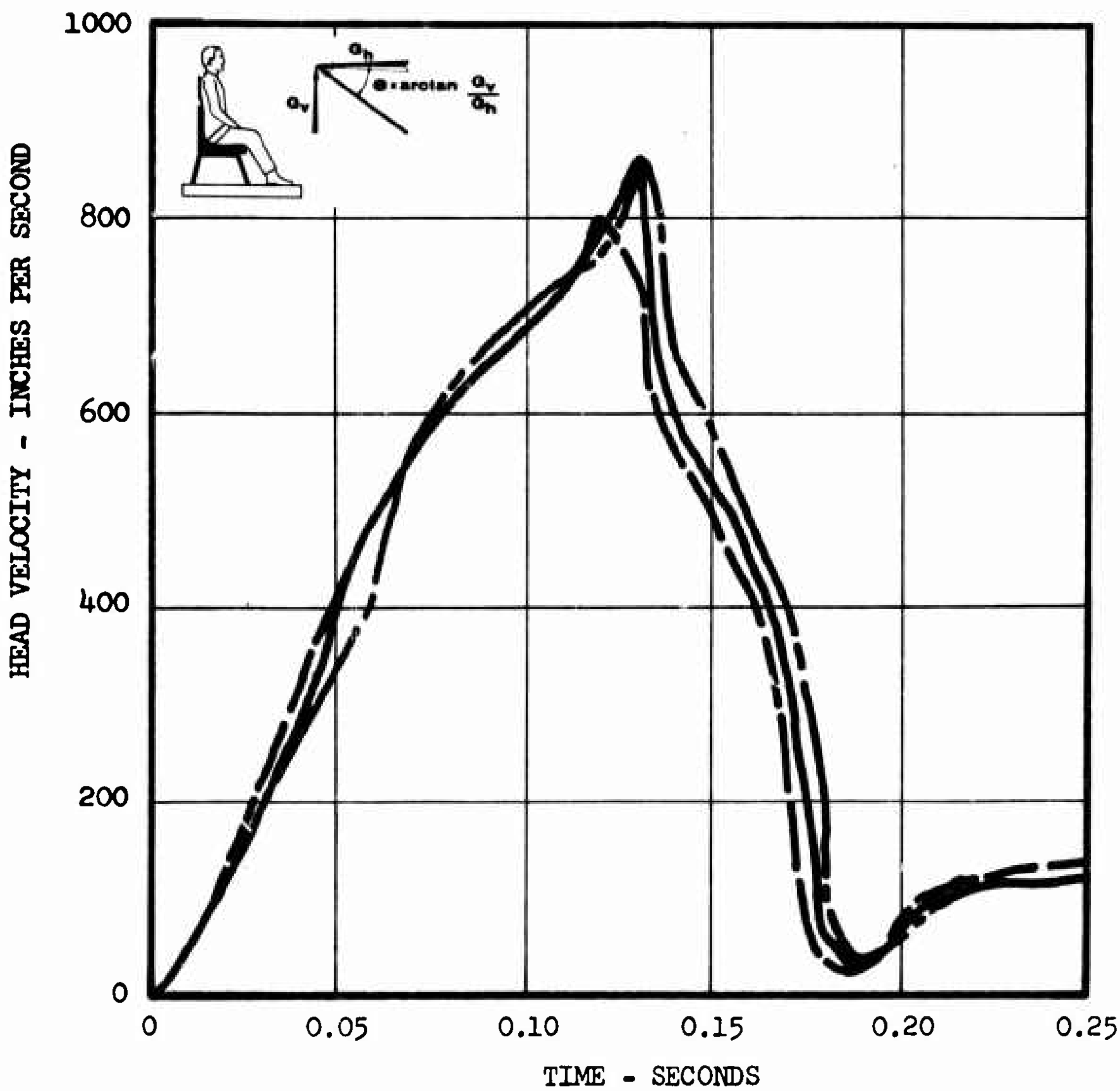

Figure 114. Head Velocity Versus Time.

Figures 115 through 123

Effects of Shoulder Harness

(See p. 49)

Pulse	No. 3* (see Figure 17)
Seat Belt	Typical (see Figure 4)
Without Shoulder Harness	————————————
With Shoulder Harness	— — — — — —
Passenger Weight	187 pounds
Load-Limiter Setting	5660 pounds
Ratio of Vertical to Horizontal Acceleration	0.2
Additional Input Conditions	See Table II, column B

Caution:
While qualitative trends and comparisons may be dependably observed in the results presented, quantitative values should be used with caution. Due to changes and improvements in the computer program during preparation of the curves, current best estimates may differ somewhat from the data presented. For example, see Appendix III, page 285.

*Seat damping coefficients are zero in computer program.

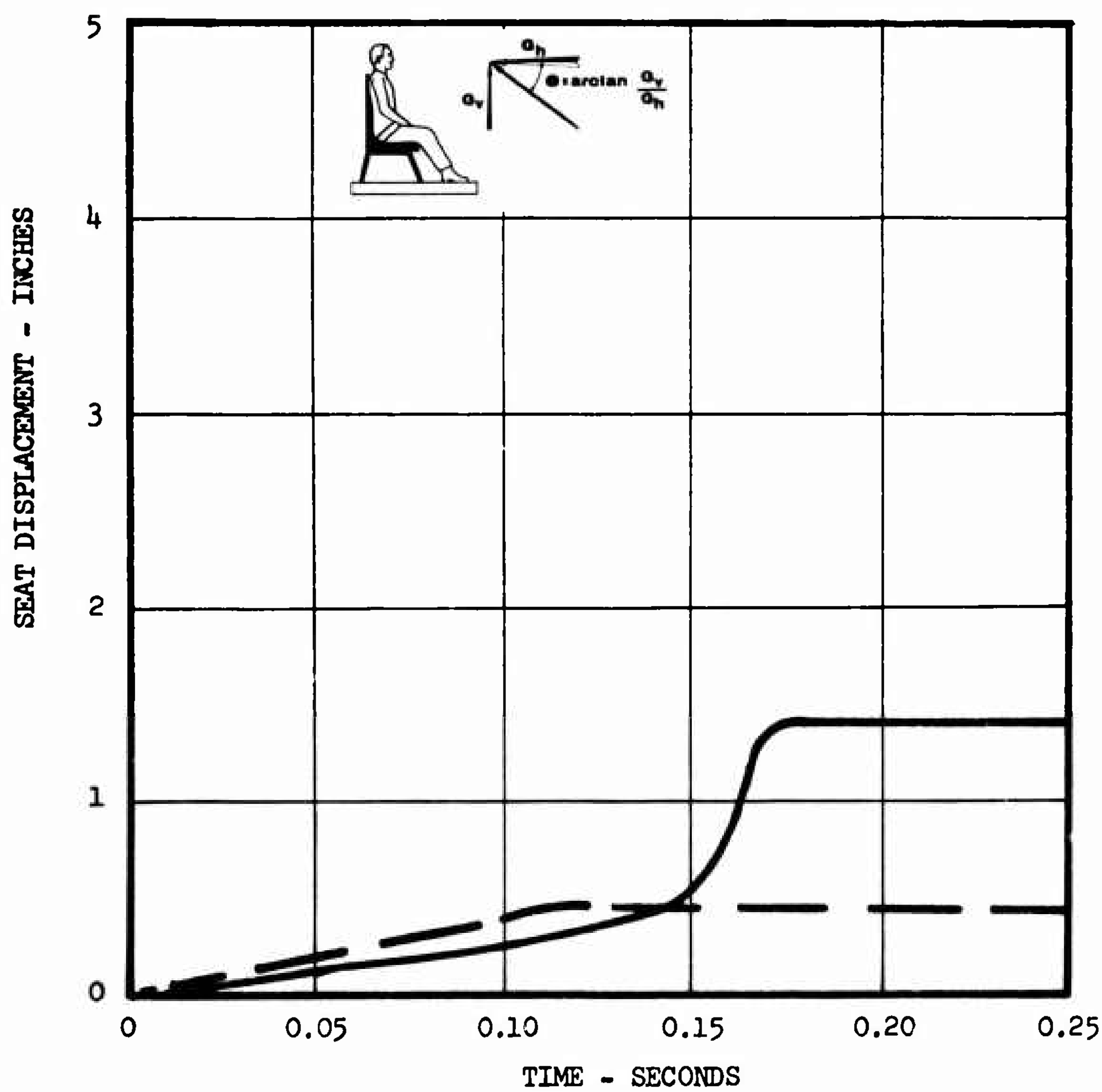

Figure 115. Seat Displacement Versus Time.

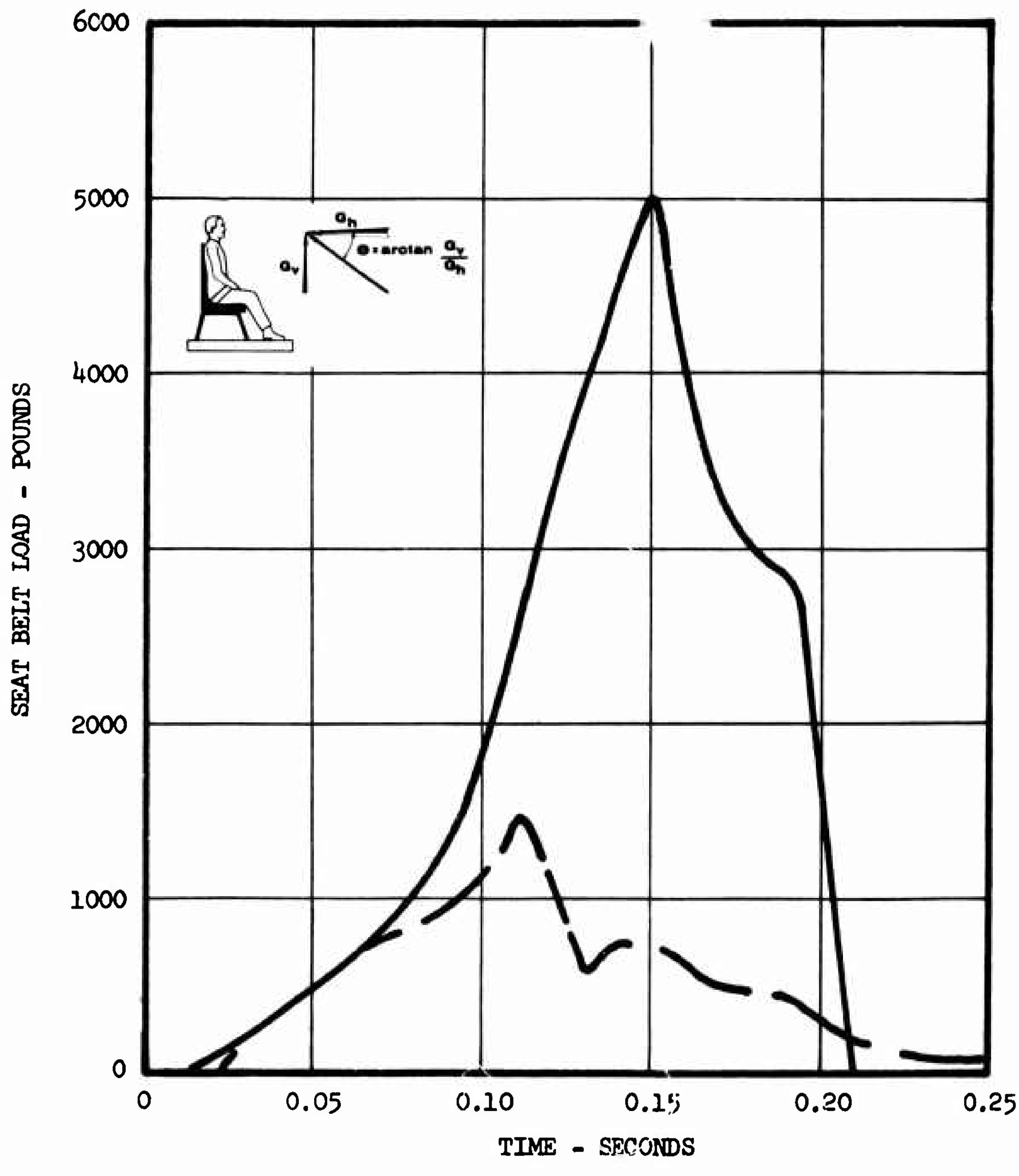

Figure 116. Seat Belt Load Versus Time.

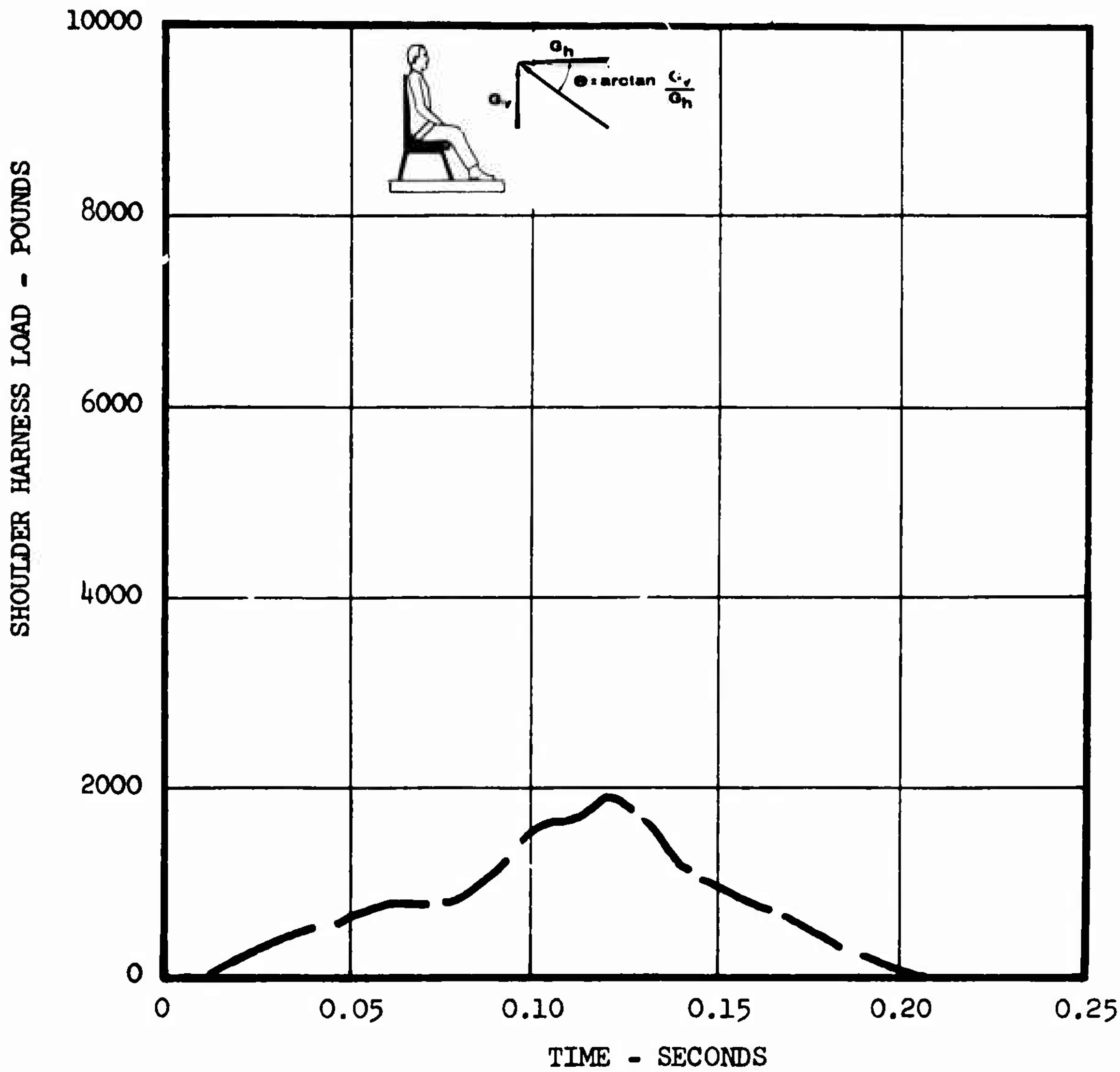

Figure 117. Shoulder Harness Load Versus Time.

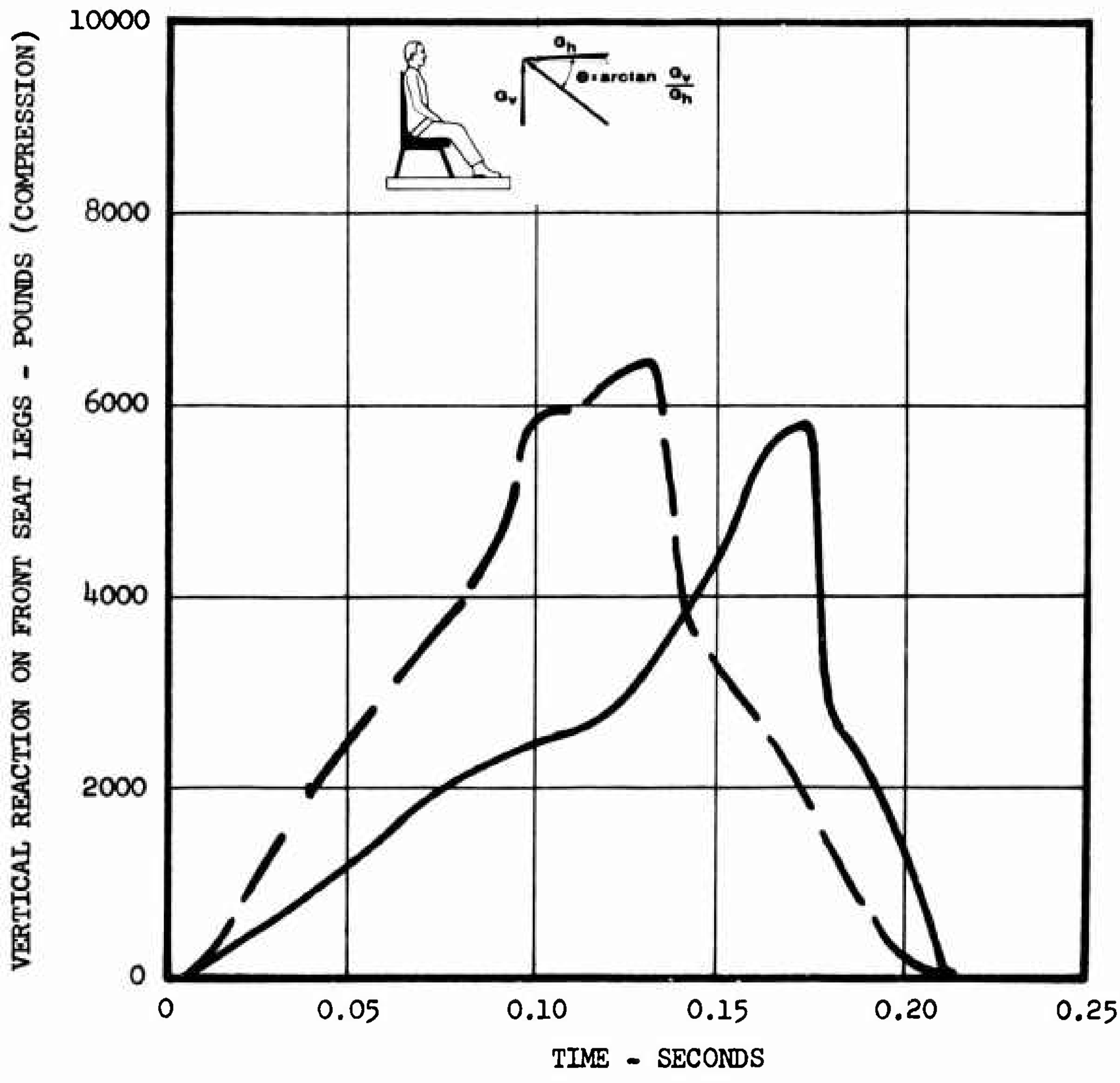

Figure 118. Vertical Reaction on Front Seat Legs Versus Time.

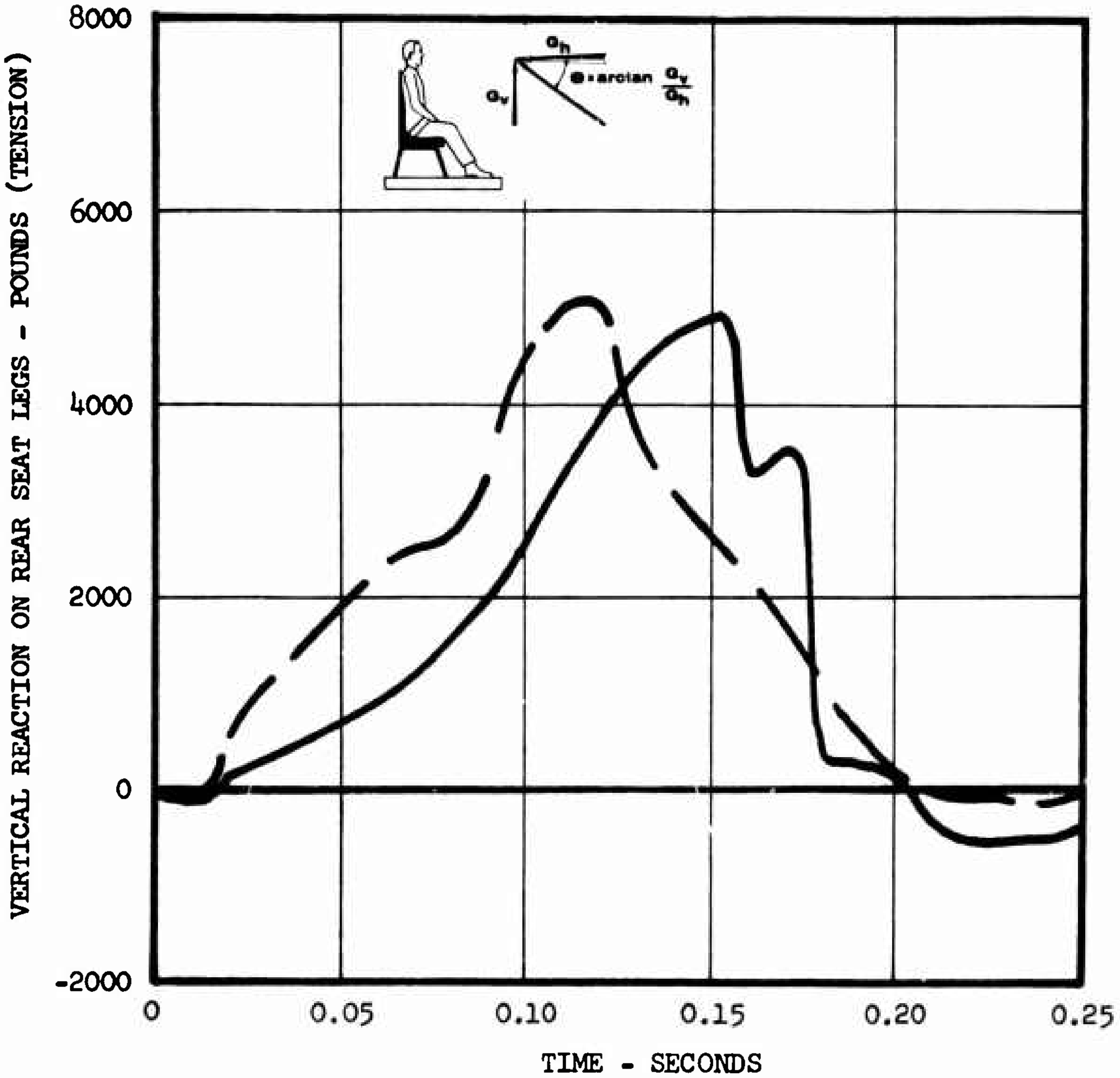

Figure 119. Vertical Reaction on Rear Seat Legs Versus Time.

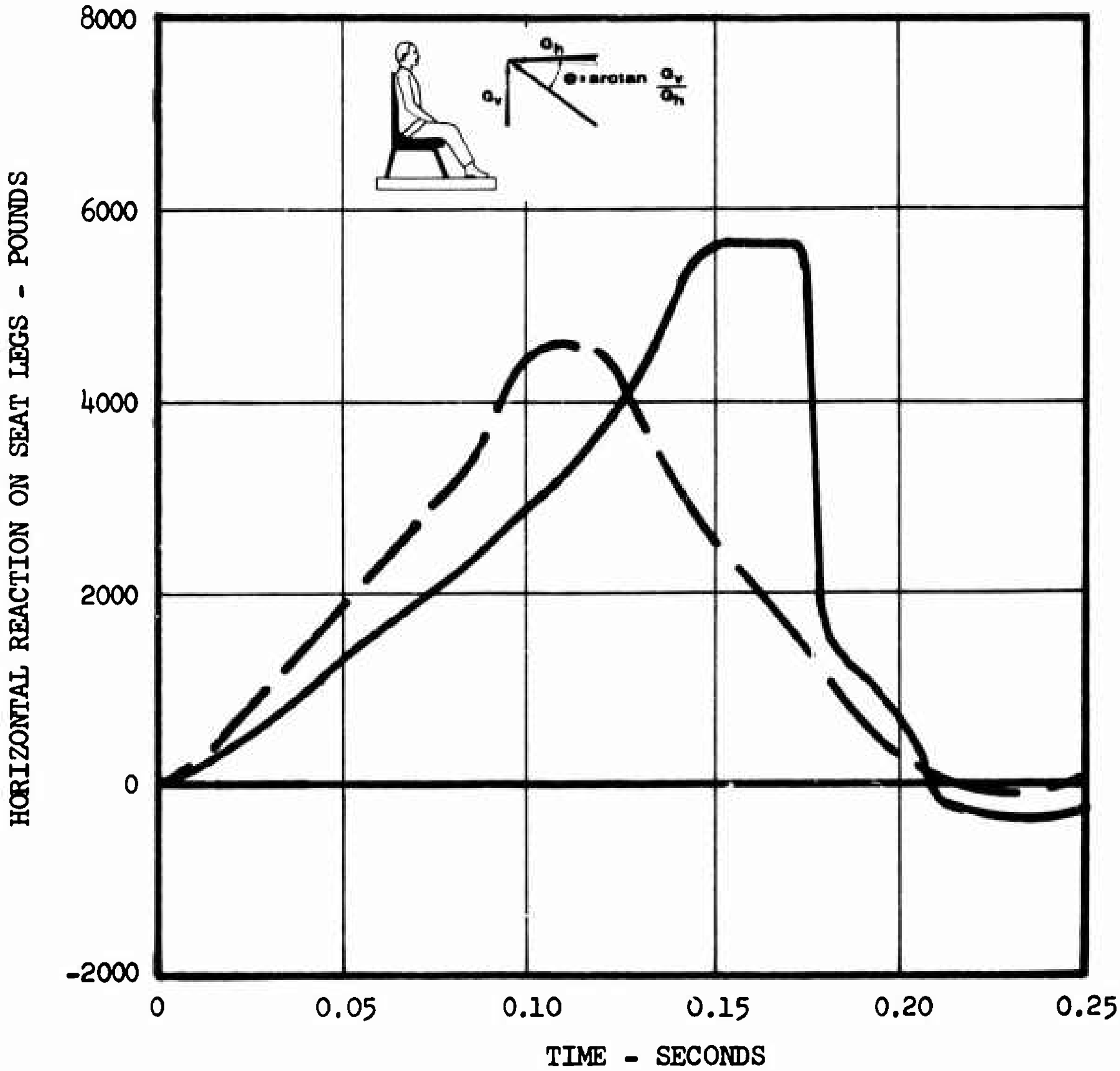

Figure 120. Horizontal Reaction on Seat Legs Versus Time.

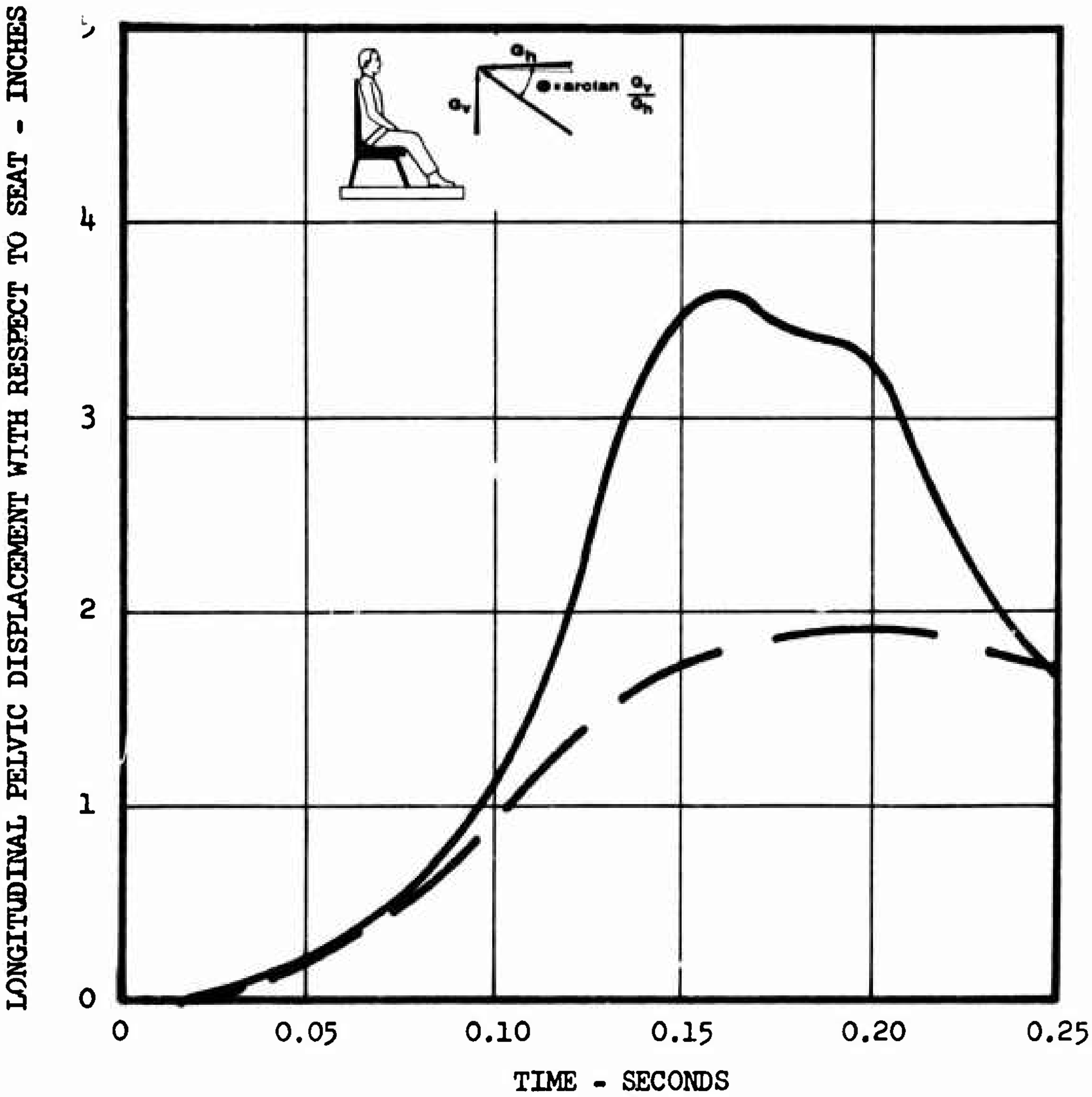

Figure 121. Longitudinal Pelvic Displacement With Respect to Seat Versus Time.

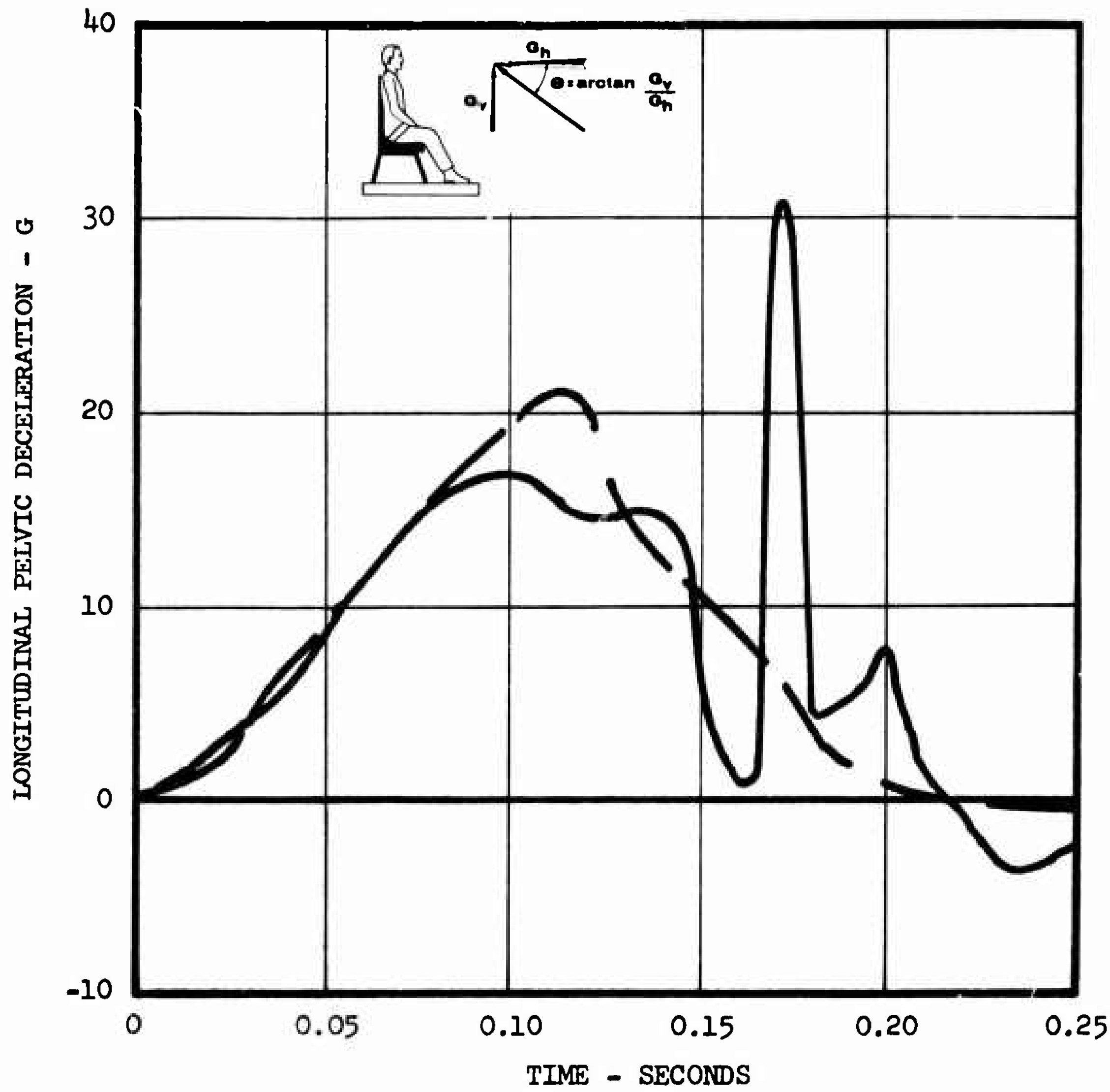

Figure 122. Longitudinal Pelvic Deceleration Versus Time.

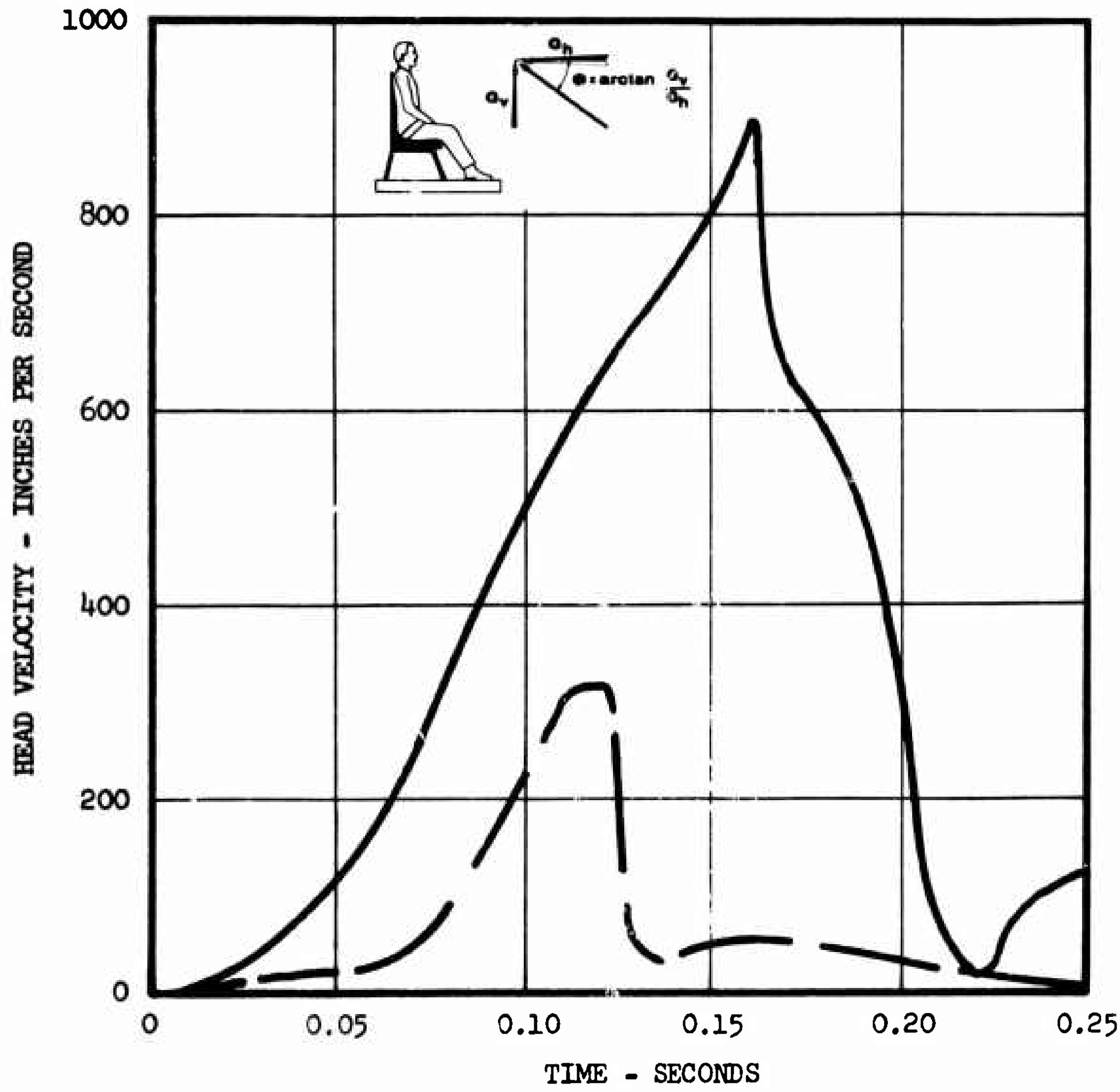

Figure 123. Head Velocity Versus Time.

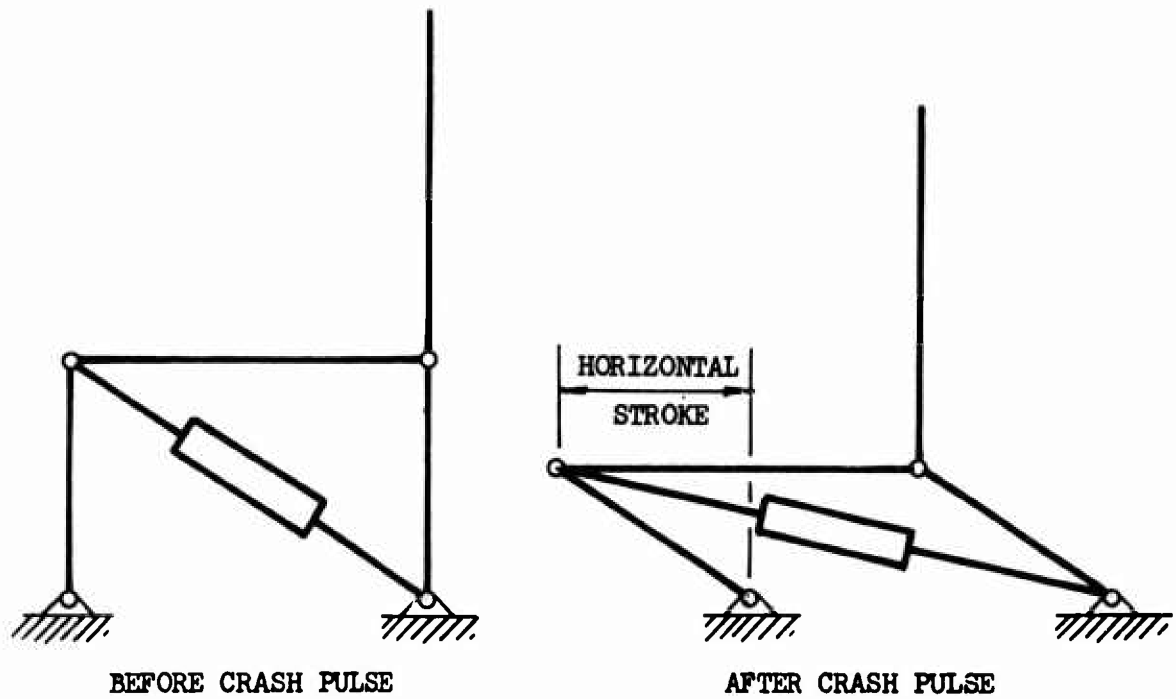

Figure 124. Structurally Integral Load Limiter Showing Seat Position Before and After Crash Pulse.

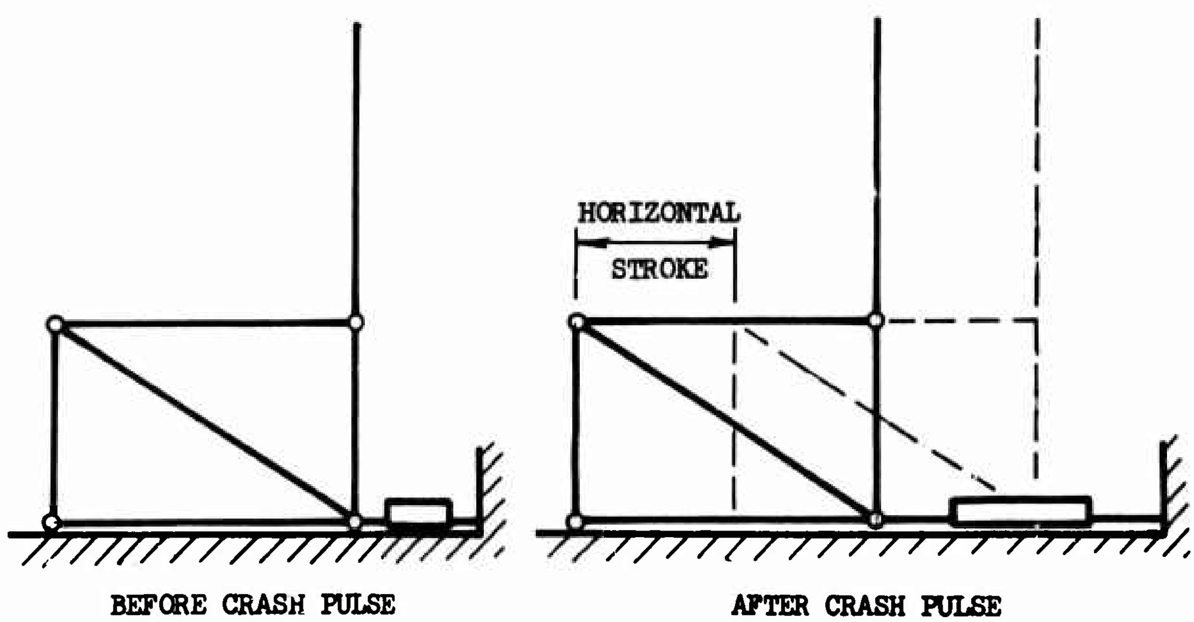

Figure 125. External Load Limiter Showing Seat Position Before and After Crash Pulse.

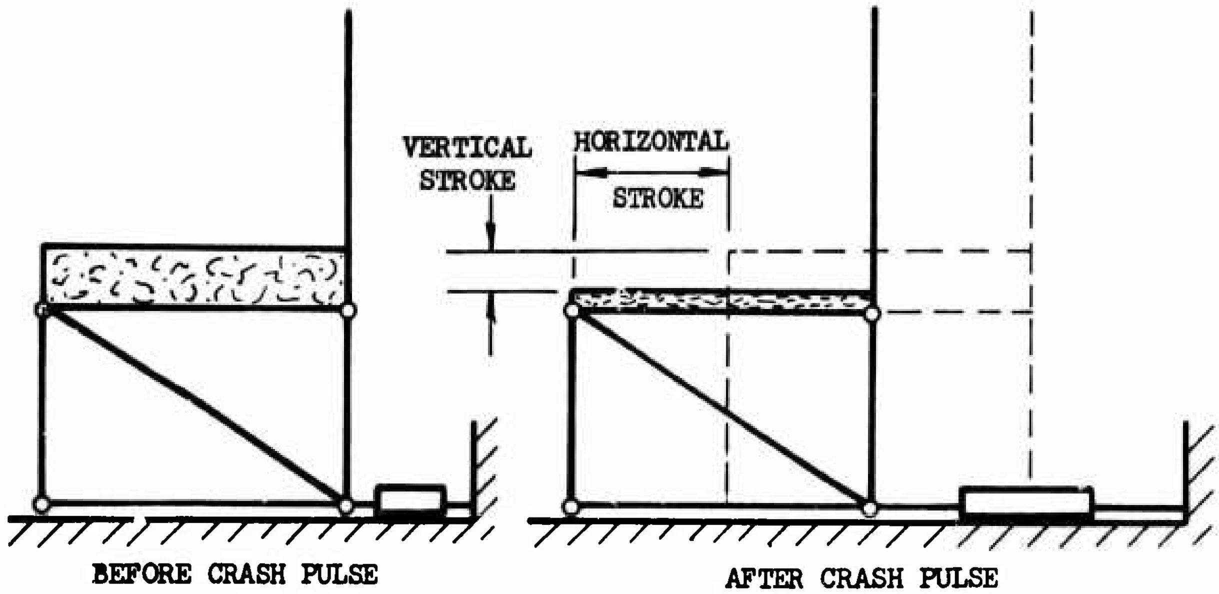

Figure 126. External Load Limiting in Two Directions Showing Seat Position Before and After Crash Pulse.

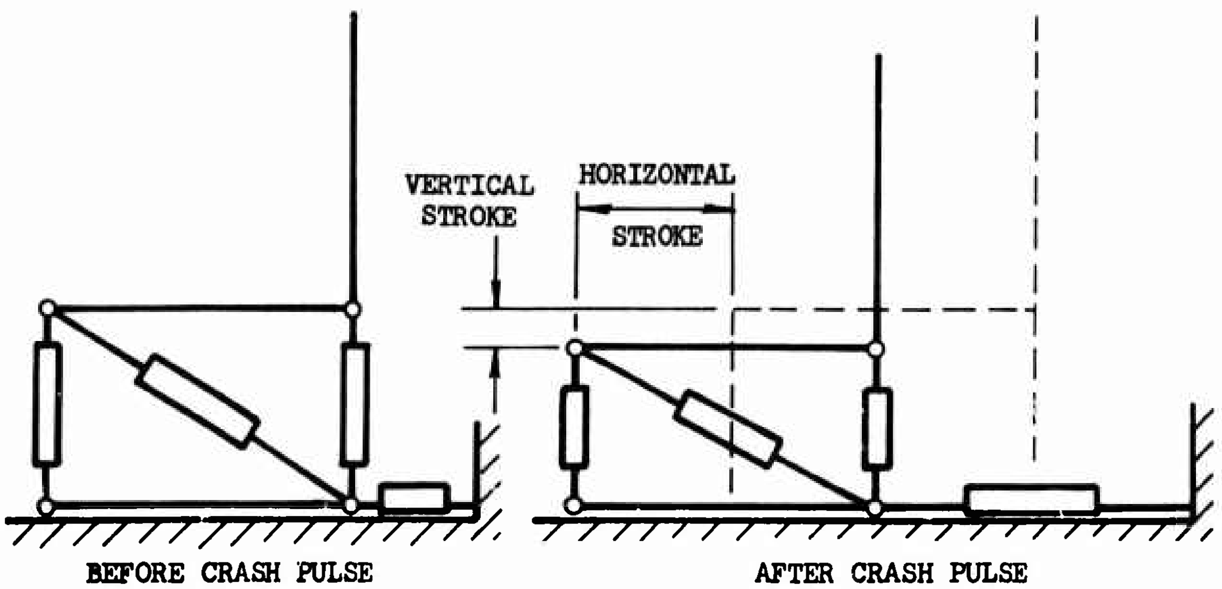

Figure 127. Combined External and Structurally Integral Load Limiting Showing Seat Position Before and After Crash Pulse.

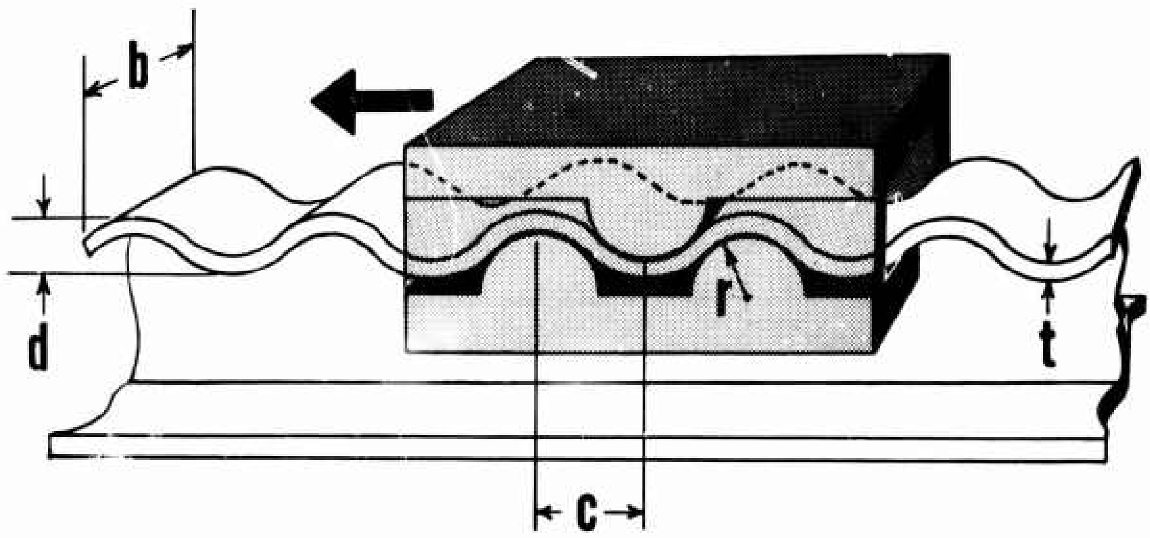

Figure 128. One Concept for a Lightweight External Load Limiter.

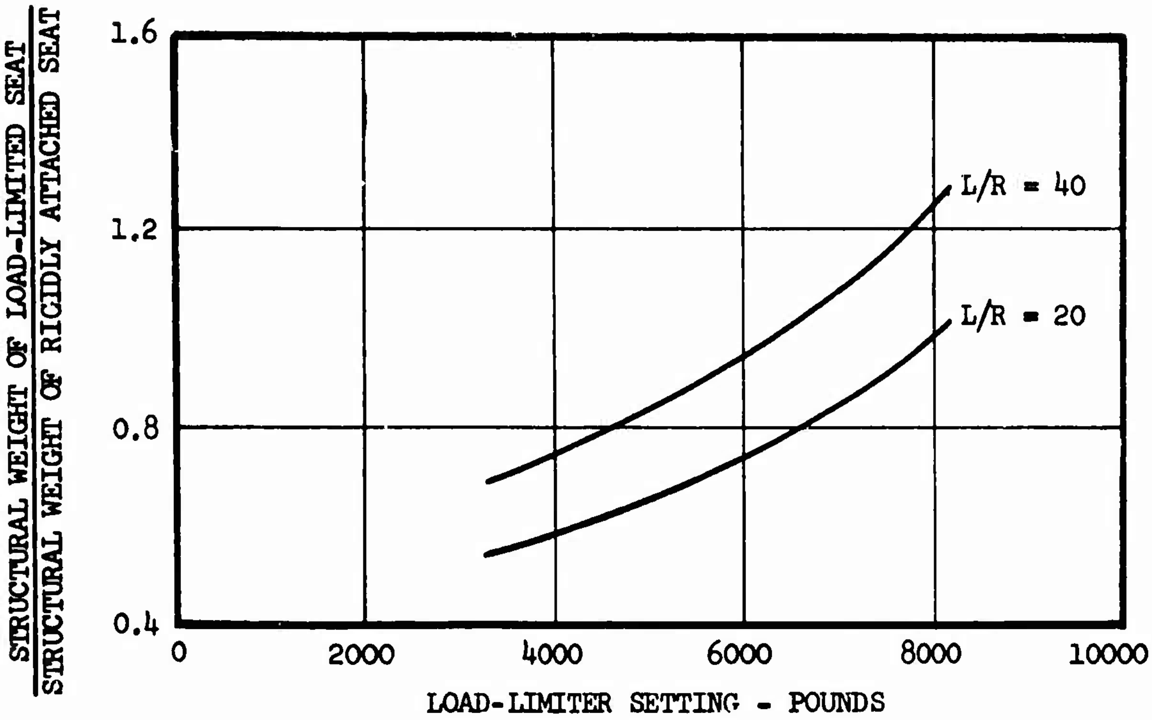

LOAD CONDITIONS FOR TYPE 3 INPUT ACCELERATION CURVE

LOAD-LIMITER SETTING	L/R = 20			L/R = 40		
	PB	PC	XMOC	PB	PC	XMOC
3396	1643	2653	12170	1643	2653	12170
5660	4027	2997	8697	4027	2997	8697
7924	5851	3112	8886	5851	3112	8886

NO SEAT DAMPING, FULL MUSCLE TENSION, NO SEAT BELT SLACK,
RATIO OF VERTICAL TO HORIZONTAL ACCELERATION = 0.2,
FRICTION COEFFICIENT BETWEEN SEAT AND PASSENGER = 0.7.
(SEE TABLE I FOR SYMBOL DEFINITIONS).

Figure 129. Structural Weight as a Function of Load-Limiter Setting as a Percentage of the Structural Weight for a Rigidly Mounted Seat Under the Same Impact Conditions.

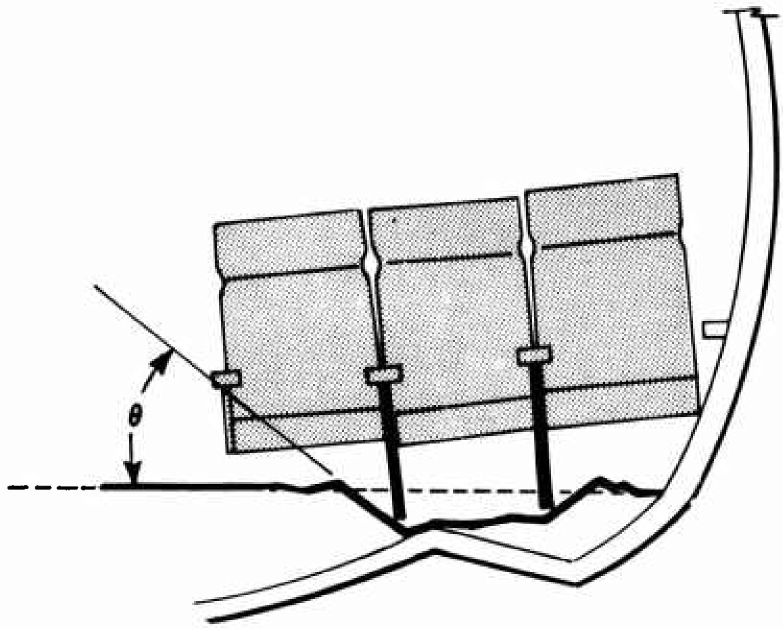

Figure 130. Schematic Diagram Showing a Bulge or Dish in Aircraft Floor in the Vicinity of the Seat Legs as a Result of Crash Loading.

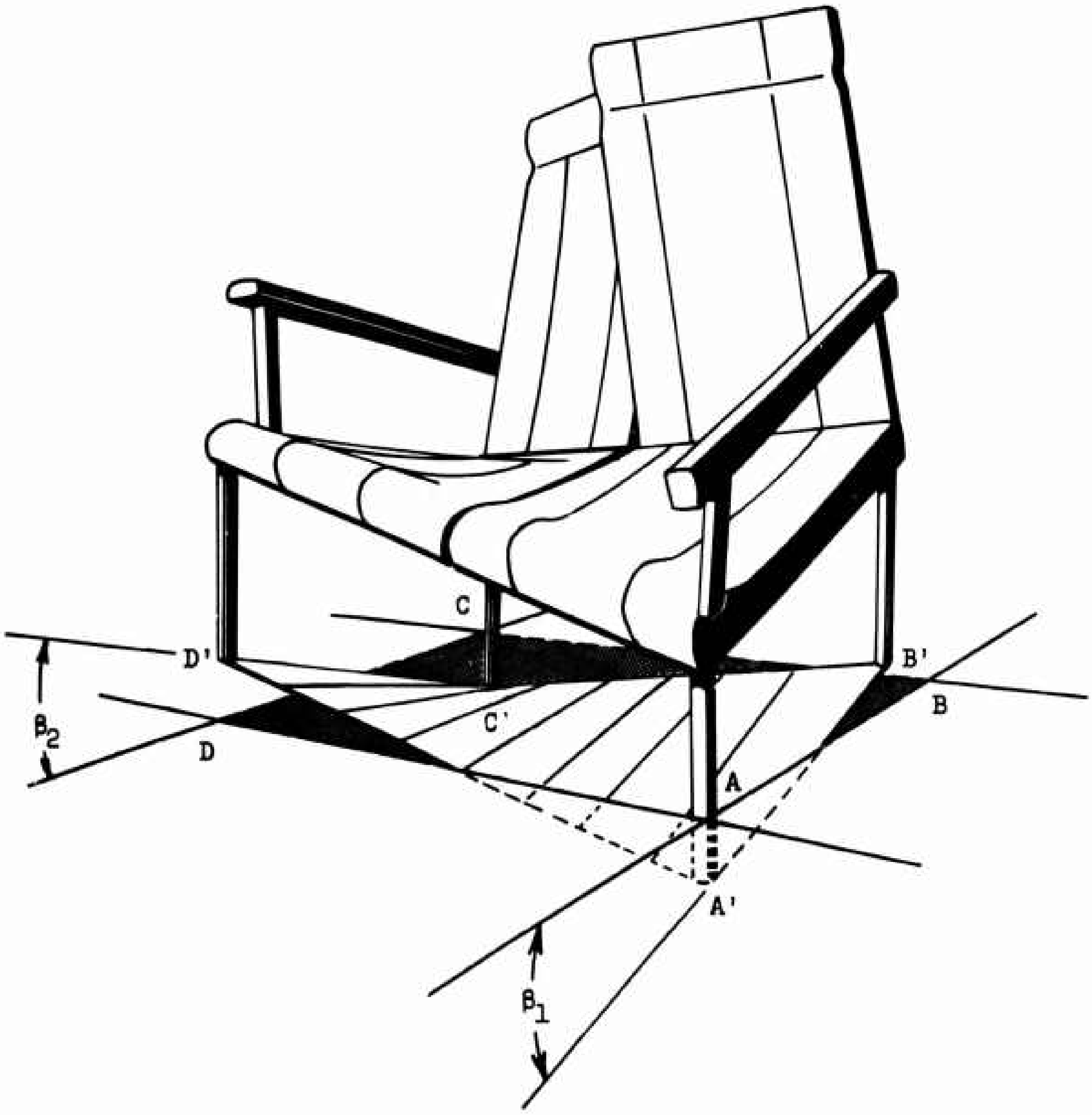

Figure 131. Schematic Diagram Showing Warpage of Floor of an Aircraft in Vicinity of Seat Legs as a Result of Crash Loading and the Resulting Twisting of the Seat.

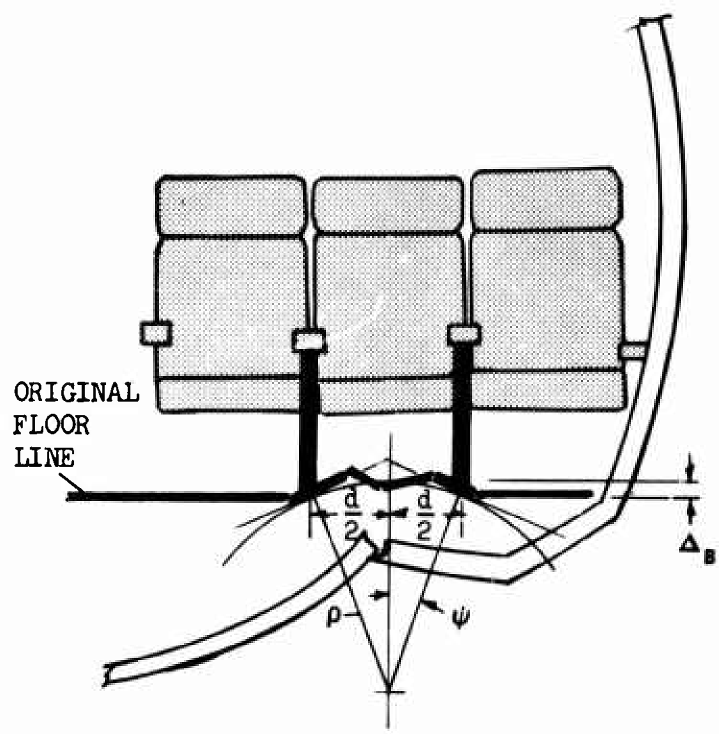

Figure 132. Sketch Showing Circle Arc Approximation for a Floor Bulge Caused by Aircraft Crash Loading.

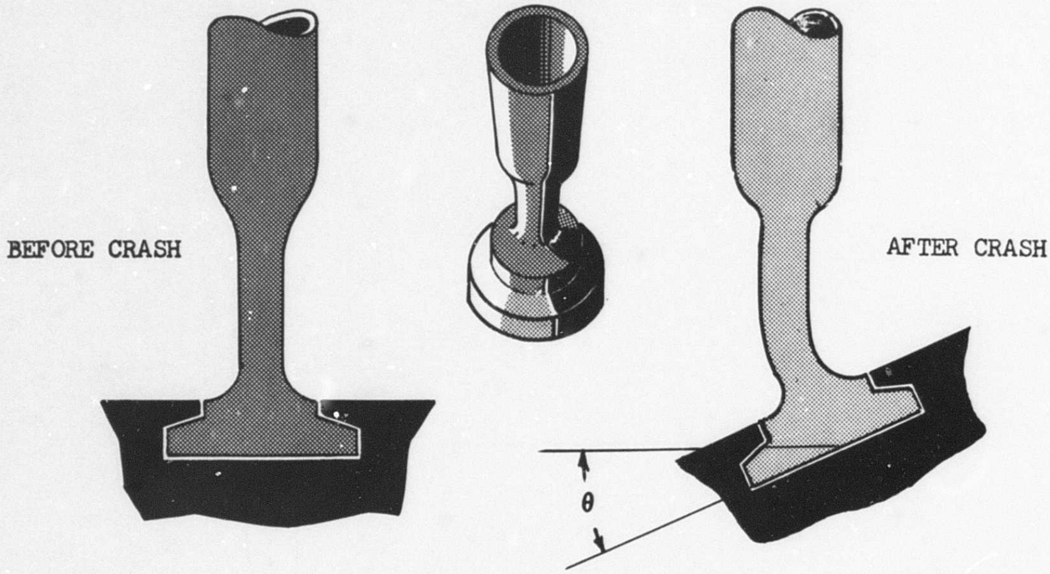

Figure 133. The Yield-Hinge Concept for Providing Large Angular Deflections in the Seat Tiedown Connections.

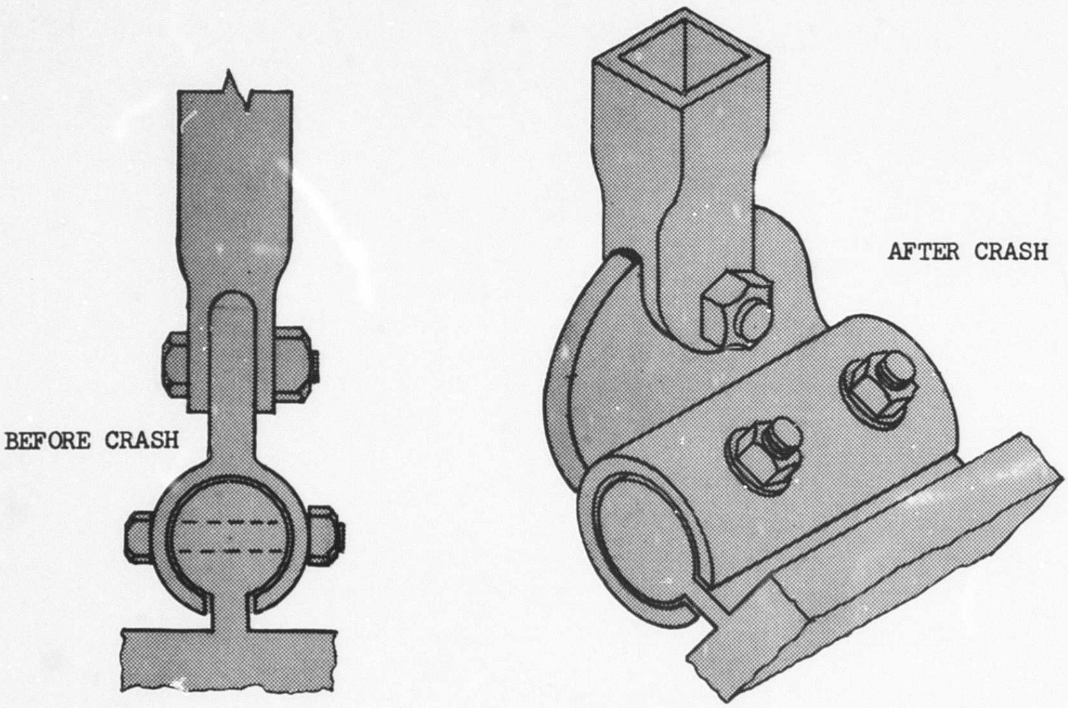

Figure 134. The Friction-Plate Concept for Providing Large Angular Deflections in the Seat Tiedown Connections.

(NOTE: ALL DIMENSIONS ARE IN INCHES)

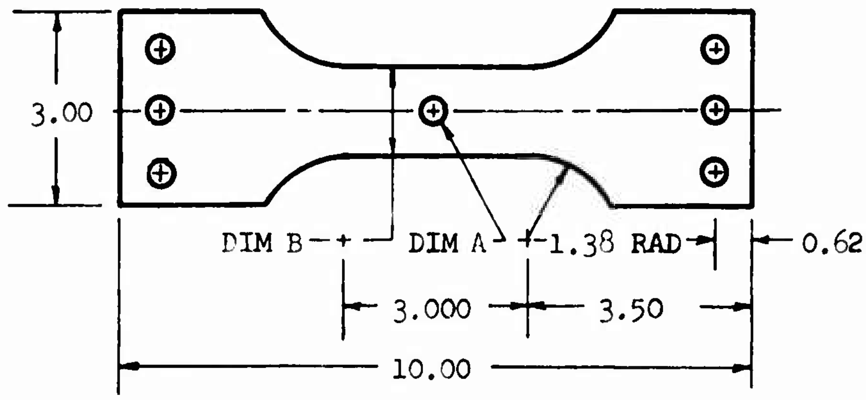

TYPE	1	2	3
DIM A	0.375 DIA	0.188 DIA	0.062 DIA
DIM B	1.375	1.188	1.062
2024-T3 ALUMINUM - 0.050-INCH BARE SHEET			

Figure 135. Hole-Type Specimen Configuration.

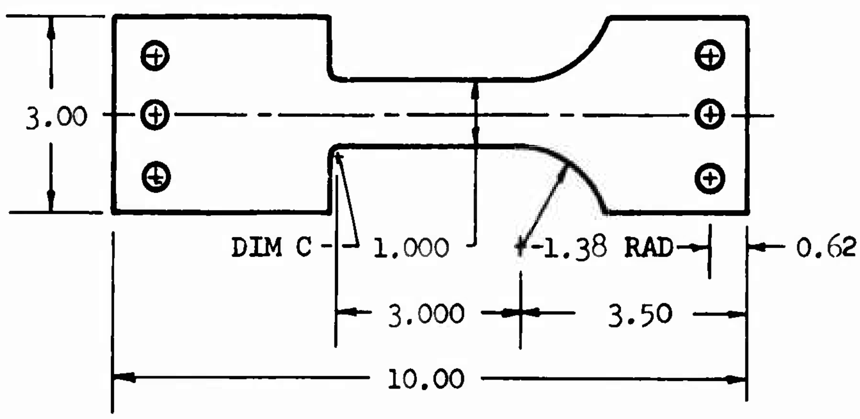

TYPE	4	5	6	7
DIM C	0.047 RAD	0.188 RAD	0.008 RAD	1.38 RAD
2024-T3 ALUMINUM - 0.050-INCH BARE SHEET				

Figure 136. Fillet-Type Specimen Configuration.

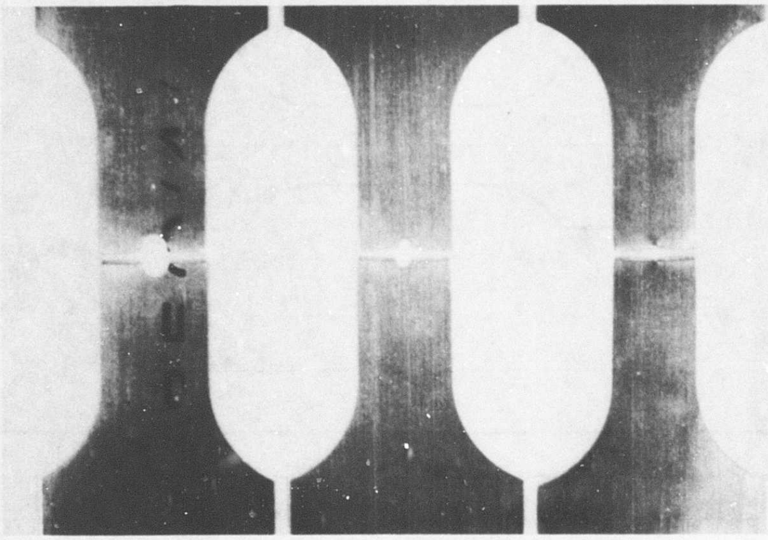

Figure 137. Typical Fracture for Hole-Type Specimens. (Left to right - Types 1, 2, 3.)

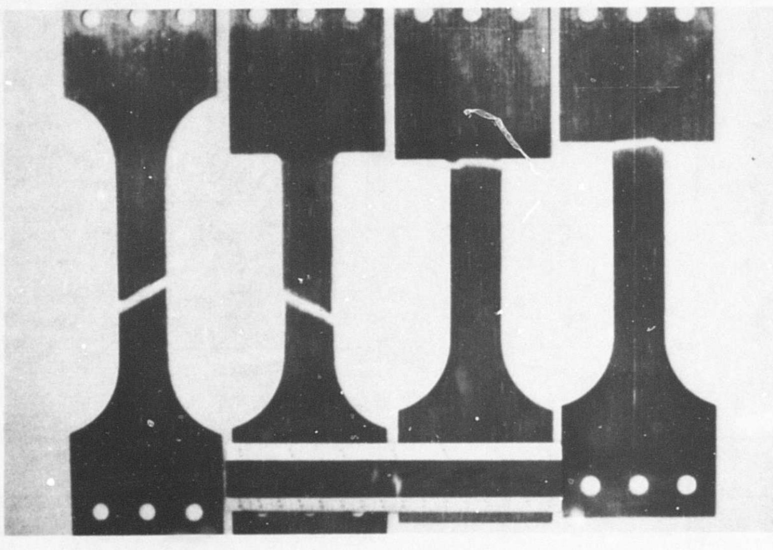

Figure 138. Typical Fracture for Fillet-Type Specimens. (Left to right - Types 7, 5, 4, 6.)

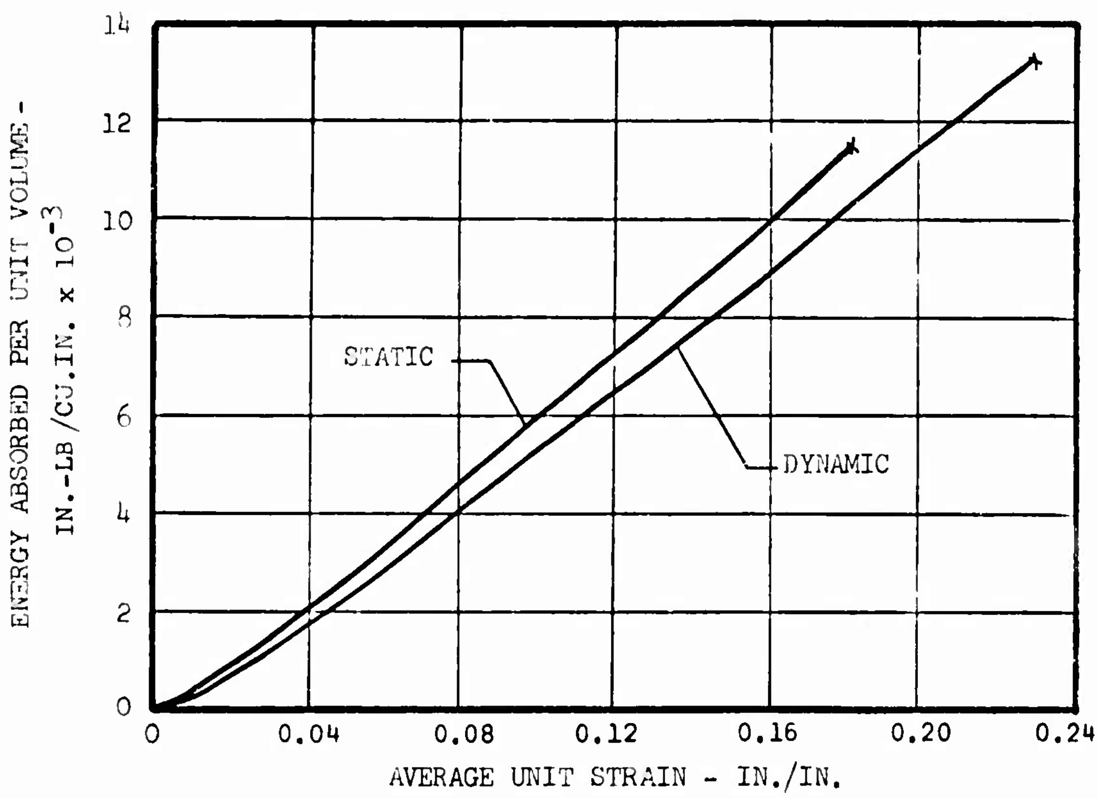

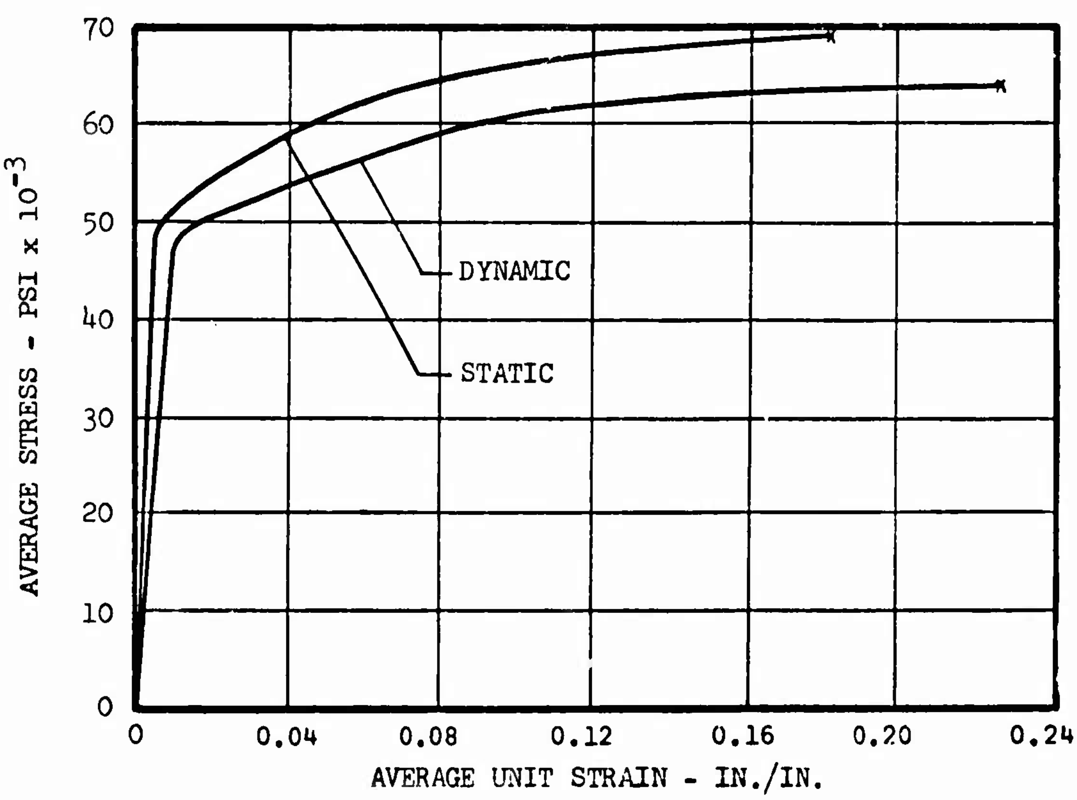

Figure 139. Static and Dynamic Stress-Strain and Energy-Strain Relations for Smooth (Type 7) Specimens.

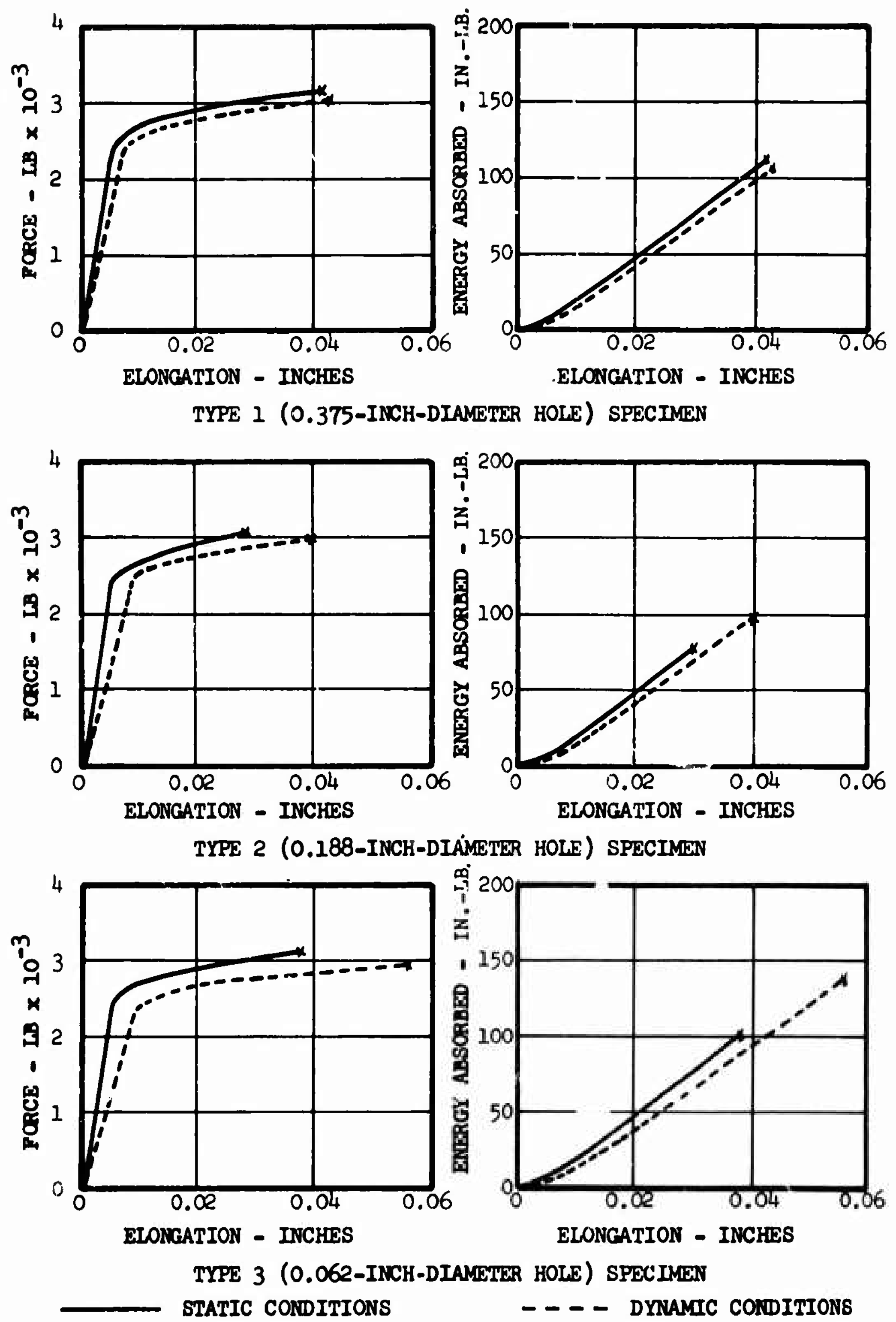

Figure 140. Static and Dynamic Force-Deformation and Energy-Deformation Relations for Hole- and Fillet-Type Specimens With 1.0-Inch Gage Length.

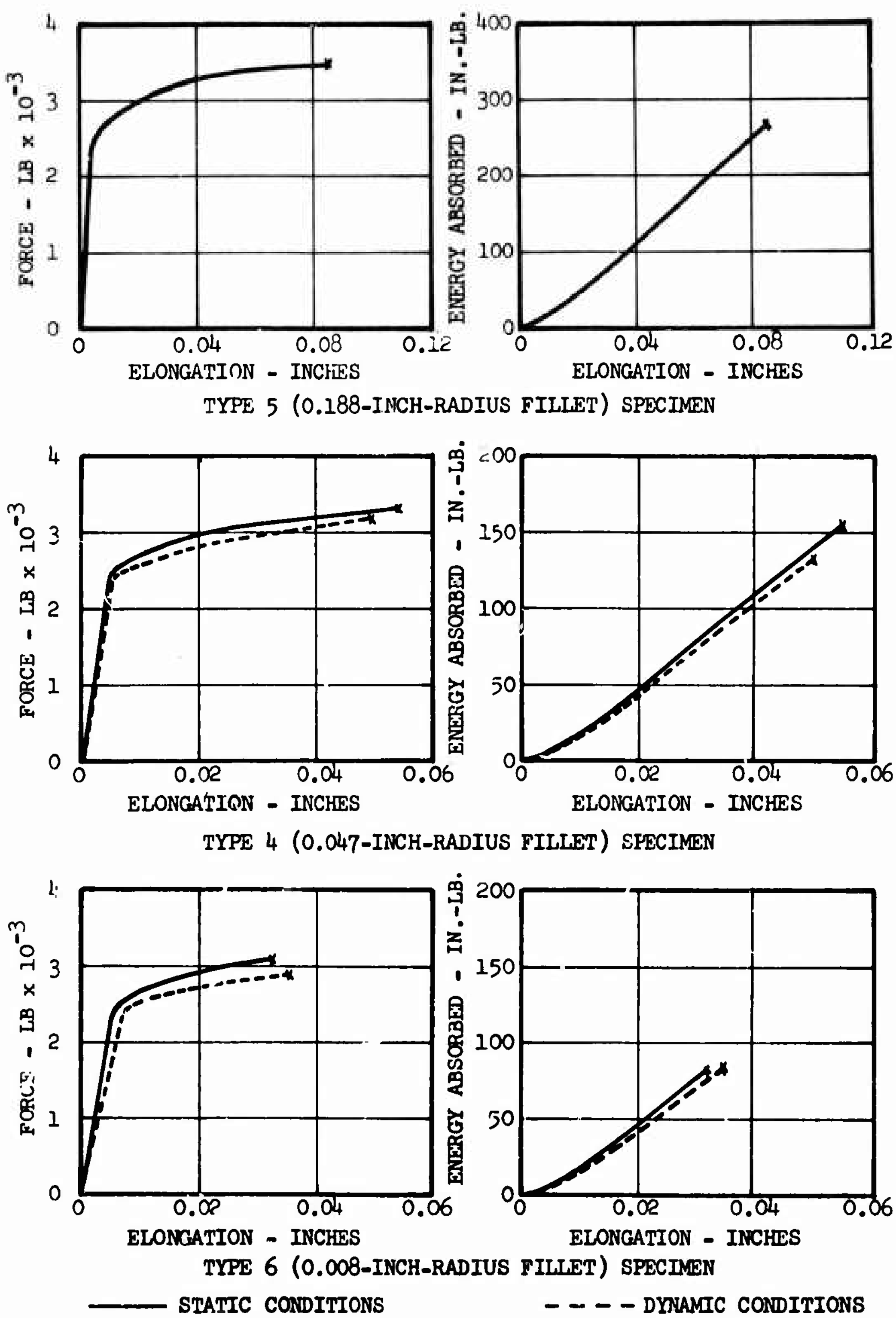

Figure 140. (contd.) Static and Dynamic Force-Deformation and Energy-Deformation Relations for Hole- and Fillet-Type Specimens With 1.0-Inch Gage Length.

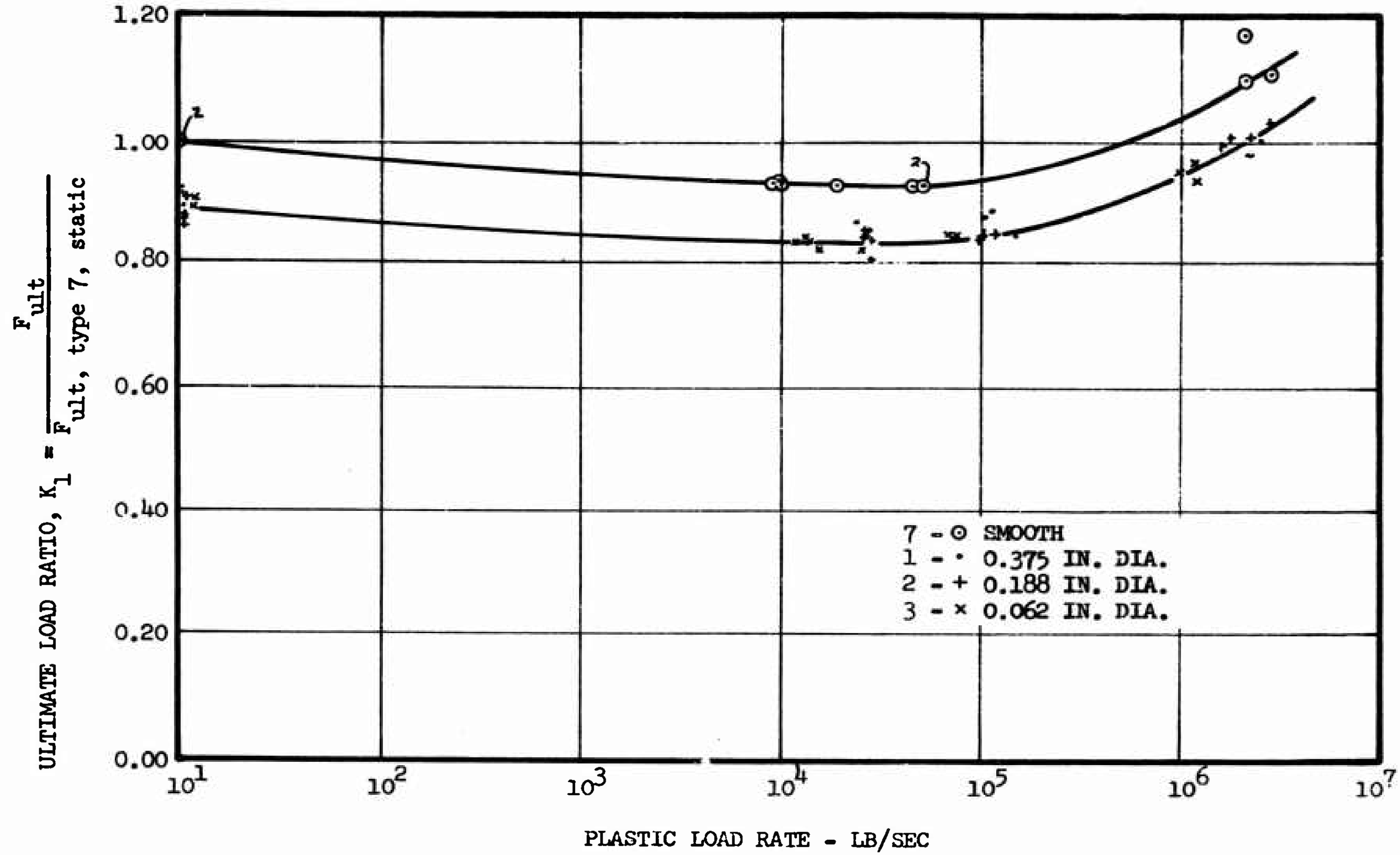

Figure 141. Effects of Geometry and Loading Rate on Ultimate-Rupture Stress-Concentration Factor for Hole-Type Specimens.

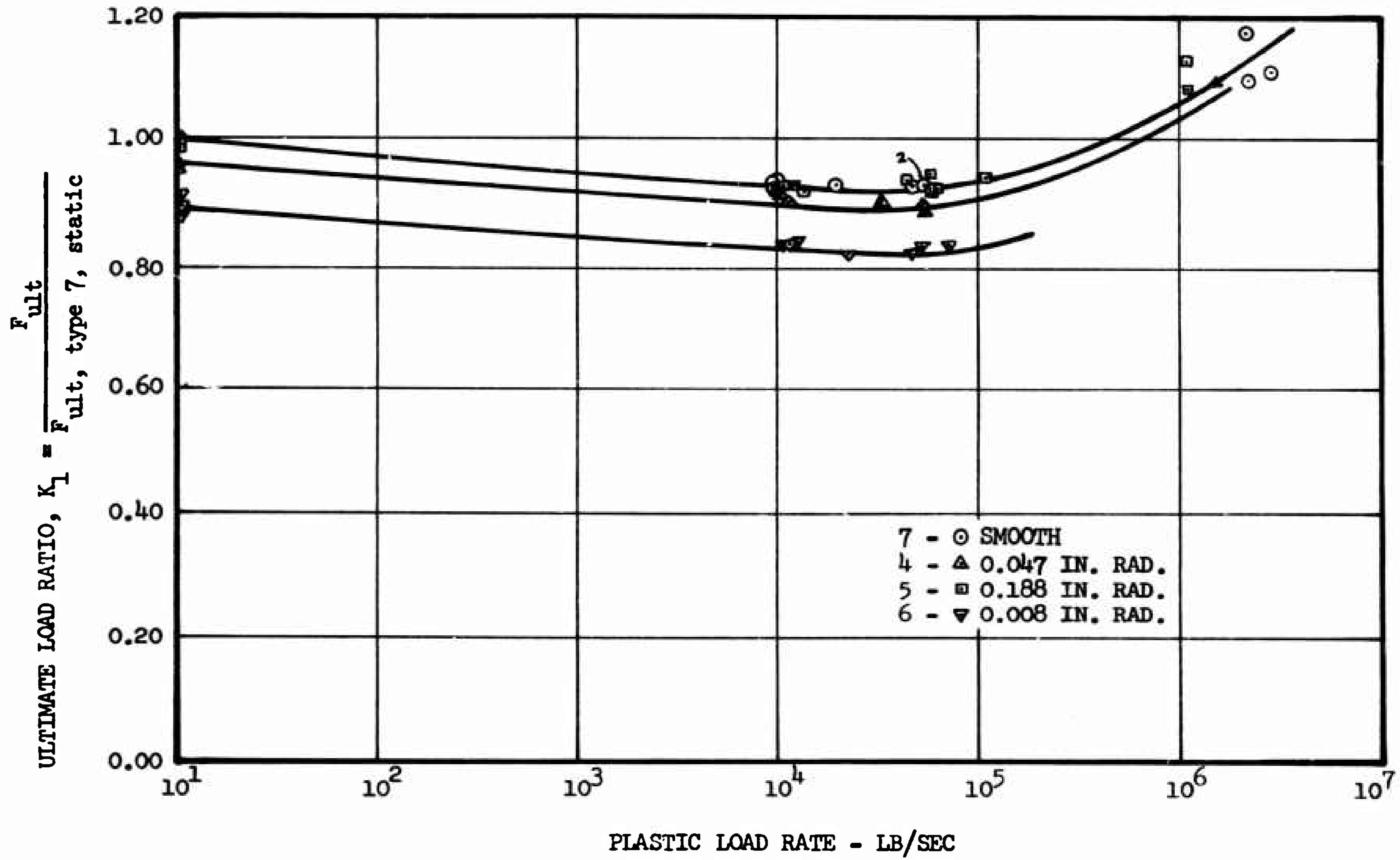

Figure 142. Effects of Geometry and Loading Rate on Ultimate-Rupture Stress-Concentration Factor for Fillet-Type Specimens.

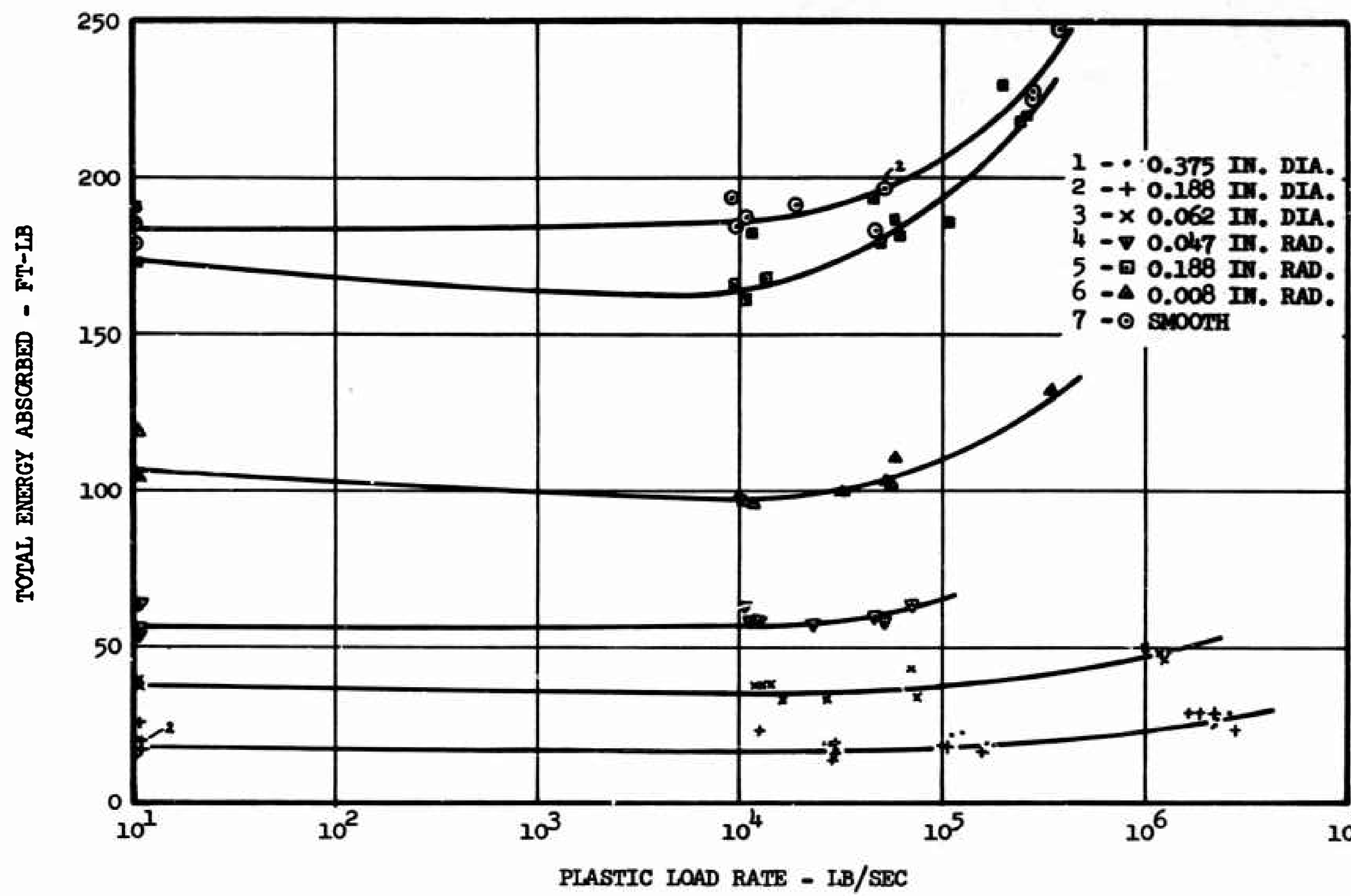

Figure 143. Effects of Geometry and Loading Rate on Total Energy Absorption in a 3.0-Inch Gage Length.

CODE:
STATIC TUBULAR
DYNAMIC TUBULAR
STATIC SHEET METAL
DYNAMIC SHEET METAL

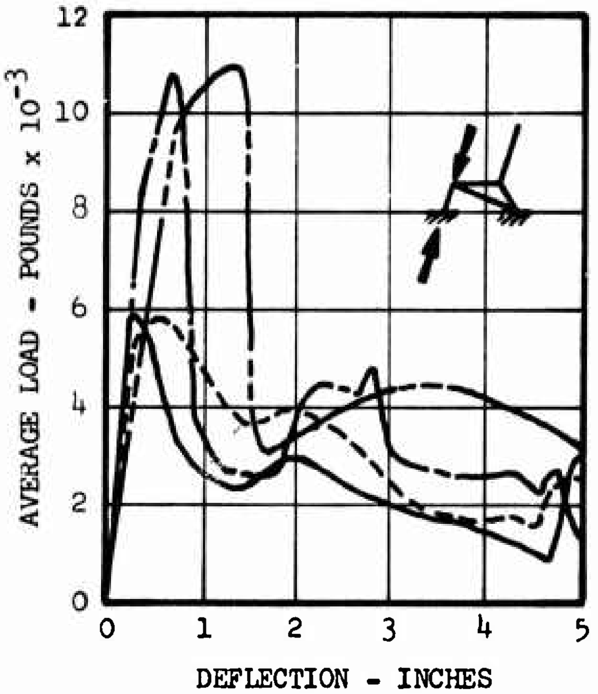

Figure 144. Compression Tests.

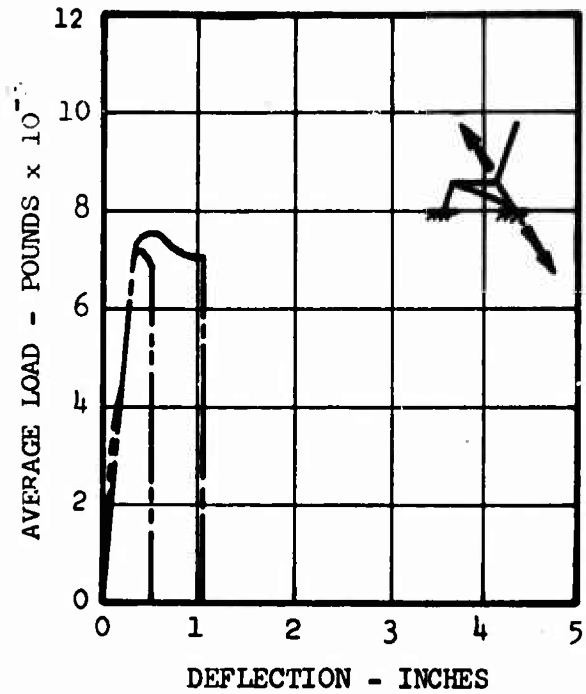

Figure 145. Tension Tests.

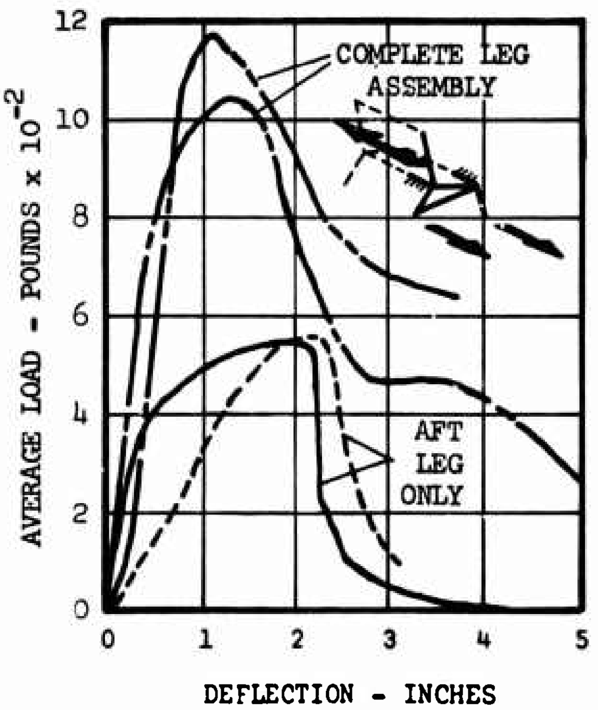

Figure 146. Side Bending Tests.

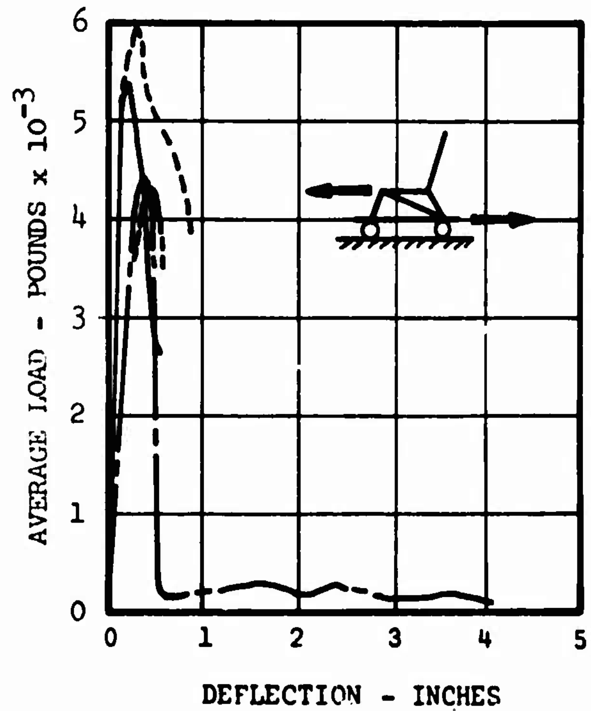

Figure 147. Forward Load Test on Complete Leg Assembly.

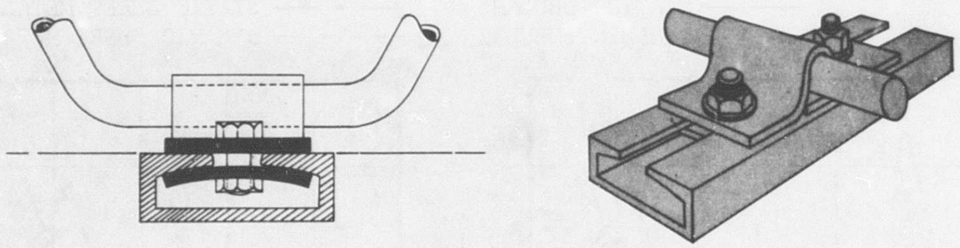

Figure 148. Friction Clamp Tiedown Connection Between Seat Leg and Floor Track.

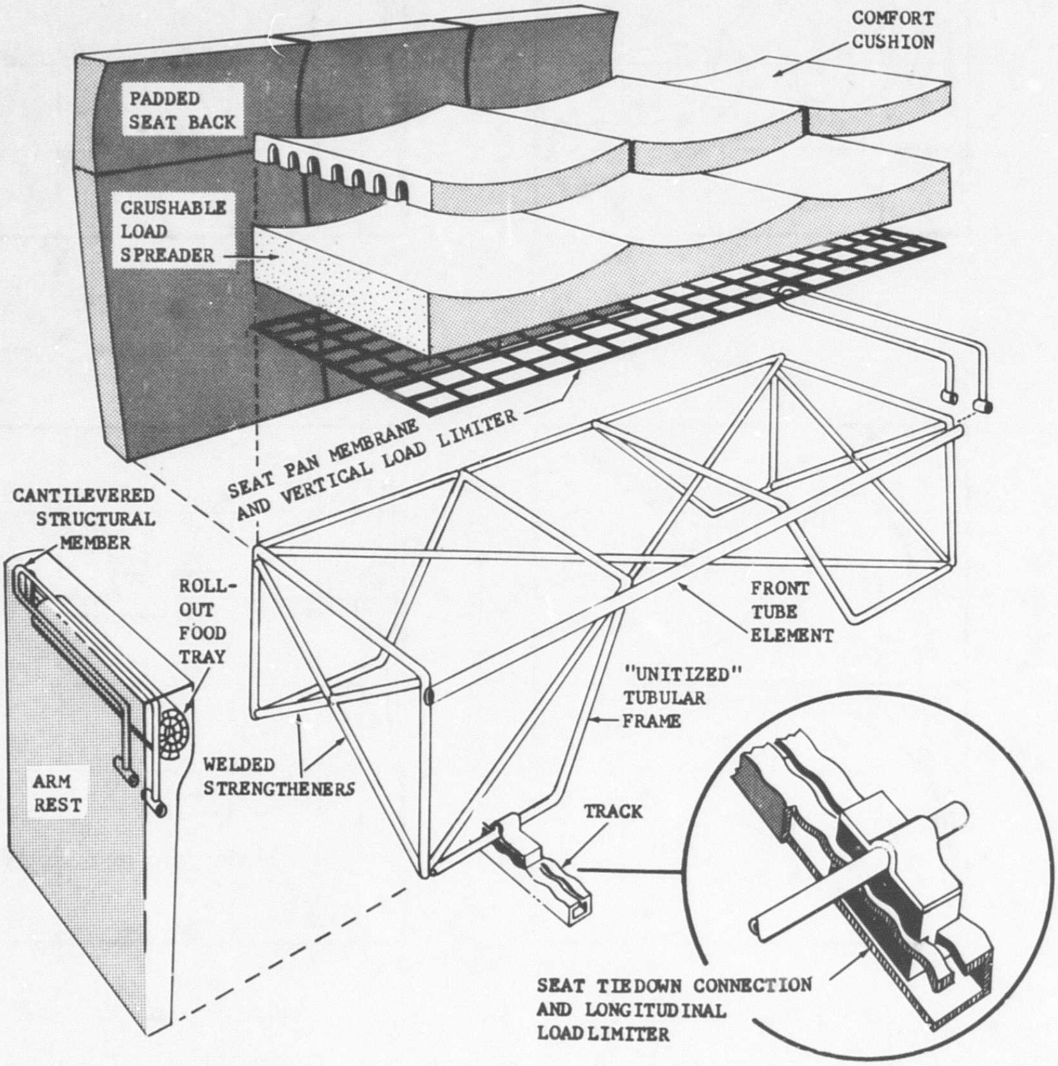

Figure 149. Hypothetical Rigid Seat With External Load Limiters and Other Design Concepts.

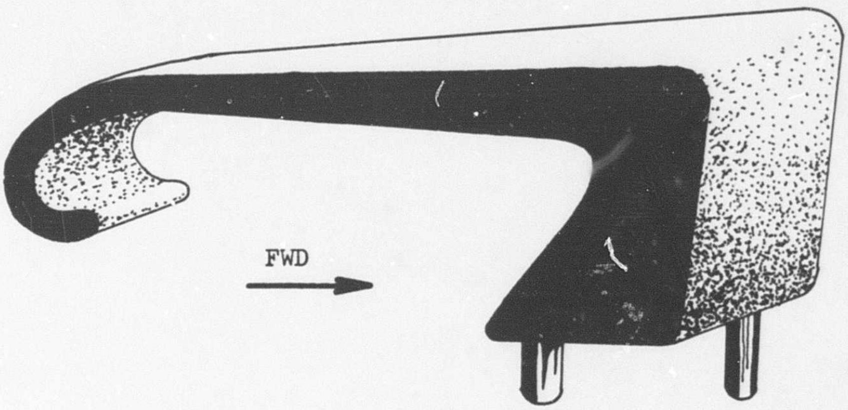

Figure 150. Cantilever Arm Rest.

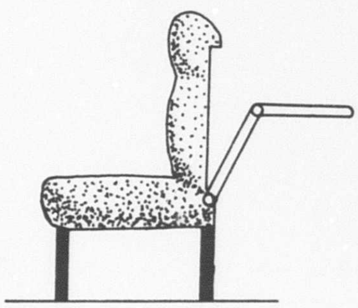

Figure 151. Standard Tray.

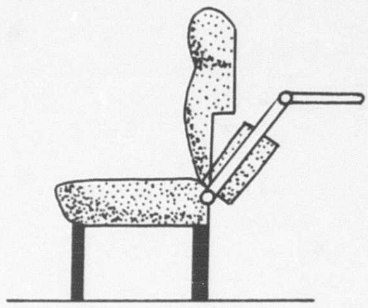

Figure 152. Telescoping Tray.

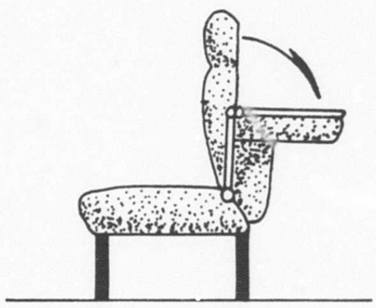

Figure 153. Split Back With Leveling Linkage.

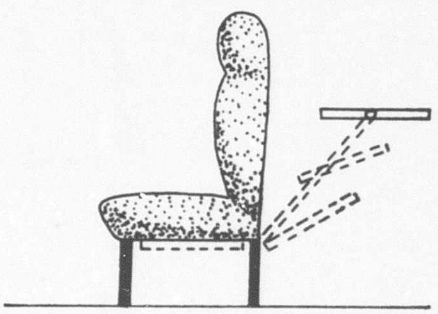

Figure 154. Under-Seat Stowage - Clean Padded Back.

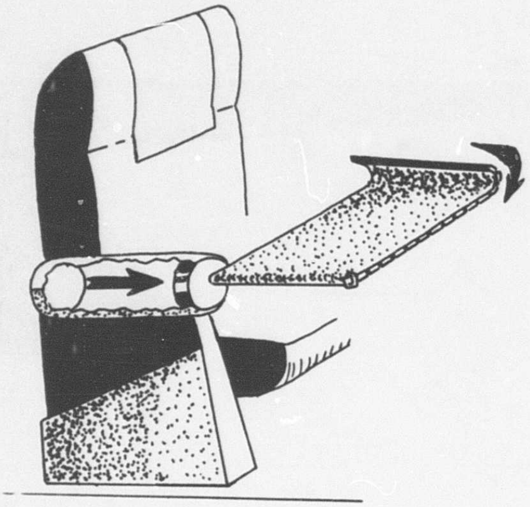

Figure 155. Arm Rest Stowage - Roll Up.

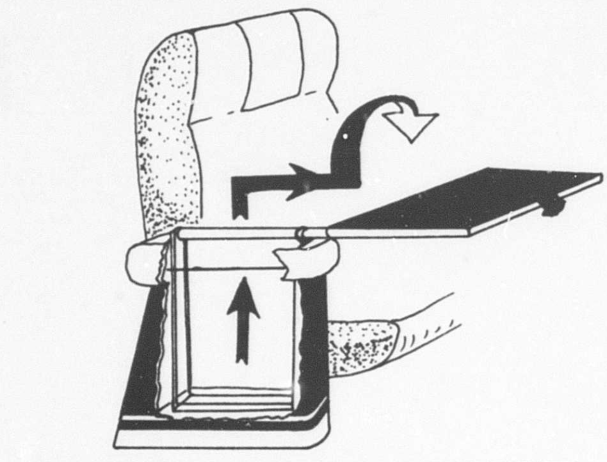

Figure 156. Arm Rest Stowage - Swing Out.

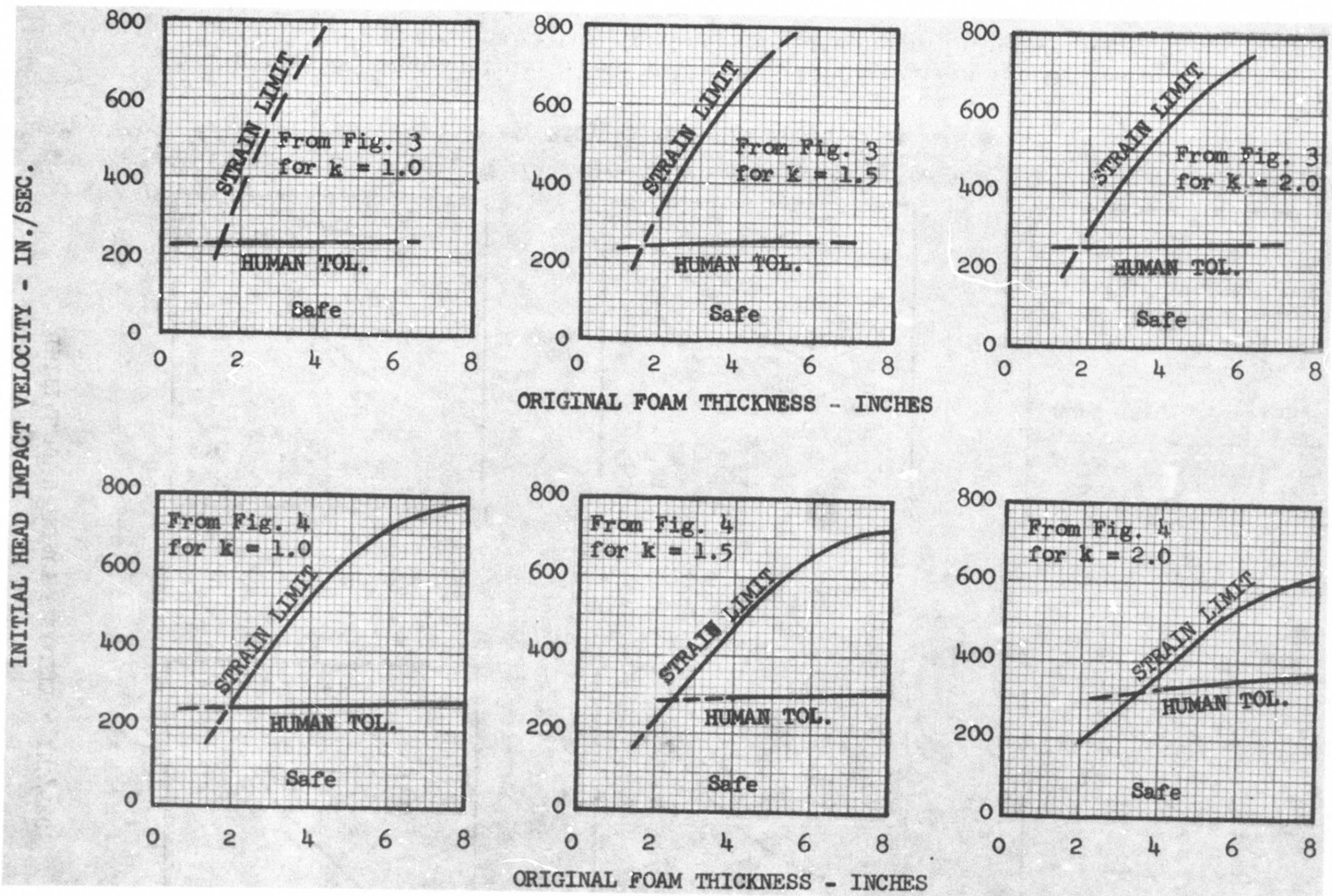

Figure 157. Human Tolerance and Material Limitations on the Determination of Original Foam Thickness and Maximum Initial Velocity.

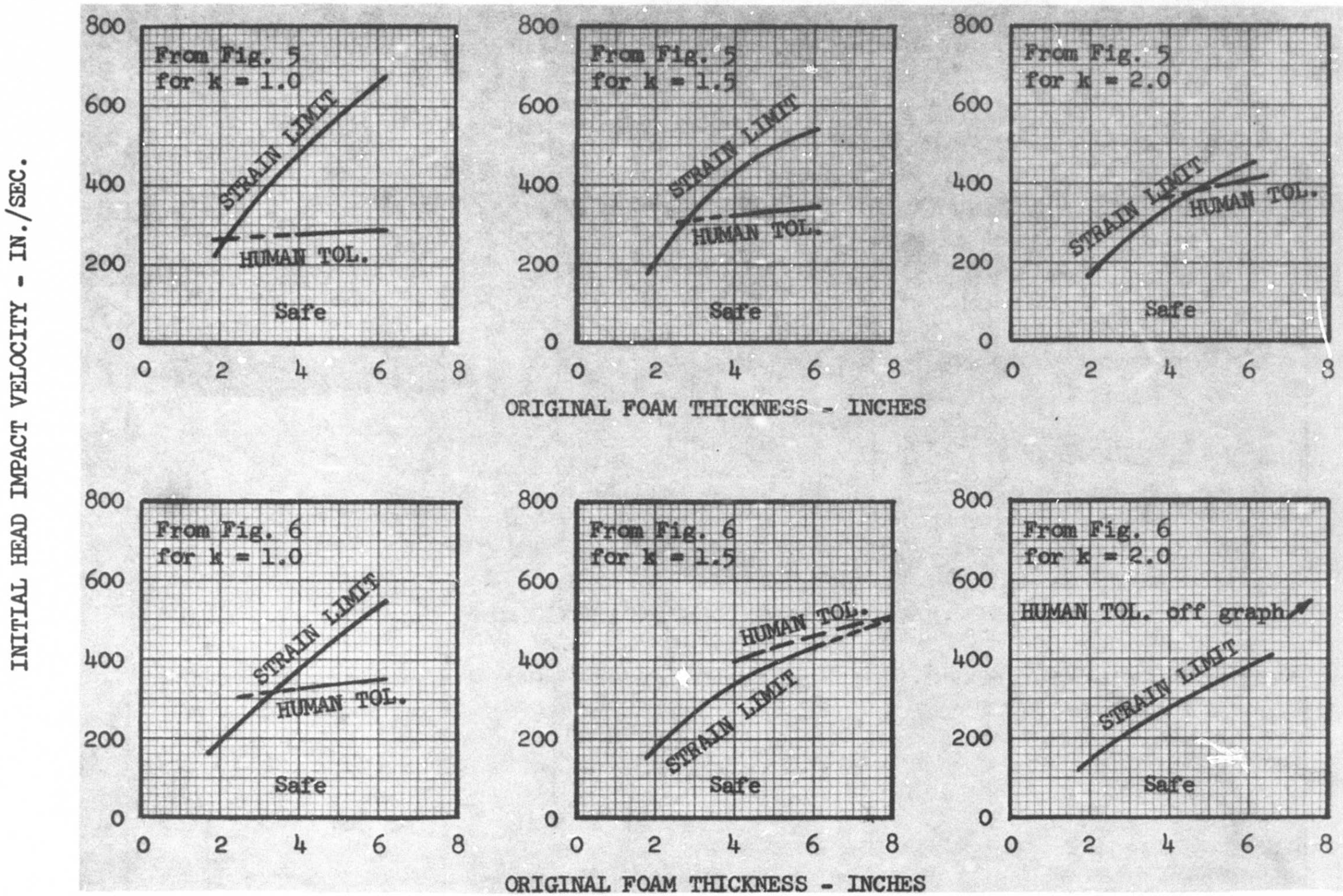

Figure 158. Human Tolerance and Material Limitations on the Determination of Original Foam Thickness and Maximum Initial Velocity.

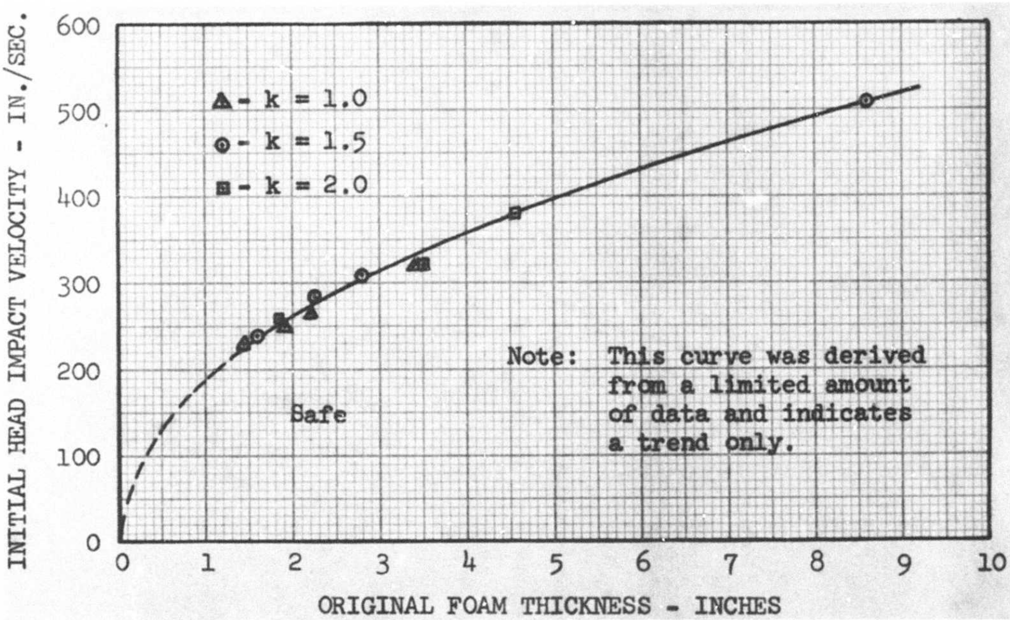

Figure 159. Lowest Value of Limiting Head Impact Velocity.

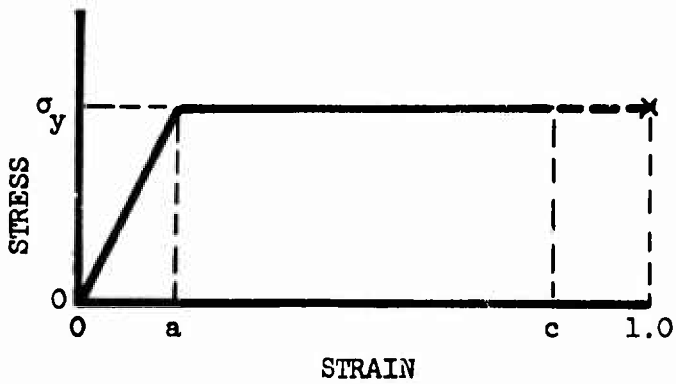

$$\sigma = \sigma_y \frac{x}{ah} \qquad 0 \le x \le a$$

$$= \sigma_y \qquad a \le x \le c$$

(NOTE THAT c = b)

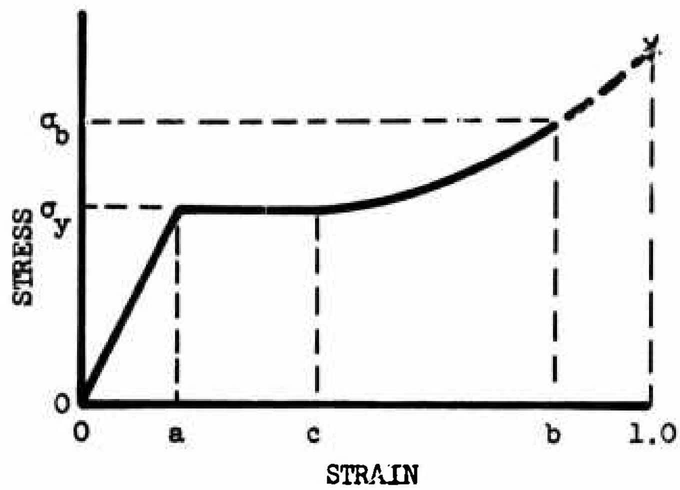

$$\sigma = \sigma_y \frac{x}{ah} \qquad 0 \le x \le a$$

$$= \sigma_y \qquad a \le x \le c$$

$$= (\sigma_b - \sigma_y) \frac{x^2 - c^2h^2}{(b^2 - c^2)h^2} + \sigma_y$$

$$c \le x \le b$$

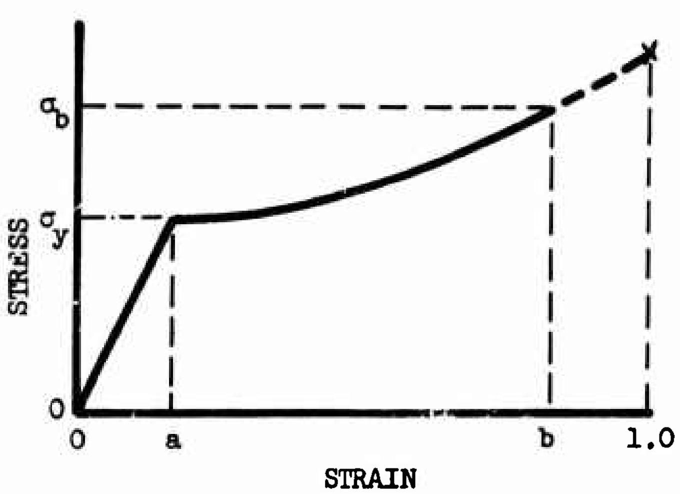

$$\sigma = \sigma_y \frac{x}{ah} \qquad 0 \le x \le a$$

$$= (\sigma_b - \sigma_y) \frac{x^2 - b^2h^2}{(b^2 - a^2)h^2} + \sigma_y$$

$$a \le x \le b$$

(NOTE THAT a = c)

Figure 160. Stress-Strain Curves Used in the Head Impact Computer Program.

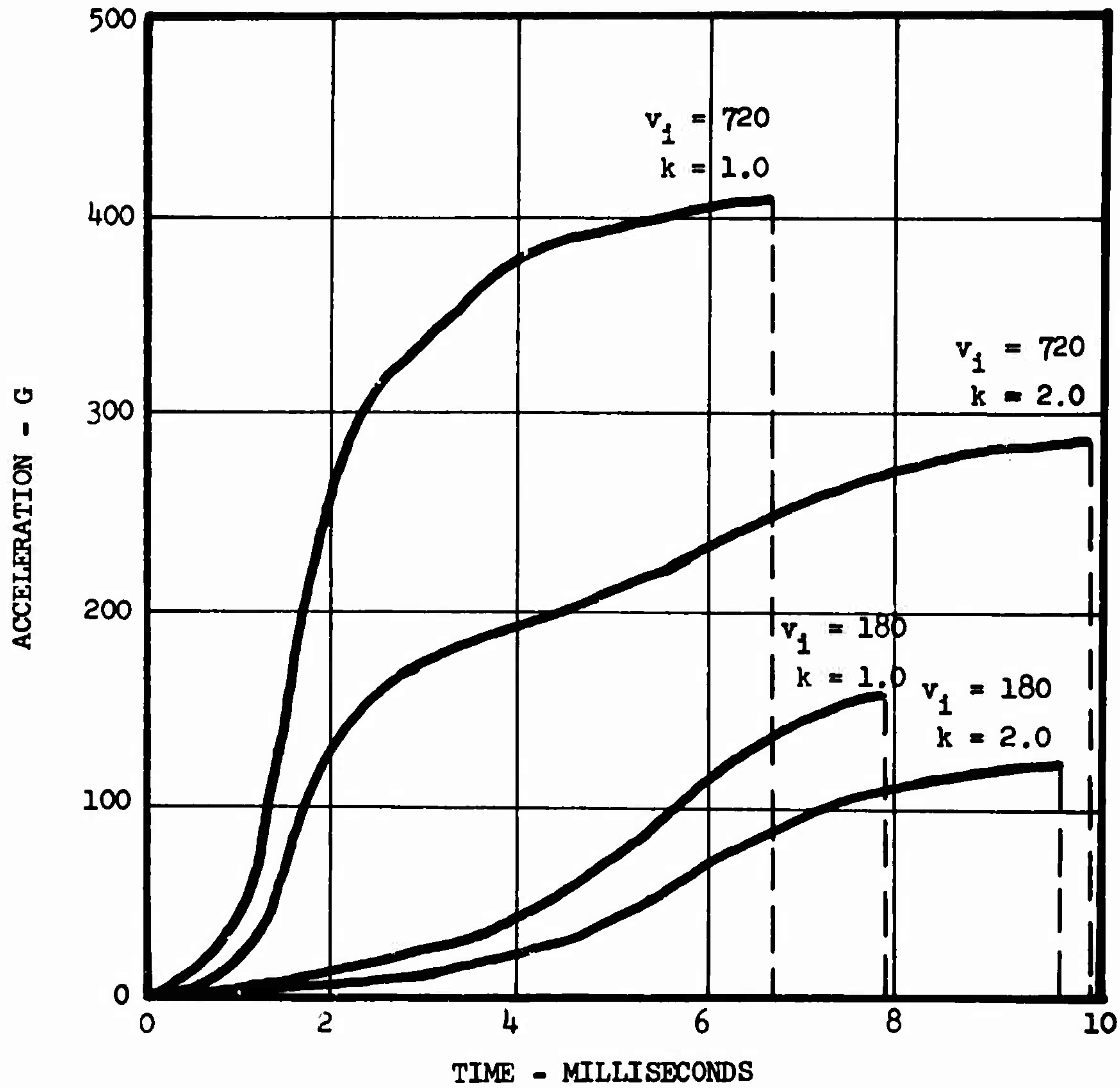

Figure 161. Acceleration-Time Curves for Foam Shown in Figure 162 for 6-Inch Original Foam Thickness.

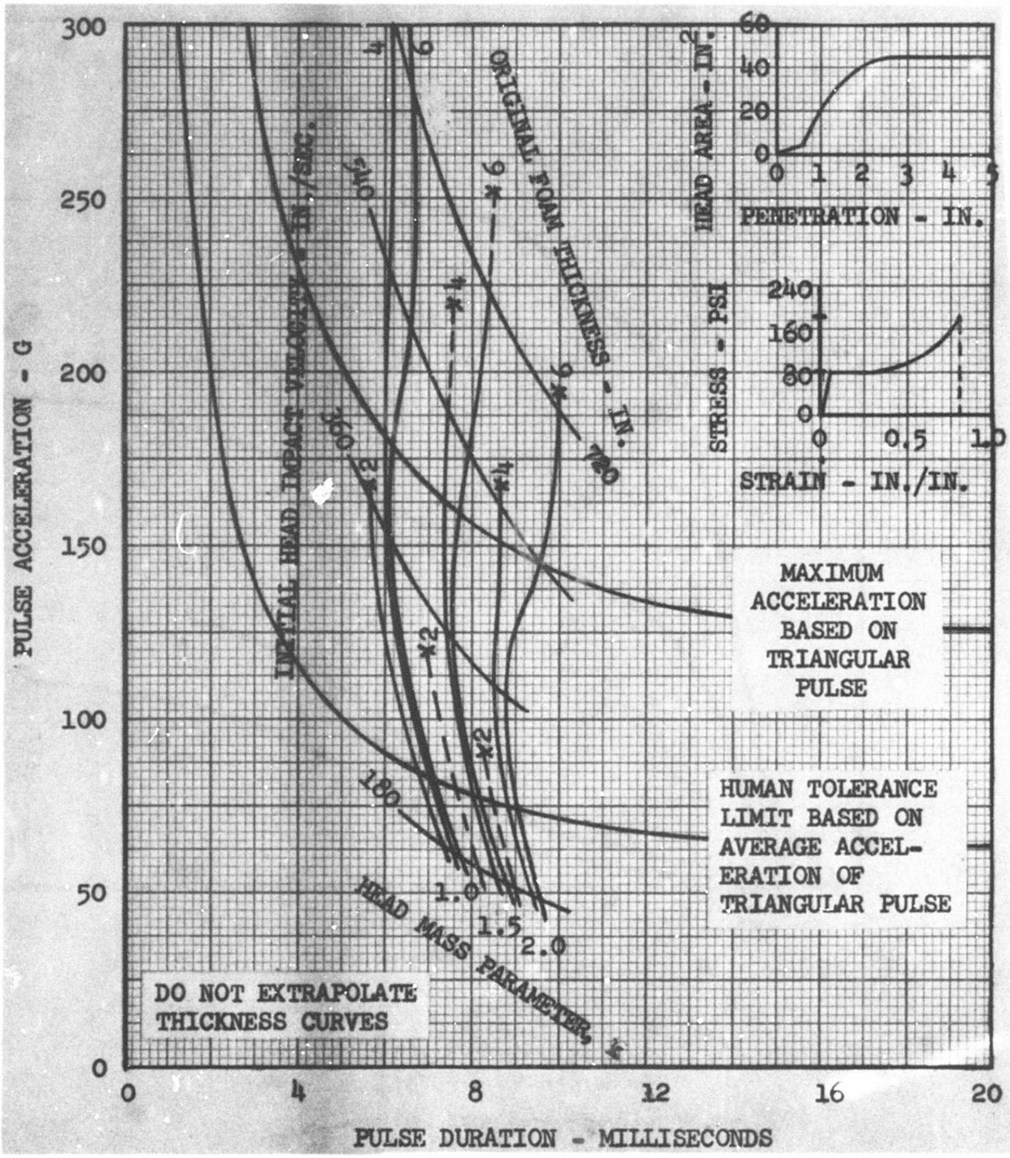

Figure 162. Design Parameters for a 3.0 lb./cu. ft. Density Styrofoam Material (Foam No. 1).

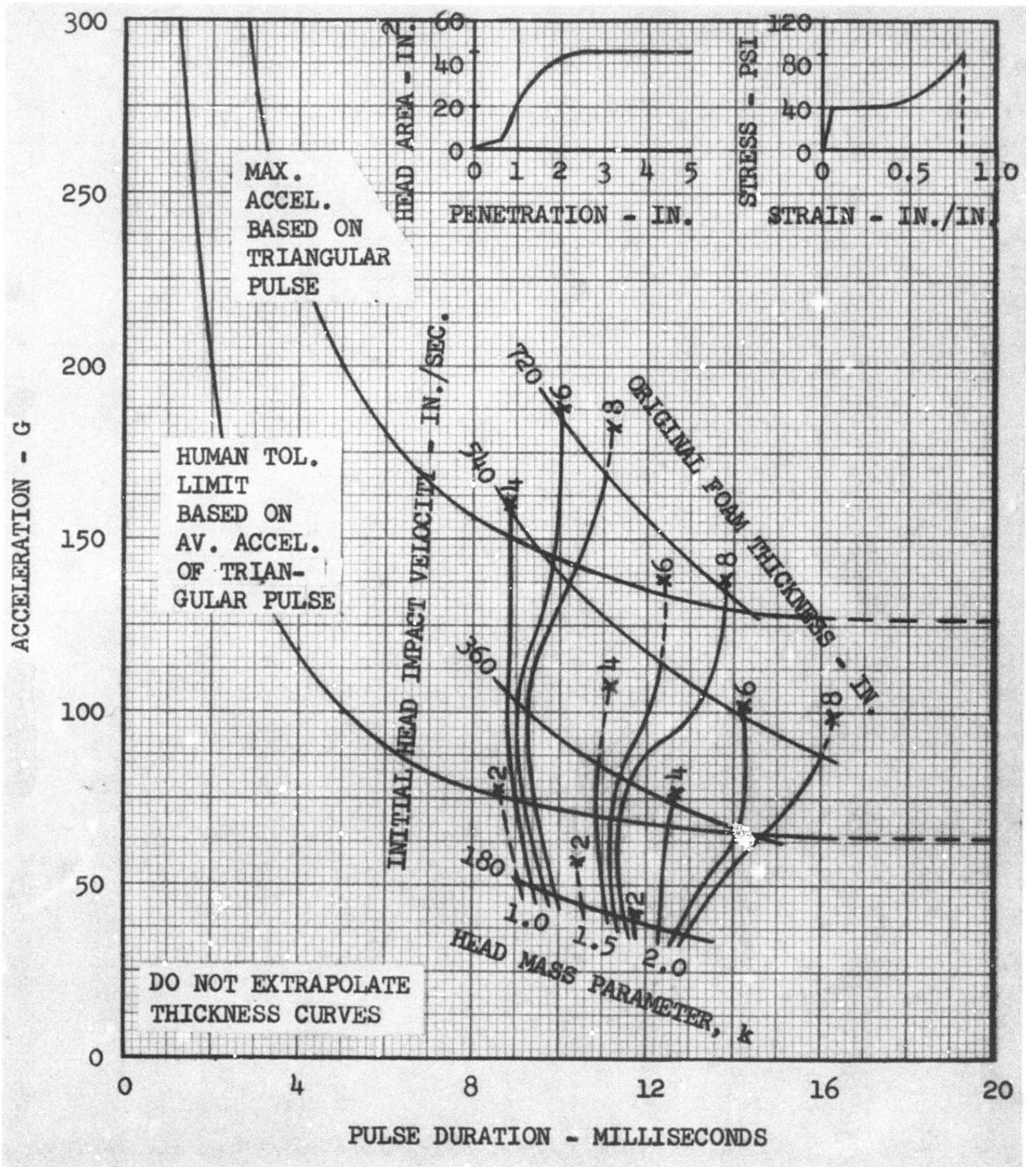

Figure 163. Design Parameters for a Hypothetical Rigid Foam Material (Foam No. 2).

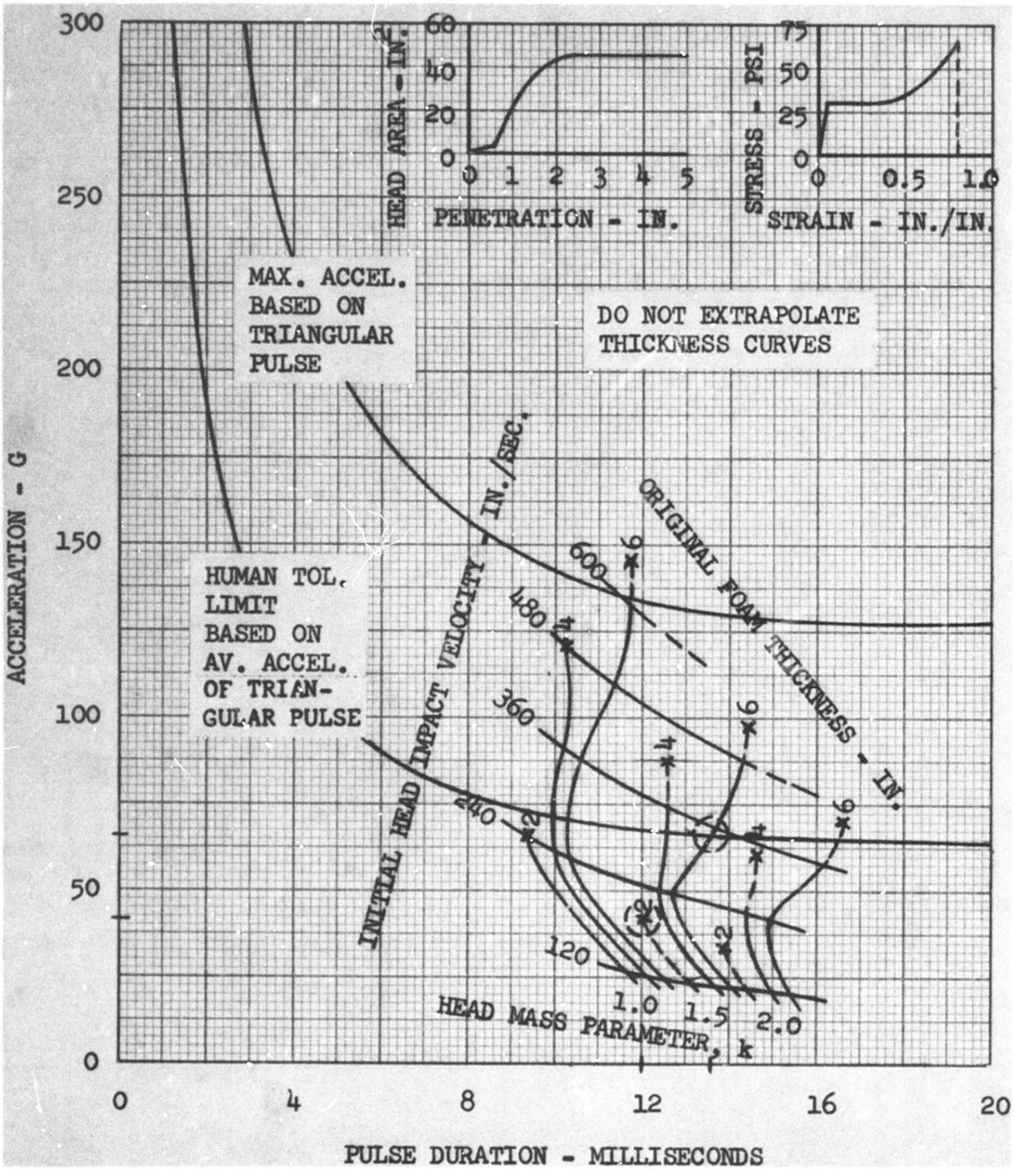

Figure 164. Design Parameters for a Hypothetical Rigid Foam Material (Foam No. 3).

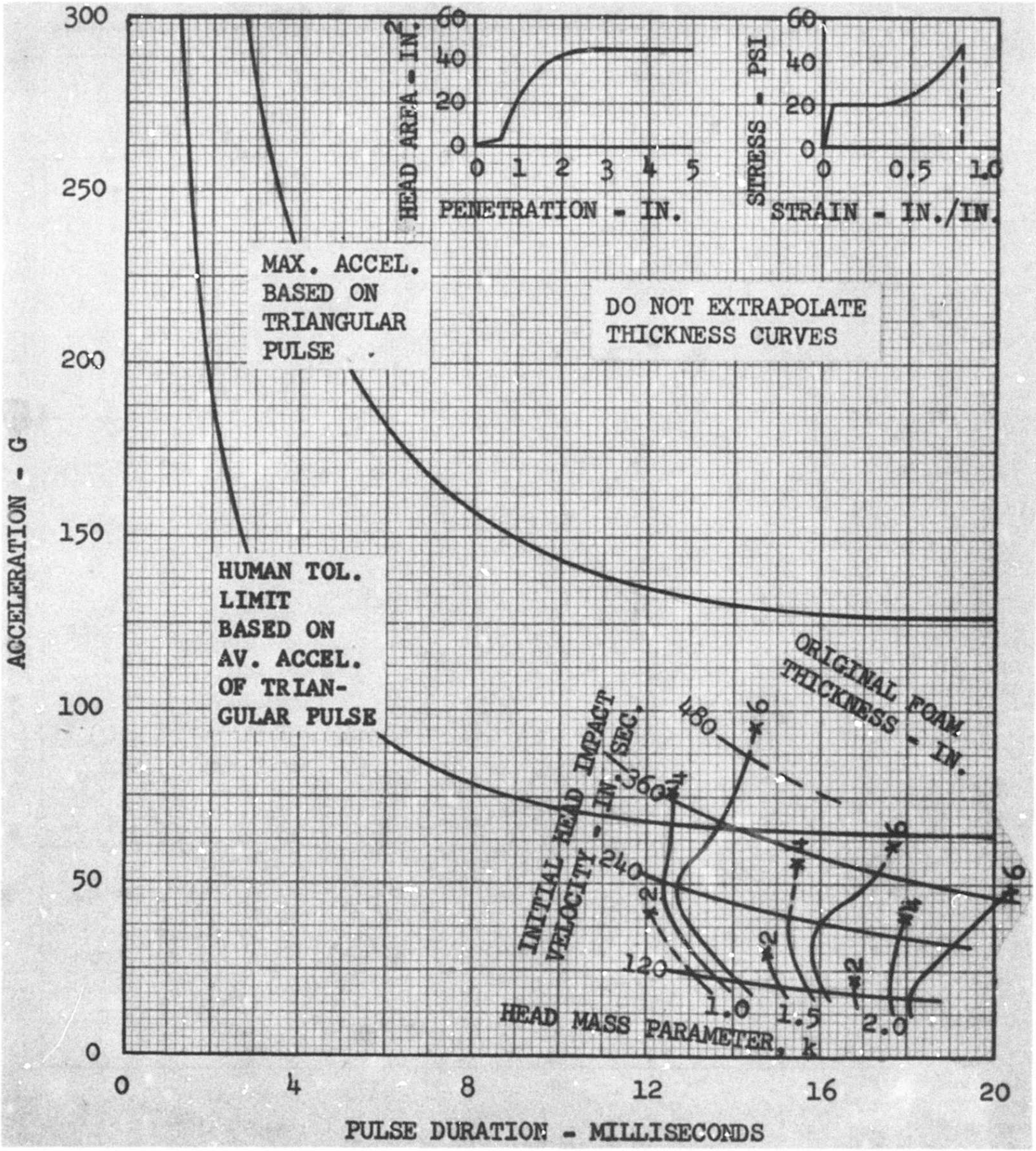

Figure 165. Design Parameters for a Hypothetical Rigid Foam Material (Foam No. 4).

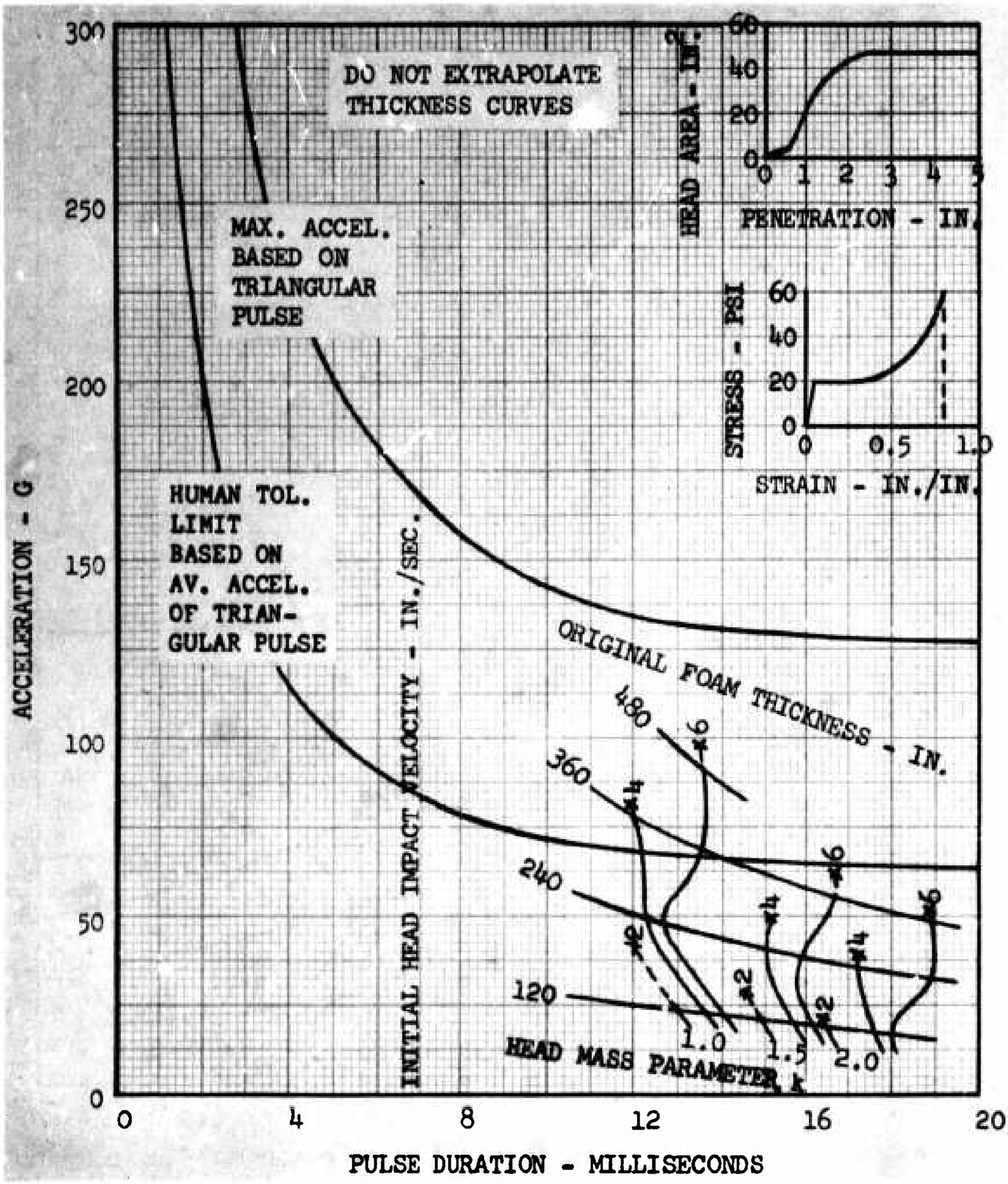

Figure 166. Design Parameters for a 2.25 lb./cu. ft. Density Foam Plastic Material (Foam No. 5).

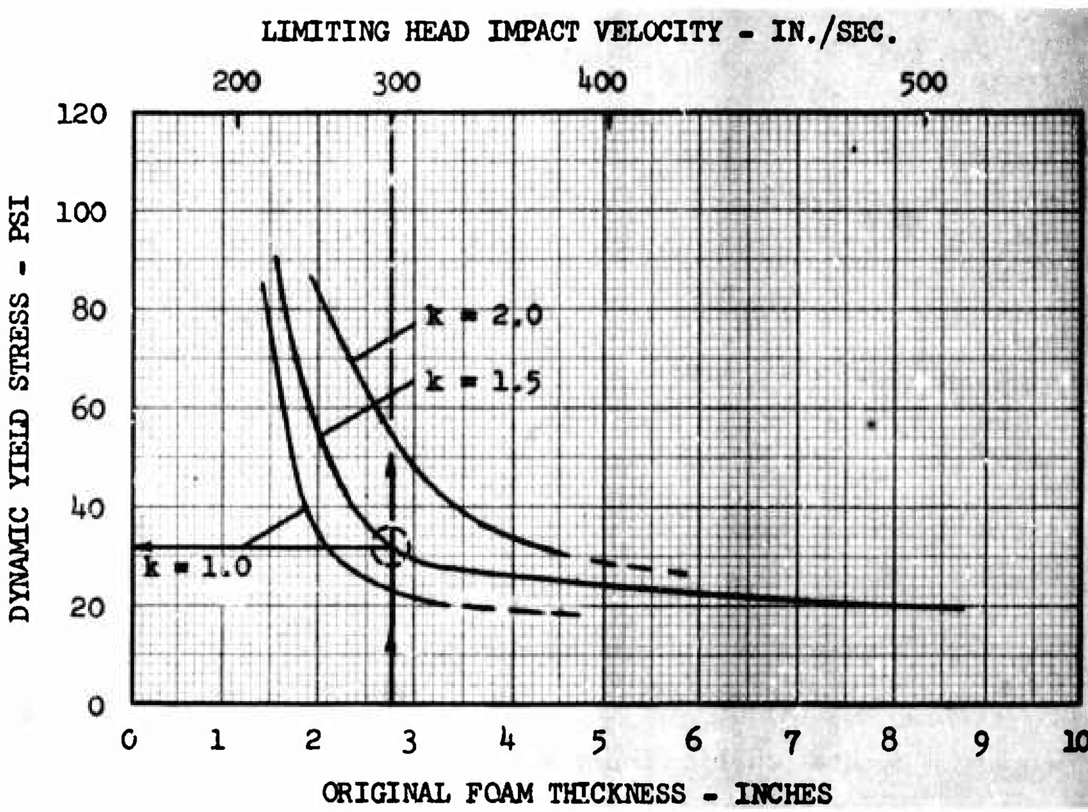

Figure 167. Design Curves for Foams Shown in Figures 162 Through 165.

TABLE I
SYMBOL NOMENCLATURE*

INPUT

ACC1 ACC2 ACC3 ACC4 ACC5 ACC6	=	Maximum accelerations for acceleration pulse shapes
AM23 BM23 AM24 BM24 AM45 BM45 AM56 BM56 AM57 BM57 AM78 BM78	=	Muscle tension coefficients
C1	=	x-distance from the seat back to the C. G. of the seat
C2	=	y-distance from the seat pan to the C. G. of the seat
CA	=	Seat cushion moment coefficient
CAB1 CAB2 CAB3 CAB4 CAB5	=	Seat belt coefficients

*For input and output:

times are in seconds
weights and forces are in pounds
elongations and displacements are in inches
velocities are in inches per second
accelerations are in inches per second squared
moments are in inch-pounds

TABLE I (contd.)

CAC1 CAC2 CAC3	=	Seat cushion coefficients
CAH1 CAH2 CAH3	=	Shoulder harness coefficients
CAX2	=	Damping coefficient for horizontal seat reaction
CAY2F	=	Damping coefficient for front seat legs
CAY2R	=	Damping coefficient for rear seat legs
CAY3R	=	Seat leg coefficient
D	=	x-distance between seat back and front leg attachment to the floor
DTI	=	Smallest time increment
DV	=	Decrease in velocity during crash
E	=	x-distance between seat back and rear leg attachment to the floor
EL2	=	Distance between lumped masses 1 and 2
EL3	=	" " " " 2 " 3
EL4	=	" " " " 1 " 4
EL5	=	" " " " 4 " 5
EL6	=	" " " " 5 " 6
EL7	=	" " " " 5 " 7
EL8	=	" " " " 7 " 8
ELB	=	Mathematical seat belt length
EYES	=	Moment of inertia of seat about the C.G.
ID	=	Pulse identification number
II	=	1 - for rigid seat 2 - for flexible seat
LIT	=	1, 2, or 3 to call for different amounts of output

TABLE I (contd.)

LL	=	1, 2, 3, 4, 5, 6, and 7 are different acceleration pulse shapes
MM	=	1 - read entire new set of input data 2 - continue reading RAG values
PI	=	Time between printouts
QUO	=	Ratio of vertical and horizontal acceleration components
RAG	=	Load-limiter setting in G's
RB	=	Buckling load of front legs
RE	=	Maximum load corresponding to elastic rear leg deflection
SB	=	Initial slack in the seat belt
SH	=	Initial slack in the shoulder harness
T1 T2 T3 T4 T5	=	Time durations defining the acceleration pulse shapes
TEST 1 TEST 2	=	Limits for accuracy test
THB1	=	Initial angle between seat belt and the horizontal
TH2I	=	" " " EL2 " " "
TH4I	=	" " " EL4 " " vertical
TH5I	=	" " " EL5 " " "
TH6I	=	" " " EL6 " " "
TH7I	=	" " " EL7 " " "
TH8I	=	" " " EL8 " " "
TMAX	=	Maximum printout time
TPT	=	Start of printout
U	=	Friction coefficient between seat and passenger
U1	=	Friction coefficient between floor and passenger's feet

TABLE I (contd.)

W1 W2 W3 W4 W5 W6 W7 W8	=	Weights of lumped masses 1 through 8
WS	=	Weight of the seat
XSE	=	Elastic horizontal deflection of the seat
YPPSC	=	Deformation at collapse of front legs
YPPSE	=	Maximum elastic deformation of front legs
YPSE	=	Maximum elastic deformation of rear legs
YSI	=	Initial vertical position of the seat pan

OUTPUT

TAC6	=	Total head acceleration in G's
ACCX1 ACCX2 ACCX3 ACCX4 ACCX5 ACCX6 ACCX7 ACCX8	=	x-accelerations of lumped masses 1 through 8 in G's
ACCXS	=	x-acceleration of the seat
ACCY1 ACCY2 ACCY3 ACCY4 ACCY5 ACCY6 ACCY7 ACCY8	=	y-accelerations of lumped masses 1 through 8 in G's

TABLE I (contd.)

AX	=	Floor acceleration in the x-direction in G's
AY	=	Floor acceleration in the y-direction in G's
DEL	=	Stretch of the seat belt
DELD	=	Velocity of stretching of seat belt
DELDD	=	Acceleration of stretching of seat belt
DT	=	Time increment that satisfies accuracy test
DX1	=	x-displacement of the pelvis with respect to the seat pan
DY1	=	y-displacement of the pelvis with respect to the seat pan
PB	=	Seat belt load
PBM	=	Maximum load on the seat belt
PC	=	Load on the seat cushion
PCM	=	Maximum load on the seat cushion
PH	=	Load on the shoulder harness
PHM	=	Maximum load on the shoulder harness
RA	=	Load-limiter setting in pounds
RSX	=	Load on the seat in the longitudinal direction
RSXM	=	Maximum load on the seat in the longitudinal direction
RYF	=	Vertical load on the front legs of the seat
RYFM	=	Maximum vertical load on the front legs of the seat
RYR	=	Vertical load on the rear legs of the seat
RYRM	=	Maximum vertical load on the rear legs of the seat
SUMS	=	Criteria for accuracy test

TABLE I (contd.)

T	=	Time coordinate
TH2	=	Angle of EL2 with respect to the horizontal
TH3	=	" " EL3 " " " " "
TH4	=	" " EL4 " " " " vertical
TH5	=	" " EL5 " " " " "
TH6	=	" " EL6 " " " " "
TH7	=	" " EL7 " " " " "
TH8	=	" " EL8 " " " " "
THB	=	Angle of seat belt with the horizontal
THS	=	Angle of seat pan with the horizontal
V6	=	Total head velocity
X1 X2 X3 X4 X5 X6 X7 X8	=	x-coordinates of lumped masses 1 through 8
XD1 XD2 XD3 XD4 XD5 XD6 XD7 XD8	=	Relative x-velocities of lumped masses 1 through 8
XDDS	=	Relative horizontal acceleration of seat
XDS	=	Relative horizontal velocity of seat
XMOC	=	Moment about hip joint due to unequal compression of the seat cushion
XS	=	Relative x-displacement of the seat

TABLE I (contd.)

Y1 Y2 Y3 Y4 Y5 Y6 Y7 Y8	=	y-coordinates of lumped masses 1 through 8
YD1 YD2 YD3 YD4 YD5 YD6 YD7 YD8	=	Relative y-velocities of lumped masses 1 through 8
YDDS	=	Relative vertical acceleration of seat
YDS	=	Relative vertical velocity of seat
YPPS	=	Deformation of the front seat leg
YPS	=	Deformation of the rear seat leg
YS	=	y-position of the seat pan

TABLE II

COMPUTER INPUT VARIABLES

Description of Computer Input Variable	Code	A	B	C	Dimension
Muscle tension coefficient	AM23	50	50	50	lb-in.
" " "	BM23	5000	5000	5000	lb-in.-sec
" " "	AM24	500	500	500	lb-in.
" " "	BM24	5000	5000	5000	lb-in.-sec
" " "	AM45	500	500	500	lb-in.
" " "	BM45	5000	5000	5000	lb-in.-sec
" " "	AM56	50	50	50	lb-in.
" " "	BM56	1000	1000	1000	lb-in.-sec
" " "	AM57	50	50	50	lb-in.
" " "	BM57	500	500	500	lb-in.-sec
" " "	AM78	10	10	10	lb-in.
" " "	BM78	500	500	500	lb-in.-sec
x-distance from the seat back to the C. G. of the seat	C_1	8	3.67	3.67	in.
y-distance from the seat pan to the C. G. of the seat	C_2	-2	5.22	5.22	in.
Seat cushion moment coefficient	CA	25	25	25	in.
Seat belt coefficient	CAB1	200	200	200	lb/in.
" " "	CAB2	-206	-206	-206	$lb/in.^2$
" " "	CAB3	84	84	84	$lb/in.^3$
" " "	CAB4	12	12	12	$lb/in.^4$
" " "	CAB5	50	50	50	lb/in./sec

TABLE II (contd.)

Description of Computer Input Variable	Code	A	B	C	Dimension
Seat cushion coefficient	CAC1	300	300	300	lb/in.
" " "	CAC2	100	100	100	$lb/in.^3$
" " "	CAC3	-50	-50	-50	lb-sec/in.
Shoulder harness coefficient	CAH1	200	200	200	lb/in.
" " "	CAH2	100	100	100	$lb/in.^2$
" " "	CAH3	50	50	50	lb-sec/in.
Damping coefficient for horizontal seat reaction	CAX2	25	25	25	lb-sec/in.
Damping coefficient for front seat legs	CAY2F	1000	1000	0	lb-sec/in.
Damping coefficient for rear seat legs	CAY2R	1000	1000	0	lb-sec/in.
Seat leg coefficient	CAY3R	4000	4000	4000	lb/in.
x-distance between seat back and front leg attachment to the floor	D	13	16.74	16.74	in.
x-distance between seat back and rear leg attachment to the floor	E	5	2.32	2.32	in.
Distance between lumped masses 1 and 2	EL2	16.6	16.6	16.6	in.
" " " " 2 " 3	EL3	20.6	20.6	20.6	in.
" " " " 1 " 4	EL4	11.0	11.0	11.0	in.
" " " " 4 " 5	EL5	10.9	10.9	10.9	in.
" " " " 5 " 6	EL6	6.8	6.8	6.8	in.
" " " " 5 " 7	EL7	11.9	11.9	11.9	in.
" " " " 7 " 8	EL8	16.2	16.2	16.2	in.

TABLE II (contd.)

Description of Computer Input Variable	Code	A	B	C	Dimension
Mathematical seat belt length	ELB	5	5	5	in.
Moment of inertia of seat about the C. G.	EYES	1.35	1.35	1.35	in.^{4}
Buckling load of front legs	RB	8000	8000	8000	lb
Maximum load corresponding to elastic limit deflection in rear leg	RE	7000	7000	7000	lb
Initial angle between seat belt and horizontal	THBI	.8522	.8522	.8522	rad
" " " EL2 " "	TH2I	.24435	.24435	.24435	rad
" " " EL4 " vertical	TH4I	-.12217	-.12217	-.12217	rad
" " " EL5 " "	TH5I	-.12217	-.12217	-.12217	rad
" " " EL6 " "	TH6I	-.17453	-.17453	-.17453	rad
" " " EL7 " "	TH7I	.01745	.01745	.01745	rad
" " " EL8 " "	TH8I	1.22172	1.22172	1.22172	rad
Friction coefficient between seat and passenger	U	.70	.70	.70	
Friction coefficient between floor and feet	U1	.50	.50	.50	
Weight of lumped mass 1	W1	46.9	46.9	25.20	lb
" " " " 2	W2	27.8	27.8	14.90	lb
" " " " 3	W3	16.7	16.7	8.96	lb
" " " " 4	W4	30.4	30.4	16.30	lb
" " " " 5	W5	35.2	35.2	18.90	lb

TABLE II (contd.)

Description of Computer Input Variable	Code	A	B	C	Dimension
Weight of lumped mass 6	W6	12.3	12.3	6.65	lb
" " " " 7	W7	12.7	12.7	6.81	lb
" " " " 8	W8	4.4	4.4	2.36	lb
Weight of the seat	WS	40.0	40.0	40.0	lb
Deformation at collapse of front legs	YPPSC	5.0	5.0	5.0	in.
Maximum elastic deformation of front legs	YPPSE	.25	.25	.25	in.
Maximum elastic deformation of rear legs	YPSE	.25	.25	.25	in.
Initial vertical position of the seat pan	YSI	18.0	12.47	12.47	in.

TABLE III

A COMBINATION OF X-ACCELERATION INPUT PULSES PROPOSED FOR USE IN STUDYING SEAT-PASSENGER RESPONSE

Effects to be Studied	Input Pulses (See Figure 17)
1. Triangular pulse, same duration, same peak, different rise times	1, 2, 3, 4, 5
2. Triangular pulse, same duration, same rise times, different peaks	3, 6, 7, 8
3. Triangular pulse, same peak, same rise time, different durations	4, 9, 10
4. Triangular pulse, same velocity change (2G-sec.)	3, 11, 12
5. Sinusoidal pulse, same velocity change (2G-sec.)	13, 14, 15, 31
6. Trapezoidal pulse, same velocity change (2G-sec.)	16, 17, 18
7. Same velocity change (2G-sec.)	1, 2, 3, 4, 5, 11, 12, 13, 14, 15, 16, 17, 18, 23, 24, 25, 26, 27, 28, 29, 30, 31
8. Sinusoidal pulse, same duration, same rise time, different peaks (compares with 2 above, except sinusoidal instead of triangular)	19, 20, 21, 22, 31
9. Early spike	1, 23, 24
10. Late spike	2, 25, 26
11. Variety of pulse shapes, same duration, same velocity change	3, 27, 28, 29, 30, 31
12. Multiple pulses, same overall duration, same velocity change (2G-sec.)	28, 29, 30

TABLE IV

CALCULATED AND MEASURED LOAD-LIMITER VALUES FOR TWO LOAD-LIMITER CONFIGURATIONS

Quantity (see Equation 67 in Chapter 3)	Case 1	Case 2
r, in.	0.5	0.5
E, psi	10^7	10^7
t, in.	0.125	0.063
S_{yp}, psi	35×10^3	35×10^3
b, in.	1.5	1.5
c, in.	0.765	0.765
d, in.	0.300	0.238
μ	0.47	0.47
n	4	4
F_{LL}, lb (calculated)	4950	1230
F_{LL}, lb (measured)	4300	1200

TABLE V

SPECIMEN STRESS CONCENTRATION FACTOR

Specimen Type (see Figures 135 and 136)	1	2	3	4	5	6	7
Theoretical Stress Concentration Factor	2.39	2.59	2.83	3.00	1.92	$\gg$3.00	1.30

TABLE VI

ENERGY ABSORBED PRIOR TO RUPTURE BY SPECIMEN TESTED DYNAMICALLY AS COMPARED TO SPECIMEN TESTED STATICALLY

	Specimen Type No.	Plastic Load Rate lb/sec	Total Energy Absorbed Dynamic in.-lb	Total Energy Absorbed Static in.-lb	% Increase (Decrease) Over Static Energy Absorption
Holes	1	2.40×10^4	107	112	(4.5)
	2	2.72×10^4	98	74	32.5
	3	1.20×10^4	139	101	37.6
Fillets	4	4.23×10^4	132	155	(14.8)
	5	-	-	264	-
	6	4.29×10^4	85	82	3.7
Smooth	7	4.46×10^4	663 (13.3×10^3) in.-lb/cu. in.	575 (11.5×10^3) in.-lb/cu. in.	15.3

TABLE VII
CUSHION MATERIAL CHARACTERISTICS

Foam	S_y psi	S_b psi	a* in./in.	b* in./in.	c* in./in.	Fig. No.
1	85	186	0.05	0.80	0.30	162
2	40	90	0.05	0.80	0.30	163
3	30	66	0.05	0.80	0.30	164
4	20	44	0.05	0.80	0.30	165
5	20	60	0.05	0.80	0.30	166

*Corresponds to the points shown on curves in Figure 160.

BIBLIOGRAPHY

1. Crashworthiness Study for Passenger Seat Design (Phase I), AvSER Technical Report 65-20, Aviation Safety Engineering and Research, Phoenix, Arizona (Unpublished).

2. Gurdjian, E. S., Lissner, H. R., and Patrick, L. M., "Protection of the Head and Neck in Sports", Journal of American Medical Association, Vol. 182, November 1962.

3. Lissner, H. R., Lebow, M., and Evans, Gaynor F , "Experimental Studies on the Relation between Acceleration and Intracranial Pressure Changes in Man", Surgery, Vol III, pp. 329-338, September 1960.

4. Turnbow, J. W., Cushioning for Air Drop, Part VII - Characteristics of Foamed Plastics under Dynamic Loading, University of Texas Structural Mechanics Research Laboratory, Austin, Texas, March 1957.

5. Shield, Richard, and Covington, Clarke, High-Velocity Impact Cushioning, Part VI, University of Texas Structural Mechanics Laboratory, Austin, Texas, September 1960.

6. Haley, J. L., Jr., and Turnbow, J. W., Helmet Design Criteria for Improved Crash Survival, USAAVLABS Technical Report 65-44, U. S. Army Aviation Materiel Laboratories, Fort Eustis, Virginia, January 1966.

7. Pinkel, I. I., et al, Seat Design for Crashworthiness, NACA Report No. 1332, Washington, D. C., 1957.

APPENDIX I
FLOW CHART FOR MAIN COMPUTER PROGRAM

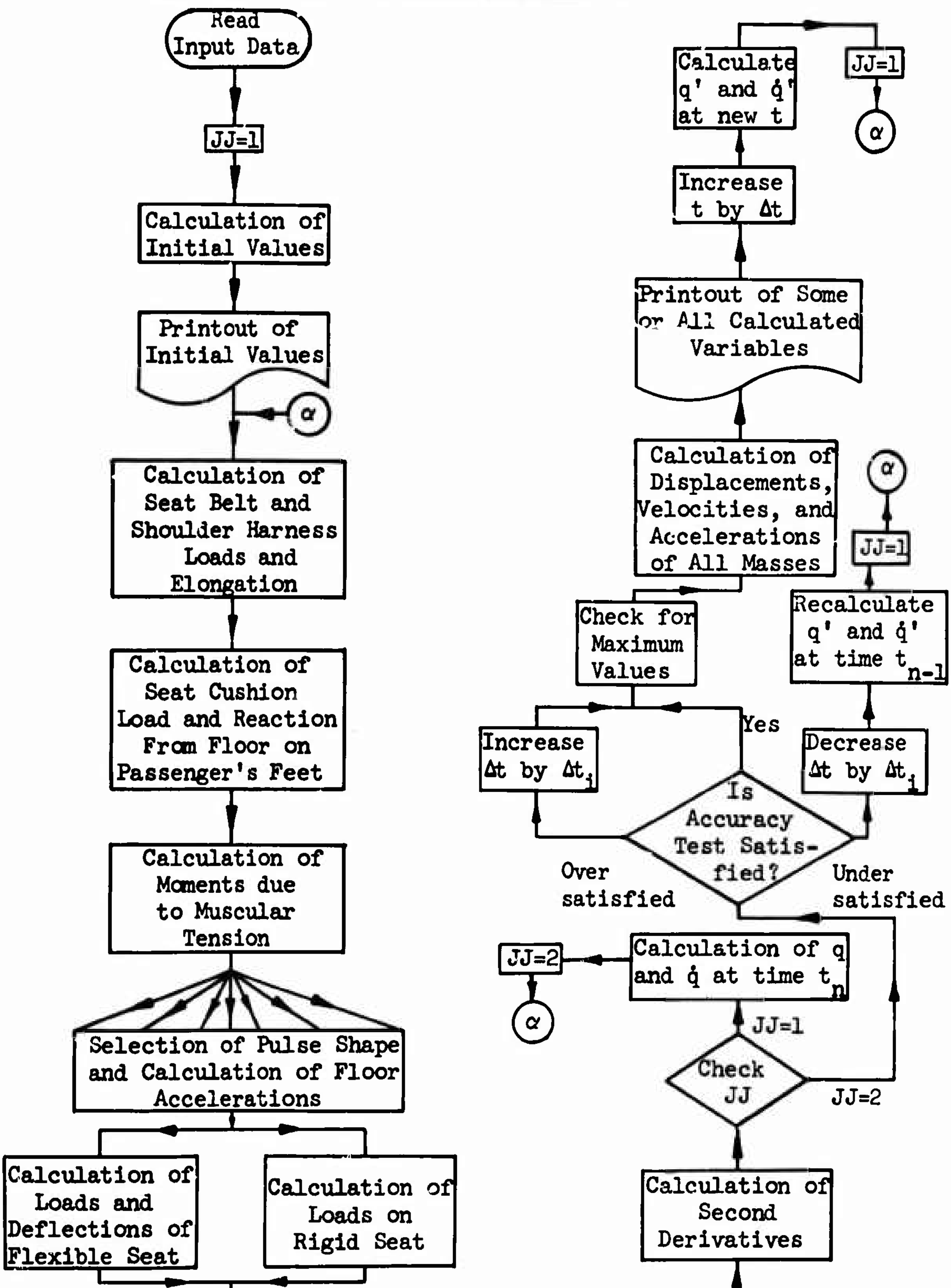

APPENDIX II

DETAILED FLOW CHART FOR SEAT ROUTINE

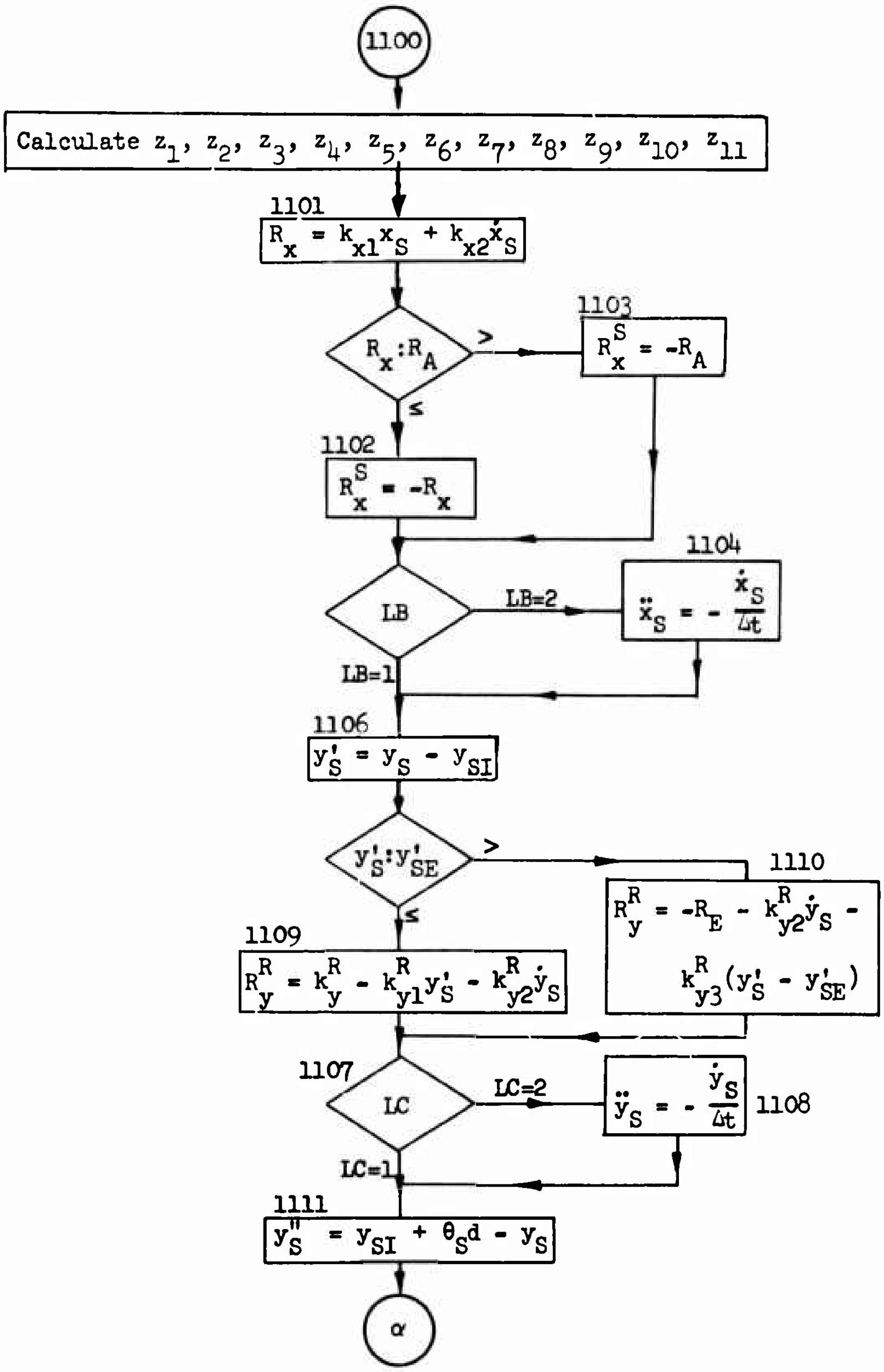

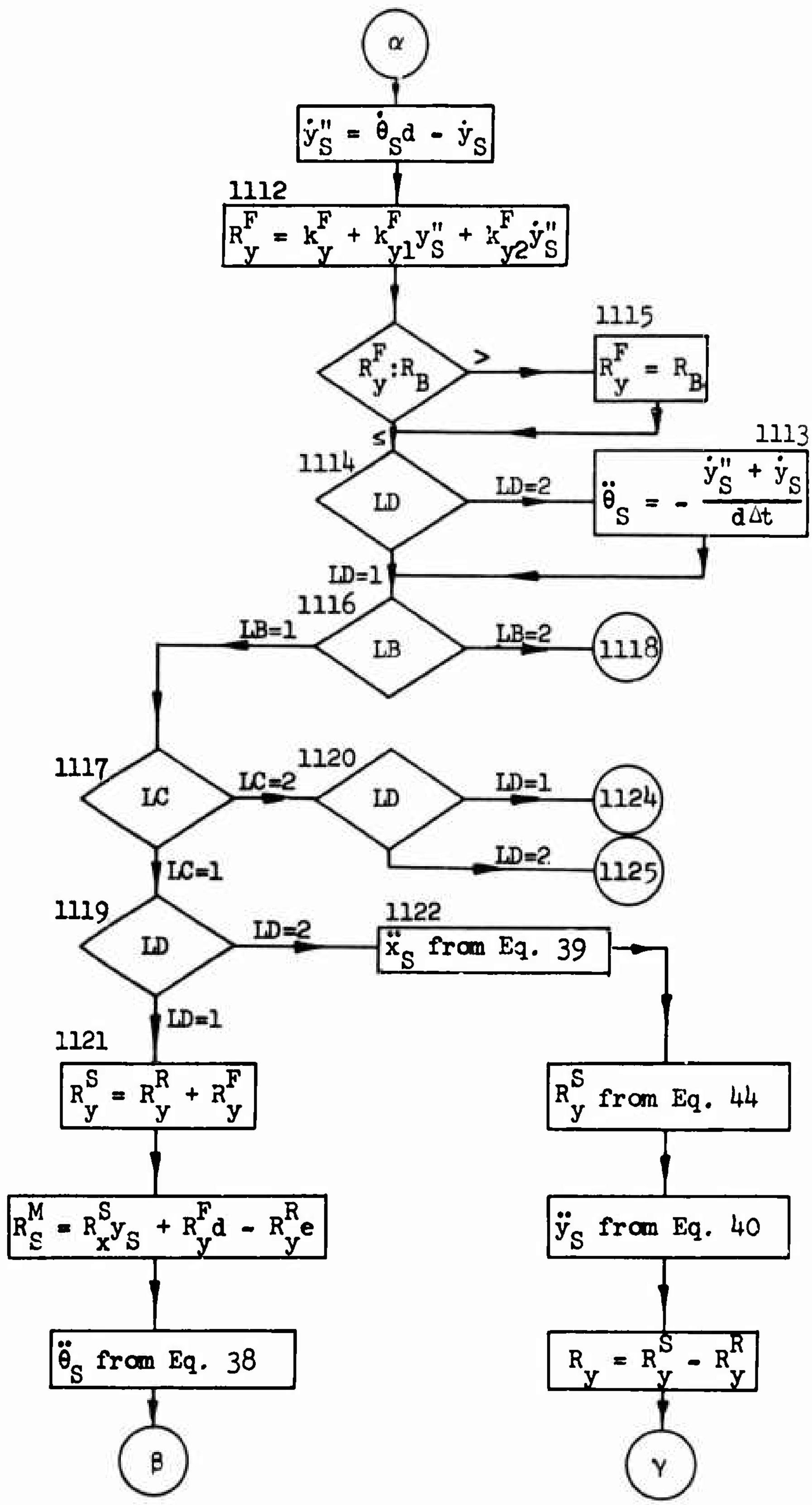
α
$\dot{y}''_S = \dot{\theta}_S d - \dot{y}_S$
1112
$R^F_y = k^F_y + k^F_{y1} y''_S + k^F_{y2} \dot{y}''_S$
$R^F_y : R_B$
>
1115
$R^F_y = R_B$
≤
1114
LD
LD=2
1113
$\ddot{\theta}_S = - \frac{\dot{y}''_S + \dot{y}_S}{d \Delta t}$
LD=1
1116
LB
LB=1
LB=2
1118
1117
LC
LC=2
1120
LD
LD=1
1124
LD=2
1125
LC=1
1119
LD
LD=2
1122
$\ddot{x}_S$ from Eq. 39
LD=1
1121
$R^S_y = R^R_y + R^F_y$
R^S_y from Eq. 44
$R^M_S = R^S_x y_S + R^F_y d - R^R_y e$
$\ddot{y}_S$ from Eq. 40
$\ddot{\theta}_S$ from Eq. 38
$R_y = R^S_y - R^R_y$
β
γ

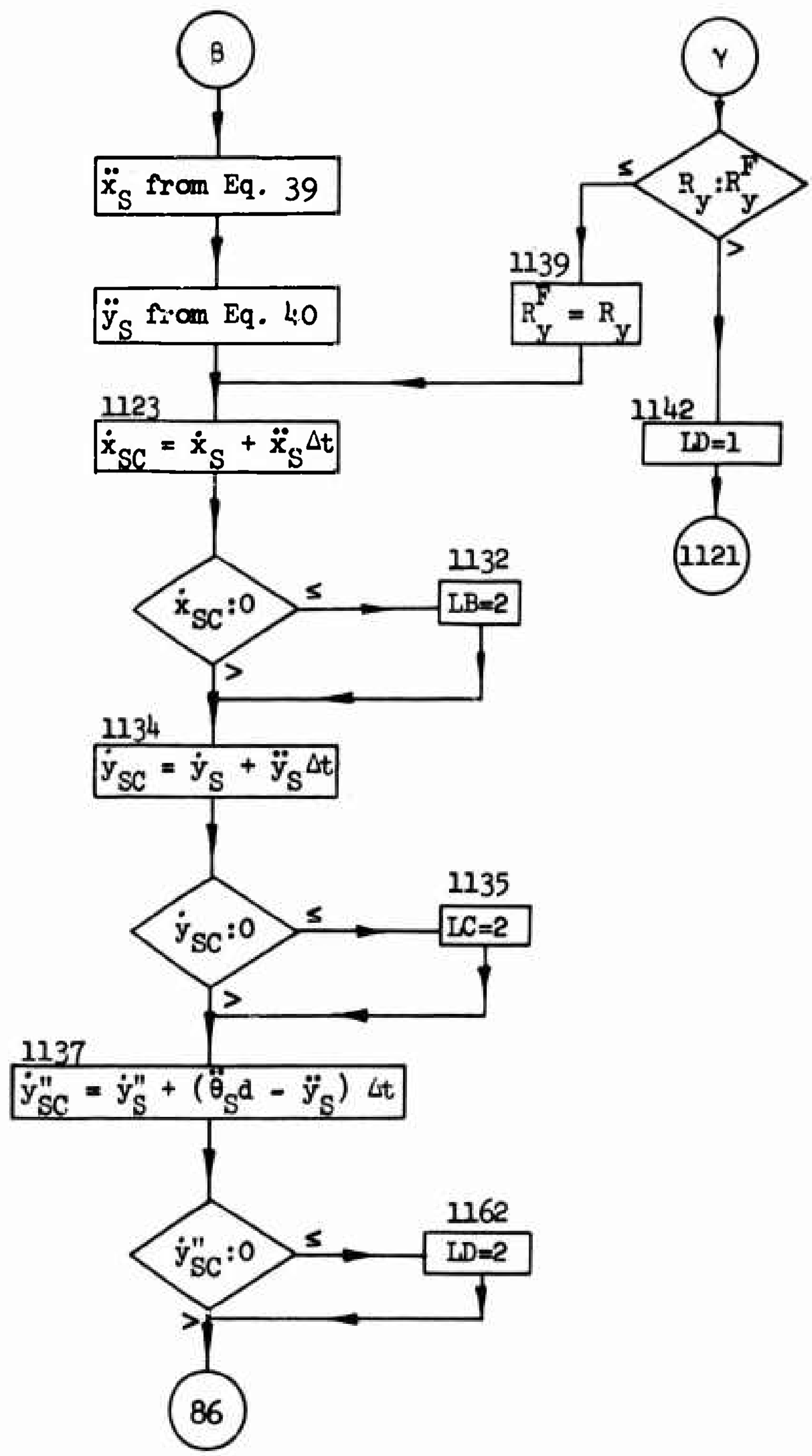
β
$\ddot{x}_S$ from Eq. 39
$\ddot{y}_S$ from Eq. 40
1123
$\dot{x}_{SC} = \dot{x}_S + \ddot{x}_S \Delta t$
$\dot{x}_{SC}:0$
≤
>
1132
LB=2
1134
$\dot{y}_{SC} = \dot{y}_S + \ddot{y}_S \Delta t$
$\dot{y}_{SC}:0$
≤
>
1135
LC=2
1137
$\dot{y}''_{SC} = \dot{y}''_S + (\ddot{\theta}_S d - \ddot{y}_S)\ \Delta t$
$\dot{y}''_{SC}:0$
≤
>
1162
LD=2
86
γ
$R_y:R^F_y$
≤
>
1139
$R^F_y = R_y$
1142
LD=1
1121

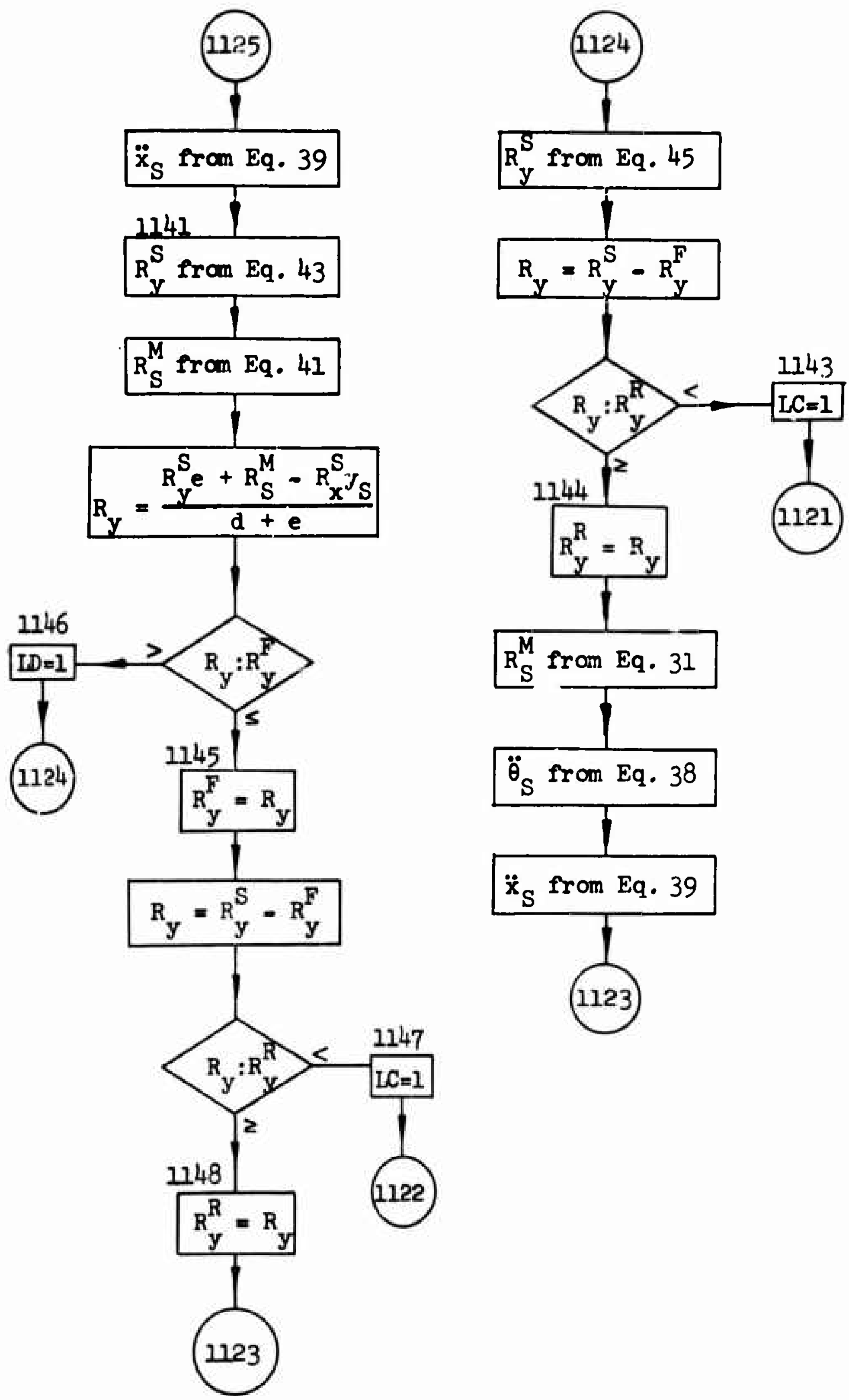
1125
ẍS from Eq. 39
1141
RyS from Eq. 43
RSM from Eq. 41
Ry = (RyS e + RSM - RxS yS) / (d + e)
1146
LD=1
>
Ry:RyF
≤
1124
1145
RyF = Ry
Ry = RyS - RyF
Ry:RyR
<
1147
LC=1
≥
1122
1148
RyR = Ry
1123
1124
RyS from Eq. 45
Ry = RyS - RyF
Ry:RyR
<
1143
LC=1
≥
1121
1144
RyR = Ry
RSM from Eq. 31
θ̈S from Eq. 38
ẍS from Eq. 39
1123

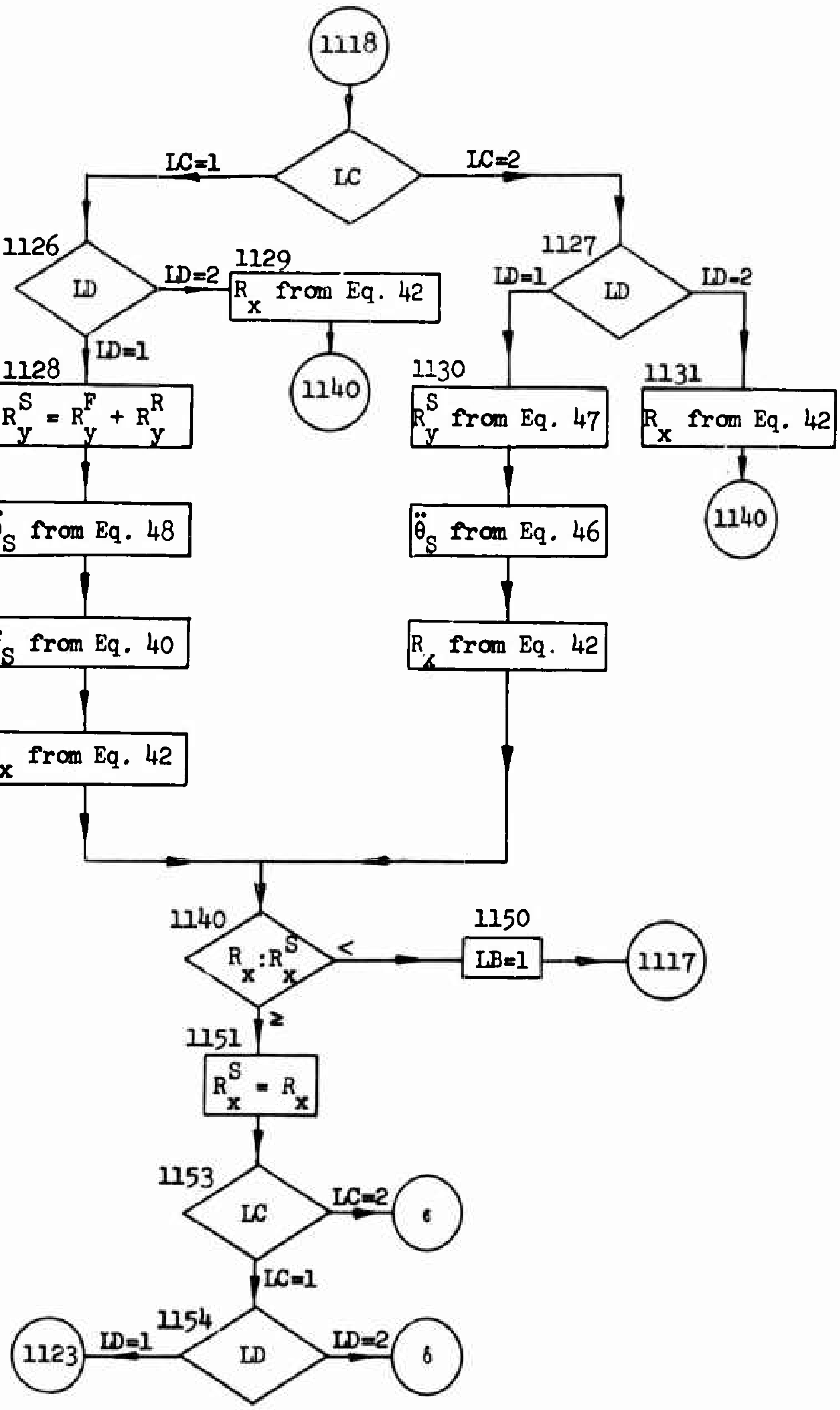
1118
LC
LC=1
LC=2
1126
LD
LD=2
1129
R_x from Eq. 42
1140
LD=1
1128
$R_y^S = R_y^F + R_y^R$
$\ddot{\theta}_S$ from Eq. 48
$\ddot{y}_S$ from Eq. 40
R_x from Eq. 42
1127
LD
LD=1
LD-2
1130
R_y^S from Eq. 47
$\ddot{\theta}_S$ from Eq. 46
R_x from Eq. 42
1131
R_x from Eq. 42
1140
1140
$R_x:R_x^S$
<
1150
LB=1
1117
≥
1151
$R_x^S = R_x$
1153
LC
LC=2
6
LC=1
1154
LD
LD=1
1123
LD=2
6

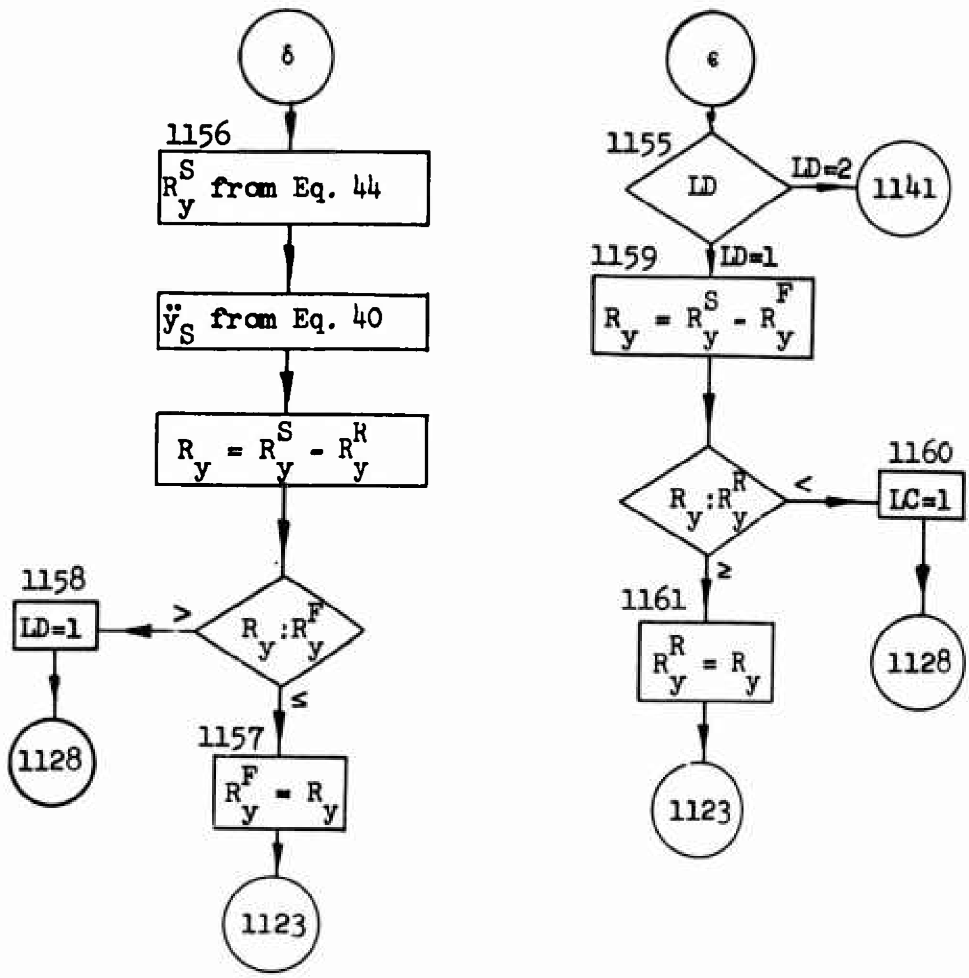

δ
1156
R_y^S from Eq. 44
$\ddot{y}_S$ from Eq. 40
$R_y = R_y^S - R_y^R$
$R_y : R_y^F$
>
1158
LD=1
1128
≤
1157
$R_y^F = R_y$
1123
ε
1155
LD
LD=2
1141
LD=1
1159
$R_y = R_y^S - R_y^F$
$R_y : R_y^R$
<
1160
LC=1
1128
≥
1161
$R_y^R = R_y$
1123

APPENDIX III
REVISED COMPUTER MODEL

Concurrently with the development of the data presented in this report, a continuing improvement in the computer simulator was being made to reduce the computational time and to improve the basic mathematical and dynamical model. Further changes and improvements to the computer program have been made after the preparation of the report as presented in the previous pages. These program changes have modified the results, as compared with those presented in the basic report, to the following extent:

1. No change in the general trend of the data has been observed.

2. The seat-belt loads and deflections and body response of the occupant are not changed appreciably in magnitude. (See comparison of the basic report and later computer runs in Figure 168.)

3. The vertical seat leg loads as presented in the basic report have been reduced in amplitude, as illustrated in Figure 169.

4. No significant change in required seat displacement for load-limited seats has been observed. (See Figure 170.)

5. The correlation between the experimental test and the computer solution as given in Figures 9 through 13 is essentially unchanged.

It can be anticipated that additional modification of the computer model as new experimental and other data are accumulated will change

the system response to some extent. Caution should thus be exercised in the applications of the results present herein, and specifically in the use of the absolute values as reported. The basic trends will probably not change.

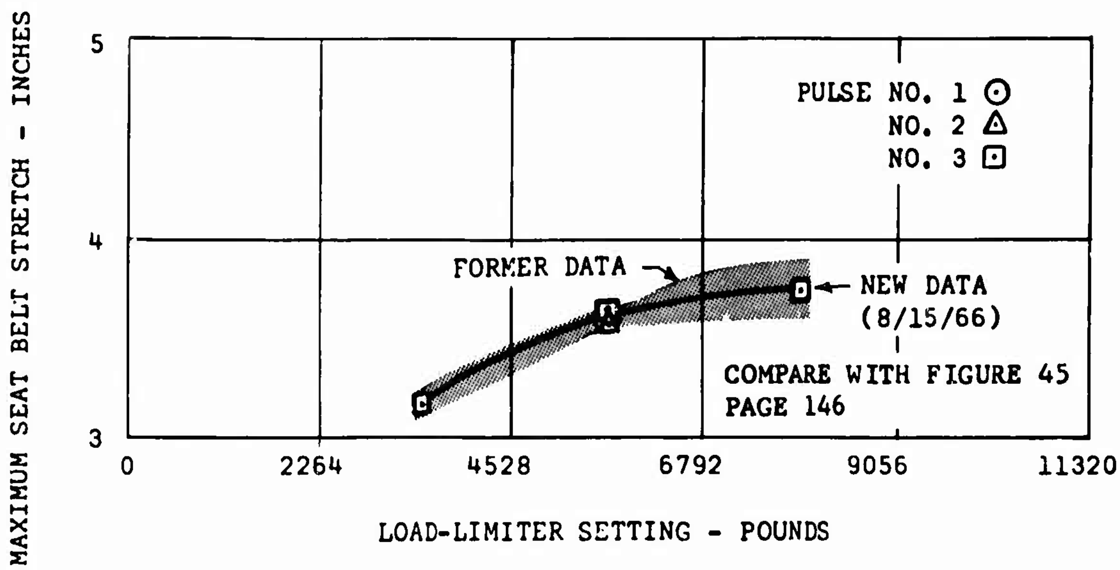

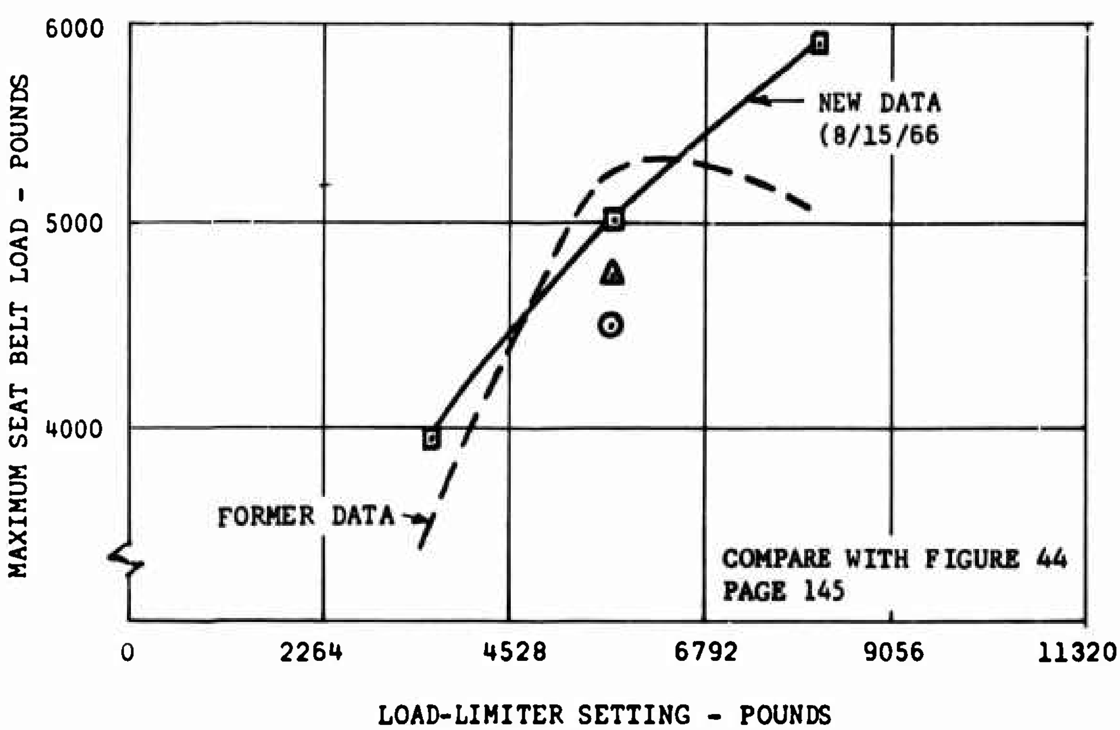

Figure 168. Comparison of Data Obtained From Revised Computer Model With Data as Presented in Figures 44 and 45.

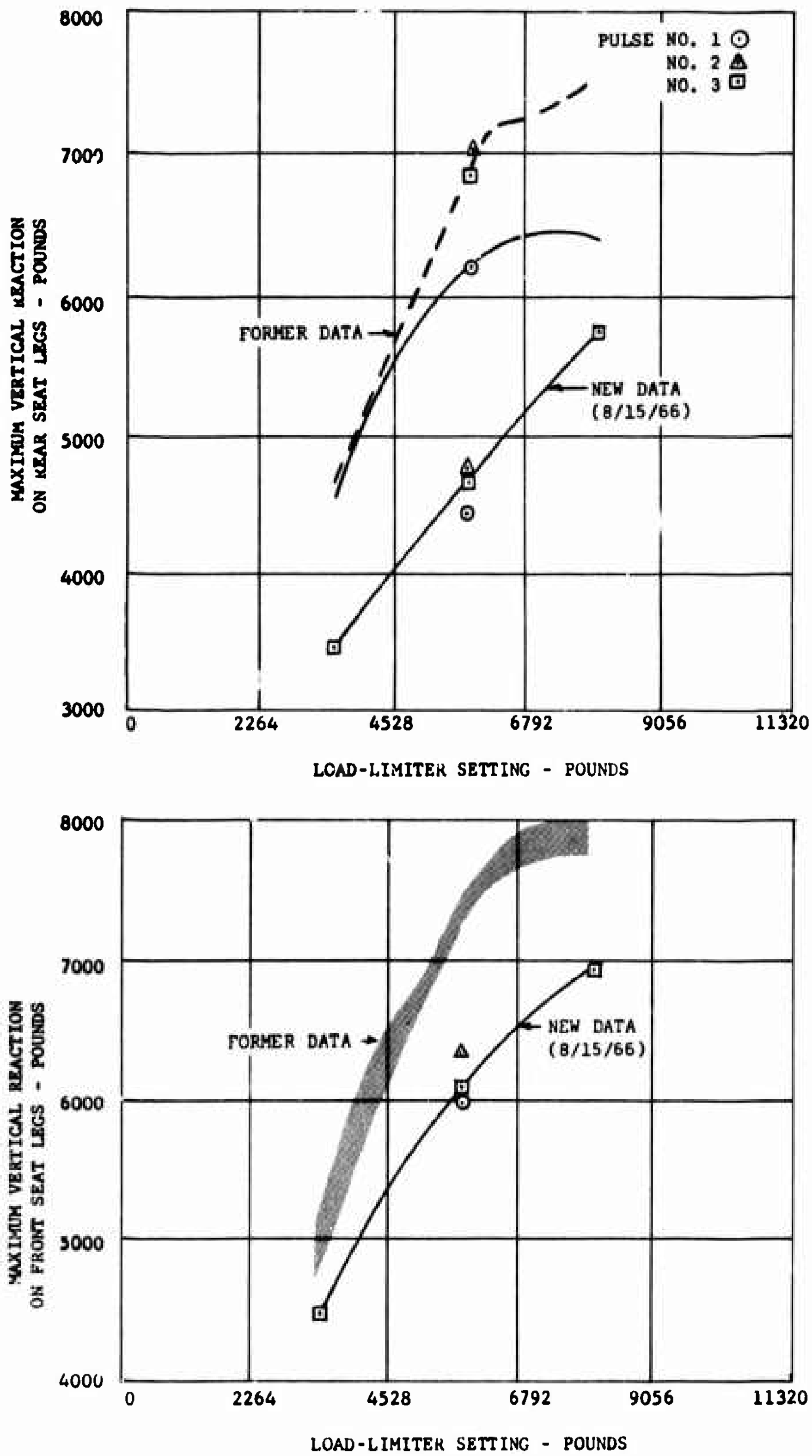

Figure 169. Comparison of Data Obtained From Revised Computer Model With Data as Presented in Figures 46 and 47.

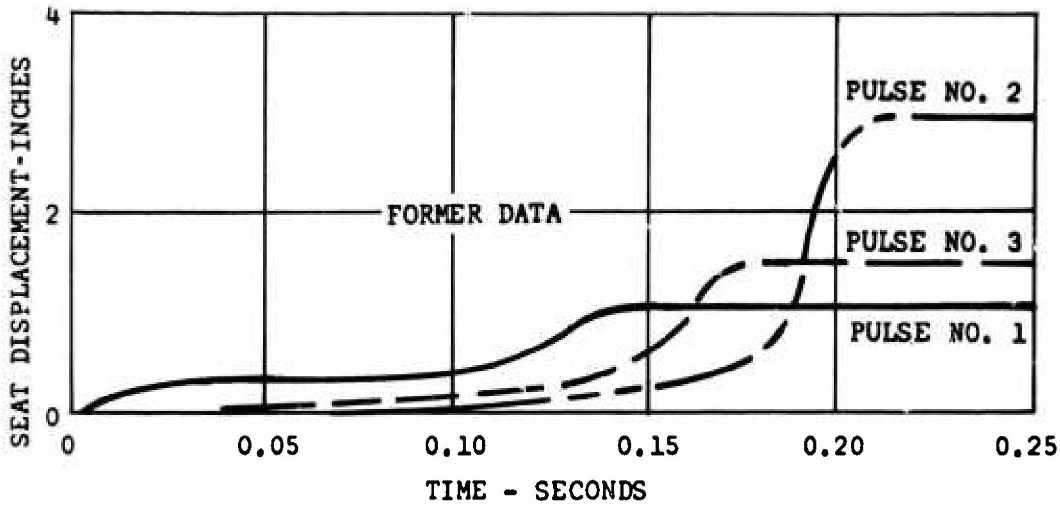

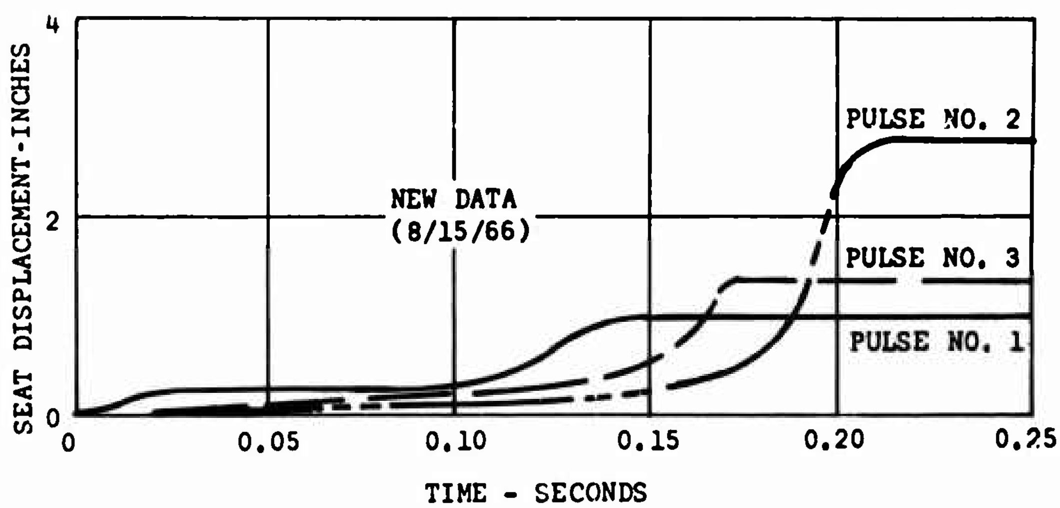

Figure 170. Comparison of Data Obtained From Revised Computer Model With Data as Presented in Figure 19.

UNCLASSIFIED
Security Classification

DOCUMENT CONTROL DATA - R&D

(Security classification of title, body of abstract and indexing annotation must be entered when the overall report is classified)

1. ORIGINATING ACTIVITY (Corporate author) Aviation Safety Engineering & Research Division of Flight Safety Foundation, Inc. Phoenix, Arizona	2a. REPORT SECURITY CLASSIFICATION Unclassified 2b. GROUP

3. REPORT TITLE

Aircraft Passenger-Seat-System Response to Impulsive Loads

4. DESCRIPTIVE NOTES (Type of report and inclusive dates)

Technical Report

5. AUTHOR(S) (Last name, first name, initial)

Turnbow, James. W.
Collins, Jack A.
Cromack, J. Robert
Myklestad, Nils P.

6. REPORT DATE	7a. TOTAL NO. OF PAGES	7b. NO. OF REFS
August 1967	313	7

8a. CONTRACT OR GRANT NO. DA 44-177-AMC-360(T)	9a. ORIGINATOR'S REPORT NUMBER(S) USAAVLABS Technical Report 67-17
b. PROJECT NO. Task 1A024701A12101	
c.	9b. OTHER REPORT NO(S) (Any other numbers that may be assigned this report)
d.	AvSER 66-20

10. AVAILABILITY/LIMITATION NOTICES

Distribution of this document is unlimited.

11. SUPPLEMENTARY NOTES	12. SPONSORING MILITARY ACTIVITY
	U.S. Army Aviation Materiel Laboratories Fort Eustis, Virginia

13. ABSTRACT

This report presents the results of an investigation of the dynamic response of typical aircraft passenger-seat systems to impulsive loading. It is divided into four chapters. Chapter 1 describes the mathematical model consisting of a visco-elastic occupant (control of joint stiffness through muscle tension) and an elastic-plastic seat structure. A comparison is made of the computer output and a full-scale dynamic test of a modern transport seat using instrumented dummies. Chapter 2 presents a spectrum of design data based on results obtained from the computer program. The design variables studied include: 1. Seat displacement with respect to the aircraft floor in the fore-aft direction. 2. Seat belt load. 3. Vertical force reaction on the front seat legs. 4. Vertical force reaction on the rear seat legs. 5. Horizontal force on the seat legs in the fore-aft direction. 6. Pelvic displacement with respect to seat. 7. Pelvic deceleration of the occupant in the fore-aft direction. 8. Maximum velocity of the occupant's head. The concept of load limiting is presented, and the effect of load limiting on the above design variables is studied. In addition, the effect of pulse shape and amplitude is presented through the use of an array of triangular, trapezoidal, and other pulses. The effects of passenger weight, seat belt slack, and shoulder harness are studied. Chapter 3 presents a discussion of load limiting and other structural and detail design concepts appropriate to maintaining good restraint of the occupant. Stress concentrations under dynamic load are explored, and the results of experimental tests are presented to show that components which have stress raisers may absorb only very small amounts of energy prior to failure. Static and dynamic tests have been conducted on typical seat components, and load-carrying capacity is compared under these conditions. Chapter 4 discusses the problem of head impact for the jackknifing passenger when restrained by seat belt alone. A computer study has been made which allows a correlation of head impact velocity and "cushioning material" thickness with the presently known human tolerance limits to deceleration. It is shown that the permissible head impact velocities will probably be in the order of one-third to one-half those which result in the 64-foot-per-second impacts described in Chapter 2.

DD FORM 1 JAN 64 1473

Unclassified
Security Classification

Unclassified
Security Classification

14 KEY WORDS	LINK A ROLE	LINK A WT	LINK B ROLE	LINK B WT	LINK C ROLE	LINK C WT
Aircraft seat design concepts.						
Stress concentration effects for rapid load stress.						
Dynamic response of aircraft passenger seat systems to impulsive loads.						
Comparison of computer output with dynamic aircraft seat tests.						

INSTRUCTIONS

1. ORIGINATING ACTIVITY: Enter the name and address of the contractor, subcontractor, grantee, Department of Defense activity or other organization *(corporate author)* issuing the report.

2*a*. REPORT SECURITY CLASSIFICATION: Enter the overall security classification of the report. Indicate whether "Restricted Data" is included. Marking is to be in accordance with appropriate security regulations.

2*b*. GROUP: Automatic downgrading is specified in DoD Directive 5200.10 and Armed Forces Industrial Manual. Enter the group number. Also, when applicable, show that optional markings have been used for Group 3 and Group 4 as authorized.

3. REPORT TITLE: Enter the complete report title in all capital letters. Titles in all cases should be unclassified. If a meaningful title cannot be selected without classification, show title classification in all capitals in parenthesis immediately following the title.

4. DESCRIPTIVE NOTES: If appropriate, enter the type of report, e.g., interim, progress, summary, annual, or final. Give the inclusive dates when a specific reporting period is covered.

5. AUTHOR(S): Enter the name(s) of author(s) as shown on or in the report. Enter last name, first name, middle initial. If military, show rank and branch of service. The name of the principal author is an absolute minimum requirement.

6. REPORT DATE: Enter the date of the report as day, month, year; or month, year. If more than one date appears on the report, use date of publication.

7*a*. TOTAL NUMBER OF PAGES: The total page count should follow normal pagination procedures, i.e., enter the number of pages containing information.

7*b*. NUMBER OF REFERENCES: Enter the total number of references cited in the report.

8*a*. CONTRACT OR GRANT NUMBER: If appropriate, enter the applicable number of the contract or grant under which the report was written.

8*b*, 8*c*, & 8*d*. PROJECT NUMBER: Enter the appropriate military department identification, such as project number, subproject number, system numbers, task number, etc.

9*a*. ORIGINATOR'S REPORT NUMBER(S): Enter the official report number by which the document will be identified and controlled by the originating activity. This number must be unique to this report.

9*b*. OTHER REPORT NUMBER(S): If the report has been assigned any other report numbers *(either by the originator or by the sponsor)*, also enter this number(s).

10. AVAILABILITY/LIMITATION NOTICES: Enter any limitations on further dissemination of the report, other than those imposed by security classification, using standard statements such as:

(1) "Qualified requesters may obtain copies of this report from DDC."

(2) "Foreign announcement and dissemination of this report by DDC is not authorized."

(3) "U. S. Government agencies may obtain copies of this report directly from DDC. Other qualified DDC users shall request through ________________."

(4) "U. S. military agencies may obtain copies of this report directly from DDC. Other qualified users shall request through ________________."

(5) "All distribution of this report is controlled. Qualified DDC users shall request through ________________."

If the report has been furnished to the Office of Technical Services, Department of Commerce, for sale to the public, indicate this fact and enter the price, if known.

11. SUPPLEMENTARY NOTES: Use for additional explanatory notes.

12. SPONSORING MILITARY ACTIVITY: Enter the name of the departmental project office or laboratory sponsoring *(paying for)* the research and development. Include address.

13. ABSTRACT: Enter an abstract giving a brief and factual summary of the document indicative of the report, even though it may also appear elsewhere in the body of the technical report. If additional space is required, a continuation sheet shall be attached.

It is highly desirable that the abstract of classified reports be unclassified. Each paragraph of the abstract shall end with an indication of the military security classification of the information in the paragraph, represented as *(TS)*, *(S)*, *(C)*, or *(U)*.

There is no limitation on the length of the abstract. However, the suggested length is from 150 to 225 words.

14. KEY WORDS: Key words are technically meaningful terms or short phrases that characterize a report and may be used as index entries for cataloging the report. Key words must be selected so that no security classification is required. Identifiers, such as equipment model designation, trade name, military project code name, geographic location, may be used as key words but will be followed by an indication of technical context. The assignment of links, rules, and weights is optional.

Unclassified
Security Classification